CRANFIELD INSTITUTE OF TECHNOLOGY

SCHOOL OF MECHANICAL ENGINEERING

Ph.D THESIS

Academic Year 1984 - 7

P. D. NGUYEN

Studies into the Failure Prediction of Brittle Materials

Supervisor : Prof. R. A. Cookson

November 1987

This thesis is submitted in partial submission for the degree of Doctor of Philosophy

SUMMARY

This thesis is divided into six chapters. The first chapter provides a brief introduction concerning the behaviour of brittle materials. It also contains the justification for the undertaking of the study as well as a brief description of the method of approach adopted, and thesis layout. Chapter two provides a critical review of the current literature available at present in the failure prediction of brittle materials. Both theoretical and experimental studies are discussed and the relevance to the present work is justified.

Chapter three deals with the numerical analyses adopted within the thesis. Five different failure criteria were utilized in the initial analysis of the results presented. Among them, the empirical model using the Principle of Independent Action satisfactorily represents the biaxial fracture behaviour of brittle materials in both tension-tension and tension-compression quadrants. Its validity has never been tested before. Various statistical fracture models were used to analyze the failure of brittle materials under multiaxial states of stress, the experimental failure data for simple tension being a starting point for their calculation. It was shown that the Energy Density theory led to a better agreement with the experiments than any other well-known fracture criterion. The study investigates methods of evaluating the Weibull parameters which were crucial in the failure prediction of brittle materials. Monte Carlo simulation techniques are also presented as a method of evaluating the data ranking for the failure probability of brittle materials.

Chapter four is devoted to the description of experimental techniques adopted in the study, using specially designed rigs. Six different tests were conducted to evaluate the performance of brittle materials in static loading and also to enable comparisons with the theoretical predictions. Attention was given to specimen casting, loading frames, alignment, measurement techniques and other relevant parameters. The use of the linear elastic fracture mechanics method to predict the behaviour of cracks in bodies, which are subjected to steady stresses, is discussed. The compliance function for the three-point notch bend specimen is presented in addition to the determination of the fracture toughness of Herculite LX plaster. The

work was also supplemented by the use of scanning electron microscopy (SEM) to failure analysis of plaster material. This is an extremely important tool in the study of brittle materials since the dimensions of small defects and fracture features on individual grains are often pertinent information to the failure analysis.

Chapter five details the analysis of the theoretical results as well as the experimental findings. Based upon the previously mentioned approaches, a comparison was made between theoretically predicted and experimentally observed data. The comparison indicates that discrepancies exist between the observed and predicted results, the reasons for the discrepancies have been justified in this work.

Chapter six provides a brief summary of conclusions derived from the complete study, together with recommendations for future work.

ACKNOWLEDGEMENTS

I would like to thank Professor R A Cookson for his wisdom and guidance throughout the work and to Dr S A Meguid for his help in the early stages. Thanks are also due to Dr E M Goodyear for the use of the fuel laboratory facilities.

I wish to thank Mr R Wilson of the Drawing Office for his quick approval of my designs. My thanks are also extended to the staff of the School of Mechanical Engineering Workshop and, in particular, to Messrs D Gadsden and G Lipinski for their help with practical difficulties.

Finally, I should like to express my gratitude to Ms S Jones for her patience and care in typing the script.

CONTENTS

LIST OF FIGURES

NOTATION

A_i	Regression constants
a	Semi-crack length
B	Total risk of rupture
b	Specimen width
β	Angle between the stress axis and the element
d	Specimen width
E	Young's modulus
F_1	Probability of failure of a single link
F_N	Probability of failure of N links
f	Probability density function (pdf)
G	Maximum coplanar strain energy release rate
g	Flaw distribution function
γ	Crack angle
Γ	Gamma function
$H(\sigma)$	Step function
i	Number of Gaussian stresses
j	Number of sampling points
K	Material constant
K_i	Stress intensity factors
K_V	Loading factor
K_{IC}	Critical stress intensity factor
k	Uniaxial compressive/tensile strength ratio
L	Limiting strength of the material
L'	Distance from the end of the bar to the load application
L( )	Likelihood function
m	Weibull modulus
$\bar{m}$	Mean of m
N	Number of samples

$N(\sigma_{cr})$	Crack density function
n	Sample size
ω	Solid angle in principal stress space
P	Applied load
P_f	Cumulative distribution function (cdf)
P_s	Probability of survival
p	Internal pressure
p/w	Plaster/water ratio
R	Disc radius
R_i	Inner radius
R_0	Outer radius
s^2	Variance
$\Sigma(V)$	Stress volume integral
$\Sigma(A)$	Stress area integral
$\bar{\sigma}$	Mean strength
σ_c	Uniaxial compressive strength
σ_{cr}	Critical normal stress
σ_{eq}	Equivalent stress
σ_f	Maximum bending stress
σ_{fv}	Unit tensile strength (volume based)
σ_{fa}	Unit tensile strength (area based)
σ_i	Principal stresses
σ_n	Stress component normal to crack length
σ_{nom}	Nominal stress
σ_0	Scale parameter (characteristic strength)
σ_r	Radial stress
σ_t	Uniaxial tensile strength
σ_θ	Circumferential stress
σ_u	Location parameter (threshold stress)

t	Disc thickness
$\tilde{\tau}_m$	Maximum in-plane shear
V	Component volume
v	Unit volume
x	Size of a defect
ν	Poisson's ratio
μ	Coefficient of friction

CHAPTER 1

INTRODUCTION

1.1 THE NEED FOR BRITTLE MATERIALS

1.1.1 Brittle Materials

In a world where competition is a vital factor for the survival of industry, the search for better and cheaper products is a must for industrial nations. With the current depletion of energy resources, industry has made every attempt to reduce its energy consumption. In a future which will presumably be short of fossil fuels and raw materials, the emphasis will continue to favour the choice of cheap and plentiful material whenever alternatives are considered. Take for example the gas turbine, it has the capacity for continued development to reach thermal efficiencies in the order of 60 per cent. But to do so, requires the hot parts to be made from exotic metals, many of which are in short supply, expensive, and come predominantly from regions of the world of somewhat uncertain political future. Alternatively, we could use components made from, say, ceramics, which in contrast are plentiful, indigeneous, and as raw materials are inexpensive. Brittle materials, particularly ceramics, have gradually been introduced to the manufacturing industries and are currently used in a wide range of applications.

The term brittle material, usually refers to materials which cannot accommodate large plastic deformations (less than, say 3 per cent) and commonly fail by brittle fracture. They include primarily the following classes of materials:

- Cast iron
- Glass
- Ceramic
- Carbon and graphite
- Cement and concrete

Of all the materials made by man, brittle materials have the longest history. Natural ceramics were selected by early man to make flint

arrow-heads and axes. The miller relied on abrasion resistance and chemical inertness of the granite mill wheel. Also, the high temperature resistance of fired clays was exploited in the early days of metal casting.

It is these same raw materials which the scientist and engineer of today and tomorrow uses and will use, to provide much more sophisticated and sometimes surprising end products.

The growing use of brittle materials arises from their basic material structure, i.e., strong chemical bonds and the ionic or covalent nature of these bonds. This results in exciting properties as follows:

- High hardness
- High stiffness
- High corrosion resistance
- High temperature resistance
- High strength
- Low specific gravity
- Low thermal expansion
- Low friction
- Low toughness
- Wide range of thermal conductivity

Because they possess a number of specialized properties, brittle material, particularly engineering ceramics are expected to be used increasingly in a number of commercial applications, ranging from components which must resist heat and wear, to electronic and optical devices.

There has been great interest shown in the design of brittle materials around the world in recent years. A recent Green paper (The Collyear Report) [1], prepared for the Department of Trade and Industry (DTI) outlined the areas of material technology that are likely to undergo revolutionary change in the coming decade. The report predicts developments which would have a major impact in three fields of mechanical and structural engineering: the base materials, fibres used to reinforce them, and the method of forming finished

shape. Leaving aside the development of electronic components, the report concluded that there are two major types of new material that will be responsible for transforming both traditional and high-technology industries: composites and ceramics. Accordingly, a UK Technical Ceramics Register was compiled jointly by the Science and Engineering Research Council (SERC) and the DTI as a reference source for academics and industrialists seeking expertise in design of brittle materials [2].

In the financial year 1985/86, about £50m has been channelled through the DTI, the Ministry of Defence, and the SERC for materials research and development. The expenditure on ceramics was about 7 per cent of the materials allocation [3]. In the USA, a committee of the National Materials Advisory Board of the National Academy of Science and Engineering [4] also encouraged the use of brittle materials in structural applications. A recent study for the US National Bureau of Standards (NBS) estimates that US shipments of engineering ceramic materials and components were $1.5 billion in 1980, then reached $7 billion in 1985, and would reach approximately $10 billion by the year 2000 if this growth rate continues [5]. In Japan, the 10-year programme initiated by the Ministry of International Trade and Industry (MITI), regarding brittle materials research and development, has been in progress since 1981 [6]. A research centre on non-destructive testing of ceramics has been set up in May 1985 [7]. West Germany is also budgeting large sums to finance research in this field [8].

1.1.2 Industrial Applications of Brittle Materials

We have grown accustomed to products made from traditional brittle materials such as glass [9] for lighting ware, optical applications, cement for construction, carbon for liquid sealing [10]. Another relatively recent area of material development is ceramics. This group of material can be assigned to three broad application categories.

ELECTRICAL OR MAGNETIC APPLICATIONS

Electrical insulation is one of the major applications of ceramics. Railway insulators, underground and overhead, controlling 400 KV from the generating station to the transmission lines, are duties handled primarily with high strength porcelain [11-14]. Other electrical applications include resistor discs for high power circuit breakers [15], radiant heating element formers [16], induction coil and arc-welding nozzles and shrouds [17]. Ceramic materials are also used as substrates or mounting fixtures for electrical circuits and devices such as the development of ceramic multi-layer capacitors [5,18], or ceramic barrier-layer capacitors [19]. These ceramic capacitors have a high capacitance per unit volume, and their construction makes them very suitable for automatic mounting.

Another unique property of ferroelectric ceramics is their ability to change shape in the presence of an applied electrical field. This conversion of electrical energy to mechanical energy is characteristic of piezoelectric materials which are used as transducers in microphones, phonograph record players [20], rotor electrodes to improve the electromagnetic interference (EMI) control over the current production rotors [21], ultrasonic equipment as x-ray tubes used in medical diagnostic [22], and in non-destructive examination of opaque materials [23].

Ceramic sensors are important in many manufacturing processes for detecting temperature, gases, humidity, and pressure [21,24,25]. Ceramic thermistors with a large positive temperature coefficient (PTC), of electrical resistance, are already being used in self-regulating heaters for automotive control. This positive temperature coefficient quality has led to applications ranging from locking the doors of front-loading washing machines [26] to helping engines run more efficiently by vapourising condensed fuel droplets to achieve more efficient combustion [27,28].

Ceramic materials with magnetic properties are important in many applications which include permanent magnets, memory units with

rapid switching times in digital computers, and circuit elements in radio, television, microwave [16,29].

The transparency of the wavelengths of electromagnetic radiation of ceramics have made them invaluable for applications in radomes to house and protect radar antennae [30] or radome nose cones for use on military missiles [16,31,32].

Ceramics are also required for a variety of applications in magnetically-confined fusion devices [33,34]. These include magnetic coil insulators, windows for heating systems, and structural uses such as first wall and blanket components in nuclear applications, armour limiters, and heat sinks.

MODERATE TEMPERATURE HARDNESS AND WEAR RESISTANCE APPLICATIONS

Their hardness and wear resistance allows novel applications in manufacturing ceramic cutting tools [13,35-46], dies for metal extrusion [17,47], roller bearings [48,49], drawing pens [50], scissors [51], artificial bones and dental implants [8,52-54], cement-free hip joint replacements [55], impellers for industrial blowers [56,57], gun barrel liners [32], and anti-ballistic personnel armour [32,58,60].

Compared with most metals, ceramics are generally resistant to corrosion. Components such as bearings, valve seals, sleeving pump shafts, and powder spraying nozzles, can successfully handle hot acids and sea water mixtures [13,36,39,61] as well as molten metal [17,62,63].

HIGH TEMPERATURE APPLICATIONS

Some effort was devoted to brittle material design for the use of ceramics as gas turbine blades in the 1940's, reactor fuel elements in the 1950's. In the 1960's, the interest in the structural use of brittle materials in aerospace vehicles arose as a result of interest in re-entry vehicles and the continuing need for propulsion systems of increased performance. Ceramic components for heat engines

of both reciprocating and turbine type are now creating immense interest around the world [13,64].

Ceramic materials have been applied to diesel engine components in the three major areas. The first area is the mass production of ceramic turbochargers to provide a useful decrease in rotor inertia and improvement in turbocharger response [65,67]. The second area of application is that of attempting to divert most of the energy extracted by the cooling system into useful mechanical energy. To do that, the cooling system should be either reduced or cut out completely, and parts such as pistons, cylinder liners, valves, cylinder heads, etc., must be insulated so that they do not experience the high temperatures [11,25,58,68-71]. The third potential application of ceramics to reciprocating engines lies in the area of materials substitution [71]. Ceramics appear to be the favoured material for glow plugs and pre-combustion chambers [6,65,72,76], and a variety of other components such as cam followers, valve seat inserts [77], positive gas seals between the monolith and container in automobile catalytic converters for exhaust emission control [78].

Ceramics are also used in turbine technology. Earlier programmes have been funded to incorporate ceramics into existing gas turbines and to design new gas turbines based upon the specific properties of the various high temperature ceramic materials. The potential applications include heat generators [79-81], rotor blades [82,83], nozzle vanes [84] and other parts of gas turbines [85,86]. Recent promising results come from the research work for the Ceramic Applications in Turbine Engines (CATE) at Massachusettes [75] and Rolls-Royce at Leavesden, Watford [87]. Apart from the production of consistently reliable turbine components, ceramics play an important, and even a critical role as solid electrolytes, electrodes and other components in vehicular batteries and load-levelling batteries, electrodes and insulators in magneto-hydrodynamic (MHD) conversion systems [88],

Ceramic materials are used increasingly in a number of high-temperature commercial applications ranging from jigs and fixtures for heat treatment, brazing, soldering and welding operations [89,90], high temperature thermal insulation uses in aerospace applications,

petrochemical and nuclear power plants [78,91], lock hopper valves in coal conversion industry [92] to ceramic foam filter used for moulds to cast automobile parts, increasing the quality and reducing the defective parts rate [93], and recently developed refractory sheet products which can be used in an unlimited variety of high temperature applications, particularly as a replacement for the medically unsafe asbestos [94-96].

Other applications which have also been developed recently are thermal barrier coatings [25,97] and integrated optical circuits [98]. The former serves as a means of increasing the system operating temperature and also provides protection to the surface of an alloy. The latter is used in fibre optic communication systems, including commercial telecommunications, military communications, and computer-to-computer data communication links.

Table 1.1 summarizes some of the most common applications of ceramic materials in industry.

1.1.3 Design Approach

Experience shows that structural design techniques which have been developed and used successfully for structures fabricated from ductile metallic materials cannot be used without modification when dealing with completely brittle materials, if the same degree of structural reliability is required. All of the considerations involved in brittle material design result from the condition that the material shows no, or insignificant, yielding prior to failure. But due to their lack of ductility, or lack of yielding, three main aspects of their characteristics must be considered by the designer. These are: the limited strain to failure, low fracture toughness, and the material inhomogeneity as exhibited by variation in strength of a given test population.

The main problem, that of the large amount of data scatter in fracture strength, precludes the use of normal design methods. To overcome this problem, designers have proposed a probabilistic approach to the design of brittle structures based, for example, on the Weibull statistical model which uses a distribution function to

TABLE 1.1 SOME APPLICATIONS OF CERAMICS

APPLICATIONS	MATERIAL	REFERENCES
Electrical or Magnetic Applications		
Insulators	Porcelain	[11,14]
Capacitors	$BaTiO_3$	[17,19]
Heat exchangers	Si_3N_4, SiC	[67]
Radomes	Si_3N_4, MgO, Al_2O_3	[30,32]
	MgF_2, ZnS, fused SiO_2	[21,24,25]
Sensors	Al_2O_3, $LiTaO_3$, $PbTiO_3$	
Tribological Applications		
Cutting tools	Al_2O_3	[13,29,30,35-46]
Metallurgical polishing	MgO, Al_2O_3	[13,39,69,97]
Sandstone and glass paper	Silica particles	[97]
Emery paper and grinding wheels	SiC	[97]
Roller bearings	Si_3N_4	[48,49,65,66]
Cylinder liners and cam followers for internal combustion engines	Si_3N_4	[48,49,65,66]
Artificial bones	Al_2O_3	[16]
Impellers for blowers	Al_2O_3, Si_3N_4, SiC	[56,57]
Armour for personnel	B_4C	[32,58-60,97]
High Temperature Applications		
Diesel engines		
Turbocharger rotors	Si_3N_4	[65,67]
Piston, piston pin and cylinder liner	Hot pressed SiC and Sintered SiC	[58,59,68,70]
Glow plug, pre-chamber parts	Si_3N_4	[6,65,72,75]
Gas Turbines		
Housing, regenerators	Lithium aluminosilicate	[39,67,69,74,81]
Rotors, stators	Sintered Si_3N_4	[75,87]

characterise the fracture strength. The inherent variability in brittle materials is too great: exact stresses must be determined statistically and parts are then designed not to exceed a specified probability of failure [99,100].

Because brittle materials cannot deform plastically, interfaces which transfer load must be highly conforming to avoid excessive local load at asperities. Extreme contact stresses, resulting from inadequate design or manufacturing processes, can cause catastrophic component failures [101]. It has been shown that if small dust particles are wedged between the undersurface of a specimen and the surface on which it is placed, the resulting stresses are sufficient to cause failure [102]. The relative motion of this interface under temperature and stress variations will introduce friction stresses, which further compound the designer's task [103,104]. In these complicated cases, simplified models may give some valuable information, especially if they use bounds on the stresses in the critical regions of the brittle component.

Apart from statistical variations in strength, another factor of major importance is the time dependence of strength [105]. such time dependent strength properties can be explained by the fracture mechanics approach to brittle fracture [106,107]. Unlike the usual stresses analysis approach, fracture mechanics consider the amount of energy needed to form new fracture surface and allow initially stable crack growth from existing flaws until sufficient growth causes instability and component failure. This theory provides a means of characterizing the stress field in the vicinity of a crack tip and thus the driving force for crack growth. Using the theories of fracture mechanics, the conditions for both crack growth and critical crack size can be established [108].

Modern design aspects also include proof testing and appropriate non-destructive evaluation (NDE) methodology. In proof-testing, the components are exposed to selected stress levels which exceed those anticipated in service to assure a minimum strength for the component [99,107,109,110]. Proof-testing of individual components offers a valuable method of quality control such that the

inherently weaker components of a batch may be identified before they are used in service. The use of proof-testing and NDE procedures for finished components are necessary means of assuring some degree of reliability, but the approach to reliability improvements must be far more fundamental than reliance on these procedures. Instead, it must depend on total process control to ensure the avoidance of defect production [111].

1.2 JUSTIFICATION FOR THE STUDY

In view of the growing interest in the use of brittle materials for structural purposes, as pointed out in section 1.1.2, this requires new approaches to design. This brittle material technology is new and will be unfamiliar to most designers who have occasion to use this class of material. Because of this, the designer usually follows the classical process of structural analysis associated with metallic materials. Ductile materials, however, flow or yield to some degree around flaws to redistribute stresses and reduce the danger of fracture. Brittle materials, on the other hand, cannot change shape. Flaws remain just as they were formed in the part, and concentrated stresses cannot be redistributed. The lack of ductility of brittle materials means that the local effects can no longer be tolerated. The second brittle characteristic is a wide scatter of strength values between nominally identical specimens due to the variation of defects.

The design process with brittle materials has not been fully exploited. Numerous references on brittle materials, have paid much attention to strength variability, and some only to the fracture mechanics aspect. In addition to these techniques, the need for statistical strength data requires simulation modelling and analysis. A design engineer requires another tool that provides additional evidence of expected system productivity and efficiency in order to add to their intuitive feel. This approach has not been taken seriously by engineers before now. Engineers frequently have difficulty obtaining information that is both pertinent to the problem at hand and understandable to someone with limited statistical training [112]. The crucial point in ceramics design is when the statistical analysis of the material is matched with stress analysis

of the design. The combined application of fracture mechanics and the empirical probabilistic method has recently been considered very sparse [102].

1.3 OBJECTIVES OF THE WORK

The main objectives of this thesis are to give the designer a better understanding of the probabilistic approach and how it can be used to predict fracture strength of brittle materials and show the problems associated with such use. Two approaches have been taken in order to serve the above-mentioned purposes. Figure 1.1 shows a block diagram of the method of approach adopted for the thesis.

1.3.1 Theoretical

Some of the theories proposed for brittle materials are discussed in order to verify which should be used. Such considerations were evolved using stress determination.

Since a most important principle of successful design with brittle materials is believed to be the use of stress analysis methods [113], finite element studies and analytical techniques in stress determination have been used extensively in this thesis.

The problem of extensive data of extrapolation on the basis of the Weibull statistical analysis may be resolved by using the Monte Carlo method. This study is conducted to compare different techniques for the estimation of the parameters of probability distributions.

1.3.2 Experimental

An experimental programme which supports the theoretical approach has been carried out. This involved measuring the mean fracture strength and its variability in plaster specimens under various multiaxial stress systems at room temperature. Different shapes of specimen and types of mechanical loading were used to achieve specimen failure as a result of well-defined stressing.

These tests are divided into two main groups. Group 1 consists of failure tests. Group 2 is the fracture mechanics tests.

1.4 LAYOUT OF THESIS

The thesis is divided into six chapters. Chapter 1 gives an introduction to brittle materials, particularly ceramics. Chapter 2 reviews literature which is available at this time on brittle materials. Considerations were given to the failure theories, probabilistic approaches to design and reliability. Chapter 3 presents the theoretical and numerical analysis. Chapter 4 presents the experimental work. The analysis of results and discussion are presented in Chapter 5 while Chapter 6 presents the final conclusions.

Numerical calculations, proofs and related matters are provided in Appendices at the end of this thesis.

CHAPTER 2

LITERATURE SURVEY

2.1 FAILURE THEORIES

At present any discussion of material failure can take one of two forms; fracture mechanics, which attempts to explain in physical terms the details of the initiation and progression of failure in the material, or the failure theories, which define material strength under complex stress conditions, but which are based on gross considerations.

The failure theories provide a quantitative statement of the stress conditions which will result in material failure, whether it be yielding or fracture. Such theories are based on overall considerations which are assumed to control material behaviour. These failure theories require empirical verification but they do provide quantitative data which can be used in design. This subject is therefore discussed here.

2.1.1 Classical Theories

- **Maximum Normal Stress Theory**

This theory assumes that the material will fracture when one of the principal stresses becomes equal to the uniaxial strength. With this theory the strength is not affected by principal stresses other than the maximum. The criterion makes no prediction of compression strength in terms of tensile strength and both values must be determined experimentally from uniaxial tests.

- **Coulomb-Mohr Theory**

The Coulomb-Mohr theory, sometimes called the internal friction theory, is based on the observations of slip lines, which are detectable on the surface of deformed metals. Mohr neglects the intermediate principal stress σ_2. A failure condition is represented by the major principal stress circle corresponding to σ_1 and σ_3 and

plotted on τ-σ axes. A number of major principal stress circles, corresponding to failure determined experimentally for various combinations of σ_1 and σ_3, can be drawn and Mohr postulates that the envelope of all of these maximum principal stress circles is the limiting curve describing failure (Fig. 2.1).

The simplest solution is to approximate the limiting envelope by a tangent to the tension and compression circles (Fig. 2.2). If we arrange the principal stresses so that $\sigma_1 > \sigma_2 > \sigma_3$, then the largest circle will be formed by σ_1 and σ_3. These two stresses and the strength are related by the equation.

$$\frac{\sigma_1}{\sigma_t} + \frac{\sigma_3}{\sigma_c} = 1$$

where σ_t = the uniaxial tensile strength

σ_c = the uniaxial compressive strength.

- Griffith's Crack Theory

Griffiths [114] in 1924 proposed a theory of rupture for brittle solids in biaxial stress condition. He used the idea, derived from Inglis's work, by assuming a small crack whose surface has the form of an elliptic cylinder and that failure occurs when a critical tensile stress is reached on the boundary of the crack.

The relationships between applied principal stresses σ_1 and σ_2 and the uniaxial tensile strength are as follows:

If $3\sigma_1 + \sigma_2$ is positive

$$\sigma_1 = \sigma_t$$

If $3\sigma_1 + \sigma_2$ is negative

$$\left(\frac{\sigma_1}{\sigma_t} - \frac{\sigma_2}{\sigma_t} \right)^2 + 8\left(\frac{\sigma_1}{\sigma_t} + \frac{\sigma_2}{\sigma_t} \right) = 0$$

From the above expressions the uniaxial compression strength is predicted as eight times the uniaxial tensile strength. Comparing the prediction with the results of tests on brittle solids, he found that the compressive strength of cast iron is about 7 times the tensile strength. In tests on stone, the compressive strength is from 7 to 11 times the tensile strength.

2.1.2 Other Theories

- **Fisher Theory**

Fisher [115] proposed a criterion by modifying the distortion energy criterion. He assumed that graphite flakes could transmit compressive stresses and act as stress concentrating cavities with respect to tensile stresses.

For tension-tension

$$K\sigma_1 = \sigma_c$$

For tension-compression

$$(K\sigma_1)^2 - K\sigma_1\sigma_2 + \sigma_2^2 = \sigma_c^2$$

For compression-compression

$$\sigma_1^2 - \sigma_1\sigma_2 + \sigma_2^2 = \sigma_c^2$$

where σ_1 : the maximum stress

σ_2 : the minimum stress

σ_c : the uniaxial compressive strength

$K = \frac{\sigma_c}{\sigma_t}$ = the uniaxial compressive/tensile strength ratio.

The results show that his criterion can be made to fit the experimental evidence quite well, particularly in the first and fourth quadrant. By comparing different theories using his own data, Mair [116] concluded that Fisher's theory is simple and in general the most satisfactory, so did Clough and Shank [117].

- Grassi and Cornet Theory

Grassi and Cornet [118,119] investigated the fracture of grey cast iron using thin wall tubes, for various ratios of axial to tangential stress ranging from pure tension to pure compression. They proposed for the tension-compression quadrant

$$\left(\frac{\sigma_1}{\sigma_t}\right)^2 - \frac{\sigma_1 \sigma_2}{\sigma_t \sigma_c} + \left(\frac{\sigma_2}{\sigma_c}\right)^2 = 1$$

In the tension-tension quadrant, the Maximum-Normal Stress theory still apply.

- Frishmuth and McLaughlin Theory

Frishmuth and McLaughlin [120] have used the plastic limit load to analyse the failure of cast irons under three-dimensional stress states. They proposed the lower and upper bounds theory, based on the observations that considerable plastic flow occurs between microflaws prior to rupture. Good agreement is obtained with the results of other researchers in both the first and second quadrants.

- Shigley Theory

Shigley [121] found that both the Maximum-Normal Stress theory and the Coulomb-Mohr theory are identical in the first quadrant. He then modified the Mohr theory to predict failure of cast iron in the fourth quadrant. The tension cut-off point in this quadrant is at the point where the σ_2/σ_1 ratio equals -1. The data from literature were plotted in the first quadrant with good agreement, but much better results were achieved in the tension-compression quadrant using his modification.

- Shaw Theory

Shaw et al. [122-124] in their investigations on a number of brittle materials, found that their results are in good qualitative agreement with Griffith's results, but in poor quantitative agreement.

The main difference is the lack of agreement between theoretical and experimental values of the uniaxial compression tension ratio. Their tests showed that this ratio is within a range of 2.51 - 5.26 while the theoretical value is 8. They proposed a new theory which assumes that the voids are circular in shapes and that the uniaxial compression-tension ratio will be 3. A better result is obtained using this theory. However, a wide range of the ratio of nominal fracture stress in uniaxial compression to that in uniaxial tension showed that this ratio is not predicted exactly by the theory.

- Babel and Sines Theory

Babel and Sines [125] have extended the Griffith analysis to cracks of finite sharpness. Their theory can now predict a compressive strength of any value from three to eight times the tensile strength depending on the sharpness of the crack.

For the first, and part of the fourth, quadrant:

$$\sigma_1 = \sigma_t - \sigma_2 \left(\frac{K - 8}{K+4+4\sqrt{K+1}} \right)$$

For the fourth quadrant:

$$\sigma_1 = \frac{1}{2} \left[2\sigma_2 - \sigma_c + (\sigma_c^2 - 8\sigma_c \sigma_2)^{1/2} \right]$$

The cross-over point between the above curves is given by:

$$\frac{\sigma_2}{\sigma_1} = - \frac{3r + 1}{r - 1}$$

where

$$r = \frac{a}{b} = \frac{-K + 2 - 2\sqrt{K+1}}{K - 8}$$

$$K = \frac{\sigma_c}{\sigma_t}$$

σ_c : uniaxial compressive strength

σ_t : uniaxial tensile strength

• McClintock and Walsh Theory

The variability of the strength ratio has also been studied by McClintock and Walsh [126]. They modified the Griffith theory by proposing that it is possible for the cracks to close, these cracks then can carry normal stresses and also shear stresses due to friction.

The condition for fracture after the cracks have closed is found to be

$$\mu\,(\sigma_3 + \sigma_1 - 2\sigma_c) + (\sigma_1 - \sigma_3)\sqrt{1+\mu^2} = 4\sigma_t\sqrt{1 - \frac{\sigma_{cr}}{\sigma_t}}$$

where σ_1, σ_3 = : the principal stresses

σ_{cr} : the critical value of applied stress at which the crack closes

σ_t : the uniaxial tensile strength

μ : the friction coefficient for crack surface.

This theory predicts a ratio of strength in simple compression to strength in simple tension of about ten.

• Paul and Mirandy Theory

Paul and Mirandy [127] recently developed a fracture criterion which takes into account the three dimensional states of applied stress. The flaw is described as a flat triaxial ellipsoidal cavity. The initial fracture criterion in principal stress space, for isotropic brittle materials containing randomly oriented flaws, is developed:

$$\left(\frac{\sigma_1 - \sigma_3}{\sigma_t}\right)^2 + 2N_1^2\left(\frac{\sigma_1 + \sigma_3}{\sigma_t}\right) + N_1^2\,(N_1^2 - 4) = 0$$

where $N_1 = 2(1-\nu) + A$

$$A = \frac{2\nu d}{E} \cdot \frac{(F-E)}{1-d^2}$$

$$d = \frac{b}{a}$$

σ_1, σ_3 : principal stresses

ν : Poisson's ratio

a,b : principal semi-diameters of ellipsoid

F,E : complete elliptic integrals of the 1st and 2nd kinds, respectively, having modulus $n = (1-d^2)^{1/2}$

$$F = \int_0^{\pi/2} [1-n^2 \sin^2 \phi]^{-1/2} \, d\phi$$

$$E = \int_0^{\pi/2} [1-n^2 \sin^2 \phi]^{1/2} \, d\phi$$

- Others

The results from tests on other materials have shown different behaviour from those obtained from tests on cast iron. Ely [128] used a modified maximum strain energy theory to fit his data on tubular graphite and magnesium silicate. The results show a weakening effect in the tension-tension quadrant. The ratios of compression to tension are approximately four for graphite and six for magnesium silicate. Tubular specimens made of reaction-sintered silicon carbide were also tested by Priddle [129], again his results show that the biaxial tension is smaller than the uniaxial tension. The work on graphite by Jortner [130] was in accordance with Ely's results. The average tensile stress at failure in the biaxial tension quadrant is less than that in uniaxial tension.

There are other theories proposed for brittle failure, such as the Coffin theory [131], the modified Tsai-Wu theory [132], the Sato biaxial failure theory [133], the mode II fracture theory [134]

but they are not discussed here either because the resultant relationship is too complex and difficult to use, or because they are seen to be questionable on the basis of the available experimental data.

2.2 STATISTICAL ANALYSIS

- Weibull Analysis

According to Freudenthal [135], three models of the distribution function of brittle fracture can be formulated:

(1) The uniform defect model produces a gamma distribution.

(2) The classical bundle model produces a Gaussian distribution.

(3) The weakest link model produces the third asymptotic distribution of smallest values.

The first and second asymptotic distributions are described in references [136,137]. The third asymptotic distribution for minimum values is the Weibull distribution which is explained in detail elsewhere [138,139].

In most cases of fracture of truly brittle materials, (ceramic, glass, etc.,) the third asymptotic distribution of smallest values will provide the best representation of the test results and the most reliable basis for extrapolation.

The Weibull theory [140-142] proposed that there is a certain probability of fracture associated with every unit volume in a body. This probability is a function of the state of stress in the element. It is important to point out that the Weibull theory assumes that fracture will take place under the action of tensile stresses. Furthermore the theory postulates that the fracture of a body occurs simultaneously with the fracture of any of its elements. This assumption is based on the idea of the weakest link concept, i.e., the failure of one link leads to total failure.

Consider a brittle material having N links in the sense of the weakest link theory. Let $F_1(\sigma)$ denote the probability of failure of a single link under a stress σ. The corresponding probability of survival is therefore $1-F_1(\sigma)$.

For N links, the overall probability of survival is $1-F_N(\sigma) = [1-F_1(\sigma)]^N \simeq \exp[-NF_1(\sigma)]$ for $N \gg 0$. This follows from the standard result $\text{Lim}\ (1-x/n)^n = \exp(-x)$ when $n \to \infty$. For an isotropic material, N will be directly proportional to the volume of the structure, so that

$$1 - F_N(\sigma) = \exp[-Vn(\sigma)]$$

where $$n(\sigma) = \frac{NF_1(\sigma)}{V}$$

Therefore, the probability of failure can be expressed as

$$P_f \equiv F_N(\sigma) = 1 - \exp[-V.n(\sigma)] \qquad (2.1)$$

Weibull suggested the following form for $n(\sigma)$ for failure under uniform tension:

$$n(\sigma) = \left(\frac{\sigma - \sigma_u}{\sigma_o}\right)^m, \quad \sigma > \sigma_u$$

$$= 0 \qquad , \quad \sigma \leq \sigma_u \qquad (2.2)$$

where σ_u is the stress at which there is zero probability of fracture and is called the location parameter or the threshold stress.

σ_o is the characteristic value and is called the scale parameter.

m is the Weibull modulus or the shape parameter. It is a measure of the variability of the fracture stress of the specimens about the mean value $\bar{\sigma}$. A low value of m implies a high spread of fracture stress about the

mean value. It can also be related to the width of the probability density curve and the steepness of this curve.

Equations (2.1) and (2.2) yield

$$P_f = 1 - \exp\left[-V\left(\frac{\sigma - \sigma_u}{\sigma_o}\right)^m\right], \quad \sigma > \sigma_u \qquad (2.3)$$

$$= 0 \qquad , \sigma \leq \sigma_u$$

or, more generally, in the case of non-uniform uniaxial tensile stresses,

$$P_f = 1-\exp\left[-\int_V\left(\frac{\sigma - \sigma_u}{\sigma_o}\right)^m .dV\right] \qquad (2.4)$$

Equation (2.3) is commonly referred as the three-parameter Weibull cumulative distribution function (cdf) and it has been shown that this satisfies all the necessary physical and statistical conditions.

The probability density function (pdf) of a random variable σ having the three-parameter Weibull distribution is:

$$f(\sigma) = m.\ \frac{(\sigma-\sigma_u)^{m-1}}{\sigma_o^{\,m}} \exp\left[-V\left(\frac{\sigma-\sigma_u}{\sigma_o}\right)^m\right] \qquad (2.5)$$

The three-parameter Weibull distribution function is not used frequently because a lot of samples are required to obtain good accuracy.

Other commonly used forms of the Weibull function are the two-parameter forms which are shown as equations (2.6) and (2.7). The probability density function (pdf) of a random variable σ having the two-parameter Weibull distribution is:

$$f(\sigma) = m.\ \frac{\sigma^{m-1}}{\sigma_o^{\,m}} \exp\left[-V\left(\frac{\sigma}{\sigma_o}\right)^m\right] \qquad (2.6)$$

and the cumulative distribution function (cdf) is:

$$P_f \equiv F(\sigma) = 1 - \exp\left[-V \left(\frac{\sigma}{\sigma_o} \right)^m \right] \qquad (2.7)$$

It is convenient to express the probability of failure in terms of non-dimensional parameters. In order to do that, a mean uniaxial strength $\bar{\sigma}$ is defined as the arithmetic mean of the sample strengths.

$$\bar{\sigma} = \sigma_u + \frac{\sigma_o}{V^{1/m}} \Gamma\left(1 + \frac{1}{m}\right)$$

where Γ is the gamma function.

when $\sigma_u = 0$, equation (2.3) can be written as

$$P_f = 1 - \exp\left[-\Gamma\left(1 + \frac{1}{m}\right)^m \left(\frac{\sigma}{\bar{\sigma}} \right)^m \right], \ \sigma > 0 \qquad (2.8)$$

$$= 0 \qquad , \ \sigma \leq 0$$

The Weibull distribution is very flexible, and by appropriate selection of the parameters, the distribution can assume a wide variety of shapes. Several Weibull distributions are shown in Figures 2.3 and 2.4. Figure 2.3(a) shows the cdf curves with σ_o=1 and m=1,2,3,4 while Figure 2.3(b) shows the cdf curves with m=2 and σ_o=1,2,3,4. Figure 2.4 shows the probability distribution function curves, i.e., equation (2.6). Figure 2.4(a) shows the pdf curves with σ_o=1 and m=1,2,3,4. Figure 2.4(b) shows the pdf curves with m=2 and σ_o=1,2,3,4.

The Weibull distribution has been suggested as a time-to-failure model on empirical grounds, and satisfactory representations have been obtained for electron tubes, relays, ball bearings and other types of failure data (137,143).

- Dukes Model

From the original work by Weibull (140-142) the probability of failure of a structural component is given by:

$$P_f = 1 - \exp\{-B\}$$

where B is the risk of rupture.

Dukes (144) gives an integral formulation of the Weibull approach which is limited to the area where the stress is positive (Fig. 2.5(a)).

$$B = KV\sigma_1^{\,m} \left[\frac{I}{I_o} \right]$$

$$\text{where } K = \frac{1}{\sigma_o^{\,m}}$$

m : Weibull modulus

σ_o : characteristic strength

m_1 = m-1

σ_u : threshold stress

V : volume of the element

$$I = \iint \left[\cos^2\phi \cos^2\Psi + \left(\frac{\sigma_2}{\sigma_1}\right) \cos^2\phi \sin^2\Psi + \left(\frac{\sigma_3}{\sigma_1}\right) \sin^2\phi - \left(\frac{\sigma_u}{\sigma_1}\right) \right]^{m} 1 \cdot \cos\phi \, d\phi \, d\Psi$$

$$I_o = I_{(\sigma_2, \sigma_3, \sigma_u = 0)}$$

- Batdorf Model

A shortcoming of the Weibull approach to the concept of probability of failure is the assumption of the Principle of Independent Action as a criterion to describe the failure mechanism of

a brittle material under a multiaxial state of stress. His theory made no explicit assumption about the nature of the flaws.

Batdorf and Crose [145] and Batdorf and Heinisch [146] have proposed an alternative model in which principal stresses interact and specific types of cracks can explicitly be considered. According to this model, if one knows the type of flaw predominant in the material of interest and the most likely failure mechanism, the probability of failure expression for a particular stress state can be written taking into account these characteristics.

Consider a body in which the predominant failure-causing flaws are distributed throughout its volume. The probability of failure of a uniformly stressed material element of volume ΔV can be written as

$$P_f = P_1 . P_2$$

where P_1 is the probability of existence in ΔV of a crack having a critical stress in the range of σ_{cr} to $\sigma_{cr} + d\sigma_{cr}$.

P_2 is the probability that a crack of critical stress σ_{cr} will be oriented in a direction such that an effective stress σ_e equals or exceeds σ_{cr}.

σ_{cr} is defined as the remote, uniaxial, normal fracture stress of a given crack.

Fracture will occur when the effective stress (a function of chosen crack configuration and fracture criterion) exceeds σ_{cr} for a particular crack. P_1 has the form:

$$P_1 = \Delta V \frac{dN}{d\sigma_{cr}} (\sigma_{cr})\, d\sigma_{cr}$$

and

$$P_2 = \frac{\omega}{4\pi}$$

where $N(\sigma_{cr})$ is the crack density function

ω is the solid angle in principal stress space containing all the crack orientations for which $\sigma_\bullet \geq \sigma_{cr}$.

Using the weakest link theory, the overall failure probability of a structure of volume V can be calculated from:

$$P_f = 1 - \exp\left[- \int_V dV \int_0^{\sigma_1} \frac{\omega}{4\pi} \cdot \frac{dN}{d\sigma_{cr}} \, d\sigma_{cr} \right]$$

The crack density function $N(\sigma_{cr})$ is a material constant and is independent of stress state. It is usually expressed as a power function of σ_{cr}, that is, $N(\sigma_{cr}) = K\sigma_{cr}^m$, where the parameters K and m can be evaluated from experimental data using uniaxial or equibiaxial tension specimens.

- Matthews and Evans Model

Uniaxial Fracture of Brittle Material

Matthews et al. [147] and Evans and Jones [148] presented an alternative technique for the treatment of failure under uniaxial tension based on the same Weakest Link Theory. This approach does not require prior assumption about the form of the flaw strength distribution term of the probability of failure

(For example, $\left(\frac{\sigma-\sigma_u}{\sigma_o}\right)^m$ in the Weibull Model of Section 2.2)

This approach was pioneered by Matthews et al. [147] in their statistical analysis of three-point flexure test failure data. Evans and Jones [148] have established a theory that allows a probability of failure analysis to be carried out on a structure starting from four-point bend test failure data. For brevity, it is referred to here as the Matthews-Evans Model.

The probability of fracture of a body of volume V can be determined

$$P_f = 1-P_s = 1-\exp\left[-\int_V dV \int_o^\sigma g(\sigma)d\sigma\right]$$

where $g(\sigma)d\sigma$ is the number of flaws per unit volume having a strength between σ and $\sigma + d\sigma$. Note that in uniaxial tension,

$\int_o^\sigma g(\sigma)d\sigma$ for the Weibull model is $\left(\frac{\sigma-\sigma_u}{\sigma_o}\right)^m$.

In the case of four-point bending, assuming volume-distributed flaws (see Figure 2.6), the resultant expression for $g(\sigma_m)$ is:

$$g(\sigma_m) = \frac{1}{2bL_1 d}\left[2\xi'(\sigma_m) + \sigma_m\ \xi''(\sigma_m)\right]$$

where σ_m is the maximum tensile stress

ξ' and ξ'' denote the first and second derivatives of $\xi(\sigma_m)$ with respect to σ_m, respectively.

The fracture probability term $\xi(\sigma_m)$ is

$$\xi(\sigma_m) = -\text{Ln}\ (1-P_f)$$

Similarly, for surface-distributed flaws,

$$g(\sigma_m) = \frac{\xi'(\sigma_m)}{2bL_1}$$

Multiaxial State of Stress

Evans [149,150] has derived a theory to predict the probability of failure of brittle structures subjected to multiaxial

states of stress, starting from basic principles of fracture mechanics and using some of the elements of the Matthews-Evans model. His theory is based on the criterion of Coplanar Strain Energy Release Rate. Crack extension (and hence, failure) occurs when the maximum Coplanar Strain Energy Release Rate, G, reaches a critical value, G_c.

$$G = \frac{(1-\nu^2)}{E} \left[K_I^2 + K_{II}^2 + \frac{1}{1-\nu} K_{III}^2 \right]$$

where E is the Young's modulus

ν is the Poisson's ratio

K_i is the stress intensity factor

I : Opening mode

II : Sliding mode

III : Tearing mode

According to the present theory, propagation will occur when

$$G = G_c = \frac{4(1-\nu^2)}{\pi E} a \left[\sigma_n^2 + \frac{4\tau_m^2}{(2-\nu)^2} \right] \qquad (2.9)$$

where a is the penny-shaped flaw radius

σ_n is the stress component normal to the crack plane

τ_m is the maximum in-plane shear

The crack extension criterion is used to obtain three basic tensile fracture conditions of practical importance in the tension-tension quadrant (equitriaxial, equibiaxial, and uniaxial).

According to Evans, the triaxial strength distribution function is

$$g_T(\sigma_T) = \left(\frac{\sigma_T - \sigma_u}{\sigma_o} \right)^m = \left(\frac{\sigma_T}{\sigma_o} \right)^m \cdot \left(1 - \frac{\sigma_u}{\sigma_T} \right)^m$$

where σ_T is the strength in equitriaxial tension

σ_u is the lower bound pertinent to the flaw population

σ_o is the scale factor

m is the Weibull modulus

The biaxial distribution is

$$g_B(\sigma_B) = \left(\frac{\sigma_B}{\sigma_o}\right)^m \int_o^{\pi/2} \left(\cos\alpha \sqrt{\cos^2\alpha + \frac{4\sin^2\alpha}{(2-\nu)^2}} - \frac{\sigma_u}{\sigma_B}\right)^m \cdot \left(\cos\alpha \sqrt{\cos^2\alpha + \frac{4\sin^2\alpha}{(2-\nu)^2}}\right) \cdot \cos\alpha \, d\alpha \qquad (2.10)$$

i.e.,

$$g_B(\sigma_B) = \left(\frac{\sigma_B}{\sigma_o}\right)^m \cdot I_B \left(m, \frac{\sigma_u}{\sigma_B}, \nu\right) \qquad (2.11)$$

where σ_B is the strength in biaxial tension

ν is the Poisson's ratio

α is the angle between the plane containing the two principal orientations and the flaw normal (Figure 2.7).

A similar functional distribution can be obtained for uniaxial tension

$$g_t(\sigma_t) = \left(\frac{\sigma_t}{\sigma_o}\right)^m \int_o^{\pi/2} \left(\cos\beta + \sqrt{\cos^2\beta \frac{4\sin^2\beta}{(2-\nu)^2}} - \frac{\sigma_u}{\sigma_t}\right)^m \cdot \left(\cos\beta \sqrt{\cos^2\beta + \frac{4\sin^2\beta}{(2-\nu)^2}}\right) \cdot \sin\beta d\beta \qquad (2.12)$$

$$g_t(\sigma_t) = \left(\frac{\sigma_t}{\sigma_o}\right)^m \cdot I_t \left(m, \frac{\sigma_u}{\sigma_t}, \nu\right) \qquad (2.13)$$

where σ_t is the strength in uniaxial tension

β is the angle between the stress axis and the element (Figure 2.8).

For failure stresses much greater than the threshold stress σ_u, the relative survival probabilities at a given strength level, for samples of equivalent stressed volume, are:

$$1-P_f(\sigma_T) = [1-P_f(\sigma_B)]^{1/I_B(m)} = [1-P_f(\sigma_t)]^{1/I_t(m)} \quad (2.14)$$

- Matsuo Model

Matsuo [151,152] has extended the Weibull distribution function which takes into account both volumetric and surface cracks. The surface cracks are assumed to be semi-elliptical cracks and the penny-shaped cracks are within the material.

The multiaxial distribution function having the three-pararameter Weibull distribution is (Figure 2.5(a) and (b)).

$$P_f = 1-\exp\left[-\int_B\left(K\int_A \sigma_{n'}{}^{m_1}\, dA\right)dV-\int_{B^*}\left(K^*\int_{A^*}\sigma_{n'}{}^{m_2}\, dA^*\right)d\omega\right]$$

where $\sigma_{n'} = \sin^2\rho\,(\sigma_1\cos^2\theta) + \sigma_2\sin^2\theta) + \sigma_3\cos^2\rho$

$$K = \frac{2m_1+1}{2\pi\sigma_{01}{}^{m_1}}$$

$$K^* = [B(m_2+\tfrac{1}{2},\tfrac{1}{2})\,\sigma_{02}{}^{m_2}]^{-1}$$

$B(,)$ is a Beta function

$dA = \sin\rho\, d\rho\, d\theta$

$dA^* = d\psi$

σ_o and m are Weibull parameters

It is found that the Strain Energy Release Rate criterion is better than the Maximum-Normal Stress criterion for calculating the fracture loci.

By taking the shear stress into consideration [153,154] Matsuo also showed that the expected fracture stresses are higher for shear sensitive cracks than those of shear insensitive ones. This was confirmed by the work of Alpa [155].

- Jayatilaka and Trustrum Model

Jayatilaka and Trustrum [156-160] developed a theory for the failure of brittle materials using the properties of the flaw size distribution and the stress necessary to fracture an inclined crack.

The strength, σ, of a brittle material is given by

$$\sigma^2 a = \frac{2}{\pi} K_{Ic}^2 \, U(\gamma)$$

where a is the semi-crack length

γ is the crack angle

K_{Ic} is the critical stress intensity factor.

For brittle materials under tensile loading, the fracture strength follows the Weibull analysis while in compression a normal distribution is more appropriate, based on the assumption that a certain proportion of cracks must fail prior to final fracture.

- Hunt and McCartney Model

Hunt and McCartney [161,162] have recently developed a statistical theory which predicts the probability of structural failure, at a given stress, from the knowledge of the expected defect population and other material properties. The probability of failure is given by:

$$P_f = \int_0^L p(L)dL = 1-\exp\{-U(L)\}$$

where p(L) is the probability of failure at a nominal applied stress in the range $L \rightarrow L + \delta L$, and

$$U(L) = \int_V \left[\int_{x(\sigma(r))}^{\infty} q(x) \right] dV$$

where $\sigma(r)$ defines the maximum principal stress at a position r in the body. $q(x)dx$ is the number of defects having size in the range $x \rightarrow x + \delta x$.

The theory has been studied extensively by both theoretical [163] and experimental approaches [164-166]. It is shown that the theory offers significant advantages for tool design [165] and failure rate prediction [167].

2.3 CONCLUSION

2.3.1 Failure Theories

Some of the theories proposed for brittle failure are discussed in section 2.1. They are summarized in Figs. 2.9 to 2.11 for biaxial stress states. Fig. 2.9 shows a comparison of most of the currently used failure theories [125]. Experimental data of Mair [116] for grey cast iron with some failure criteria [120] is shown in Fig. 2.10. Fig. 2.11 illustrates results obtained by Broutman and Cornish [169] on ceramics.

For biaxial tension, all of the theories except that of Babel and Sines give results identical with those obtained from the maximum normal stress concept, which slightly overestimates the fracture stress for equi-biaxial tension.

For tension-compression, two theories, one of Frishmuth and the other of Paul appear to fit the experimental data well. All other theories underestimate the fracture stress.

None of the theories agrees with all of the data in the compression-compression quadrant. This may be explained by Mair's difficulty in experimentally ascertaining exact failure loads under biaxial compression [116].

Further results of various investigators are given in Figs. 2.12 and 2.13. Fig. 2.12 shows the results which have been collected from reference [168] for ceramics in the range $1.0 \geq \sigma_2/\sigma_1 \geq -4$. Fig. 2.13 summarizes the biaxial strength data for graphite. Most researchers report weakening in the tension-tension quadrant, while neither strengthening nor weakening predominate among results reported for the tension-compression quadrant. The biaxial weakening observed in the tension-tension quadrant by most investigators is consistent with statistical fracture theory.

2.3.2 Statistical Analysis

As a result of the significant degree of variability in the strength of most brittle materials, it is necessary to analyze fracture of these materials from a statistical point of view. Various statistical models for the analysis of failure of brittle materials have been reviewed.

Attempts to specify the strength of brittle materials, as a function of failure probability, were made by Weibull in 1939, and a great deal of additional work has been conducted since. Weibull established a model to describe a material containing flaws of random size and distribution. His model has a very simple form, and it generally provides an accurate characterization of failure under uniaxial tension. He assumed, further, that compressive stresses and shear stresses do not contribute to the probability of failure. The two assumptions are the drawbacks of the Weibull theory. The asymptotic forms which had previously been proposed do not necessarily characterize the real distributions for various materials. The latter

approach is inherently not conservative due to the fact that not only the contributions to failure from each individual principal stress component are considered, neglecting the effects of combined principal stresses. Recently, other approaches have been suggested by Batdorf et al. [145,146]. Evans [148-150], and Matsuo [151-154] marking a significant step forward in the statistical theory of brittle fracture under multiaxial stress states.

CHAPTER THREE

NUMERICAL ANALYSIS

3.1 FAILURE THEORIES

It has long been observed that the nature of a stress state in a brittle body is as significant as its magnitude in so far as fracture is concerned.

Consideration is given in this section to the correlation of fracture data with different failure theories.

3.1.1 Maximum Normal Stress Theory

The phenomenological theory most commonly applied to brittle materials, the Maximum Normal Stress Theory, postulates that fracture will occur when the maximum principal stress in a body is equal to the uniaxial strength. This theory has been found to agree qualitatively with fracture data on brittle materials at normal temperatures and pressures.

3.1.2 Coulomb-Mohr Theory

This criterion of failure has been reviewed in Chapter Two. For simplicity, only the two-dimensional stress system will be considered, i.e., $\sigma_3=0$. It can be shown that σ_1 can be related by means of the expression:

$$\frac{\sigma_1}{\sigma_t} - \frac{\sigma_2}{\sigma_c} = 1$$

Where σ_t and σ_c are the uniaxial tensile and uniaxial compressive strengths, respectively.

It must be noted that σ_2 is the minimum principal stress in this case. When σ_1 and σ_2 are both tensile stresses, the minimum principal stress is σ_3, which is equal to zero. Therefore fracture occurs when the larger of the two principal stresses reaches the value

σ_t. A similar analysis can be carried out when both σ_1 and σ_2 are compressive. The failure diagram is given in Fig. 3.1.

3.1.3 Griffith Theory

Griffith's theory is based on the fact that rupture occurs when the stress at any point on the surface of the crack reaches a specific tensile stress. The effects of other cracks and of the distribution of these cracks in a body are neglected. In a biaxial stress system, his theory is based on the formula:

$$(\sigma_1 - \sigma_2)^2 + 8\sigma_t\ (\sigma_1 + \sigma_2) = 0$$

Fig. 3.1 shows the failure diagram according to Griffith's theory.

3.1.4 Weibull Theory

Weibull proposed that there is a certain probability of fracture associated with every unit volume in a body, and that this probability is a function of the state of stress in the element. Furthermore, fracture may occur on one of an infinite number of planes in the element. The probability function is therefore associated with all possible modes of failure of the element.

It was pointed out that the fracture strength of a body can be defined in terms of B′, the risk of fracture at each point in the body, and that B′ can be of the form:

$$B' = \iint n_1(\sigma)\ \cos\phi.d\phi.d\Psi$$

where $n_1(\sigma)$ is the material function, σ denotes the stress state at the point at which B′ is to be evaluated, and ϕ and Ψ are defined in Fig. 2.5(a). If each point in a body is subjected to a system of biaxial stresses, the normal stress, σ, in a particular direction may be defined in terms of the principal stresses, σ_1 and σ_2 by the relation:

$$\sigma = \cos^2\phi\ (\sigma_1\ \cos^2\Psi + \sigma_2\ \sin^2\ \Psi)$$

Furthermore, if $n_1(\sigma)$ is assumed to be of the form

$$n_1(\sigma) = K_1 \sigma^m$$

then the risk of fracture, B', becomes

$$B' = 2K_1 \int_0^{\pi/2} \cos^{2m+1} \phi . d\phi \int_{-\Psi_o}^{\Psi_o} (\sigma_1 \cos^2 \Psi + \sigma_2 \sin^2 \Psi)^m \ . \ d\Psi$$

where $$K_1 = \frac{2m + 1}{2\pi} K$$

K : constant

m : Weibull modulus

If σ_1 and σ_2 are both tensile stresses

$$\Psi_o = \frac{\pi}{2}$$

If one of the principal stresses is negative or compressive.

$$\tan \Psi_o = \sqrt{\frac{\sigma_1}{-\sigma_2}}$$

If the ratio of the principal stresses is defined as

$$C^2 = \frac{\sigma_2}{\sigma_1}$$

then

$$B' = 2K_1 \sigma_1^m \int_0^{\pi/2} \cos^{2m+1} \phi d\phi \int_{-\Psi_o}^{\Psi_o} (\cos^2 \Psi + C^2 \sin^2 \Psi)^m \ d\Psi$$

The total risk of rupture, B of a body of a volume, V, becomes

$$B = \int_V B' dV = B'V$$

The Weibull Theory was analysed in this work and a computer programme was developed for predicting the failure of plaster under combined stresses. The results of this analysis are presented in Table 3.1 and Fig. 3.1. The methods used in the determination of the theory for biaxial stresses on plaster are described in detail in Appendix A.

3.1.5 Stanley Theory

Stanley and Sivill[171] have recently proposed a theory which is based on the Independent Action Criterion, i.e., the effect of any one of the principal stresses is independent of the other. They then defined an equivalent stress function for the biaxial stress state in the form:

$$\sigma_{eq} = \left[\frac{\sigma_1}{H(\sigma_1)}\right]^K + \left[\frac{\sigma_2}{H(\sigma_2)}\right]^K$$

where $H(\sigma)$ is a step function equal to 1 for a tensile (positive), and to minus the ratio of the compressive to the tensile strengths, for σ compressive (negative).

K is a material parameter.

This theory was proposed as a satisfactory mathematical description of experimental biaxial failure data in the tension-tension quadrant. Its validity in other quadrants has not been tested [171].

This function is plotted in Fig. 3.1 for values of K=m=6.6727 and $H(\sigma)=\sigma_c/\sigma_t = -2.3111$. In the tension-tension quadrant, the theory conforms with the experimental results of ring-on-ring disc tests. In the tension-compression quadrant, the usefulness of the theory as a

TABLE 3.1 RISK OF FRACTURE FOR PLASTER SUBJECTED TO BIAXIAL STRESSES. m=7

Principal Stress Ratio $C^2=\sigma_2/\sigma_1$	Risk of Fracture B	$\frac{\sigma_1}{\sigma_t}$	$\frac{\sigma_2}{\sigma_t}$
1.0	4.7739	1.25	1.25
0.8	2.5839	1.15	0.92
0.667	1.9213	1.10	0.73
0.333	1.2512	1.03	0.34
0.0	1.0000	1.00	0.00
-0.333	0.8582	0.98	-0.33
-0.667	0.7634	0.96	-0.64
-0.8	0.7336	0.96	-0.77
-1.0	0.6947	0.95	-0.95
-2.0	0.5641	0.92	-1.84
-3.0	0.4873	0.90	-2.71
-4.0	0.4352	0.89	-3.55
-5.0	0.3969	0.88	-4.38
-6.0	0.3672	0.87	-5.20
-7.0	0.3432	0.86	-6.01
-8.0	0.3235	0.85	-6.81

design tool was validated by the test data yielded by the Brazilian disc tests. Furthermore, with the aid of this theory a prediction of the compressive strength, in terms of the equivalent strength, can be made. This cut-off has never been predicted by other theories.

3.2 THE EFFECT OF STRESS STATE ON FAILURE

3.2.1 Biaxial Tension

*Weibull Analysis of Failure

- Uniaxial State of Stress

The primary purpose of a uniaxial test is to determine the value of distribution parameters which are material properties and which can later be used to predict the probability of failure of a structural component under different loading conditions. The Weibull distribution parameters can be obtained by calculating the closest Weibull distribution curve fit to the experimental results for uniaxial data (see section 3.3.3)

From section 3.3.3

$m = 6.6723$

$\sigma_o = 0.6461$

The two-parameter Weibull probability of failure expression is:

$$P_f = 1-\exp\left(-6.9696 \times 10^{-6}\ \sigma^{6.6723}\right)$$

The experimental results and the distribution function are shown in Fig. 4.12.

- Multiaxial State of Stress

The stress distribution in a ring-on-ring disc test is investigated in section 4.5. The next step in this analysis of

statistical failure prediction models for brittle materials is to compare the probability of failure corresponding to a multiaxial state of stress, based on uniaxial fracture data with experimental results for the same state of stress. For reasons of simplicity, a biaxial state of stress is a convenient choice.

From the previous section, the probability of failure under biaxial stress can be written as:

$$P_f = 1-\exp\,[-B']$$

where

$$B' = 2K_1 \int_{-\Psi_o}^{\Psi_o} \int_{o}^{\pi/2} \cos^{2m+1} \rho(\sigma_1 \cos^2\Psi + \sigma_2 \sin^2\Psi)^m \, d\rho \, d\Psi$$

If σ_1 and σ_2 are both tensile stresses

$$B' = 4K_1 \sigma_1^{\,m} \int_{o}^{\pi/2} \cos^{2m+1} \rho d\rho \int_{o}^{\pi/2} (\cos^2\Psi + \frac{\sigma_2}{\sigma_1} \sin^2\Psi)^m \, d\Psi$$

For equibiaxial tension with Weibull modulus $m = 6.6723$, $K_1 = (2m+1)K/2\pi$ and $K = 6.9696 \times 10^{-6}$, the probability of failure distribution function for the ring-on-ring disc test is:

$$P_f = 1-\exp\,[-3.3276 \times 10^{-5} \sigma^{6.6723}]$$

This equation is plotted in Fig. 3.2 together with the experimental results of section 4.5.

Freudenthal Analysis

A frequently used approximate treatment of fracture statistics for a multiaxial stress state assumes that the probability of survival is the product of the probabilities of survival of the structure for the principal stresses applied individually [135], i.e.,

$$P_s(\sigma_1,\sigma_2,\sigma_3) = P_s(\sigma_1).P_s(\sigma_2).P_s(\sigma_3)$$

where P_s is the probability of survival

σ_i is the principal stress

For the case of equibiaxial tension, the above equation reduces to

$$P_s(\sigma,\sigma) = [P_s(\sigma,0)]^2$$

or

$$\text{Ln } P_s(\sigma,\sigma) = 2 \text{ Ln } P_s(\sigma,0)$$

From uniaxial failure data (section 3.2.2)

$$Pf(\sigma,0) = 1-P_s(\sigma,0) = 1-\exp(-6.9696 \times 10^{-6} \ \sigma^{6.6723})$$

Hence

$$\text{Ln } P_s(\sigma,0) = -6.9696 \times 10^{-6} \ \sigma^{6.6723}$$

$$\text{Ln } P_s(\sigma,\sigma) = -1.3939 \times 10^{-5} \ \sigma^{6.6723}$$

The probability of failure for equibiaxial tension becomes

$$P_f(\sigma,\sigma) = 1-P_s(\sigma,\sigma) = 1-\exp(-1.3939 \times 10^{-5} \ \sigma^{6.6723})$$

This approximation is plotted in Fig. 3.3 together with the experimental results of the ring-on-ring disc test of section 4.5.

*Batdorf Analysis

According to the Batdorf model (section 2.2), the probability of survival can be shown to be:

$$P_s = \exp\left[-\int dV \int \frac{\omega}{4\pi} \cdot \frac{dN(\sigma_{cr})}{d\sigma_{cr}} \cdot d\sigma_{cr}\right]$$

where σ_{cr} is the critical stress, defined as the remote tensile stress that will cause fracture when applied normal to the crack plane.

$N(\sigma_{cr})$ is the crack density function

ω is the solid angle in the principal stress space enclosing the normals to crack planes so that an effective stress, σ_e, which is a function of the principal stresses and crack orientation, exceeds σ_{cr}.

For analytical simplicity, the crack size distribution characterizing the volume flaws is assumed to be of the form

$$N(\sigma_{cr}) = K\sigma_{cr}^{m}$$

then

$$P_s(\sigma,\sigma) = \exp\,[-VK\sigma^m]$$

$$P_s(\sigma,0) = \exp\,[-VKm\int_0^{\sigma}\frac{\omega}{\pi}\,\sigma_{cr}^{m-1}\,d\sigma_{cr} = \exp\,[-VK'\sigma^m]$$

where

$$K' = Km\int_0^1\frac{\omega}{\pi}\,x^{m-1}dx$$

$$x \equiv \frac{\sigma_{cr}}{\sigma}$$

The relation between uniaxial and equibiaxial fracture statistics can thus be expressed in the form:

$$\frac{\text{Ln } P_s(\sigma,\sigma)}{\text{Ln } P_s(\sigma,0)} = \frac{K}{K'} = [m\int_0^1\frac{\omega}{\pi}\,x^{m-1}dx]^{-1}$$

and is shown in Fig. 3.4 for different fracture criteria [172]. Curves 1 to 3 represent the Normal Stress criterion. Curve 2 is for Griffith cracks while curve 3 is for penny-shaped cracks. Curves 4 and 5 correspond to the Strain Energy Release Rate criterion with curve 4 for Griffith cracks and curve 5 for penny-shaped cracks. Curves 6 and 7 used the Energy Density theory while curve 8 is obtained from Griffith's stress criterion. Curves 6 and 7 are for Griffith and penny-shaped cracks, respectively.

These curves can now be used to analyse the experimental results of ring-on-ring disc tests of section 4.5. The uniaxial data for four-point beam bend tests are taken as given (section 3.2.2).

$$P_f(\sigma,0) = 1-P_s(\sigma,0) = 1-\exp\,(-6.9696 \times 10^{-6}\ \sigma^{6.6723})$$

With the Weibull modulus m = 6.6723, the K/K′ ratios for various fracture criteria may be found. The corresponding equibiaxial fracture probability expressions are:

curve 1: $P_f = 1-\exp(-3.2548 \times 10^{-5}\ \sigma^{6.6723})$

curve 2: $P_f = 1-\exp(-2.8227 \times 10^{-5}\ \sigma^{6.6723})$

curve 3: $P_f = 1-\exp(-2.6833 \times 10^{-5}\ \sigma^{6.6723})$

curve 4: $P_f = 1-\exp(-2.3345 \times 10^{-5}\ \sigma^{6.6723})$

curve 5: $P_f = 1-\exp(-2.0560 \times 10^{-5}\ \sigma^{6.6723})$

curve 6: $P_f = 1-\exp(-2.0909 \times 10^{-5}\ \sigma^{6.6723})$

curve 7: $P_f = 1-\exp(-1.6727 \times 10^{-5}\ \sigma^{6.6723})$

curve 8: $P_f = 1-\exp(-1.2685 \times 10^{-5}\ \sigma^{6.6723})$

These expressions are plotted in Figs. 3.5 and 3.6 with the experimental data on equibiaxial bending of plaster discs. As expected, the Energy Density criterion leads to fairly good agreement

with experiment for the case of penny-shaped cracks (curve 7). A similar result was also obtained by Batdorf himself in analysing various experimental results from the literature [172].

*Matthews and Evans Analysis

Matthews and Evans' approach for the statistical analysis of fracture under a multiaxial state of stress (section 2.2) was used to analyse the fracture data of ring-on-ring disc tests.

Two functional relations for $g(\sigma)$ are thus needed in order to proceed with the analysis.

The biaxial distribution

$$g_B(\sigma_B) = \left(\frac{\sigma_B}{\sigma_o}\right)^m \cdot I_B\left(m, \frac{\sigma_u}{\sigma_B}, \nu\right)$$

and the uniaxial distribution

$$g_t(\sigma_t) = \left(\frac{\sigma_t}{\sigma_o}\right)^m \cdot I_t\left(m, \frac{\sigma_u}{\sigma_t}, \nu\right)$$

A computer programme was written which incorporates the subroutine DϕlAKF of the NAG Library [170]. This is an adaptive integrator, using the Gaussian quadrature which calculates an approximation to the integrals of I_B (Equation 2.10) and I_t (Equation 2.12). This subroutine is suitable for non-singular oscillating integrands. Values of I_B obtained for a range of σ_u/σ_B for ν=0.2 with m as variable are plotted in Fig. 3.7. Similarly, values of I_t obtained for a range of σ_u/σ_t are shown in Fig. 3.9. Values of I_B and I_t for a range of m when σ_u/σ_B and σ_u/σ_t equal 0 are plotted in Fig. 3.8.

From uniaxial data

$$P_f(\sigma,0) = 1-P_s(\sigma,0) = 1-\exp(-6.9696 \times 10^{-6}\ \sigma^{6.6723})$$

with the values of I_B and I_t obtained from Fig. 3.9 and equation (2.14) of section 2.2, the probability of failure expression for equibiaxial tension is

$$P_f(\sigma,\sigma) = 1- [\exp(-6.9696 \times 10^{-6} \ \sigma^{6.6723)} \ ]^{3.3559}$$

Similarly, for equitriaxial tension

$$P_f(\sigma,\sigma,\sigma) = 1- [\exp(-6.9696 \times 10^{-6} \ \sigma^{6.6723}) \ ]^{7.5586}$$

These expressions are compared with the measured equibiaxial strengths of ring-on-ring disc tests in Fig. 3.10. This model underestimates the equibiaxial strengths.

*Matsuo Analysis

By taking the shear stresses into account, Matsuo [153] obtained the expression for the probability of failure in equibiaxial tension

$$P_f(\sigma,\sigma) = 1-\exp\left[-V_o I_2 \left(\frac{\sigma}{\sigma_o}\right)^m\right]$$

where V_o is the total volume

σ_o is the scale parameter

m is the Weibull modulus

$$I_2 = \int_o^{\pi/2} \left[\sin^2\rho + \frac{4}{(2-\nu)^2} \cos^2\rho \right]^{m/2} \cdot\cos^m\rho \sin\rho \, d\rho$$

Where ν is the Poisson's ratio

ρ is the angle defined in Fig. 2.5 ($\rho = 90°-\phi$)

From the experimental data of Chapter Four:

$m = 6.6723$

$\sigma_o = 0.6461$

$$V_o = 1.9635 \times 10^{-6} \ m^3$$

The value of I_2 was obtained for ν=0.2 from a similar computer programme to that described in the previous section.

$$I_2 = 0.4761$$

The equibiaxial probability of failure distribution function is given by:

$$P_f(\sigma,\sigma) = 1-\exp(-1.7248 \times 10^{-5} \ \sigma^{6.6723})$$

This equation is plotted in Fig. 3.11 together with the experimental results of ring-on-ring disc tests.

3.2.2 Uniaxial Compression

Stanley Analysis of Failure

It is well known that brittle materials are often used as a structural material in compression, rather than in tension, since tension can give rise to catastrophic failure. The Weibull analysis has been extended by Stanley et al. [173] to brittle materials subjected to uniaxial compression by defining a step function:

$H(\sigma) = 1$ For positive (tensile) values of σ.

$= -\alpha$ For negative (compressive) values of σ.

where α is the ratio of compressive to tensile strength.

$$P_f = 1-\exp\left[-\Gamma \left(1+\frac{1}{m}\right)^m \left(\frac{1}{\bar{\sigma}_{fv}}\right) \frac{V}{v} \left(\frac{\sigma}{H(\sigma)}\right)^m \right]$$

where Γ is the gamma function

m is the Weibull modulus

$\bar{\sigma}_{fv}$ is the mean tensile failure stress of unit volume of the material

V is the component volume

v is the unit volume

Using values of m = 6.6723, $\bar{\sigma}_{nom}$ = 5.5338 MPa, the probability of failure of a uniaxial compression test was obtained from Appendix B.

$$P_f = 1 - \exp[-1.4899 \times 10^{-6} \ \sigma^{6.6723}]$$

Fig. 3.12 plots the above equation with the experimental data from the uniaxial compression tests of section 4.7.

3.2.3 Tension-Compression

Stanley et al. [171,173,176] have developed an equation to cover the case of a component subjected to non-uniform multiaxial stresses, which may include compressive stresses.

$$P_f = 1 - \exp\left[-\left(\frac{1}{m}! \right) \left(\frac{\sigma_{nom}}{\bar{\sigma}_{fv}} \right)^m \frac{V}{v} \Sigma(V) \right]$$

where

$$\Sigma(V) = \frac{1}{V}\int_V \left(\frac{\sigma_{eq}}{\sigma_{nom}} \right)^m dV = \frac{1}{v} \int_V \left[\left(\frac{\sigma_1}{\sigma_{nom} H(\sigma_1)} \right)^K \left(\frac{\sigma_2}{\sigma_{nom} H(\sigma_1)} \right)^K \right]^{m/K} dV$$

m is the Weibull modulus

σ_{nom} is a nominal stress

$\bar{\sigma}_{fv}$ is the mean tensile fracture stress of unit volume of the material (i.e., the unit tensile strength)

V is the volume of the component

v is the unit volume

$\Sigma(V)$ is the stress integral

σ_{eq} is the equivalent stress

$\sigma_1, \sigma_2, \sigma_3$ are the principal stresses

An alternative assumption is that fracture always indicates on the surface of the component. This assumption leads to an equation of the form:

$$P_f = 1 - \exp\left[-\left(\frac{1}{m}!\right)^m \left(\frac{\sigma_{nom}}{\bar{\sigma}_{fa}}\right)^m \frac{A}{a}\Sigma(A)\right]$$

where

$$\Sigma(A) = \frac{1}{A}\int_A \left[\left(\frac{\sigma_1}{\sigma_{nom}H(\sigma_1)}\right)^K + \left(\frac{\sigma_2}{\sigma_{nom}H\sigma_2)}\right)^K\right]^{m/K} dA$$

A is the surface of the component

$\bar{\sigma}_{fa}$ is the mean tensile fracture stress of unit surface area of the material

Finite element stress calculations were performed using the PAFEC computing package (see section 4.6). Stress and model geometry data were stored in output files for subsequent stress integral calculations. A post-processing computer code was developed and employed to access the stored finite element results on an, element by element, basis. To improve the accuracy of the stress integral calculation, the integration was actually performed over the integration points of the model elements.

The Brazilian disc test was selected for evaluating the accuracy of the failure prediction methodology described above. To determine specimen failure probabilities using the Stanley model, different parameters are required. These parameters were computed in Appendices C and D.

The probability of failure assuming volume flaws can be expressed as:

$$P_f = 1.0 - \exp\left[-1.035\ \sigma_{nom}^{6.6723}\right]$$

For surface-distributed flaws

$$P_f = 1-\exp\left[-4.906 \times 10^{-4}\ \sigma_{nom}^{6.6723}\right]$$

Both equations are plotted in Fig. 3.13 together with the results of section 4.6.4. There is a substantial discrepancy between predicted results and experimental data.

3.3 EVALUATION OF WEIBULL PARAMETERS

It has been found that the distribution function that best describes the test results is that due to Weibull, as mentioned in Chapter Two.

If flaws are volume distributed, the Weibull probability of failure equation can be written:

$$P_f = 1-\exp\left[-V\left(\frac{\sigma-\sigma_u}{\sigma_o}\right)^m\right]$$

where V : volume of the structure under stress σ

σ_u : the threshold stress below which the probability of failure is zero

σ_o : a distribution parameter with unit of (stress) (volume)$^{1/m}$

m : the Weibull modulus

For simplification and a conservative design approach [177] the value of σ_u will be assumed to be zero.

From the experimental point-of-view, two important questions were raised. The first concerns the number of samples which is required for an accurate determination of the Weibull parameters. The second is how to estimate m and σ_o for a material, given a set of failure strengths for nominally identical specimens.

3.3.1 Sample Size

It is well-known that the fracture stress of brittle materials shows a large variability. In order to obtain reliable information for structural purposes it is necessary to test more specimens than for ductile materials. The decision on the number of specimens used involves time and expense. Taking into consideration the ease of calculation of the parameters, specimen preparation as well as studies dealing with sample size [99,177-180], a sample size of at least 30 is chosen to be sufficient in obtaining both failure strengths and Weibull parameters.

3.3.2 Weibull Paramater Estimation

Flexure tests are often used to determine the material properties of brittle materials. They are commonly used in place of the preferred uniaxial tensile test because of the great difficulty involved in aligning specimens for tensile tests. The type of flexure test most often used is four-point bending (Fig. 3.14).

The basic Weibull equation describing the probability of failure, P_f, as a function of fracture stress, σ_f, is:

$$P_f = 1-\exp\left[-V.K_v . \left(\frac{\sigma_f}{\sigma_o} \right)^m \right]$$

where K_v is a loading factor derived in Appendix E.

$$K_v = \frac{m + 3}{6(m+1)^2}$$

Taking the natural logarithm of the inverse of both sides of the Weibull equation twice gives,

$$\mathrm{LnLn}\left(\frac{1}{1-P_f}\right) = m\,\mathrm{Ln}\,\sigma_f + \mathrm{Ln}\,K_v.V - m\mathrm{Ln}\sigma_o$$

It can be seen that a plot of the distribution function will be linear in a system of rectangular coordinates in which $LnLn(1/1-P_f)$ is the ordinate and Ln σ_f the abscissa. In addition, m and $LnK_{V.}V-mLn\sigma_o$ will be the slope and intercept of the distribution function in those coordinates, respectively.

To fit this equation, the strength observations (values of failure stresses) are ranked in increasing order. The failure probability P_f^j associated with the jth strength observation in a sample of N specimens is defined as the mean value or mean rank

$$P_f^j = \frac{j}{N+1}$$

Another value which was commonly used is the median value or median rank [181]. An approximation to the median rank value is given by:

$$P_f^j = \frac{j-0.3}{N+0.4}$$

The mean value is used because the mean is commonly taken as the representative value of a sample from a distribution. However, in highly skewed distributions, the median may be a better descriptor [182].

To facilitate the evaluation of $LnLn\ (1/1-P_f)$, a computer code was written to generate both mean and median ranks for any sample of N specimens.

Several methods of estimating m have been proposed [183]. They include the least squares procedures and the method of maximum likelihood.

3.3.3 The Least-Squares Procedures

The model for obtaining the estimates is:

$$Ln[-Ln(1-P_f)] = m\ Ln\ \sigma_f + Ln\ K_{V.}V - m\ Ln\ \sigma_o$$

If m and σ_o were chosen to minimize

$$\Sigma \{Ln [-Ln(1-P_f)]-[m Ln \sigma_f + Ln K_{V.} V-m Ln \sigma_o] \}^2$$

then the slope m and intercept $Ln K_{V.} V - m Ln \sigma_o$ can be obtained. This was done for the four-point bending tests using the routine G02 CAF of the NAG Library [184]. Table 3.2 lists results of the analysis of 50 fracture stresses of four-point beam bend tests.

TABLE 3.2 LEAST-SQUARES ESTIMATES OF WEIBULL PARAMETERS

	MEAN RANK	MEDIAN RANK
m	6.4266	6.6723
$LnK_{V.} V-mLn\sigma_o$	-11.4445	-11.8735
σ_o	0.5977	0.6461

3.3.4 The Method of Maximum Likelihood

The likelihood function [185] for the two-parameters Weibull distribution is:

$$L(\sigma_1,\ldots,\sigma_n;m,\sigma_o) = \sum_{i=1}^{N} \frac{m}{\sigma_o} \left(\frac{\sigma_i}{\sigma_o}\right)^{m-1} \exp\left[-\left(\frac{\sigma_i}{\sigma_o}\right)^{m}\right]$$

where σ_i : fracture stress

N : sample size

Differentiating L with respect to σ_o and m in turn and equating to zero

$$\frac{\partial L}{\partial \sigma_o} = \left(\frac{m}{\sigma_o}\right) \left[-N + \sum_{i=1}^{N}\left(\frac{\sigma_i}{\sigma_o}\right)^{m}\right] = 0$$

$$\frac{\partial L}{\partial m} = \left(\frac{1}{\beta}\right) \left[N + \sum_{i=1}^{N} Ln\left(\frac{\sigma_i}{\sigma_o}\right)^{m} - \left(\frac{\sigma_i}{\sigma_o}\right)^{m} Ln\left(\frac{\sigma_i}{\sigma_o}\right)\right] = 0$$

On eliminating σ_o between these two equations we obtain

$$\frac{\Sigma\ \sigma_i^{\,m}\ \mathrm{Ln}\ \sigma_i}{\Sigma\ \sigma_i^{\,m}} - \frac{1}{m} - \frac{\Sigma\ \mathrm{Ln}\ \sigma_i}{N} = 0$$

which may now be solved for an estimate of m, using a Newton-Raphson procedure:

$$\hat{m} = \frac{N \sum_{i=1}^{N} \sigma_i^{\,m}}{N \sum_{i=1}^{N} \sigma_i^{\,m}\ \mathrm{Ln}\ \sigma_i - \sum_{i=1}^{N} \sigma_i^{\,m} \sum_{i=1}^{N} \mathrm{Ln}\ \sigma_i}$$

Having estimated m, σ_o is estimated by

$$\hat{\sigma}_o = \left(\frac{\sum_{i=1}^{N} \sigma_i^{\,m}}{N} \right)^{1/m}$$

3.3.5 Comparison Between the two methods

The Weibull parameter estimation is illustrated for a data set of 25 observations which was generated from the Weibull distribution with m=2 and $\sigma_o^{\,m} = 4$.

4.1505	1.6173	0.6461	3.0466	1.3545
1.8889	1.0509	0.6288	1.3592	3.0530
0.7500	1.7708	0.5903	1.9310	1.8889
0.7705	1.7172	1.5319	1.5700	0.3761
1.3162	1.6560	1.7961	1.8802	1.8487

Both the Least-squares and Maximum Likelihood methods are applicable. These parameter estimations are compared with their theoretical counterparts in Table 3.3 and provide some indication as to the accuracy of the methods used.

TABLE 3.3 COMPARISON OF WEIBULL PARAMETERS OBTAINED BY THE LEAST-SQUARES AND MAXIMUM LIKELIHOOD METHODS

PARAMETER	EXACT	LS-ESTIMATION	ML-ESTIMATION
m	2	2.0555	2.0351
σ_o	2	1.8281	1.8194
σ_o^m	4	3.4556	3.3820

3.3.6 Simulation Method

Another method for estimation of Weibull parameters is simulation using direct Monte-Carlo methods. Monte-Carlo methods comprise that part of experimental mathematics concerned with experiments on random numbers.

With probabilistic problems, the simplest Monte-Carlo approach is to observe random numbers, selected in such a way that they directly simulate the physical random processes of the problem at hand, and to deduce the required solution from the behaviour of these numbers.

The two-parameters Weibull distribution can be written in the form [186]:

$$P_f = 1-\exp\left\{ -\left[\Gamma\left(1+\frac{1}{m}\right) \left(\frac{\sigma}{\bar{\sigma}}\right) \right]^m \right\}$$

where Γ is the gamma function

m is the Weibull modulus

σ is the failure stress

$\bar{\sigma}$ is the mean strength

As the gamma function is constant, this equation can be expressed in a simpler form:

$$\sigma = \left[\text{Ln} \left(\frac{1}{1-P_f} \right) \right]^{1/m}$$

on putting $\bar{\sigma} = \Gamma \left(1 + \frac{1}{m} \right)$

Random samples, $\sigma_1, \sigma_2, \ldots, \sigma_n$, were then generated and ranked in ascending order. The m estimate is computed by using the least-squares method. Random sample of sizes n=10,20,30,40 and 50 were simulated, and for each n, KMAX = 1000,2000,3000,4000 samples were generated from a population in which $m_o = 7$. Only small variation in the Weibull modulus and variance was observed for the range of KMAX values considered. Hence, it was deemed unnecessary to carry out calculations for higher values of KMAX. The following plotting positions [177,182,186] were used:

$$P_f = \frac{j}{N+1}$$

$$P_f = \frac{j-1/2}{N}$$

$$P_f = \frac{j-0.3}{N+0.4}$$

$$P_f = \frac{j-3/8}{N+1/4}$$

The RND function of the VAX computer was used in the simulation procedure to generate uniformly distributed random numbers. In addition, the RANDOMIZE statement was used to change the starting condition and generate a truly random number [187].

The Weibull modulus and the variance for each estimator were estimated. A flow chart for the simulation is shown in Fig. 3.15.

The performance of least-squares analysis for the Weibull modulus m was compared with the results of Bain and Antle [188], Thoman et al. [189], Jayatilaka [186], Jeryan [178], and Cohen and Whitten [183] in Tables 3.4-3.6 where appropriate. These tables show the mean calculated values of m/m_o employing the different methods of estimating the Weibull modulus. The value of m is the average of $\bar{m}$ at several consecutive KMAX values while m_o was chosen arbitrarily. For an unbiased estimator the mean value should be close to 1. The results of the first two plotting positions of Table 3.6 agree closely with those reported by Jayatilaka [186] and those of the last two plotting positions are close to the results of Jeryan [178] in Table 3.4.

The variance of the Weibull modulus was derived as a function of sample size from statistical theory [179] as

$$s^2 \simeq \frac{m_i^2}{N}$$

Where N is the number of samples.

The coefficient of variance is given by:

$$C.V. = \frac{s}{\bar{m}} = \frac{\sqrt{\frac{m_i^2}{N}}}{\bar{m}}$$

where $\bar{m}$ is the mean of m_o at a particular n and KMAX.

Fig. 3.16 shows the dependency of Weibull modulus m on sample size where the coefficient of variation is defined as the standard deviation divided by the mean value of the parameters. The standard deviation is the square root of the variance [190]. There is a good agreement between the Monte Carlo technique and the equation derived from statistical theory. From this result, the choice of sample size of 50 specimens for each test of Chapter Four should give an acceptable degree of reproducibility.

The difference between four plotting positions was better described by plotting $\Delta m/m_o$ versus sample size where $\Delta m = |\bar{m} - m_o|$. It can be seen from Fig. 3.17 that the anomalous behaviour of the last

two plotting positions at small sample size makes the second one the best in the determination of the statistical reproducibility of the Weibull modulus. The same conclusion can be reached from examining Table 3.6 in which the second plotting position gives the smallest bias.

TABLE 3.6 COMPARISONS OF MEAN (m/m_o) FOR ESTIMATION OF WEIBULL MODULUS

n \ P_f	$\frac{j}{N+1}$	$\frac{j-1/2}{N}$	$\frac{j-0.3}{N+0.4}$	$\frac{j-3/8}{N+1/4}$
10	0.866	1.057	0.969	1.001
20	0.894	1.020	0.959	0.978
30	0.905	1.010	0.960	0.976
40	0.922	1.003	0.968	0.980
50	0.931	0.999	0.973	0.979
100	0.953	0.999	0.976	0.987

3.4 SUMMARY

None of the classical theories appears to fit the experimental data, particularly in the tension-compression quadrant. The reason lies in the fact that they ignored the shapes of existing defects and the contribution of each stress component in a stress state.

A recent empirical theory proposed by Stanley and Sivill [171] has been shown to fit the experimental data quite well. Furthermore, only with this theory can the tension cut-off in the tension-compression quadrant be explained.

An alternative approach is to consider separately each stress state. Two plaster configurations were experimentally tested, and the resulting failure distributions were compared with calculated

TABLE 3.4 COMPARISONS OF MEAN (m/m_o) FOR ESTIMATION OF WEIBULL MODULUS

n	JAYATILAKA [180]				BAIN & ANTLE [182]			THOMAN ET AL. [183]		JERYAN [178]		
	LS(*)	LS(+)	MLE	ME	ESTIMATOR I	GUMBEL	MILLER & FREUND	MENON	MLE	MLE	PLE	ME
10	0.867	1.055	1.165	1.102	1.00	1.04	0.85	0.78	0.859	0.997	0.961	1.116
20	0.894	1.019	1.078	1.049	1.04	1.06	0.93	0.88	0.931	1.004	0.961	1.060
30	0.910	1.008	1.048	1.031	1.05	1.07	0.96	0.92	0.955			
40	0.920	1.002	1.035	1.021					0.966			
50	0.924	0.996	1.025	1.014					0.973			

LS(*) : $P_f = j/1+N$

LS(+) : $P_f = j-0.5/N$

LS : Least-Squares Estimator

MLE : Maximum Likelihood Estimator

ME : Moment Estimator

PLE : Pseudo-Least-Squares Estimator

TABLE 3.5 COMPARISONS OF MEAN (m/m_o) FOR ESTIMATION OF WEIBULL MODULUS

n	COHEN & WHITTEN [183]									
	ME	MME-I	MME-II	MME-III	MLE	MLE-I	MLE-II	MLE-III	MLE-IV	MLE-V
10	1.976	1.333	1.333	1.791	N.A.	1.222	1.232	1.114	1.006	1.042

ME : Moment Estimator

MME : Modified Moment Estimator

MLE : Maximum Likelihood Estimator

better results have been obtained by using Matsuo's equation [153]. Compared with other theories, these methods have been found to lead to a more accurate prediction because the shear stresses have been taken into account. The Brazilian disc test represented the tension-compression quadrant. Because analytical predictions of the failure characteristics of the test specimens could only be obtained with difficulty or were sometimes impossible for this quadrant, the numerical approach is an alternative. Stanley's model [171] deduced from the Principle of Independent Action has predicted the data conservatively.

Finally, different methods for evaluating the Weibull parameters were assessed. The present results showed that the least-squares method procedure is adequate in obtaining these parameters. It can be seen in Fig. 4.12 that there is a good correspondence between the experimental data and the two-parameter Weibull curve. Additional simulation has been used to gain more confidence in choosing experimental data ranking. The ranking is not an important factor as long as the number of tests is greater than 30 in any one investigation.

CHAPTER FOUR

EXPERIMENTAL WORK

The objective of this chapter is to develop the engineering knowledge necessary to describe the mechanical behaviour of brittle materials.

For ductile materials, such as most metals, the mean strength (yield or fracture) may be used reliably in the design of engineering structures. The strength of a brittle material, on the other hand is sensitive to local stress concentrations, i.e., flaw, voids, microcracks or inclusions. As a result, the fracture of a brittle material was found to be affected by size and state of stress to which it was subjected.

Two main steps have been taken in these attempts to obtain the strength of brittle materials:

(1) The selection of a material suitable for investigation.

(2) The planning of experiments.

4.1 SELECTION OF MATERIAL

4.1.1 Plaster as a Modelling Material

The material used in this investigation is Herculite LX plaster, which is manufactured by the British Gypsum Limited in Nottingham. This is a strong plaster designed for use when light strength, surface hardness, and accurate dimensions are essential: i.e., copy milling, checking fixtures, precision patterns, motor trade tooling, moulds for epoxy resin patterns. It is available in 50Kg sacks and costs about £13.80 for each sack.

The selection of Herculite LX plaster as a modelling material has been considered by recognizing some of the following properties:

(1) The material must be representative of brittle materials.

(2) Reproducibility from specimen to specimen is essential for proper control of the tests.

(3) The ease of fabrication and the cost of the material.

(4) It possesses a reasonably high strength and is therefore easy to handle and test.

4.1.2 Microstructure

The microstructure of hardened gypsum paste affects most of the physical and engineering properties of the material, and in particular its rigidity. The rigidity is due to the skeleton of interlocking crystals, and the strength will depend on:

(1) The size and shape of the component crystals.

(2) The strength of the bond between the crystals.

(3) The possibility that impurities built into the crystals will harden them or predispose them to fracture.

(4) The amount of empty space in the set mass which will in turn be determined by the water content of the mixture.

Therefore the microstructure should be understood, as well as the physical properties of the material. The microstructure of set plasters were examined using scanning electron microscopy.

Samples were prepared by taking a small portion of the specimen after casting and a thin section of the fracture surface of

the strength test specimen. They were then gold plated and examined using the 'Stereo Scan 250 MK3' scanning electron microscope.

Set plaster consists of a mass of fine interlocking needles of $CaSO_4 .\frac{1}{2}H_2 0$. Figs. 4.1 and 4.2 show the microstructure of uniaxial compression and disc specimens which were allowed to fully set. There is a slight difference between the two surfaces shown, resulting from the relative movement occurring between the cast and mould surfaces during extraction. The surface of the uniaxial compresion specimen was flattened because the specimens were pushed along the mould surface during extraction (Fig. 4.1). For the case of the disc specimens, neither surface suffered from the sliding effect (Fig. 4.2).

The chemical elements of plaster specimens can simultaneously be analysed. This analysis was conducted using the Link System of Energy Dispersive Analysis of X-rays (EDAX) for the presence of major elements Ca and S, and trace elements K and Si. A typical result is shown in Fig. 4.3. The elements Au and Pd were from specimen surface coating.

4.1.3 Properties

Gypsum is a natural hydrated sulphate of calcium ($CaSO_4 .2H_2 0$) [191]. When gypsum is heated to a temperature of about 130°C, it loses a proportion of its water of crystallization and forms the quick setting cement known as Beta hemihydrate or plaster ($CaSO_4 .\frac{1}{2}H_2 0$) [192,193]. When water is added again during processing as building material, a process of recrystallization takes place [194]. This is an isothermic reaction with a maximum temperature rising up to approximately 45°C [195]. The chemical reaction of hydration required 18.6 lb. of water for each 100 lb. of plaster; any excess of water above this makes the mixture more fluid and it eventually evaporates, leaving behind a porous structure. This porosity determines the major physico-mechanical properties such as mechanical strength, thermal conductivity, permeability, etc.

The specification of the present material was based on the data provided by the Industrial Products Division of British Gypsum Limited [196] and was as follows:

	HERCULITE LX
Plaster/water proportions by weight (for pourable mix)	100/40 2.49Kg/litre
Vicat initial set	20-35 mins.
Compressive strength (24 hrs)	17.2 MN/m^2
Compressive strength (dry)	37.2 MN/m^2
Surface hardness (BS1191) Dropping ball penetration)	3.4 mm
Net expansion on setting	0.05%
Yield of set plaster per 50Kg dry plaster	approx. 0.035 m^3

The Young's moduli are also provided [197]. The values relate to dry set plaster.

PLASTER/WATER RATIO (p/w ratio)	YOUNG'S MODULUS (MN/m^2)
100/40	1.38×10^4
100/50	1.10×10^4
100/60	0.83×10^4
100/70	0.69×10^4

The Poisson's ratio is of the order of 0.2 and is little changed for varying p/w ratio. This ratio is very close to that of concrete [198,199].

4.1.4 Casting Preparation

*Mixing Procedures

Successful mixing of industrial plaster requires strict adherence to specific standards and procedures. The improvements in plaster formulations, made in recent years, have resulted in more uniform products, but to obtain the full benefit of these improved products, these procedures must be standardized. Mixing the plaster slurry can be considered the most important step in making the cast [200]. The following information covers the mixing process used in the investigation:

- water purity: organic impurities in mixing water cause variations in setting time. Drinkable water is suitable for mixing plaster slurries [201,202].

- Water temperature: Gypsum has maximum solubility between 70° and 100°F (21° and 37°C). Therefore, crystallization should take place in a uniform temperature environment somewhere in this range. Further, variations in water temperature will produce variations in setting time, which can cause difficulty in the control of the mixing time. Hot and cold water were blended to ensure a constant water temperature between 65° and 80°F (18° and 27°C) [203].

- Plaster to water ratio (p/w ratio) : a plaster/water proportion of 100/66 (1.5Kg/litre) has been found to be suitable in practice. The plaster and water are always weighed carefully for every mix.

- Mixing: mixing the plaster slurry is one of the most important steps in producing plaster casts with maximum strength, hardness and other important properties [202]. Hand mixing is generally acceptable for small batches. However, since optimum physical

properties are in direct relation to energy input in mixing, hand mixing will not result in a plaster slurry with the best of properties [204-206].

A direct drive, propeller-type mixer with a speed of 900 rpm was used (Fig. 4.4). The propeller should be off centre from the bottom, 10-15° from the vertical, and 20-30° from the top diameter of the bucket. This mixer position creates a correct flow pattern of the slurry [207].

Also, the strength of the cast is practically determined by mixing time as it is well known that the strength increases with mixing time. However, the slurry would be too stiff to pour from the bucket if the mixing time is long. A mixing time of 4-5 minutes was found to be suitable for a p/w ratio of 100/66. The details of specimen casting procedure will be discussed in section 4.3.1.

*Drying Plaster Casts

Two methods were used in the drying of the plaster casts, both were aimed at controlling the free moisture content of the casts. The same drying action takes place whether the plaster cast dries in the workroom, outdoors or in a dryer. The use of a forced-hot-air dryer only speeds and controls the drying procedures.

In the first case, the casts were dried in a drying chamber (Fig. 4.5). The main physical limitation in drying a plaster cast is the maximum temperature at which the dryer can operate and not calcine the cast. The recommended temperature is 40-45°C [195,196,201,208-211]. Operating much above this temperature range results in excessive calcination; that is, surfaces of the casts, especially those in front of hot-air ducts, become soft and powdery.

A drying cabinet is specially designed to dry the casts at room temperature in the second case (Fig. 4.5). In both cases, the weight of the cast was carefully checked.

Preliminary tests were carried out to determine the best method of drying the plaster casts. Two sets of beam specimens were prepared, one was placed in air for 24 hours then placed in an oven

provided with air circulation and adequate ventilation for removal of moisture, so that the air may be maintained at a temperature of 104 to 110°F (40 to 43°C) and with a relative humidity not to exceed 50 per cent for 24 hours [196]. The humidity was monitored by using the psychrometer Therm 2246 of Texcel Limited (Hertfordshire) [212]. It was found that the relative weight reduction ratio, which is the ratio of weight reduction after drying for 24 hours over initial weight, was always in the range of 0.200 to 0.250.

Another set of beam specimens was dried in air and the weight of the cast was checked daily. It took about 6 or 7 days until the relative weight reduction ratio of this set was within the limits shown. For both methods of drying, a further increase in drying time did not vary this ratio. The drying process was considered to be completed for both sets.

The strength of the former set was found to be much less than that for the latter. Microscopic examination showed that there were many cracks which appeared on the surface of this set because of the drying process. This method of drying was consequently abandoned. Table 4.1 shows the results from two sets of beam cast under different drying processes and subjected to four point bending.

TABLE 4.1 THE EFFECT OF DRYING PROCESS

NO. OF SPECIMENS	DRYING PROCESS	MEAN STRENGTH (MPa)	STANDARD DEVIATION
21	7 days at room temperature	3.7032	0.6292
35	24 hrs at room temperature then 24 hrs at 40°C	3.3674	0.5706

* Surface Finish

It has been well known in the glass industry that an edge flaw and stress concentration often propagate until they become damaging cracks. Bevelling of the edges and at the same time

producing a smoothed or polished surface would be necessary to ensure a high survival probability. The surface finish has been the subject of practical interest in design with brittle materials [213,214].

The surface finish of plaster casts was measured using the Surface Texture Measuring Instrument Surfcom 300B. This system indicates integrated values of Centerline Average Roughness (Ra) and records in both forms:

(1) An enlarged graph of real profiles, roughness profiles and waviness profiles.

(2) By interfacing to a PET model 4032 computer, a hard copy containing additional information about the measurement of surface finish can be obtained [213,214]. A sample is shown in Table 4.2.

The Average Roughness (Ra) values are given in Table 4.3 together with some expected values from common production processes [213]. The meter cut-off of 0.25 mm and a magnification of 500 were chosen. It can be seen that the plaster casts had a good surface quality.

4.2 PLANNING OF EXPERIMENTS

The main difficulty in testing brittle materials is a wide scatter in results when apparently identical tests are conducted on identical specimens of the same material. The difficulty in relieving residual stresses and the presence of defects from the manufacturing process all contribute to the characteristic high variability in mechanical properties of brittle materials.

At the present time the development of test methods for brittle materials has not reached the stage where completely satisfactory methods can be defined. Hence the approach adopted here is to consult the literature [144,164,186,215,216] and select the test technique on the basis of its relative simplicity, and accept a simple stress distribution within the specimen. Reliance is then placed on accuracy and reliability of the available analyses for converting the measurements into proper data.

TABLE 4.2 A TYPICAL PRINT-OUT FOR MEASUREMENT OF SURFACE ROUGHNESS

SURFACE FINISH PARAMETERS

SPECIMEN - DISK02 DATE - 2411 TIME - 14:46

CUT-OFF - .25 M.M. RANGE- X 500

AVERAGE ROUGHNESS	(RA)	=	1.46	MICRONS
RMS ROUGHNESS	(RQ)	=	1.87	MICRONS
SKEWNESS	(RSK)	=	-.22	
KURTOSIS		=	2.95	
TEN POINT HEIGHT	(RZ)	=	3.68	MICRONS
AV PEAK TO VALLEY HEIGHT	(RTM)	=	3.86	MICRONS
PEAK TO VALLEY HEIGHT	(RT)	=	14.28	MICRONS
AVERAGE ROUGHNESS DEPTH	(R3Z)	=	3.39	MICRONS
PEAK HEIGHT	(RP)	=	2.1	MICRONS
AVERAGE WAVELENGTH	(LA)	=	78.4	MICRONS
HIGH SPOT COUNT	(HSC)	=	14.15	PER M.M.
MEAN SLOPE		=	6.78	DEGREES
MEAN HIGH SPOT SPACING	(SM)	=	80.1	MICRONS
MEAN PEAK RADIUS OF CURVATURE		=	35.4	MICRONS
MEAN VALLEY RADIUS OR CURVATURE		=	-42.23	MICRONS

TABLE 4.3 THE AVERAGE ROUGHNESS PRODUCED BY PLASTER CAST AND COMMON PROCESSES

PROCESS		AVERAGE ROUGHNESS Ra(μm)
PLASTER CAST*	DISC	1.2 (Plate surface)≠ 2.3 (Mould surface)≠
	BEAM	1.6 (Plate surface)≠ 2.2 (Mould surface)≠
	HOLLOW CYLINDER	2.0 (Outer surface) 1.8 (Inner surface)
	SOLID CYLINDER	2.6 (Wall surface, as cast) 2.8 (Wall surface, turning) 2.5 (End, surfacing)
GRINDING		0.6 - 1.6
TURNING		0.4 - 6.3
BORING		0.4 - 6.3
MILLING		0.8 - 6.3

* Each value is an average of at least ten measurements

≠ Plate surface is the surface of the specimen which is facing the separating plate between two moulds during casting. While the mould surface is the surface of the specimen facing the bottom of the mould.

There have been two types of tests made in the attempts to obtain information on brittle materials. The first type are strength tests. The closest practical approximation to uniaxial testing is obtained in bend tests, cylinder burst tests and compression tests.

Biaxial stress fields are produced by testing the ring-on-ring disc test and the Brazilian disc test. Fig. 4.6 shows the allocation of tests before the testing was performed.

The second type of test is the fracture mechanics test. To use the fracture mechanics analysis effectively, it is necessary to adopt a reliable procedure for introducing sharp precracks into specimens. The notch-beam technique was used to determine the toughness.

4.3 FOUR-POINT BEAM BEND TEST

4.3.1 Introduction

Because of its simplicity, the tensile strength of ductile materials is measured by uniaxial tensile testing. However, it is extremely difficult to perform a satisfactory tensile test on a brittle material [99,213,217,226]. Gripping a brittle test piece in jaws, or using a screw thread or other clamping device leads to such stress concentration that failure is most likely at the grip, possibly before the test proper is under way. Furthermore, a slight misalignment of the axial load produces premature failure at the loading grip.

A simple method for overcoming these difficulties is the use of flexure tests. The majority of strength data for various ceramic heat exchangers [227], adiabatic engines [228,229], and ceramic turbine programs [230-232] have been obtained by modulus of rupture (or flexure) tests in which simple shapes are subjected to three or four-point bending until fracture occurs. While the solutions for fibre stresses and elastic behaviour are more complicated than the simple tensile method, the relative ease in producing specimens and conducting the tests have made the bend tests extremely popular with both material researchers and product developers [229]. The simplest configuration is in three-point bending but four-point bending gives a uniform stress field on the surface within the inner rollers. Also, the shear stresses for the three-point bending are developed over the full span, thus deviating from the ideally uniaxial stress state present in the four-point bending. A further term in use is third-point bending [186] which refers to the case where the distance

between adjacent support and loading point in four-point bending is one-third of the span between support points. A four-point bend test is shown in Fig. 4.7.

Factors such as load mislocation, twisting of the specimen, friction at the knife edge, local stresses, contact point tangency shift, and specimen surface conditions can introduce errors, for which there are correction factors. In this regard, an overview of the sources of error arising from the method of load application in bending has been given by many reseachers [99,186,233,238].

4.3.2 Experimental Procedures

A four-point bend fixture was designed for the testing of small plaster specimens with a squared cross section of b=d=10 mm. The length of L' is 46 mm and of the outer span L is 138 mm. The design of this fixture incorporates ideas presented in review literature [99,186,233-238]. Corner flaws resulting from chipping or cracking during the extracting operation are sources of low-strength failure [233,239]. Strength results obtained from edge-dominated failure would not be representative of the material as a whole and their use could lead to serious error in predictions of the failure probabilities for engineering components subject to complex stress states.

Series of tests on both bevelled and unbevelled squared-section beams have been performed. The difference between the two sets is that the former set has its four corners bevelled with c=0.1 mm, as depicted in Fig. 4.7. The data of the two sets are shown in Table 4.4 and there is a difference in strength for the two types of specimens. These results show the importance of edge-dominated failure.

TABLE 4.4 4-POINT BEAM BEND TEST RESULTS FOR BEVELLED AND UNBEVELLED SPECIMENS

	Number of Specimens	Mean Strength (MPa)	Standard Deviation (MPa)
Unbevelled	50	4.2349	0.8086
Bevelled	50	5.53338	0.9460

The beam specimens were cast with a mould as shown in Fig. 4.8. Important aspects of the mould design include:

(i) A controlled, constant rate of mould filling was achieved by using a specially designed pouring basin.

(ii) Bottom feeding to the beam moulds was used to avoid agitation and to allow steady filling.

(iii) Plasticine and rubber bands were used to seal and hold together the mould assembly while the plaster was setting.

(iv) The test specimens were cast in a vertical position to ensure that rising air bubbles would not be trapped on principal surfaces thus impairing the surface finish.

Various plaster/water ratios were considered in order to observe the effects on the cast specimens. It was found that a plaster/water ratio of 100/66 was ideal for obtaining a maximum number of perfect specimens from one cast.

Once the beams had been produced they were left for a short time before they were extracted from the mould using an extraction device shown in Fig. 4.9. This modified lathe slide allowed both the extraction of the beam and disc specimens.

The number of defective specimens were in the range of 8-10 per cast. The perfect castings were left in the drying cabinet for seven days to allow the plaster to dry and harden.

They were bevelled and tested using the four-point bend fixture shown in Fig. 4.10. Although this figure does not show the configuration usually used in a four-point bend test and is perhaps nearer to a value of 20 mm for the parameter L'. When the beam was in place, water was allowed to drain into the bottom container and hence loaded the beam. When fracture occurred the flow of water was stopped and the bottom container was weighed.

Examples of perfect, flawed, and fractured specimens obtained from this test are shown in Fig. 4.11. From the weight of the water it was then possible to calculate the mean fracture load.

4.3.3 Stress Distribution

The extreme fibre stresses at failure were calculated from the usual equation for maximum bending stress (Fig. 4.7), σ_f:

$$\sigma_f = \frac{3PL'}{bd^2}$$

where P is the total applied load at failure.

L' is the distance from the end of the bar to the load application points.

b is the width of specimen.

d is the depth of specimen.

4.3.4 Results and Discussion

The tests were performed in a dry environment, with short loading times, to minimize the influence of slow crack growth. Fig. 4.12 shows a plot of failure probabilities, i.e., $\text{LnLn}(1/1-P_f)$ versus stresss σ, where P_f was defined by both mean ranking:

$$P_f = \frac{j}{n+1}$$

and median ranking

$$P_f = \frac{j-0.3}{N-0.4}$$

where j is the ranking number of a specimen in a sample size N in increasing order of fracture stress, σ.

From data of section 3.2.2 of Chapter 3, the Weibull modulus and the scale parameter are calculated as 6.6723 and 0.6461, respectively.

Fig. 4.13 shows an example of the fracture surface obtained from four-point beam bending. The fracture feature that may be clearly observed is the concave crack front profile which shows the approximate origin of the crack from inside. The fracture origin is indicated by the arrow in the figure. Note also that the microstructure had a dual pore distribution, with small pores ($\bar{r}$=100-120 μm) and large pores ($\bar{r}$=200-300 μm). The large pores are roughly spherical and can result from air entrapment during casting. The small pores are capillary ones.

Scanning electron micrographs of specimen surfaces after casting (Figs. 4.1 and 4.2) and the fracture surface (Fig. 4.14) gave evidence supporting the uniformity in plaster casting with different moulds.

The fractographic examination for the origin of the cracks seems to show that fracture is caused by the pores in the bulk of the material on some specimens. The importance of edge dominated failure has also been shown. From these observations it can be seen that failure can be caused either by edge cracks or by volume flaws.

Microscopic examination of the contact areas of specimens with both loading and support rollers showed no evidence of the effect of contact stresses.

4.4 CYLINDER BURST TESTS

4.4.1 Introduction

As mentioned in section 4.3.1, parasitic tensile stresses due to the gripping jaws and to specimen misalignment are not relaxed and can be of sufficient magnitude to distort seriously the form of the measured strength distribution. The expanded cylinder or cylinder burst test was developed by Sedlacek and Halden [218] to overcome these difficulties with regard to strength measurements in ceramics. Another advantage of this method is that, since tensile stress is applied to all parts of the specimen, a larger effective volume can be tested than with bend tests.

Some information obtained from burst tests of brittle materials is summarized in Table 4.5.

4.4.2 Experimental Procedures

From the above information a suitable apparatus can be designed and built. Fig. 4.15 shows the arrangement of the cylinder burst test unit. Fig. 4.16 shows the specimen holder which consists of two annular steel plates. Hydraulic pressure is applied radially to the cylinder from the inside through a flexible rubber cylinder which is sealed by a conical plug at the upper end. Another conical plug in the lower steel plate seals the lower end and provides entrance for the air. Spacer blocks are provided to separate the steel plates, to prevent extrusion of the rubber cylinder between the specimen and the fixture, and finally to maintain the cavity alignment.

Bursting pressure is recorded by monitoring the hydraulic pressure of the two gauges. One is on the pump, the other is a changeable test gauge.

TABLE 4.5 SUMMARY OF CYLINDER BURST TESTS

SPECIMEN DIMENSIONS	MATERIAL	RESULTS	REFERENCES
O.D.55.88 mm I.D.50.80 ht. 6.35 12.70 25.40	Acrylic Plastic Alumina (97.6% Al_2O_3)	Mean tensile burst strength is two times smaller than the mean bend strength	[218]
O.D.27.90 I.D.25.40 ht. 7.60	HPSN	Mean tensile burst strengths are up to ~ 2.3 times smaller than the mean bend strengths	[221]
O.D.28.45 I.D.25.40 ht. 12.70	CVDSiC		
O.D.30.50 I.D.25.40 ht. 7.60	RBSN		
O.D.50.80 I.D.48.26 ht. 12.70	Tungsten Carbide (16%CO,84% WC)	The fracture strength in the disc compression test (Indirect Tensile test) is higher than the tensile burst strength	[240]
O.D.37.00 I.D.31.60 ht. 7.80	Sintered Silicon Nitride	Mean tensile burst strengths are 1.4 to 2.5 times smaller than the mean bend strengths	[241]
O.D.398.78 I.D.379.73 ht. 19.05	Slip Cast Fused Silica (SCFS)	The mean tensile burst strength (4.145 KSI) is smaller than the mean bend strength (6.952 KSI)	[242]

A mould for casting the cylinder is shown in Fig. 4.17. When the plaster began to set in the mould, the cores were turned slightly with a special tool to prevent the specimens sticking to the mould wall. The mould was inverted and supported by pillars from an extraction table. The plaster specimens were then pushed out by a press as shown

in Fig. 4.18, and left drying out in the cabinet for two days. This is the time required for the relative weight reduction ratio (see section 4.1.4) of the cylinder to be in the range 0.200 to 0.250. Fig. 4.19 shows a special device which was used for preparing the specimen by cutting and then sanding the cut faces flat and parallel, to the required dimensions.

Fig. 4.20 shows three types of plaster specimens, specimens as cast with defects are shown on the left, specimens as cast without defects are in the centre and the prepared specimens are on the right. The measured dimensions of the specimen were within $\pm$0.1 mm of the nominal dimensions for all casts (Fig. 4.21).

4.4.3 Stress Distribution

Data from the burst tests were analyzed using the elastic theory of thick-walled cylinders [243]. This theory indicates that the stresses at the inside surface are higher than those at the outside surface. According to this theory, the circumferential stress σ_θ, in the specimen is of the form:

$$\sigma_\theta = \frac{R_i^2\ p}{R_o^2 - R_i^2}\left(1 + \frac{R_o^2}{R^2}\right)$$

where R_i is the radius of the inside surface

R_o is the radius of the outside surface

p is the internal pressure

R is the radius at which the stress is being determined.

It can be seen that the circumferential stress at the inside surface, σ_θ, is (when $R=R_i$):

$$\sigma_\theta = \left(\frac{R_o^2 + R_i^2}{R_o^2 - R_i^2}\right)p$$

4.4.4 Results and Discussion

The burst test results are shown in Fig. 4.22. The results can be seen to follow a relatively smooth curve with either no outliers or very few as shown in the figure. The type of test and the geometry of the specimen probably contribute to this situation.

Fractographic examination was performed on all specimens. The cylinders exhibited a noteworthy behaviour when subjected to the burst test. Forty-six cylinders fractured into numerous fragments which made it impossible to identify the primary failure site. However, fifteen cylinders generally ruptured into only a few fragments, as shown in Fig. 4.20. Optical examination indicated that fracture was invariably initiated at bulk sites in these specimens.

The standard deviation which is a useful descriptor of the dispersion or spread of a sample of data was calculated for both four-point beam bend and cylinder burst tests. Table 4.6 shows the calculations for the two tests. Thus the standard deviation of the former test is greater than that of the latter. This indicates that the cylinder burst test method is well-suited to tensile strength determination of brittle materials.

TABLE 4.6 RESULTS OF 4-POINT BEAM BEND TESTS AND CYLINDER BURST TESTS

TEST METHOD	NUMBER OF SPECIMENS	MEAN STRENGTH (MPa)	STANDARD DEVIATION (MPa)
4-point beam bend test	50	5.5338	0.9460
cylinder burst test	46	4.6693	0.5436

After fracture, the fracture surface was gold coated and examined. As shown photographically in Fig. 4.23, a similar

microstructure of set plaster was obtained. Fig. 4.24 of the same surface shows the dual pore distribution. The inside of a capillary pore was also shown in Fig. 4.23.

Because of the dual pore distribution and because there could be other potential sources of inaccuracy in this test related to frictional forces and the development of parasitic stresses, the experimental results were used only as supplementary data for the four-point bend tests.

4.5 RING-ON-RING TESTS

4.5.1 Introduction

Uniaxial strength tests, such as three-or four-point bending tests, have been used extensively in the past to determine ceramic strength. On one hand, they are low cost test methods in terms of complexity of test technique, but on the other hand they have a significant disadvantage in that it is very difficult to eliminate undesirable edge failure [244-247]. Furthermore, these flexure tests may provide only a partial characterization of load-bearing capacity since service applications of brittle materials generally involve multi-axial loads.

The biaxial flexure test is becoming increasingly popular as a means of measuring the strength of glass [248-251] and ceramic materials [245,246,252-258]. This is due to the fact that the measured strength is free from edge condition and a relatively large area of the specimen is subjected to a uniform stress.

4.5.2 Experimental Procedures

The ring-on-ring test is based on an existing loading method which has been of considerable use in flexural strength testing of brittle materials [171,126,259,260]. The test fixture consists of a loading ball, alignment pillars (Fig. 4.43), and a load cell.

The test involves the creation of a state of uniform axisymmetric tension stress in the central portion of one of the faces

of a circular plate. This can be accomplished by placing the plate on a circular ring and by applying on its upper surface a load transmitted through a circular ring concentric with, and having a smaller diameter than, the support ring. The three guide pillars, integral with the lower ring, ensure this concentricity. The loading ball has only three short line contacts with the inserts to minimize friction.

Force plate design

A strain gauged load cell was designed to measure the applied load. The supported top plate consisted of a circular plate of 11 mm thickness. This plate was supported by three cantilever blocks. The top plate rested on rounded steel supports, machined hemispherically at one end, and screwed to the cantilever blocks. The cantilever support beams (machined from a single billet of high tensile steel alloy) were mounted to a steel base plate which was 240 mm square and 11 mm thick.

For force and weight measurements below 227 Kgs, the bending beam design is usually chosen [261].

Instrumentation

The heart of the strain gauged load cell is the three cantilever beams to which the strain gauge Wheatstone bridge network, shown in Fig. 4.25, is bonded. In this design, two strain gauges were attached on top and two directly underneath, near the supported end of the cantilever. They were wired as shown in Fig. 4.26 for each cantilever beam to increase the sensitivity of the measuring system [262].

Following the criteria for foil gauge selection [263], it would appear that the most suitable gauge is one made by Welwyn Strain Measurement Limited of Basingstoke, Hampshire, designated EA-06-250BG-120, and costing £18.49 for a package of five. As the gauge can only perform as well as the installation will permit [264], the associated gauge installation procedure has been followed [265] with M-Bond 200 adhesive and M coat A and C coating.

All experiments used a Strain Gauge Amplifier MK111 S/No. 122 connected to a Fluke 8800A Digital multimeter. The applied force signal was outputted to an attached x-y recorder. The instrumentation is shown in Fig. 4.27. The top plate has been removed to expose the three supporting cantilever beams. The load cell was mounted on the hydraulic testing machine as shown in Fig. 4.28.

Testing and calibration

The weights were measured and then stacked on the platform while the voltage indicated by the voltmeter was recorded. The applied force signal was recorded simultaneously by the x-y recorder for each weight increment. The calibration results are given in Fig. 4.29 for the voltage indicator showing the highly linear nature of the load cell calibration throughout the loading range.

Specimen casting

To produce a large number of discs quickly and efficiently a casting method was used similar to that discussed in section 4.3.2.

The disc mould used the same pouring basin and bottom fixture as was used in the beam mould assembly. This is shown in Fig. 4.30. Using this assembly, it was possible to produce 28 disc specimens in one cast, and of these, approximately 20 were perfect and could be used for either ring-on-ring or diametral testing. The importance of the mould design, as discussed in section 4.3.2, still applies.

Several casts were made in order to obtain enough specimens for use in each test. The same plaster/water ratio as described in section 4.3.2 was used. Once the discs had been made in their moulds they were extracted using small steel pins, and using the modified lathe slide shown in Fig. 4.9. They were then left exposed to air in the drying cabinet for two days. This is the time required for the relative weight reduction ratio (see section 4.3.1) of the disc specimen to be in the range 0.200 to 0.250.

Fig. 4.31 shows samples of the commonly obtained disc castings. On the left are specimens with casting defects. The perfect casts are on the right. The common deffects were either air bubbles on the surface or out-of-circularity of the disc caused by inherent setting effects. The specimens with defects were discarded.

4.5.3 Stress Distribution

In this test a circular plate specimen is supported on a coaxial ring and loaded at the centre with a smaller coaxial ring (Fig. 4.32). Equibiaxial tensile stress is developed on the bottom fibres in the central area of the disc.

The test specimen is a disc, 25 mm diameter and of 4 mm thickness. It is supported on a ring of 20 mm in diameter. Load is applied to the specimen centre by a loading ring of 10 mm in diameter.

For thin, rigid elastic discs, the frictionless bending stresses are given below [259].

If $0 \leq r \leq b$

$$\sigma_r = \sigma_\theta = \frac{3Pz}{2\pi t^3}\left[2(1+\nu)\mathrm{Ln}\frac{a}{b} + \frac{(1-\nu)(a^2 - b^2)}{R^2}\right]$$

If $b \leq r \leq a$

$$\sigma_r = \frac{3Pz}{2\pi t^3}\left[2(1+\nu)\mathrm{Ln}\frac{a}{r} + \frac{(1-\nu)(a^2-b^2)}{R^2} - \frac{(1-\nu)(r^2-b^2)}{r^2}\right]$$

$$\sigma_\theta = \frac{3Pz}{2\pi t^3}\left[2(1+\nu)\mathrm{Ln}\frac{a}{r} + \frac{(1-\nu)(a^2-b^2)}{R^2} + \frac{(1-\nu)(r^2-b^2)}{r^2}\right]$$

where P is applied load

t is disc thickness

a is radius of support ring

b is radius of loading ring

R is radius of the disc

ν is Poisson's ratio.

The uniform maximum stress occurs within the centre region, bounded by the loading ring, and is given by [243,249,253].

$$\sigma = \frac{3P}{4\pi t^2}\left[2(1+\nu)\mathrm{Ln}\frac{a}{b} + \frac{(1-\nu)(a^2-b^2)}{R^2}\right]$$

Two-dimensional finite element analysis of the ring-on-ring test and other tests is considered the valid basis for stress analysis. The finite element programme used was PAFEC which stands for 'Program for Automatic Finite Element Calculations', developed by Pafec Limited of Nottingham. This is a software package with the capability to solve a wide range of engineering problems ranging from static displacement and stress analysis, thermal analysis, dynamic and vibration calculations to non-linear static analysis [266,267].

Two idealizations of the disc bending have been employed. They are shown in Figs. 4.33 and 4.34. Fig. 4.33 shows the first idealization with 64 eight-noded isoparametric curvilinear quadrilateral elements [268]. A fine mesh grid of elements is required for accurate calculations at the location of stress perturbations [269]. By virtue of symmetry only a half specimen need be considered.

Fig. 4.34 shows the second idealization with 63 eight-noded facet shell elements [268]. Since the problem has symmetric geometry, properties, and boundary conditions, only one quarter of the region was utilized. The displaced shapes for both idealizations are shown in Fig. 4.35.

Figs. 4.36 and 4.37 show the stress distribution at the tensile face of the disc of the present finite element analysis with the analytical solution [259] for both idealizations. The second idealization (Fig. 4.37) shows a better agreement with the analytical

solution in the centre region of the disc where the stress state was assumed to be in equibiaxial tension. The stress uncertainty in the region around the support point in the first idealization disappeared in the second one.

Only the stress contours of the first idealization were shown in Figs. 4.38, 4.39, and 4.40. Here it can be seen that the most compressive stresses occur at the loading and support points. The equibiaxial stress state is also revealed. The combined effect of these stresses may be found by calculating the equivalent stress:

$$\sigma_{eq} = 2^{-\frac{1}{2}} [(\sigma_x-\sigma_y)^2 + (\sigma_y-\sigma_z)^2 + (\sigma_z-\sigma_x)^2 + 6\ (\tau_{xy}^2 + \tau_{yz}^2 + \tau_{zx}^2)\ ]^{\frac{1}{2}}$$

Once the stresses have been determined it is possible to predict the failure initiation. The Failure Criterion module enables a failure code to be expressed graphically and in printed output. It is assumed that failure occurs when the maximum principal stress meets the failure criterion:

$$\sigma_1 = \sigma_t$$

where σ_t is the uniaxial tensile strength.

The state of stress at each stressing point in an element is examined. If any of these points indicates a failure then the complete element is assumed to have failed.

The failure is found to start in the vicinity of the loading ring on the tensile face. Thus the code C2 in Fig. 4.41 refers to the failure which has occurred. After initiation of the first crack, the fracture grows rapidly towards the centre of the disc. This is in absolute agreement with the fractographic examination.

4.5.4 Results and Discussion

All biaxial tests were conducted in air at room temperature with a crosshead speed of 5 mm/min., conditions chosen to minimize the effect of slow crack growth on strength. Fig. 4.42 shows the test

results, both mean and median rankings were used. The loading system is shown in Fig. 4.43. Measured strength value is summarized in Table 4.7.

TABLE 4.7 FRACTURED STRENGTH OF RING-ON-RING TESTS

NO. OF TESTS	MEAN STRENGTH (MPa)	STANDARD DEVIATION (MPa)
69	4.9425	0.5997

Fracture surfaces of all specimens were examined microscopically. Each disc specimen apparently had failure initiated within the loading ring. Crack branching was also observed, resulting in the fracture pattern shown in Fig. 4.44. This fracture morphology is similar to that observed in earlier investigations, on different materials, using the biaxial disc tests [245,255,257,270].

The fracture surface of a typical specimen is shown in Figs. 4.45 and 4.46. Fig. 4.45 reveals the dual pore distribution. Fig. 4.46 shows the same fracture surface with crack front profiles on the left side towards the boundary. Crack branching (Fig. 4.44) and crack front profiles (Fig. 4.46) suggest that the fracture origin is initiated from the inside of the specimen.

The present results are consistent with the finite element analysis. The fracture morphology proved that the biaxial strength test described in this section will significantly contribute to the generation of reliable data.

4.6 BRAZILIAN DISC TESTS

4.6.1 Introduction

It was shown in section 4.3.1 that the measurement of the tensile strength of brittle materials, using the conventional tension

test, presents difficulties both in the specimen preparation and in alignment during the test. As an alternative, bending tests are often made because they are comparatively simple to carry out and better suited to field conditions. However, the flexure test may give results considerably in excess of the true tensile strength [271-273] and true uniaxial tensile stressing occurs very rarely in components, hence a large number of less conventional specimens have been proposed for measurement of tensile strength [217,274,277]. One of the most interesting of these is the diametral compression of a solid disc shown in Fig. 4.47 which allows for easier specimen preparation and load application. It was developed independently in Japan by Akazawa and in Brazil by Carneiro and Barcellos [271,278], and is now known as the "splitting tensile", the "indirect tension" or the "Brazilian" disc test. It has been used to measure the tensile strength of concrete [219,272,278-284], rocks [285], coals [286], polymers [287-289], tungsten carbide [122], graphite [273], and ceramics [274,290,291].

4.6.2 Experimental Procedure

A simple design test fixture, as shown in Fig. 4.64, was used in the Brazilian disc tests. The discs were compressed between two identical anvils which were ground with high accuracy. The top anvil was allowed to move freely in a linear bearing while the lower anvil was fixed in-situ by a 6 mm screw. The base of the fixture was ground to ensure good contact with the testing machine during the test. The ground base surface was used as a reference in boring the locating holes for both the linear bearing and the lower anvil to ensure the alignment of the top and bottom anvils. The end of the top anvil was machined to a spherical shape to minimize the side forces during testing. A 'safety pin' was fitted through the top anvil to prevent it from dropping, after the fracture of the test specimen, and causing damage to the anvils.

Two pairs of loading anvils with different contact profiles were made. One pair was machined with a loading arc of 12.5 mm radius, the other with a 16.0 mm radius.

A vertical block with an adjusting circular disc was used to ensure the positioning of the disc specimen between two anvils.

To produce a large number of disc specimens quickly and efficiently, the same casting method and disc mould which were discussed in sections 4.3.2 and 4.5.2 were used.

4.6.3 Stress Distribution

*Elasticity solution

An elastic analysis of the stresses within a circular disc with concentrated loads on the diameter (Fig. 4.47), gives the following expressions [292]:

$$\sigma_x = \frac{-2P}{\pi t}\left[\frac{(R-y)x^2}{r_1^4} + \frac{(R+y)x^2}{r_2^4} - \frac{1}{D}\right]$$

$$\sigma_y = \frac{-2P}{\pi t}\left[\frac{(R-y)^3}{r_1^4} + \frac{(R+y)^3}{r_2^4} - \frac{1}{D}\right]$$

$$\tau_{xy} = \frac{2P}{\pi t}\left[\frac{(R-y)^2 x}{r_1^4} - \frac{(R+y)^2 x}{r_2^4}\right]$$

where t is the disc thickness

For points on the diameter perpendicular to the loads, the x-axis,

$$y = 0$$

$$r_1 = r_2 = \sqrt{x^2 + R^2}$$

$$\sigma_x = -\frac{2P}{\pi tD}\left[\frac{16D^2x^2}{(D^2+4x^2)^2} - 1\right] = \frac{2P}{\pi tD}\left[\frac{D^2-4x^2}{D^2+4x^2}\right]^2$$

$$\sigma_y = -\frac{2P}{\pi tD}\left[\frac{4D^4}{(D^2+4x^2)^2} - 1\right].$$

$$\tau_{xy} = 0$$

On the y-axis, where

$$x = 0$$

$$r_1 = R-y$$

$$r_2 = R+y$$

$$\sigma_x = \frac{2P}{\pi tD}$$

$$\sigma_y = -\frac{2P}{\pi tD}\left[\frac{2}{D-2y} + \frac{2}{D+2y} - \frac{1}{D}\right]$$

$$\tau_{xy} = 0$$

The stresses at the centre are

$$\sigma_x = \frac{2P}{\pi tD}$$

$$\sigma_y = -\frac{6P}{\pi tD}$$

Therefore, the compressive strength needs to be at least three times the tensile strength in order to ensure a tensile failure.

*Finite Element Analysis

By virtue of symmetry only a simple quadrant of the disc need be considered. Figs. 4.48 and 4.49 show two idealizations which were employed. In Fig. 4.48 there are 63 eight-noded isoparametric curvilinear quadrilateral elements [268] while in Fig. 4.49 there are 6 six-noded isoparametric curvilinear triangular elements and 52 eight-noded isoparametric curvilinear quadrilateral elements. It is found that both idealizations give the same results, hence only results of the former are presented.

The stresses obtained by the finite element method are plotted along both the x and y-axis. It is thus possible to compare the finite element solution with the analytical one when different finite element idealizations are employed. All stress distributions were calculated under constant loads which gave the same net section stress $\sigma_n = 2P/\pi tD$.

Fig. 4.50 shows how the principal stresses vary with x/R position for both the classical theory and finite element solutions. Excellent agreement is obtained between the 63-element solution and the exact solution.

Fig. 4.51 shows the variation of principal stresses along the y-axis. It is seen that the finite element analysis gives a very good agreement up to y/R = 0.8.

The shear stresses along the x and y-axes were also shown in Figs. 4.52 and 4.53, respectively. Again, very good agreement with the analytical solution was obtained.

These results have shown that the Pafec programme has been used successfully to produce reliable data for stress analysis. In practice, however, the applied load is transmitted to the disc through some finite area. Consequently a second run in which the applied load was modified to reflect the finite load distribution is needed. The load is now distributed on an arc of 30 degrees conforming with the experimental results (Fig. 4.54).

The displaced shapes for both cases are shown in Fig. 4.55. It can be seen that the point load causes much more deformation at the loading point than does the distributed load.

A comparison is shown in Figs. 4.56, 4.57, 4.58 and 4.59 of the stress distributions as obtained from the point load and 30-degree arc load. Stresses along the x-axis did not change except in the central region where they are smaller for the arc load case. A similar trend is observed along the y-axis. The principal stresses are also more uniformly distributed. So are the shear stresses.

The maximum principal, minimum principal and equivalent stress distributions are shown in Figs. 4.60 to 4.62 respectively. Notice a high tensile stress is located at the boundary in Fig. 4.60. This explains the additional fracture site which was also observed in the experiments.

With the assumption that the maximum tensile stress is the cause of fracture, the state of stress at each stressing point in an element of the whole disc is examined. It is found in Fig. 4.63 that the fracture starts from the free boundary as well as from the centre of the disc. Thus the code C2 refers to the failures which have occurred.

4.6.4 Results and Discussion

Preliminary tests were performed using smaller pair of anvils (12.5 mm radius) and P.T.F.E. tape placed between the anvils and the disc. Although great care was exercised, local crushing was observed. During this preliminary experiment, 115 specimens were tested, but only 31 produced fracture due to tensile stresses.

The anvils were replaced by those with the bigger loading arc. Each test was run with a sheet of white paper and carbon paper placed between the specimen and the anvil. These papers were used to obtain a measure of the contact width after the test. After testing, the padding was observed and the measurement of contact width was made. The mean result of contact width is 6.55 mm which results in a mean effective value for β of 0.524 radian (30°). Crushing under platens was never observed. Typical fractures are shown in Fig. 4.65.

Some specimens were fractured by the triple-cleft mode of tensile fracture. A typical fracture pattern with varying degress of fragmentaion is shown in Fig. 4.66. This secondary fracture has been observed on testing different materials [283,290,291,293].

Examination of the fracture surface reveals no particular features of fracture. Fig. 4.67 shows the microstructure of a typical fracture surface with short stubby needles.

Fig. 4.68 shows the distribution of strength, plotted as a cumulative probability of failure against nominal failure stress of disc specimens in diametral compression. Strength results for plaster specimens is given in Table 4.8.

TABLE 4.8 FRACTURED STRENGTH OF BRAZILIAN DISC TESTS

NO. OF TESTS	MEAN STRENGTH (MPa)	STANDARD DEVIATION (MPa)
77	3.8556	0.5754

4.7 UNIAXIAL COMPRESSION TESTS

4.7.1 Introduction

It is well known that brittle materials are often used as structured materials in compression, rather than in tension, since tension gives rise to catastrophic failures. It was decided, therefore, to examine the materials in uniaxial compression. The uniaxial compression tests have long been studied to determine the strength of brittle materials, especially cement [294], concrete [186], rock and graphite [295]. It has also been used extensively for food texture investigations [296].

4.7.2 Experimental Procedure

The usual compression test is intended to obtain the strength of a material in a uniaxial-compressive-stress state. The word 'uniaxial' implies that there is only one stress acting upon the body. This stress is compressive and has constant magnitude and direction throughout the body.

The specimen usually chosen for the purpose of simulating this stress state is a right prism or a right circular cylinder. In practice, however, due to friction at the two loading platens, the stress distribution in the material is significantly altered near to

the loading platens. In fact, biaxial compressive stresses are built up in this region. The result is the conical region of severe destruction, shown in Fig. 4.69(b).

If the friction at the ends is fairly low, then the specimen will fail by splitting across the centre, in a vertical plane (Fig. 4.69(a)). Therefore, it is clear that the friction between the loading platens and the specimen end is an important factor which influences the measured compressive strength of a brittle material.

A new mould was designed to cast the specimen (Fig. 4.70). Similar procedures of casting and extracting the cylinder to those described in section 4.4.2, were used. The diameter of specimen was 24.0 $\pm$ 0.1 mm. The height of specimen was chosen to be twice the diameter in order to insure more uniform stress distribution in the gauge section. After casting, the specimens were left for four days to dry out. Both ends of the specimen were then machined by surfacing. Fig. 4.71 shows the specimens as cast and after machining.

Compression of the plaster specimens was carried out using a universal tension-compression machine with a pair of specially designed platens. One method of reducing the frictional effect is by introducing a material with a very low coefficient of friction between the specimen end and the loading platen. A PTFE sheet of 0.9 mm thickness was used for this purpose. Fig. 4.72 shows the experimental set up.

4.7.3 Results and Discussion

Fig. 4.73(a) shows a cylinder in the testing machine prior to loading. The load was applied at the rate of 2 mm/min. When the cylinder failed it usually split axially with some shattering. A typical break is shown in Fig. 4.73(b) which illustrates the splitting action when the frictional effect is very low.

Fig. 4.74 shows the test results, both mean and median rankings were used. The measured strength value is summarized in Table 4.9.

TABLE 4.9 FRACTURED STRENGTH OF UNIAXIAL COMPRESSION TESTS

NO. OF TESTS	MEAN STRENGTH (MPA)	STANDARD DEVIATION (MPA)
50	12.7891	1.2174

4.8 NOTCH-BEAM TESTS

4.8.1 Introduction

By comparison with most ductile metals and alloys the toughness of brittle materials measured by a conventional impact testing machine is indeed very low, but nevertheless is measurable. Fracture toughness testing is a basic prerequisite of any effective assessment of a brittle material. Most of the commonly used techniques of toughness measurement were first developed for testing metals [297], but they can be applied equally, with a few modifications, to brittle materials. The usual technique for brittle materials is to put a notch in a test bar and load it slowly in a testing machine. Although several different specimen configurations are available, the most commonly used for brittle materials is the notched beam tested in bending, primarily because of its simplicity, the ease of machining samples and the economy of material.

Recent literature evidence [298-302] supports the conclusion that accurate values of the fracture surface energy of brittle materials and hence the critical stress intensity factor of brittle materials can be obtained from bend tests on specimens containing saw-cut notches, provided that the notches are sufficiently narrow and deep (e.g., between 0.12 and 0.8 mm wide and deeper than 1 mm).

4.8.2 Experimental Procedures

Plaster specimens similar to those used in the beam bend tests of section 4.3 were employed. Notches were cut in the centre of the beam with a thin steel blade using a circular saw table shown in Fig. 4.75. The notch dimensions were checked by means of an optical

microscope. The major dimensions were within $\pm 10\mu m$, tool wear being very slight. Great care was taken to cut and sand both ends of the specimen flat and parallel to the required dimensions (Fig. 4.77) using a specially designed table shown in Fig. 4.76. The prenotched beams were loaded to failure in the three-point bending test rig shown in Fig. 4.78. More than twenty specimens were used for each experimental condition.

The fracture surfaces of the toughness specimens were examined on a 'Stereo Scan 250 MK 3' scanning electron microscope. Plaster is a non-conductor and so surfaces were coated with a vacuum deposited gold-palladium alloy.

4.8.3 The Determination of Fracture Toughness

Using the specimen geometry and loading configuration shown in fig. 4.77, K_{Ic} is calculated using the following form of the Griffith relation [297]:

$$K_{Ic} = Y. \frac{6Ma^{\frac{1}{2}}}{bW^2}$$

where M is the applied bending moment at fracture. Y is a dimensionless parameter which depends on a/w and on the type of loading as follows:

$$Y = A_o + A_1 \left(\frac{a}{w}\right) + A_2 \left(\frac{a}{w}\right)^2 + A_3 \left(\frac{a}{w}\right)^3 + A_4 \left(\frac{a}{w}\right)^4$$

For three-point bending and s/w=8, the coefficients A have the following values:

$A_o = 1.96$

$A_1 = -2.75$

$A_2 = 13.66$

$A_3 = -23.98$

$A_4 = 25.22$

and the K calibration is

$$K_{Ic} = \frac{PS}{b(w)^{3/2}}\left[\ 2.94\ \left(\frac{a}{w}\right)^{\frac{1}{2}} - 4.12\ 5\left(\frac{a}{w}\right)^{3/2} + 20.\ 49\ \left(\frac{a}{w}\right)^{5/2} - 35.97\left(\frac{a}{w}\right)^{7/2} + 37.83\left(\frac{a}{w}\right)^{9/2}\ \right]$$

4.8.4 Results and Discussion

Table 4.10 lists the average K_{Ic} values obtained for five groups of different a/w ratios. The results of the K_{Ic} determination are shown in Fig. 4.79. Each point represents at least 21 specimens. Notch depth has a significant effect with a maximum at a/w≈0.33. Anomalous notch weakening and strengthening at other a/w ratios were also observed. A comparison of fracture toughness of plaster with some engineering materials is given in Table 4.11.

Although the general curve fits the data in Fig. 4.79 well, there is much scatter due to the small values of K_{Ic}. The standard deviation of K_{Ic} in Table 4.10 is much less than the standard deviation of the 4-point bend test in Table 4.4. The critical stress intensity factor is ideally a material constant, but a constant value is unlikely with flaw sizes comparable to microstructure features. Variation in the value of K_{Ic} is due to subcritical crack growth (105). Significant variation in the fracture toughness of cementous materials with crack length should be expected (106). Thus, for inherent flaws it is conceptually difficult to discuss strength in terms of an independent crack size and stress intensity factor. The K_{Ic} values obtained should be treated with some caution.

The notch effect observations are in agreement with previous work. Simpson [300] has reported the same phenomenon in both single edge-notched (SEN) beam and double-cantilever-beam (DCB) specimens of SiC with a maximum fracture energy ($\gamma=(1-\nu^2)K_{Ic}/2E$) at a/w≈0.3. Brown [303] determined the fracture toughness of cement paste and mortar using similar specimens. The fracture toughness values increased with a/w ratio, up to a maximum at a/w around 0.3, then decreased. Cook

TABLE 4.10 K_{Ic} DATA FOR HERCULITE LX PLASTER OBTAINED WITH SPECIMENS CONTAINING SAW-CUT NOTCHES

SET NO.	a/w	NUMBER OF SPECIMENS	MEAN VALUE OF K_{Ic} ($MN/m^{**}1.5$)	STANDARD DEVIATION
1	0.13	37	0.1374	0.0163
2	0.23	35	0.1334	0.0230
3	0.33	31	0.1527	0.0252
4	0.43	30	0.1360	0.0278
5	0.53	30	0.1322	0.0306
6	0.63	21	0.1480	0.0302

TABLE 4.11 FRACTURE TOUGHNESS VALUES FOR SEVERAL MATERIALS

MATERIAL	K_{Ic} ($MN/m^{**}1.5$)	REFERENCES
POLYESTER	0.5	[309]
CONCRETE	0.2	[309]
MARBLE	0.9	[309]
EPOXIES	0.6	[310]
GLASS	0.25	[305]
PLASTER	0.15	

and Crookham [304] used the notched beam technique to study the notch depth effect on polymer concrete. Their results showed that the fracture toughness increases with the notch-to-depth ratio and attains a limiting value at an a/w ratio of between 0.35 to 0.42. It then decreases beyond this range. Carpinteri [305] also observed the same

phenomenon in SEN specimens of marble, mortar and concrete. The K_{Ic} values increased for small crack depth and decreased for large depth. The maximum K_{Ic} values were obtained at a/w=0.3.

The variations in apparent fracture toughness with a/w ratios are not easily explained. Simpson [300] using a notch crack combination model from Bowie's solution showed that a maximum in fracture energy and hence in fracture toughness can be obtained at a/w=0.4, not far from present results. While Jenq and Shah [306] proposed a two-parameter fracture model, namely the critical stress intensity factor and crack tip opening displacement, to explain the size effect of notched beam specimens. Cotterel and Mai [307] used the crack growth resistance curve to predict the experimentally observed size effects. This size and geometry dependency may be attributed to slow crack growth and nonlinearity due to geometrical interlock effects [302].

Carpinteri [309] has studied the variability of K_{Ic} with geometry. Based on Dimensional Analysis, he deduced the brittleness number:

$$s = \frac{K_{Ic}}{\sigma_u . b^{\frac{1}{2}}}$$

where K_{Ic} : fracture toughness

σ_u : ultimate strength

b : specimen depth

For an elastic brittle material, fracture data of three-point beam bending are valid only if $s \leq 0.5$ [308]. It is possible to obtain the test brittleness number for the present study:

$$s = \frac{0.1527}{5.5338 \times 0.01^{\frac{1}{2}}} = 0.276$$

The agreement with published data and the fact that the brittleness number s is less than 0.5 suggests that the notch-beam technique can be used for fracture toughness measurements on brittle materials.

Since the plaster surface was non-reflective and crack-opening displacements were so small, no direct observation or measure of crack length was possible during the tests. In addition, fracture surfaces were not different in appearance as they usually are for metals. Consequently, all crack lengths were determined during the testing by a compliance calibration. A general notch configuration is given in Fig. 4.80. In order to interpret the notch effect, two samples each at different a/w ratios were examined using the scanning electron microscope. No mirror and related features can be distinguished on these fractures because of the roughness of the fracture topography on the microscale due to the large grain and pore size. The only feature that can be clearly observed is the macroscopic pore structure (Fig. 4.81).

In most materials it has been found necessary to introduce a fatigue crack into the material prior to testing in order to provide reliable crack initiation. This is unlikely to be necessary with plaster because the pores acted as cracks within the material. Subsequent fatigue damage will not improve on this crack initiator.

4.9 STRESS INTENSITY FACTOR

4.9.1 Introduction

In the engineering application of the concepts of linear fracture mechanics to the prediction of strength and life of cracked structures, a knowledge of the crack tip stress intensity factor as a function of applied load and geometry of the structure is necessary.

The importance of determining stress intensity factors in connection with fracture investigations has promoted the search for practical methods that can be used for this purpose.

There are many methods of calculating stress intensity factors. These methods have been reviewed in the literature [311-314]. Among them, the finite element method is suggested as the best candidate at the present time for obtaining approximate stress

intensity factors [315], particularly when exact solutions are not available.

4.9.2 Computational Methods for Stress Intensity Factors

The methods for determining stress intensity factors using finite elements can be grouped into the following three categories:

(a) Direct methods

(b) Indirectly by considering changes in energy due to the presence of a crack.

(c) Method involving special crack tip elements.

The stress field near to the crack tip can be divided into three basic types, each associated with a local mode of deformation as illustrated in Fig. 4.82. They are the opening, sliding and tearing mode and often referred to as Mode I,II and III crack extensions, respectively. In isotropic materials under essentially elastic conditions cracks loaded both statically and cyclically, tend to grow in Mode I irrespective of initial orientation. The opening mode stress intensity factor, K_I, is therefore of greatest importance in fracture investigations. Attention in this section is confined to this mode. As regards the determination of the mode II and mode III stress intensity factors, the procedure will generally be the same.

The stress method correlates the stresses at the nodal points of the finite element mesh with those at the crack tip which are given by:

$$\sigma_{ij}(r,\theta) = \frac{K_N}{\sqrt{2\pi r}} f_{ij}(\theta)$$

Where r,θ are polar coordinates centred at the crack tip and $f_{ij}(\theta)$ is a known function of θ (Fig. 4.83). For the opening mode (N=I) the full set of stress and displacement fields are [316]

$$\sigma_x = \frac{K_I}{(2\pi r)^{\frac{1}{2}}} \cos\left(\frac{\theta}{2}\right)\left[1-\sin\frac{\theta}{2}\sin\frac{3\theta}{2}\right]$$

$$\sigma_y = \frac{K_I}{(2\pi r)^{\frac{1}{2}}} \cos\left(\frac{\theta}{2}\right)\left[1+\sin\left(\frac{\theta}{2}\right)\sin\left(\frac{3\theta}{2}\right)\right]$$

$$\sigma_z = \nu(\sigma_x + \sigma_y)$$

$$\tau_{xy} = \frac{K_I}{(2\pi r)^{\frac{1}{2}}} \sin\left(\frac{\theta}{2}\right)\cos\left(\frac{\theta}{2}\right)\cos\left(\frac{3\theta}{2}\right)$$

$$\tau_{xz} = \tau_{yz} = 0$$

$$u = \frac{K_I}{G}\left(\frac{r}{2\pi}\right)^{\frac{1}{2}}\cos\left(\frac{\theta}{2}\right)\left[1-2\nu+\sin^2\left(\frac{\theta}{2}\right)\right]$$

$$v = \frac{K_I}{G}\left(\frac{r}{2\pi}\right)^{\frac{1}{2}}\sin\left(\frac{\theta}{2}\right)\left[2-2\nu-\cos^2\left(\frac{\theta}{2}\right)\right]$$

$$\omega = 0$$

Where ν is the Poisson's ratio, G is the shear modulus of elasticity, u,v, ω are the displacements in the x,y and z directions respectively.

4.9.3 Finite Element Implementation

A plane strain finite element program using a combination of six-noded isoparametric curvilinear triangular and eight-noded isoparametric curvilinear quadrilateral elements [268] were used to analyse the three-point notched beam specimen (Fig. 4.84). For the efficient numerical solution of fracture problems it is advantageous to employ special crack tip elements which directly model the near tip elastic strain field singularity. The crack tip module [268] is used

for this purpose. The program adapts any isoparametric elements in the region of the crack tip to produce an appropriate singularity.

Due to symmetry only one half of the specimen of Fig. 4.84 need be considered. Two idealizations were employed. In each case, the analysis was conducted over the range of notch to depth (a/w) ratios 0.2 to 0.8. Notches of different lengths were simulated by imposing appropriate boundary constraints in the plane of the cracks. Fig. 4.85 shows the mesh employed for an a/w ratio of 0.2 of the first case. A typical mesh of the second idealization with a/w = 0.8 is shown in Fig. 4.86. The former has a coarser mesh than the latter.

Both displacement and stress extrapolation techniques were used. With the displacement extrapolation method, K_I is found by extrapolating the displacement along the crack face. The analytical expressions for the displacement variation along radial lines emanating from the crack tip are given in section 4.9.2. Substituting the values of u or v and r for nodal points along a radial line emanating from the crack tip as shown in Fig. 4.87 allows a plot of K_I against radial distance r to be drawn. The best straight line is found by linear regression. The regression constant will then be used as an estimate for K_I. The stress extrapolation method for determining the crack tip stress intensity factor is similar to the displacement method.

A Fortran computer program was written to evaluate the stress intensity factors. A finite element analysis was performed for each notch to depth ratio a/w. Nodal coordinates and either nodal displacements or nodal stresses were inputted to this computer program. The stress intensity factors were evaluated for each nodal point along the chosen radius according to the equations of section 4.9.2. These values were then extrapolated to r=0 using the routine G02CAF of the NAG Library [184].

4.9.4 Results and Discussion

The results obtained from the finite element solutions are compared to results given by the ASTM formula [297] in Figs. 4.88 and 4.89. Fig. 4.88 shows the K_I values obtained from the stress

extrapolation method while Fig. 4.89 shows the results from the displacement extrapolation technique. In general, a better agreement with the ASTM formula is obtained using the displacement extrapolation method. The reason is that the nodal stresses are less accurate than the displacements [317]. It has also been shown that the most accurate results are given by using the first idealization. Remember that the crack tip elements were employed in both idealizations. Errors can arise in the evaluation of stress intensity factors by this approach, if the crack tip element is too small to fully capture the $1/\sqrt{r}$ strain singularity behaviour. This is likely to be the case as the crack tip elements of the second idealization are much smaller than those in the first idealization (Fig. 4.85 and 4.86). The accuracy of the present procedure may also be judged from Fig. 4.90 which compares the computed $K_1/\sigma_o \sqrt{a}$ with those given in references [297,318,319].

The experimental data points shown in Fig. 4.90 indicate a curve of the form y=f(x). A least-squares fit involving these four data points can be carried out with a computer program. The plot of data first suggests a quadratic curve having the form:

$$y = C_1 + C_2 x^2$$

Other polynomials of n-1 degree are also used. They have the form:

$$y = C_1 + C_2 x + C_3 x^2 + \ldots + C_n x^{n-1}$$

where the $C_1, C_2 \ldots C_n$ are regression constants. They are listed in Table 4.12. The solution curves with the experimental data were plotted in Fig. 4.91. It can be seen that the 3rd, 4th and 5th degree polynomials equally fit the experimental data well. A comparison of Figs. 4.90 and 4.91 suggests that the best fit is obtained with the 5th degree polynomial.

An equation for estimating K_I for the configuration shown in Fig. 4.84 was derived:

$$K_I = \frac{M}{b(w)^{3/2}} \left[A + B\left(\frac{a}{w}\right) + C\left(\frac{a}{w}\right)^2 + D\left(\frac{a}{w}\right)^3 + E\left(\frac{a}{w}\right)^4 + F\left(\frac{a}{w}\right)^5 \right]$$

Where M is the moment. The constants A,B,C,D,E,F, are listed in Table 4.13.

Thus in conclusion, it can be seen that the use of special crack tip elements is beneficial for stress intensity factors evaluation by displacement extrapolation.

TABLE 4.12 REGRESSION CONSTANTS C_i (i=1,6)

	C_1	C_2	C_3	C_4	C_5	C_6
QUADRATIC	0.9769	7.9844	-	-	-	-
2ND DEGREE	3.4332	-11.7356	19.3561	-	-	-
3RD DEGREE	0.2342	13.7046	-37.7704	38.0844	-	-
4TH DEGREE	1.0264	5.4582	-8.9303	-3.0851	20.5714	-
5TH DEGREE	1.6670	-0.4240	5.9957	-6.7374	-5.3333	21.333

TABLE 4.13 CONSTANTS FOR STRESS INTENSITY FACTOR (K_I) FORMULA

REGRESSION CONSTANT	(x10**3)
A	0.835
B	-0.212
C	3.000
D	-3.370
E	-2.665
F	10.650

CHAPTER FIVE

ANALYSIS AND DISCUSSION OF RESULTS

5.1 EXPERIMENTAL WORK

5.1.1 Plaster Casting

Two key practical points for the preparation and use of plaster specimens need to be emphasized. First, it is necessary to cast moulds in a logical, efficient way. Araldite and perspex were chosen for the present work because of their chemical inertness, ease of machining and availability. In addition, the preparation of specimens required for a test needed minimum machining. In the five failure tests, only the uniaxial compression specimens required workshop machining. The second important requirement is the casting technique, which includes the removal and drying of the plaster casts. A simple but effective procedure for casting plaster specimens as described in section 4.1.4 has been followed throughout. It is important to separate the cast from the mould at the correct time. Plaster becomes warm during setting and the final set is reached when the cast is at maximum temperature. Lifting should be effected just prior to this stage as separation is easy at that point. Various extraction devices have been designed and they proved to be very effective in minimizing the removal time. After setting, the cast should be dried correctly so as to prevent excessive loss from being too wet, too dry, and thermal shock. The drying of plaster specimens will obviously depend upon the sectional depth of the casts. As different types of specimens have been required, a method of weighing the specimens was devised (see section 4.1.4). Although cast at different times, control of the relative weight reduction ratio ensured a high degree of consistency among various sets of specimens.

5.1.2 Mechanical Testing

Fracture strengths of Herculite LX plaster were evaluated at room temperature in five tests. Four-point bend test, cylinder burst test, ring-on-ring test, Brazilian disc test and uniaxial compression test. In designing the mechanical tests, both the testing rig and the

specimen extraction device had to be considered. The latter must be considered to be as important as the former, especially in the case of brittle materials such as plaster which do not possess a very high strength. The weight of the rig must be reduced wherever possible. Another difficulty in testing brittle materials is the edge cracking and spalling phenomena. Experimental measurements using a specially designed anvil that permits a bigger applied-load angle have proved successful in the Brazilian disc tests.

A method of reducing the frictional effect of the compression testing was also introduced by using a P.T.F.E. interlayer between the loading plates and the specimen ends. All of the specimens failed by splitting across the centre, in the vertical plane.

5.2. THEORETICAL AND NUMERICAL ANALYSIS

5.2.1 Finite Element Analysis

As indicated in Chapter Three, the probability of failure is a function of the applied state of stress. In many cases, a closed form solution for the stress distribution on the given structure does not exist and therefore an exact estimate for the probability of failure cannot be obtained. The Finite Element (F.E.) method is a very common technique used to obtain an approximate solution for the stress distribution on the structure.

Over the past ten years, probabilistic structural mechanics with the advent of modern digital computers and the F.E. method has begun to emerge as a tool for assessing the structural risk and reliability of a variety of components and structures in many industries [320,321]. In consequence, it is advantageous to have a probability to failure analysis formulation that can be readily incorporated in a finite element code.

The F.E. method has proved to be very useful in the present work. Stress distributions show very good agreement with analytical solutions. The only drawback are the stress discontinuities at the support point, but this problem can be overcome by using a different type of element as shown in section 4.5.

The F.E. analysis also provides an estimate of the positional failure on certain assumed stress conditions. It can be seen that these failure predictions did occur in experiments.

The usefulness of the F.E. method for the computation of crack tip stress intensity factors is demonstrated. Although several approaches have been developed for estimating the stress intensity factors for a single-edge-notch (SEN) beam subjected to three-point bending, the ASTM formula [297] is commonly used for comparison with the results of other solutions [318,319,322,323]. However the assumptions made in this formula have limited its application to a certain range of span to depth [324]. The results presented in section 4.9 and Fig. 4.92 agree fairly well with published results.

5.2.2 Applicability of the Weibull Distribution

Properties of brittle materials make it necessary to treat the failure in a statistical manner. A theory proposed by W. Weibull [140-142] does this. He proposed that failure of a structure will occur when the stress acting on the weakest flaw exceeds a critical value. This idea is comparable to the case of a loaded chain, where failure of an individual link produces total failure. The name Weakest Link Theory (WLT) is thus often used to denote this approach.

The Weibull distribution function of section 2.2 has a very convenient analytical form and its parameters can be adjusted to closely fit experimental data. Fig. 4.12 illustrates this fact for the case of a two-parameter distribution. The results suggest that the two-parameter Weibull distribution is an adequate description of the experimental failure data.

5.2.3 Shortcomings of the Weakest Link Concept

A major limitation of the WLT is that it does not adequately model situations where compressive stresses are predominant, because in such situations crack growth is not an unstable phenomenon. Unlike the situation in tensile stress states, splitting of the structure by a single crack does not necessarily imply catastrophic failure. The

short-comings of the WLT presented in Fig. 3.12, shows that indeed the probability of failure equation based on this model underestimates the failure stress of the uniaxial compression tests. A more realistic approach to the problem has been suggested by Jayatilaka and Trustrum [159]. Catastophic failure of a brittle material under uniaxial compression can only take place after a proportion of the cracks present in the material have failed. McClintock and Zaverl [325] proposed a similar model assuming that the first crack is stable. Increases in applied stress are then required to cause further cracking. Instability occurs only after a number of cracks have developed.

Batdorf [327] has suggested that the WLT should not be applied in cases where the principal compressive stress exceeds in magnitude the value of the principal tensile stress by a factor of about three.

5.2.4 Limitations of the Principle of Independent Action

The Weibull model is often used in conjunction with the Principle of Independent Action (PIA) to evaluate the probability of failure for the state of multiaxial stress. The PIA ignores the possibility of structural failure taking place under the combined actions of two or three principal stresses [145,171], but the Weibull-Principle of Independent Action approach to multiaxial fracture remains very much in use because it is a simple useful function, in which the dependency of strength on volume can be incorporated into a reliability analysis.

5.2.5 Multiaxial Failure Criterion

Among the numerous failure criteria reviewed, the one proposed by Stanley and Sivill [171] proved to fit quite well the multiaxial failure strengths in both the tension-tension and tension-compression quadrants. The WLT has some drawbacks as pointed out in section 5.2.3 but it does work in this case, since the largest compressive stresses are less than about three times the maximum tensile stress, allowing the method to be applied with confidence

[326]. The compressive/tensile strength ratio for Herculite LX plaster is 2.3.

The Weibull theory, which is a statistical approach, described at length in the literature [140-142], also provides a basis for predicting material failure under multiaxial stress states. However, because the resultant relationships are complex and difficult to use, the theory has been misinterpreted. The results of section 3.1.4 have shown that the Weibull theory could predict either weakening or strengthening relative to the uniaxial tensile strengths in both the tension-tension and tension-compression quadrants. This prediction depends on the Weibull modulus. If m is big, say 12, the theory would predict the biaxial tensile strength to be less than the uniaxial strength. Present results with m=7 show a reversed prediction in the tension-tension quadrant.

One group of ceramics, typified by titania and magnesium silicate [327], exhibit weakening in the tension-tension stress state and strengthening in the tension-compression stress state. This pattern of behaviour is consistent with the statistical fracture theories. In contrast, reaction-sintered silicon carbide showed biaxial strengthening in the tension-tension stress state. A fracture mechanics analysis which was presented by Shetty et al. [327] indicated that the above trend can be expected in those ceramics that fail from spherical defects. There were still other materials such as alumina which showed a transition from an apparent biaxial strengthening to an expected biaxial weakening due to slow crack growth [328]. Various theories which were proposed recently by Matsuo [152], Alpa [155], and Batdorf [172] can be used to explain the strengthening effect with increasing Weibull modulus. However, the reported data are insufficient to determine whether the Weibull modulus has a significant effect on the reported results [168].

5.2.6 Multiaxial Failure Strengths

In biaxial tension, both the Freudenthal analysis, which is based on the Principle of Independent Action (PIA), and the Batdorf model, which includes the possibility of failure under combined principal stresses, can be used to predict the equibiaxial tension

tests (Figs. 3.3 and 3.6). Several versions of the Batdorf model exist for the treatment of fracture due to the presence of different criteria. Among them, the Energy Density criterion assuming penny-shaped cracks, leads to a quite good agreement with experiment. But the best agreement is the Matsuo model which takes into account the contribution of shear to crack propagation. There is not much difference whether the PIA was used or not, because the compressive-tensile strength is less than three.

It was to be expected that of the two Energy Density solutions the one based on the use of penny-shaped cracks is in best agreement with experiment; since such cracks are more closely related to naturally occurring cracks than Griffith cracks. The SEM observations revealed the circular flaws which are probably the point of failure initiation.

The Matthews-Evans model does not require any particular functional form for the strength distribution, and that makes it attractive in cases where a Weibull distribution may not adequately represent the fracture statistics. This formulation of the problem is not very useful, however, because equitriaxial tension is considered first, and then the results corresponding to equibiaxial and uniaxial states of stress are derived in terms of parameters associated with equitriaxial tension. The inverse would have been more appropriate, because material-dependent parameters are normally calculated from uniaxial results, and equitriaxial tension is a state of stress that cannot be obtained in practice. The latter approach has been taken to obtain the results which were presented in Fig. 3.10. There is a large discrepancy between the model and the experiment, and the model is more conservative (i.e., exhibits the lower failure stress).

5.2.7 Estimation of Weibull Parameters

Many techniques exist for the estimation of the parameters of probability distributions. The methods vary in their underlying assumptions and theoretical procedures and, in general, provide somewhat different results. Two methods currently used to estimate the Weibull parameters are discussed in the present work. These were the method of least-squares and the method of maximum likelihood. For

the two methods, both estimates of the normalizing factor σ_o and the Weibull modulus m were very close (see Tables 3.2 and 3.3). It is suggested that the maximum likelihood method is to be used since it is completely objective, simple, and involves no arbitrary assumptions. However, when computing time is not at a premium and other extra statistical data are required, then it is recommended that the method of least-squares be employed.

A Monte Carlo study was conducted to compare the different methods of data ranking. The second plotting position was found to be the best in the determination of the Weibull modulus. However, an examination of Fig. 4.12 discloses that both the first and third plotting positions gave similar results with accuracy sufficient for engineering purposes.

CHAPTER SIX

CONCLUSIONS

In view of the growing interest in the use of brittle materials for structural purposes, this work has been prepared to provide the designer with the best current practice. The theoretical work was carried out using a finite element analysis, and the experimental work using six types of tests on samples of Herculite LX plaster for the latter. The findings are summarized below:

(1) Herculite LX plaster with the plaster/water ratio of 1.5 Kg/litre can be used as a model material to study the influence of the main physical parameters on the fracture properties of brittle materials.

(2) The casting technique was shown to be satisfactory in producing homogeneous casts and accurate dimensional specimens. A minimum of skill and equipment was required to handle the material.

(3) For a tensile state of stress and for a limited range of stress ratio in the compression-tension quadrant (up to a ratio of principal compressive stress to principal tensile stress of approximately -3 according to section 3.2.1 and Appendix B) the Weakest Link theory adequately represents the statistical characteristics of the fracture of brittle materials.

(4) The theory proposed by Stanley has been verified to accuracies acceptable in predicting the failure of brittle components.

(5) The Principle of Independent Action ignores the possibility of structural failure taking place under the combined actions of different stresses. The validity of that approximation has been challenged by the model of Matsuo which combines both normal and shear stresses.

(6) Simulating cracks can be produced in samples of Herculite LX plaster by sawing.

(7) Fracture toughness increases with the crack length and approaches a limiting value at crack-to-depth ratios of approximately 0.3, and then decreases after this point.

(8) Methods of deriving the stress intensity factors from finite element results have been discussed, and two different methods have been identified. In general it has been found that the displacement extrapolation method can give better stress intensity estimates, especially when used with quarter-point crack tip elements.

(9) This work does demonstrate the depth to which analysis of failure of brittle materials is possible using a combination of the finite element method for stress analysis combined with statistical failure data for the material to give an estimate of reliability.

(10) A technique for the prediction of the mean failure load of a Brazilian disc, derived from the above approach, should prove to be an extremely powerful tool in the analyisis of brittle structural components with all types of geometries when subjected to multiaxial stress states.

(11) Experimental results and finite element analysis have been shown to give good agreement in predicting the positional failure for the ring-on-ring and Brazilian disc tests.

(12) To measure the uniaxial strengths, the four-point bending tests are easy to perform. The results of section 3.2 and Fig. 3.1 suggested that either the ring-on-ring or the Brazilian disc test could replace uniaxial tests as a means of evaluating probability of failure parameters for subsequent use.

(13) The cylinder burst tests measure specimen strengths in the uniaxial stress state. It is not easy to perform and its success depends on the material strength, and on a careful experimental procedure.

(14) The use of P.T.F.E. sheet placed between the platens and specimen ends has been shown to reduce the pressure concentrations due

to inevitable geometric mismatches of the contact surfaces of the uniaxial compression tests.

(15) Fractography using the scanning electron microscope provides valuable information about the failure of brittle materials.

(16) The two-parameter Weibull probablity distribution adequately describes all the test failure strength distributions.

(17) Common methods of estimating the Weibull parameters are discussed. Either the method of Least-Squares or the method of Maximum Likelihood could be used.

(18) Computer simulation is used to obtain the statistical properties of different estimators. It is recommended that the Least-Squares estimate with a sample size of about 30 and the plotting position $P_f=(j-1/2)/N$ be used.

RECOMMENDATIONS FOR FUTURE WORK

The author believes that there exists three distinct areas related to this work for further improvement and investigation.

(1) Further experimental work on other brittle materials with different ratios of principal compressive stress to principal tensile stress is necessary to establish a more general failure criterion for brittle materials.

(2) Utilization of brittle materials in applications such as heat engines, bearings, cutting tools, where high contact loads can occur, requires a thorough understanding of contact stress distributions and their related effects on crack initiation and propagation.

(3) The Weibull distribution is often employed to model the statistical variation of strength of brittle materials. It is assumed that a single distribution of flaws is present uniformly throughout the material. However, it is only a model, and extrapolations are only valid if the model is accurate. Different flaw populations may

be present in a set of specimens. Therefore, multiple flaw distributions should be studied in order to model the results more accurately.

REFERENCES

1. THE COLLYEAR REPORT
HMSO, 1985.

2. RILEY, F. L. and MILSOM, S. J.
"Ceramics in engines - process requirements and research activity". Materials Science and Technology, 9, 2, 891-894, 1986.

3. SINCLAIR, T. J.
"Organization and financing of ceramics research and development - An overview". Ibid., 9, 2, 889-890, 1986.

4. STRUCTURAL CERAMICS
Committee on Structural Ceramics, NMAB, National Research Council, Report NMAB-32, 1975.

5. CHARLES RIVER ASSOC. INC.
"Advanced Ceramic Materials - Technological and Economic Assessment". Noyes Publications, New Jersey, 1985.

6. SUZUKI, H.
"Recent trends in the development of fine ceramics in Japan". Materials Science and Engineering, 71, 211-226, 1985.

7. JOHNSTONE, B.
"Ceramics faces its big test". New Scientist, No.1473, 41-43, 12 Sept. 1985.

8. BELL, J.
"The ceramics age dawns". Ibid., No.1394, 11-12, 26 Jan. 1984.

9. DOYLE, P. J.
"Sixty years in 'Glass'". Glass, 60, 8, 273-281, 1983.

10. WAKELY, K. W.
"Engineering in Carbon". Engineering, I-IV, April 1985.

11. BRISCOE, E. M.
"A new era for engineering ceramics ?". Journal of the Royal Society of Arts, CXXXII, 782-796, 1984.

12. BRISCOE, E. M.
"Ceramic materials". Materials in Engineering Design, 25-26, October 1985.

13. BROOK, R. J.
"Engineering Ceramics". Proceedings of the First Conference on Materials Engineering, A. N. Bramley, Ed., Institution of Metallurgists, 33-35, 1984.

14. NITRASIL - Reaction Bonded Silicon Nitride "Application Data Sheet - Electrical Applications". AE Developments Ltd., Engineering Ceramic Unit, Warwickshire, 1985.

15. NEWS PRODUCTS
Toshiba Ceramics News, 7, 1986
Toshiba Ceramics Co. Ltd., Japan.

16. MORELL, R.
"Handbook of Properties of Technical and Engineering Ceramics". HMSO, I985.

17. MITCHELL, V.
"Engineering with Ceramics". Engineering Designer, March/April, 24-25, 1986.

18. HAGEMANN, H. J., HENNINGS, D. and WERNICKE, R.
"Ceramic multilayer capacitors". Philips Technical Review, 41, 3, 89-98, 1983/4.

19. MANCZOK, R. and WERNICKE, R.
"Ceramic boundary-layer capacitors". Ibid., 41, 11/12, 338-346, 1983/4.

20. THORNTON, P. A. and COLANGELO, V. J.
"Fundamentals of Engineering Materials'. Prentice-Hall, Inc., New Jersey, 1985.

21. MICHELI, A. L., KUO, W. C. and SPRAGUE, R. L.
"Ceramic distributor rotor for electromagnetic interference (EMI) control". International Journal of Vehicle Design, 6, 6, 811-816, 1985.

22. HARTL, W. PETER, D. and REIBER, K.
"A metal/ceramic diagnostic X-ray tube". Philips Technical Review, 41, 4, 126-134, 1983/4.

23. HART, W. PETER, D. and REIBER, K.
"Metal/ceramic X-ray tubes for non-destructive testing". Ibid., 41, 1, 24-29, 1983/4.

24. SHEPPARD, L. M.
"Ceramics for Sensors". Advanced Materials and Processes, 2, 9, 19-25, 1986.

25. TOVELL, J. F.
"Ceramics and the Reciprocating Internal Combustion Engine". Materials and Design, v, 5, 215-220, 1984.

26. CERAMICS
Developments in Technology, National Westminster Bank, Plc., 3-4, Sept. 1985.

27. PAGANELLI, J. V.
"PTC ceramics heat automotive controls". Automotive Engineering, 31-35, June 1984.

28. HUMPHREY, T.
"The use of PTC heaters in diesel fuels". International Journal of Vehicle Design, 6, 4-5, 469-474, 1985.

29. 3M Brand 210 - Aluminium Oxide/Titanum Carbide Composite
Product Bulletin, 98-0400-0429-7 (105.05) R1, Ceramic Material Department/3M, Minnesota, USA, 1986.

30. BARTA, J. and MANELA, M.
"Si_3N_4 and Si_2N_2O for high performance radomes". Materials Science and Engineering, 71, 265-272, 1985.

31. HIGH ALUMINA CERAMICS
Wade (Advanced Ceramics) Ltd., Leicester, 1985.

32. NEWLAND, B. G.
"Ceramics - Materials at the sharp end of defence". Metals and Materials, 2, 6, 334-339, 1986.

33. PORZ, F., GRATHWOHL, G. and THUMMLER, F.
"SiC as a structural material in the plasma chamber of nuclear fusion reactors". Materials Science and Engineering, 71, 273-282, 1985.

34. CLINARD, Jr. F. W.
"Ceramics for Fusion Devices". Journal of Materials for Energy Systems, 100-106, March 1984.

35. Ibid.(5), 380-449.

36. INDUSTRIAL APPLICATIONS : HPSN
Advanced Materials Engineering Ltd., Worcestershire.

37. BURGAM, M.
"Taking advantage of new ceramics". Manufacturing Engineering, 60-63, Feb. 1985.

38. JACK, K. H.
"Sialon tool materials". Metal Technology, 297-301, July 1982.

39. JACK, K. H.
"Engineering applications of sialons". Ibid.(3), 65-72, 1984.

40. HIped Ceramics - W80.NB90S.NB90M
Sumiden Hardmetal UK Ltd., Bucks., 1986.

41. JACK, D. H.
"Cemented Carbide as an engineering material". Material Engineering, 125-131, 10-12 July 1984.

42. JACK, D. H.
"Ceramic tool materials". Hi-Tech 6 International Conference, 28-29 March 1985, Hi-Tech Communications Ltd.

43. JACK, D. H.
"Ceramic Cutting Tool Materials". Materials and Design, 7, 5, 267-273, 1986.

44. NORTH, B.
"Substitution of ceramics for conventional cutting tools". Materials and Society, Pergamon Press Inc., 257-270, 1984.

45. OBRZUT, J. J.
"Ceramic tooling has what it takes but few takers". Iron Age, Chilton Co. Inc., 38-39, 17 July 1978.

46. WHITNEY, E. D.
"Modern Ceramic Cutting Tool Materials". Powder Metallurgy International, Verlag Schmid GmbH, 201-205, April 1983.

47. PARTIALLY STABILISED ZIRCONIA - Transformation Toughned.
Nilcra Ceramics Pty., Ltd., Victoria, Australia, 1986.

48. SIBLEY, L. B. and ZLOTNICK, M.
"Considerations for tribological application of engineering ceramics". Materials Science and Engineering, 71, 283-293, 1985.

49. NITRASIL - Reaction Bonded Silicon Nitride
"Applications Data Sheet - Tribological and Gauging Applications". Ibid.(14), 1985.

50. PENTEL
Technical Catalogue, Surrey, 1985.

51. Toscut scissors into the market
Toshiba Ceramics News, 8, 1987
Toshiba Ceramics Co. Ltd., Japan.

52. SHEPPART, L. M.
"Cure it with ceramics". Advanced Material & Processes, 2, 5, 26-31, 1986.

53. HENCH, L. L. and WILSOM, J.
"Surface - Active Biomaterials". Science, 630-636, 9 Nov. 1984.

54. PRODUCT PROFILE - P-30 Resin Bonded Ceramic
Dental Products, 3M Health Care, Leicestershire, 1986.

55. HASTINGS, G. W. and WILLIAM, D. F., Eds.
"Mechanical Properties of Biomaterials". John Wiley and Sons, 1980.

56. HAMADA FINE CERAMIC SYSTEM
Hamada Blower Co. Ltd., Japan, 1985.

57. Anti-abrasive-wear fine ceramics materials used on I.D.F impeller blades.
MSG No.86F-099, Dengyosha Machine Works Ltd., Japan, 1-15, 1985.

58. BRISCOE, E. M.
"Ceramic materials - Some product design considerations". Materials & Design, 7, 1, 38-43, 1986.

59. Applications of Glass Ceramics
Developments in Technology, National Westminster Bank Plc., 6, March 1985.

60. Diamond Diced Ceramic Armour
Industrial Diamond Review, 46, 513, 55-56, 1986.

61. REFEL SILICONE CARBIDE - Today's engineering ceramic. BNFL Publication, Cheshire, 1985.

62. NITRASIL - Reaction Bonded Silicon Nitride
"Application Data Sheet - Handling molten metals".
Ibid.(14), 1985.

63. New pouring filter improves casting quality
Ceramic products for metal casting. Certech, New Jersey, 1986.

64. Research and development in ceramics - Dublin University leads the pack.
The Engineer, 21-22, 10 Jan. 1985.

65. PARKER, D. A.
"Ceramic technology - Application to engine components". Proceedings of the Institution of Mechanical Engineers, 199, A3, 135-150, 1985.

66. HARMON, R. A. and LARSEN, R. P.
"Ceramic turbochargers boost engine performance".
Mechanical Engineering, 44-57, Oct. 1984.

67. LASKER, M. F., CRAIG, R. P. and MASON, J. L.
"Evaluation of ceramics for passenger car turbochargers". ASME Paper No.85-IGT-149, 1985.

68. BUTLER, E. P.
"Critical assesment - Transformation - Toughned Zirconia ceramics". Materials Science and Technology, 1, 6, 417-432, 1985.

69. WATERMAN, N. A.
"Materials for the 80's and 90's". Ibid.(13), 1-7, 1984.

70. WALZER, P., HEINRICH, H. and LANGER, M.
"Ceramic components in passenger-car diesel engines". Materials & Design, 7, 2, 75-80, 1986.

71. PARKER, D. A.
"Requirements for ceramics in reciprocating engines". Ibid.(2), 9, 2, 900-901, 1986.

72. WALZER, P., HEINRICH, H. and LANGER, M.
"Ceramic components : key to improve diesel effiviency ?". Automotive Engineering, 93, 5, 44-50, 1985.

73. MATSUOKA, H., KAWAMURA, H. and TOEDA, S.
"Development of ceramic pre-combustion chamber". JSAE Review, 13, 32-39, 1984. Also International Journal of Vehicle Design, 7, 1/2, 151-162, 1986.

74. KATZ, R. N.
"Applications of high performance ceramics in heat engine design". Materials Science and Engineering, 227-249, 1985.

75. BURGAM, M.
"Taking advantage of new ceramics". Manufacturing Engineering, 60-63, Feb. 1985.

76. NEWLAND, B. G.
"Challenging time for technical ceramics". CME, 33, 1, 28-30, 1986.

77. Ceramic cut out cooling
Engineering, 432-433, July/August 1985.

78. Ceramic Materials/3M - A commitment to quality
Ceramic Materials Department/3M, 98-0400-0510-4 (26.5) 11, Minnesota, 1986.

79. RAHNKE, C. J. and VALLANCE, J. K.
"Reliability and durability of ceramic regenerators in gas turbine". Trans. ASME, Journal of Engineering for Power, 100, 73-81, 1978.

80. CLEVELAND, J. J., FRITSCH, C. W. and KLEINER, R. N.
"Fracture strength and thermal shock resistance of thick and thin-walled magnesium-aluminum-silicate ceramic heat regenerators". Ibid., 100, 136-139, 1978.

81. GETTINGS, M.
"Regenerative ceramic burner has highest efficiency". CME, 33, 1, 38-40, 1986.

82. ANDERSON, C. A., BRATTON, R. J., COHN, A., SANDAY, S. C. and LANGE, F. F.
"Progress on ceramic rotor blade development for industrial gas turbine". Trans. ASME, Journal of Engineering for Power, 100, 1, 58-65, 1978.

83. ELKINS, R. T., HEATH, B. B. and YONUSHONIS, T.
"Innovative design of ceramic utility gas turbine". Ibid., 101, 4, 556-562, 1979.

84. NAPIER, J. C.
"Application of all-ceramic nozzle to radial flow turbine". Ibid., 102, 2, 239-243, 1980.

85. TRANTINA, G. and GRONDAHL, C.
"Demonstration of ceramic design methodology for a ceramic combustor liner". Ibid., 101, 320-323, 1979.

86. SHIEMBOB, L. T., STEWART, O. L. and BILL, R. C. "Development of sprayed ceramic seal system for turbine gas path sealing". Ibid., 101, 549-555, 1979.

87. BELL, J. "Small gas turbine". New Scientist, No.1394, 19, 26 Jan. 1984.

88. BOWEN, H. K. "Basic research needs on high temperature ceramics for energy applications". Material Science and Engineering, 44, 1-56, 1980.

89. NITRASIL - Reaction Bonded Silicon Nitride "Application Data Sheet - Jigs and Fixture". Ibid.(14), 1985.

90. INDUSTRIAL APPLICATIONS : RBSN Advanced Materials Engineering Ltd., Worcestershire.

91. ZIRCONIA, Alumina Products Zircar fibrous ceramics, Zirca Products Inc., Florida, 1986.

92. CAPPIELLO, C. C., BENNET, J. G. and GAC, F. D. "Review of Valve Design for Coal-Gasification Lockhopper Service". Report No.LA-10024-MS, Los Alamos National Laboratory, 1984.

93. Ceramic Foam Filter Toshiba Ceramics Publication, TC 068-85.8.1A.

94. Refractory Sheet Products Ibid.(91), 4.86A, 1986.

95. Fiberfrax Manual 1986 Carborundum Resistant Materials, Form G-F019(E), 1985.

96. FRYATT, J. "Ceramic fibres for the Automotive Industry". Paper presented at the Second I.A.V.D. Congress on Vehicle Design and Components, Geneva, 4-6th March 1985.

97. RICHERSON, D. W. "Modern Ceramic Engineering". Marcel Dekker, Inc., 1982.

98. Ibid.(5), 257-316.

99. CREYKE, W. E. C., SAINSBURY, I. E. J. and MORREL, R. "Design with Non-ductile Materials". Applied Science Publishers Ltd., 1982.

100. BITTENCE, J. C. "Ceramics : A Brittle material shatters ductile traditions". Materials Engineering, 18-22, August 1978.

101. BENNET, A.
"Requirements for engineering ceramics in gas turbine engines". Materials Science and Technology, 2, 9, 895-899, 1986.

102. LAWN, B. R. and WILSHAW, T. R.
"Fracture of Solids". Cambridge University Press, 1975.

103. FESSLER, H. and FRICKER, D. C.
"The Design of Ceramic Turbine Blade Roots". Proceedings of British Ceramic Society, 26, 81-96, 1978.

104. FESSLER, H. and FRICKER, D. C.
"Friction at Broad and Narrow Contacts Between Silicon Nitride and Hardened Steel". Ibid., 34, 129-143, 1984.

105. DAVIDGE, R. W.
"Combination of fracture mechanics, probability, and micromechanical models of crack growth in ceramic systems". Metal Science, 14, 8-9, 459-462, 1980.

106. DAVIDGE, R. W.
"Strength and toughness in ceramic systems". Phil. Trans. Roy. Soc. London, A310, 113-125, 1983.

107. DAVIDGE, R. W.
"Engineering performance prediction for ceramics". Ibid.(2), 9, 2, 902-909, 1986.

108. PLETKA, B. J. and WIEDERHORN, S. M.
"A comparison of failure predictions by strength and fracture mechanics techniques". Journal of Materials Science, 17, 5, 1247-1268, 1982.

109. ANTHONY, F. M., MARCUS, L. and MISTRETTA, A. L.
"Selection techniques for brittle materials". Technical Report No.65-209, Vol.1, Air Force Materials Laboratory, Wright-Patterson Air Force Base, Dayton, Ohio, 1965.

110. BARNETT, R. L., COSTELLO, J. F., HERMANN, P. C. and HOFER, K. E.
"The behavior and design of brittle structures". Technical Report No.AFFDL TR 65-165, Air Force Flight Dynamics Laboratory, Wright-Patterson Air Force Base, Dayton, Ohio, 1965.

111. EVANS, A. G.
"Structural Reliability : A Processing-Dependent Phenomenon". Journal of the American Ceramic Society, 65, 3, 127-137, 1982.

112. HAHN, G, J. and MEEKER, Jr. W. Q.
"An engineer's guide to books on statistic and data analysis". Journal of Quality Technology, 16, 4, 196-218, 1984.

113. BRAIDEN, P. M.
"Techniques for stress analysis of ceramics". Proceedings of British Ceramic Society, 32, 315-332, 1982.

114. GRIFFITH, A. A.
"The theory of rupture". Proceedings of the First International Congress for Applied Mechanics, Part 1, 55-63, 1924.

115. FISHER, J. C.
"A criterion for the failure of cast iron". ASTM Bulletin, No.181, TP76-77, 74-75, April 1952.

116. MAIR, W. M.
"Fracture criteria for cast iron under biaxial stresses". Journal of Strain Analysis, 3, 4, 254-263, 1968.

117. CLOUGH, W. R. and SHANK, M. E.
"The deformation and rupture of gray cast iron". Transactions of American Society for Metals, 49, 241-262, 1957.

118. GRASSI, R. C. and CORNET, I.
"Fracture of gray-cast iron tubes under biaxial stresses". Journal of Applied Mechanics, 16, 178-182, 1949.

119. CORNET, I. and GRASSI, R. C.
"A study of the theories of fracture under combined stresses". Trans. ASME, Journal of Basic Engineering, 83, 39-44, 1961.

120. FRISHMUTH, R. E. and McLAUGHLIN, P. V.
"Failure analysis of cast irons under general three-dimensional stress states". Trans. ASME, Series H, 98, 1, 69-75, 1976.

121. SHIGLEY, J. E.
"Mechanical engineering design". McGraw Hill, Third Edtion, 173-175, 1977.

122. TAKAGI, J. snd SHAW, M. C.
"Brittle fracture initiation under complex stress states". Trans. ASME, Journal of Engineering for Industry, 105, 3, 143-148, 1983.

123. SHAW, M. C.
"A critical review of mechanical failure criteria". Trans. ASME, Journal of Engineering Materials and Technology, 106, 219-226, 1984.

124. SAMPATH, W. S., LEE, Y. M. and SHAW, M. C.
"Tool fracture probability under steady state cutting conditions". Trans. ASME, Journal of Engineering for Industry, 106, 161-170, 1984.

125. BABEL, H. W. and SINES, G.
"A biaxial fracture criterion for porous brittle materials". Trans. ASME, Journal of Basic Engineering, 90, 285-291, 1968.

126. McCLINTOCK, F. A. and WALSH, J. B.
"Friction on Griffith cracks in rocks under pressure". Proceedings of the Fourth U.S. National Congress of Applied Mechanics, ASME, 1015-1021, 1962.

127. PAUL, B. and MIRANDY, L.
"An improved fracture criterion for three-dimensional stress states". Trans. ASME, Journal of Engineering Materials and Technology, 98, Series H, 2, 159-163, 1976.

128. ELY, R. E.
"Strength of magnesium silicate and graphite under biaxial stresses". Ceramic Bulletin, 47, 5, 489-492, 1968.

129. PRIDDLE, E. K.
"Effects of multiaxial stresses on the fracture strength of silicon carbide". Journal of Strain Analysis, 4, 2, 81-87, 1969.

130. JORTNER, J.
"Biaxial mechanical properties of AXF-5Q graphite to 4000° F". Proceedings Conference on Continum Aspect of Graphite Design, CONF-701105, 514-532, 1970.

131. COFFIN, Jr. L. F.
"The flow and fracture of brittle material". Journal of Applied Mechanics, 17, 233-248, 1950.

132. PRIDDLE, T. G.
"A fracture theory for brittle anisotropic materials". Trans. ASME, Journal of Engineering Materials and Technology, 96, Series H, 2, 91-96, 1974.

133. SATO, Y.
"Fracture of brittle materials under biaxial stresses". Trans. JSME, 39, 320, 1096-1105, 1973.

134. AWAJI, H.
"Macroscopic brittle fracture criterion under multi-axial stress". Trans. ASME, Journal of Engineering Materials and Technology, 102, 3, 257-263, 1980.

135. FREUDENTHAL, A. M.
"Statistical approach to brittle fracture". Fracture - An advanced treatise, H. Liebowitz, Ed., Volume II, Academic Press, 1968.

136. HAHN, G. J. and SHAPIRO, S. S.
"Statistical Models in Engineering". John Wiley & Sons, 1967.

137. THOFT-CHRISTENSEN, P. and BAKER, M. J.
"Structural reliability theory and its applications". Springer-Verlag Berlin, Heidelberg, 1982.

138. GUMBEL, E. J.
"Statistics of Extreme". Columbia University Press, New York, 1958.

139. O'CONNOR, P. D. T.
"Practical reliability engineering". John Wiley & Sons, Second Edition, 1985.

140. WEIBULL, W.
"A statistical theory of the strength of materials". Ingeniorsvetens kapsakademiens, Handligar NR151, 5-45, 1939.

141. WEIBULL, W.
"The phenomenon of rupture in solids". Ibid., 5-55, 1939.

142. WEIBULL, W.
"A statistical distribution function of wide applicability". Trans. ASME, Journal of Applied Mechanics, 18, 293-297, 1951.

143. MONTGOMERY, D. C.
"Introduction to statistical quality control". John Wiley & Sons, 1985.

144. DUKES, W. H.
"Handbook of brittle material design technology". Agardograph No.152, 1971.

145. BATDORF, S. B. and CROSE, J. G.
"A statistical Theory for the Fracture of Brittle Structures Subjected to Nonuniform Polyaxial Stresses". Trans. ASME, Journal of Applied Mechanics, 41, 2, 459-464, 1974.

146. BATDORF, S. B. and HEINISCH, Jr. H. L.
"Fracture Statistics of Brittle Materials with Surface Cracks". Engineering Fracture Mechanics, 10, 831-841, 1978.

147. MATTHEWS, J. R., McCLINTOCK, F. A. and SHACK, W. J.
"Statistical Determination of Surface Flaw Density in Brittle Materials". Journal of the American Ceramic Society, 59, 7-8, 304-308, 1976.

148. EVANS, A. G. and JONES, R. L.
"Evaluation of a Fundamental Approach for the Statistical Analysis Fracture". Ibid., 61, 3-4, 156-160, 1978.

149. EVANS, A. G.
"A General Approach for the Statistical Analysis of Fracture". Fracture Mechanics of Ceramics, R. C. Bradt et al. Eds., Vol.3, Plenum Press, 31-49, 1977.

150. EVANS, A. G.
"A General Approach for the Statistical Analysis of Multiaxial Fracture". Journal of the American Ceramic Society, 61, 7-8, 302-308, 1978.

151. MATSUO, Y. and SATO, H.
"A Probability Treatise of Rupture of Brittle Rotating Disks". Bulletin of the JSME, 22, 172, 1368-1373, 1979.

152. MATSUO, Y.
"A Probabilistic Analysis of the Brittle Fracture Loci under Biaxial Stress State". Ibid., 24, 188, 290-294, 1981.

153. MATSUO, Y.
"On the Relative Coefficients of the Multiaxial Probability Distribution Function for Fracture". Ibid., 24, 189, 495-500, 1981.

154. MATSUO, Y.
"Statistical fracture theory for Multiaxial Stress States using Weibull's three-parameter function". Ibid., 26, 219, 1461-1467, 1983.

155. ALPA, G.
"On the Statistical Approach to Brittle Rupture for Multiaxial States of Stress". Engineering Fracture Mechanics, 19, 5, 881-901, 1984.

156. JAYATILAKA, A. De S. and TRUSTRUM, K.
"Designing with brittle materials subjected to complex loading systems". Conference organized by the British Ceramics Society, London, 155-165, 1977.

157. JAYATILAKA, A. De S. and TRUSTRUM, K.
"Statistical approach to brittle fracture". Journal of Materials Science, 12, 1426-1430, 1977.

158. JAYATILAKA, A. De S. and TRUSTRUM, K.
"Application of numerical methods in predicting strengths of brittle materials". International Conference on Numerical Methods in Fracture Mechanics, Swansea, 765-773, 1978.

159. JAYATILAKA, A. De S. and TRUSTRUM, K.
"Fracture of brittle materials in uniaxial compression". Journal of Materials Science, 18, 2, 455-457, 1978.

160. JAYATILAKA, A. De S. and TRUSTRUM, K.
"Application of a statistical method to brittle fracture in biaxial loading systems". Ibid., 12, 2043-2048, 1978.

161. HUNT, R. A.
"Reliability Technology". National Physical Laboratory, Report IMA A(1), December 1976.

162. HUNT, R. A. and McCARTNEY, L. N.
"A new approach to Weibull's statistical theory of brittle fracture". International Journal of Fracture, 15, 4, 365-375, 1979.

163. GEE, M. G.
"The failure probability of bend test specimens". Res Mechanica, 4, 295-313, 1982.

164. ALMOND, E. A.
"Strength of hardmetals". Metal Science, 12, 12, 582-592, 1978.

165. ALMOND, E. A., GEE, M. G. and McCARTNEY, L. N.
"Application of reliability technology in tool design". Met. Soc. Book 278, The Metal Society, London, 183-189, 1982.

166. GEE, M. G.
"Brittle fracture of hard metals : Dependence of strength on defect size distribution". International Journal of Mechanical Science, 26, 2, 85-91, 1984.

167. GEE, M. G. and McCARTNEY, L. N.
"Statistical theory of failure for ceramic in aggressive environments". Proceedings of British Ceramic Society, 32, 133-147, 1982.

168. DUCKWORTH, W. H. and ROSENFIELD, A. R.
"Effects of Stress State on ceramic Strength". Energy and Ceramics, F. Vincenzini et al., Eds., Elsevier, Amsterdam, 645-660, 1980.

169. BROUTMAN, L. J. and CORNISH, R. H.
"Effect of Polyaxial Stress States on Failure Strength of Alumina Ceramics". Journal of the American Ceramic Society, 48, 10, 519-524, 1965.

170. NAG Fortran - Library Manual, Mark 11, Volume 1.
Chapter D01 - Quadrature
Numerical Algorithms Group, Oxford, 1984.

171. STANLEY, P. and SIVILL, A. D.
"On the biaxial fracture strength of Reaction-Bonded Silicon Nitride". Proceedings of British Ceramic Society, 26, 97-111, 1978.

172. BATDORF, S. B.
"Comparison of the Best Known Fracture Criteria". Proceedings of the International Symposium on Absorbed Specific Energy and/or Strain Energy Density Criterion, G. C. Sih, E. Czoboly and F. Gillemot Eds., 243-251, 1982.

173. STANLEY, P., FESSLER, H. and SIVILL, A. D.
"An engineer's approach to the prediction of failure probability of brittle components". Proceedings of British Ceramic Society, 22, 453-487, 1973.

174. ABRAMOWITZ, M. and SEGUN, I. A.
"Handbook of Mathematical Functions". Dover Publications, Inc., New York, 1968.

175. NAG Fortran - Library Manual, Mark 11, Volume 6.
Chapter S - Approximation of Special Functions
Numerical Algorithms Group, Oxford, 1984.

176. STANLEY, P., FESSLER, H. and SIVILL, A. D.
"The unit strength concept in the interpretation of beam test results for brittle materials". Proceedings of Institution of Mechanical Engineers, 190, 49/76, 585-595, 1976.

177. TRUSTRUM, K. and JAYATILAKA, A. De S.
"On estimating the Weibull modulus for a brittle material". Journal of Materials Science, 14, 1080-1084, 1979.

178. JERYAN, R. A.
"Use of Statistis in Ceramic Design and Evaluation". Ceramics for high performance application II, J. J. Burke, E. N. Lenoe and R. Katz, Eds., Brook Hill Publishing, Chesnut Hill, Mass., 35-51, 1978.

179. RITTER, Jr. J. E., BANDYOPADHYAY, N. and JAKUS, K.
"Statistical Reproducibility of the Dynamic and Static Fatigue Experiments". American Ceramic Society Bulletin, 60, 8, 798-806, 1981.

180. KAMIYA, N. and KAMIGAITO, O.
"Estimation of Weibull parameters by omission of some data in a sample". Journal of Materials Science, 19, 4021-4025, 1984.

181. OSAKI, S.
"Stochastic system reliability modelling". World Scientific Publishing Co., Pte., Ltd., 1985.

182. KAPUR, K. C. and LAMBERSON, L. P.
"Reliability in Engineering Design". John Wiley & Sons, Inc., 1977.

183. COHEN, A. C. and WHITTEN B.
"Modified maximum likelihood and modified moment estimators for the three-parameter Weibull distribution". Commun. Statist. Theor. Meth., 11, 23, 2631-2656, 1982.

184. NAG Fortran - Library Manual, Mark 11, Volume 2.
Chapter E02 - Curve and Surface Fitting
Numerical Algorithms Group, Oxford, 1984.

185. GIBBON, D. I. and VANCE, L. C.
"A simulation study of estimators for the 2-parameter Weibull distribution". IEEE Transactions on Reliability, R-30, 1, 61-66, 1981.

186. JAYATILAKA, A. De S.
"Fracture of Engineering Brittle Materials". Applied Science Publishers, Ltd., 1979.

187. VAX - BASIC
User's Guide
Order No. AA-L335A-TK including AD-L335A-TI.

188. BAIN, L. J. and ANTLE, C. E.
"Estimation of Parameters in the Weibull Distribution". Technometrics, 9, 4, 621-627, 1967.

189. THOMAN, D. R., BAIN, L. J. and ANTLE, C. E.
"Inferences on the Parameters of the Weibull Distribution". Ibid., 11, 3, 445-460, 1969.

190. McCUEN, R. H.
"Statistical Methods for Engineers". Prentice-Hall, Inc., New Jersey, 1985.

191. KIRK-OTHMER
"Calcium Sulfate". Concise Encyclopedia of Chemical Technology, John Wiley & Sons, 196-197, 1985.

192. GREEN, G. W.
"Gypsum Analysis with the Polarizing Microscope". ASTM STP 861, R. A. Kuntze, Ed., 22-47, 1984.

193. PRESSLER, J. W.
"Gypsum". Mineral Facts and Problems, U.S.D.O.I., Bureau of Mines, 1985.

194. DICKSON, T.
"Gypsum - Building from the depths". Industrial Minerals, 130, 17-31, 1978.

195. RUFFER, C. V., KROKER, V. and JOERKE, E.
"Plaster of Paris in the southern 'Harz'-mountain". Borgardts - Sachsenstein GmbH, Austria.

196. British Gypsum Industrial Plaster
"Herculite and Crystacal industrial plaster for engineering, pattern making, tooling". British Gypsum Limited, Newark, Nottingham.

197. PRIESTLEY, R.
British Gypsum Limited, Private communication, Sept. 1985.

198. AZEVEDO, M. C. and ESTEVES FERREIRA, M. J.
"Construction of Models of Concrete damps for elastic tests". Technical Paper No.232, Laboratorio Nacional de Engenharia Civil, Lisbon, 1964.

199. HOSSDORF, H.
"Model analysis of structure". Van Nostrand Reinhold, Co., Ltd., 1974.

200. Casting plasters - For Arts and Crafts
Georgia Pacific Gypsum Division
Georgia Pacific Corporation, 1984.

201. Annual Book of ASTM Standards
Section 4 - Construction
Volume 04.01 - Cement; Lime; Gypsum, 1983.

202. Quality control in the plaster mold shop
Tooling and Casting Division
United States Gypsum, Bulletin No.TAC-161, 1978.

203. Testing Gypsum Cements & Plasters
Tooling and Casting Division
United States Gypsum, Bulletin No.TAC-206, 1979.

204. ANSI/ASTM C 842-76
Standard Specification for Application of Interior Gypsum Plaster.

205. Plaster and Gypsum Cements for the Ceramic Industry
United States Gypsum, Bulletin No.TAC-159/USG, 1978.

206. Nitto Gypsum Technical Information
Nitto Gypsum Division, Noritake Co., Ltd., Japan, 1985.

207. Industrial Tooling - Products and Techniques
Georgia Pacific Corporation, Georgia, 1984.

208. U.S.G. Industrial Plasters & Gypsum Cements
United States Gypsum, TAC-217/rev., 10-82.

209. Catalogue & Information 1986
South Western Industrial Plasters, Wiltshire.

210. REDA YOUSSEF, M. A. and DIETZ, A. G. H.
"Potentialities of Egyptian Gypsum for Housing".
Proceedings of the American Society of Civil Engineers, 107, ST4, 671-688, 1981.

211. Catalogue des méthodes d'essais des plâtres
Syndicat National des Industries du Plâtre, Paris, 1983.

212. VAN WYLEN, G. J.
"Fundamentals of Classical Thermodynamics". John Wiley & Sons, 1985.

213. NICOLLS, M. O.
"The measurement of the surface finish". De Beers Industrial Diamond Division, 1978.

214. Talysurf 10
Operator's Handbook
Rank Taylor Hobson, 1977.

215. ALMOND, E. A., ROEBUCK, B. and GEE, M. G.
"Mechanical testing of hard materials". Metals and Materials, 2, 2, 76-82, 1986.

216. SHOOK, W. B.
"Critical Survey of Mechanical Property Test Methods for Brittle Materials". AF Materials Laboratory, Technical Report No. ASD-TDR-63-491, 1963.

217. BORTZ, S. A. and LUND, H. H.
"The brittle ring test". Mechanical Properties of Engineering Ceramics, W. W. Kriegel and H. Palmour III, Eds., Interscience Publishers, 383-406, 1961.

218. SEDLACEK, R. and HALDEN, F. A.
"Method for Tensile Testing of Brittle Materials". Review Scientific Instrument, 33, 3, 298-300, 1962.

219. DAVIES, J. B. and BOSE, D. K.
"Stress distribution in splitting tests". Journal of the American Concrete Institute, 65, 8, 662-669, 1968.

220. CHEN, W. F.
"Double Punch Test for Tensile Strength of Concrete". Ibid., 67, 993-995, 1970.

221. JONES, R. L. and ROWCLIFFE, D. J.
"Tensile Strength Distribution for Silicon Nitride and Silicon Carbide Ceramics". American Ceramic Society Bulletin, 58, 836-844, 1979.

222. MARGETSON, J. and SHERWOOD, P. J.
"Statistical analysis of the brittle fracture of sintered tungsten". Journal of Materials Science, 14, 11, 2575-2580, 1979.

223. AWAJI, H. and SATO, S.
"Diametral compressive testing method". Trans. ASME, Journal of Engineering Materials and Technology, 101, 2, 139-147, 1979.

224. CHEN, W. F. and YUAN, R. L.
"Tensile strength of concrete : Double-punch test". Journal of the Structural Division, ASCE, 106, ST8, 1673-1693, 1980.

225. TRUSTRUM, K.
"Reply to comments on 'Estimating the Weibull modulus for a brittle material'". Journal of Materials Science, 17, 11, 3883, 1982.

226. FESSLER, H. and FRICKER, D. C.
"Multiaxial strength tests for brittle materials". Journal of Strain Analysis, 19, 3, 197-208, 1984.

227. BLIEM, C. et al.
"Ceramic Heat Exchanger Concept and Materials Technology". Noyes Publications, New Jersey, 1985.

228. GOVILA, R. K., HERMAN, J. A. and ARNON, N.
"Stress Rupture Test Rig Design for Evaluating Ceramic Material Specimens". ASME Paper No. 85-GT-181, 1985.

229. LENOE, E. M., NEAL, D., VANGEL, M., BOEHMER, M. and SIEBELS, J. E.
"Interlaboratory comparison of flexural strength of structural ceramics". ASME Paper No. 85-GT-225, 1985.

230. MESSIER, D. R., SCHIOLER, L. J. and QUINN, G. D.
"Fracture Behavior and Strength of Reaction-Bonded Si_3N_4 Turbine Shrouds". American Ceramic Society Bulletin, 60, 8, 812-817, 1981.

231. MESSIER, D. R., SCHIOLER, L. J., QUINN, G. D. and NAPIER, J. C.
"Fracture Analysis of Reaction-Bonded Silicon Nitride Turbine Shrouds". Army Materials and Mechanics Research Center, Watertown, Mass., Technical Report no. AMMRC TR 82-43, June 1982.

232. QUINN, G. D., MESSIER, D. R. and SCHIOLER, L. J.
"Characterization of Ceramic Vane Materials for the 10KW Turbo-alternator". Ibid., Technical Report No. AMMRC TR 83-18, April 1983.

233. NEWNHAM, R. C.
"Strength tests for brittle materials". Proceedings of British Ceramic Society, 25, 281-293, 1975.

234. HOAGLAND, R. G., MARSCHALL, C. W. and DUCKWORTH, W. H.
"Reduction of Errors in Ceramic Bend Tests". Journal of the American Ceramic Society, 59, 5-6, 189-192, 1976.

235. Flexural Strength of High Performance Ceramics at Ambient Temperatures.
Army Materials and Mechanics Research Center, Watertown, Mass., MIL-STD-1942(MR), 21 Nov. 1983.

236. MIL-STD-1942 Changes
Ibid., 15 March 1985.

237. QUINN, R. J., BARATTA, F. I. and CONWAY, J. A.
"Commentary on U.S. Army Standard Test Method for Flexural Strength of High Performance Ceramics at Ambient Temperature". Ibid., Technical Report No. AMMRC 85-21, August 1985.

238. BARATTA, F. I.
"Requirements for Flexure Testing of Brittle Materials". ASTM STP 844, 194-222, 1984.

239. DAVIES, D. G. S.
"The Statistical Approach to Engineering Design in Ceramics". Proceedings of British Ceramic Society, 22, 429-452, 1973.

240. SHAW, M. C., BRAIDEN, P. M. and DeSALVO, G. J.
"The Disk Test for Brittle Materials". Trans. ASME, Journal of Engineering for Industry, 97, Series B, 1, 77-87, 1975.

241. KATAYAMA, Y. and HATTORI, Y.
"Effects of Specimen Size on Strength of Sintered Silicon Nitride". Communications of the American Ceramic Society, C-164, 1982.

242. NEAL, D. M. and LENOE, E. M.
"Examination of size effects in the failure prediction of ceramic material". Fracture Mechanics of Ceramics, R. C. Bradt, A. G. Evans, D. P. H. Hasselman and F. F. Lange, Eds., 5, 387-401, 1983.

243. ROARK, R. J. and YOUNG, W. C.
"Formulas for Stress and Strain". McGraw Hill International Book co., 1975.

244. KAO, R., PERRONE, N. and CAPPS, W.
"Large-Deflection Solution of the Coaxial-Ring-Circular-Glass-Plate Flexure Problem". Journal of the American Ceramic Society, 54, 11, 566-571, 1971.

245. GIOVAN, M. N. and SINES, G.
"Biaxial and Uniaxial Data for Statistical Comparisons of a Ceramic's Strength". Ibid., 62, 9-10, 510-515, 1979.

246. RITTER, Jr. J. E., JAKUS, K., BATAKIS, A. and BANDYOPADHYAY, N.
"Appraisal of Biaxial Strength Testing". Journal of Non-Crystalline Solids, 38-39, 419-424, 1980.

247. MARSHALL, D. B.
"An Improved Biaxial Flexure Test for Ceramics". American Ceramic Society Bulletin, 59, 5, 551-553, 1980.

248. VITMAN, F. F., BARTENEV, G. M., PUKH, V. P. and TSEPKOV, L. P.
"A method for measuring the strength of sheet glass". Glass Ceram, 19, 8, 412-414, 1962.

249. VITMAN, F. F. and PUKH, V. P.
"A method for determining the strength of sheet glass". Industrial Laboratory, 29, 863-867, 1963.

250. SIMIU, E. et al.
"Ring-on-Ring Tests and Load Capacity of Cladding Glass". NBS Building Science Series 162, National Bureau of Standards, 1984.

251. SIMIU, E. and REED, D. A.
"Ring-on-Ring Tests and the Modelling of Cladding Glass Strength by the Weibull Distribution". IUTAM Symposium, S. Eggwertz and N. C. Lind, Eds., Springer-Verlag, Berlin, Heidelberg, 263-269, 1985.

252. WACHTMAN, Jr. J. B., CAPPS, W. and MANDEL, J.
"Biaxial Flexure Tests of Ceramic Substrates". Journal of Materials, JMLSA, 7, 2, 188-194, 1972.

253. SHETTY, D. K., ROSENFIELD, A. R., McGUIRE, P., BANSAL, G. K. and DUCKWORTH, W. H.
"Biaxial Flexure Tests for Ceramics". American Ceramic Society Bulletin, 59, 12, 1193-1197, 1980.

254. GAC, F. D. et al.
"Design Analysis of an Automotive Exhaust Gas Sensor". Ceramic Engineering and Science Proceedings, 1, 7-8, 593-608, 1980.

255. SHETTY, D. K., ROSENFIELD, A. R., BANSAL, G.K. and DUCKWORTH, W. H.
"Biaxial Fracture Studies of a Glass-Ceramic". Journal of the American Ceramic Society, 64, 1, 1-4, 1981.

256. WILLIAMS, R. M. and SWANK, L. R.
"Use of Weibull Statistics to Correlate MOR, Ball-on-Ring, and Rotational Fast Fracture Tests". Ibid., 66, 11, 765-768, 1983.

257. SHETTY, D. K., ROSENFIELD, A. R., DUCKWORTH, W. H. and HELD, P. R.
"A Biaxial-Flexure Test for Evaluating Ceramic Strengths". Ibid., 66, 1, 36-42, 1983.

258. SOLTESZ, U., RICHTER, H. and KIENZLER, R.
"The concentric-ring-test and its application for determining the surface strength of ceramics". High Tech Ceramics, P. Vincenzini, Ed., Elsevier Science Publishers B. V., 149-158, 1987.

259. FESSLER, H. and FRICKER, D. C.
"A Theoretical Analysis of the Ring-on-Ring Loading Disk Test". Journal of the American Ceramic Society, 67, 9, 582-588, 1984.

260. GODFREY, D. J.
"Fabrication, formulation, mechanical properties, and oxidation of sintered Si_3N_4 ceramics using disc specimens". Materials Science and Technology, 1, 7, 510-515, 1985.

261. STORY, J. R.
"Bonded Strain Gage Load Cells". Process Instruments and Control Handbook, D. M. Cosidine, Ed., McGraw-Hill Book Co., Third Edition, 7.32-7.38, 1985.

262. SCOTT, K. and OWENS, A.
"Instrumentation". Strain Gauge Technology, A. L. Window and G. S. Holister, Eds., Applied Science Publishers, 139-207, 1982.

263. POPLE, J.
"BSSM Strain Measurement Reference Book". The British Society for Strain Measurement, 1979.

264. MORDAN, G. C.
"Adhesives and Installation Techniques". Ibid.(262), 39-83, 1979.

265. Strain Gauge Installation with M-Bond 200 Adhesive Instruction Bulletin B-127-5. Welwyn Strain Measurement Limited, 1976.

266. WHEELER, P. M.
"Pafec : The Pafec Finite Element Analysis System". Structural Analysis Systems, A. Nikulari, Ed., Pergamon Press, Volume 1, 151-159, 1986.

267. DINEEN, K. J.
"Application of the Pafec 75 Software Package". National Physical Laboratory, Technical Report No.QU66, August 1983.

268. Data Preparation.
User Manual Level 6.1, Pafec Ltd., 1984.

269. ROCKEY, K. C., EVANS, H. R., GRIFFITHS, D. W. and NETHERCOT, D. A.
"The Finite Element Method". Granada Publishing Ltd., 1983.

270. RICE, R. W.
"Ceramic Fracture Features, Observations, Mechanism, and Uses". ASTM STP 827, 5-103, 1984.

271. L'ECRIVAIN, L. and LAMBERT, B.
"Application de 'L'essai brésilien' à l'étude des produits céramiques". L'industrie Céramique, 534, 367-372, 1961.

272. McNEELY, D. J. and LASH, S. D.
"Tensile Strength of Concrete". Journal of the American Concrete Institute, 60, 6, 751-761, 1963.

273. SRINIVASAN, M. and SESHADRI, S. G.
"Probabilistic Design and Reliability of Silicon Carbide Ceramics". Journal of Mechanical Design, 635-642, 1982.

274. BROCH, E. and FRANKLIN, J. A.
"The Point-load Strength Tests". International Journal of Rock Mechanics and Mineral Science, 9, 6, 669-697, 1972.

275. De WITH, G.
"Note on the use of the diametral compression test for the strength measurement of ceramics". Journal of Materials Science Letters, 3, 11, 1000-1002, 1984.

276. FERBER, M. K., TENNERY, V. J., WATERS, S. B. and OGLE, J.
"Fracture strength characterization of tubular ceramic materials using a simple C-ring geometry". Journal of Materials Science, 21, 8, 2628-2632, 1986.

277. ALMOND, E. A., ROEBUCK, B. and GEE, M. G.
"Mechanical testing of hard materials". Metals and Materials, 2, 2, 76-82, 1986.

278. GRIEB, W. E. and WERNER, G.
"Comparison of splitting tensile strength of concrete with flexural and compressive strength". Proceedings of ASTM, 62, 972-995, 1962.

279. WRIGHT, P. J. F.
"Comments on an indirect tensile test on concrete cylinders". Magazine of Concrete Research, 87-96, 1955.

280. THAULOW, S.
"Tensile Splitting Test and High Strength Concrete Test Cylinders". Journal of the American Concrete Institute, 53, 699-706, 1957.

281. ABELES, P. W.
"Discussion of a paper by Sven Thaulow : Tensile Splitting Test and High Strength Concrete Test Cylinders". Ibid., 53, 1315-1325, 1957.

282. HONDROS, G.
"The evaluation of Poisson's ratio and the modulus of materials of a low tensile resistance by the Brazilian (Indirect tensile) test with particular reference to concrete". Australian Journal of Applied Science, 10, 243-268, 1959.

283. MITCHELL, N. B.
"The Indirect Tension Test for Concrete". Materials Research & Standards, 1, 10, 780-788, 1961.

284. SPOONER, D. C.
"Measurement of the Tensile Strength of Concrete by an Indirect Method. The Cylinder Splitting Test". Cement and Concrete Association, Technical Report TRA 419, May 1969.

285. VARDAR, O. and FINNIE, I.
"An analysis of the Brazilian disc fracture test using Weibull probabilistic treatment of brittle strength". International Journal of Fracture, 11, 3, 495-508, 1975.

286. BERENBAUM, R. and BRODIE, I.
"Measurement of the tensile strength of brittle materials". British Journal of Applied Physics, 10, 281-287, 1959.

287. PRICE, H. L. and MURRAY, K. H.
"Finite Element Analysis of the Diametral Test of Polymer Moldings". Trans. ASME, Journal of Engineering Materials and Technology, 95, Series H, 3, 186-191, 1973.

288. ODA, J. and YAMAZAKI, K.
"On the New Indirect Tension Test of Brittle Materials". Trans. JSME, 44, 378, 478-484, 1978.

289. TSURUSAKI, A. and ODA, J.
"An Evaluation Method for the Tensile Strength of Britlle Materials by means of New Indirect Tension Test". Ibid., 50, 453, 1062-1067, 1984.

290. SPRIGGS, R. M., BRISSETTE, L. A. and VASILOS, T.
"Tensile Strength of Dense Polycrystalline Ceramics by the Diametral-Compression Test". Materials Research & Standards, 4, 218-220, 1964.

291. MARION, R. H. and JOHNSTONE, J. K.
"A Parametric Study of the Diametral Compression Test for Ceramics". American Ceramic Society Bulletin, 56, 11, 998-1002, 1977.

292. FROCHT, M. M.
"Photoelasticity". John Wiley & Sons, Inc., Volume 2, 1948.

293. RUDNIK, A., HUNTER, A. R. and HOLDEN, F. C.
"An Analysis of the Diametral-Compression Test". Materials Research & Standards, 3, 4, 283-289, 1963.

294. KITTL, P. and ALDUNATE, R.
"Compression fracture statistics of compacted cement cylinder". Journal of Materials Science, 18, 2947-2950, 1983.

295. AWAJI, H.
"Brittle Fracture under Compressive Stresses". Bulletin of the JSME, 25, 203, 713-719, 1982.

296. BAGLEY, E. B., CHRISTIANSON, D. D. and WOLF, W. J.
"Frictional Effects in Compressional Deformation of Gelatin and Starch Gels and Comparison of Material Response in Simple Shear, Torsion, and Lubricated Uniaxial Compression". Journal of Rheology, 29, 1, 103-108, 1985.

297. BROWN, Jr. W. F. and SRAWLEY, J. E.
"Plane Strain Crack Toughness Testing of High Strength Metallic Materials". ASTM STP 410, 1966.

298. DAVIDGE, R. W. and TAPPIN, G.
"The Effects of Temperature and Environment on the Strength of Two Polycrystalline Aluminas". Proceedings of British Ceramic Society, 47-60, 1970.

299. BARNBY, J. T. and TAYLOR, R. A.
"The Fracture Resistance of Reaction-Sintered Silicon Nitride". Special Ceramics 5, P. Popper, Ed., British Ceramic Association, 311-328, 1972.

300. SIMPSON, L. A.
"Use of the Notched-Beam Test for Evaluation of Fracture Energies of Ceramics". Journal of the American Ceramic Society, 57, 4, 151-154, 1974.

301. ROSE, A. P. G.
"Evaluation of Fracture Toughness of Nuclear Graphite". Proceedings 'Carbonne 84', Bordeaux, 416-417, 1984.

302. JENQ, Y. S. and SHAH, S. P.
"A Fracture Toughness Criterion for Concrete". Engineering Fracture Mechanics, 21, 5, 1055-1069, 1985.

303. BROWN, J. H.
"Measuring the fracture toughness of cement paste and mortar". Magazine of Concrete Research, 24, 185-196, 1972.

304. COOK, D. J. and CROOKHAM, G. D.
"Fracture toughness measurements of polymer concretes". Ibid., 30, 205-214, 1978.

305. CARPINTERI, A.
"Mechanical Damage and Crack Growth in Concrete". Martinus Nijhoff Publishers, Dordrecht, 1986.

306. JENQ, Y. S. and SHAH, S. P.
"A Two Parameter Fracture Model for Concrete". Internal Report, Northwestern University, Evanston, Illinois, 1985.

307. COTTEREL, B. and MAI, Y. W.
"Crack growth resistance curve and size effect in the fracture of cement paste". Journal of Materials Science, 22, 2734-2738, 1987.

308. CARPINTERI, A.
"Notch sensitivity in fracture testing of aggregative materials". Engineering Fracture Mechanics, 16, 4, 467-481, 1982.

309. ASHBY, M. F. and JONES, D. R. H.
"Engineering Materials". Pergamon Press, 1980.

310. WILLIAMS, J. G.
"Fracture Mechanics of Polymers and Adhesives". Fracture of Non-Metallic Materials, K. P. Herrman and L. H. Larsson, Eds., D. Reidel Publishing Co., 227-255, 1987.

311. AAMODT, B.
"Application of the finite element method to problems in linear and nonlinear fracture mechanics". Report No.74-1, The Norwegian Institute of Technology, University of Trondheim, Norway, 1974.

312. CARTWRIGHT, D. J. and ROOKE, D. P.
"Evaluation of Stress Intensity Factors". Journal of Strain Analysis, 10, 4, 217-224, 1975.

313. CHELL, G. G.
"Some sub-critical crack growth parameters and their evaluation". CEGB Report No.RD/L/R2007, 1981.

314. PARKER, A. P.
"The Mechanics of Fracture and Fatigue". E.& F. N. Spon Ltd., London, 1981.

315. ZIENKIEWICZ, O. C.
"The Finite Element Method". McGraw Hill Book Co.(UK) Ltd., 1977.

316. PARIS, P. C. and SIH, G. C.
"Stress Analysis of Cracks". ASTM STP 381, 30-83, 1965.

317. BANKS-SILLS, L. and SHERMAN, D.
"Comparison of methods for calculating stress intensity factors with quarter-point elements". International Journal of Fracture, 32, 2, 127-140, 1986.

318. NALLATHAMBI, P. and KARIHALOO, B. L.
"Stress Intensity Factor and Energy Release Rate for Three-point Bend Specimens". Engineering Fracture Mechanics, 25, 3, 315-321, 1986.

319. GO, C. G., SWARTZ, S. E. and HU, K. K.
"Stress Intensity Factors for Single-Edge-Notch Beam". Journal of Engineering Mechanics, 110, 4, 629-632, 1984.

320. BALKEY, K. R., MEYER, T. A. and WITT, F. J.
"Probabilistic Structural Mechanics : Chances are...". Mechanical Engineering, 108, 7, 56-62, 1986.

321. DERBALIAN, G.
"Successful Failure Analysis using Finite Elements". Ibid., 108, 9, 76-83, 1986.

322. CHAN, S. K., TUBA, I. S. and WILSON, W. K.
"On the finite element methods in linear fracture mechanics". Engineering Fracture Mechanics, 2, 1-17, 1970.

323. HU, K. K., HUANG, C. M. J. and SWARTZ, S. E.
"Finite Element Model to Determine K_I ". Journal of Engineering Mechanics, 109, 4, 1103-1113, 1983.

324. GROSS, B. and SRAWLEY, J. E.
"Stress-Intensity Factors for Three-Point Bend Specimens by Boundary Collocation". NASA Technical Note TN D-3092, December 1965.

325. McCLINTOCK, F. A. and ZAVERL, Jr. F.
"An analysis of the mechanics and statistics of brittle crack initiation". International Journal of Fracture, 15, 2, 107-118, 1979.

326. BATDORF, S. B.
"Fundamentals of the Statistical Theory of Fracture". Fracture Mechanics of Ceramics, R. C. Bradt, D. P. H. Hasselman and F. F. Lange, Eds., Plenum Press, 3, 1-29, 1977.

327. SHETTY, D. K., ROSENFIELD, A. R. and DUCKWORTH, W. H.
"Biaxial Stress State Effects on Strength of Ceramics Failing from Pores". Ibid., 5, 531-542, 1983.

328. SHETTY, D. K., ROSENFIELD, A. R. and DUCKWORTH, W. H.
"Statistical Analysis of Size and Stress State Effects on the Strength of an Alumina Ceramic". ASTM STP 844, 57-80, 1984.

APPENDIX A

NUMERICAL CALCULATION OF THE WEIBULL THEORY FOR BIAXIAL STRESSES ON PLASTER

The risk of rupture B′ is defined by (section 3.1.4) :

$$B' = 4K_1\sigma_1^m \int_0^{\pi/2} \cos^{2m+1}\phi \, d\phi \int_{-\psi_o}^{\psi_o} (\cos^2\psi + c^2\sin^2\psi)^m \, d\psi$$

A numerical example with m = 3, c^2 = 0.8 was performed in order to check the accuracy of the computer code in calculating the above integrals

$$\int_0^{\pi/2} \cos^{2m+1}\phi \, d\phi = \int_0^{\pi/2} \cos^7\phi \, d\phi = \frac{2.4.6}{3\cdot5\cdot7} = \frac{48}{105} = 0\cdot4571$$

With $c^2 = 0.8 > 0$, the second integral can be written as

$$\int_{-\psi_o}^{\psi_o} (\cos^2\psi + c^2\sin^2\psi)^m \, d\psi = \int_0^{\pi/2} (1 - k^2\sin^2\psi)^m \, d\psi$$

where $k^2 = 1-c^2 = 1-0.8 = 0.2$

Using the binomial theorem, the integral can be expanded as

$$\int_0^{\pi/2} (1 - k^2\sin^2\psi)^m \, d\psi = \int_0^{\pi/2} \left[1 - mk^2\sin^2\psi + \frac{m(m-1)}{2!}k^4\sin^4\psi - \frac{m(m-1)(m-2)}{3!}k^6\sin^6\psi + \cdots\right] d\psi$$

With m = 3 the integral becomes

$$\int_0^{\pi/2} (1 - 0\cdot6\sin^2\psi + 0\cdot12\sin^4\psi - 8\times10^{-3}\sin^6\psi) \, d\psi = 1\cdot1663$$

A computer code which called the subroutine D01AKF of the NAG Library (170) was developed to compute these two integrals. The results with m = 3, c^2 = 0.8, and the relative accuracy of 1/1000 were outputted.

$$\int_0^{\pi/2} \cos^7\phi \, d\phi = 0\cdot4571$$

$$\int_0^{\pi/2} (\cos^2\psi + 0\cdot8\sin^2\psi)^3 \, d\psi = 1\cdot1663$$

It can be seen that a very good agreement was obtained.

The computer code was used to compute these two integrals with different values of c^2 and m = 7. The risk of fracture in the biaxial stress state was then computed.

In assuming that both the biaxial and uniaxial stress states have the same total risk of fracture, we have

$$\frac{B_B}{B_t} = \frac{4 k_1 \sigma_1^m V \int_0^{\pi/2} \cos^{2m+1}\phi \, d\phi \int_{-\psi_o}^{\psi_o} (\cos^2\psi + c^2 \sin^2\psi)^m \, d\psi}{k \sigma_t^m V} = 1$$

where $k_1 = \frac{2m+1}{2\pi} k$

σ_1 is the maximum pricipal stress

σ_t is the fracture strength in simple tension

With m and c^2 are now known, the ratio of σ_1/σ_t can be obtained, so can the σ_2/σ_t ratio. These ratios were presented in Table 3.1.

APPENDIX B

NUMERICAL CALCULATION OF THE PROBABILITY OF FAILURE FOR THE UNIAXIAL COMPRESSION TEST

Stanley et al.(173) have proposed an equation for the failure probability distribution of specimens subjected to uniform uniaxial compressive stress.

$$P_f = 1 - \exp\left[- \left(\frac{1}{m}!\right)^m \left(\frac{1}{\bar{\sigma}_{fv}}\right)^m \left(\frac{V_c}{v}\right) \left(\frac{\sigma}{H(\sigma)}\right)^m \right]$$

The first function [(1/m)!] is associated with strength variability

$$\left(\frac{1}{m}!\right)^m = \Gamma\left(1+\frac{1}{m}\right)^m = \Gamma\left(1{\cdot}1499\right)^{6{\cdot}6723} = 0{\cdot}6296$$

Where

Γ is the Gamma function. The Gamma function can be read from table (174), graph (99), or can be computed by using a subroutine (175). The subroutine S14AAF of the NAG Library has been used to obtain the values of Gamma functions.

m is the Weibull modulus obtained from least-squares analysis of section 3.2.2.

The second function $(1/\bar{\sigma}_{fv})^m$ is derived from a calibration test of the four-point beam bending (section 4.3.2).

$$\bar{\sigma}_{nom} = 5{\cdot}5338$$

$$\sigma(V) = \frac{m+3}{6(m+1)^2} = 0{\cdot}0274$$

$$V = Lbd = 1{\cdot}38 \times 10^{-5}\ m^3$$

$$\bar{\sigma}_{fv} = \bar{\sigma}_{nom} \left[\frac{V\,\sigma(V)}{v}\right]^{1/m} = 0{\cdot}6032$$

Where

$\bar{\sigma}_{nom}$ is the mean value of the nominal failure stress.

$\sigma(V)$ is the stress-volume integral.

V is the volume of the beam.

$\bar{\sigma}_{fv}$ is the mean tensile fracture stress of unit volume of the material.

The step function $H(\sigma)$ is determined by

$$H(\sigma) = \frac{\sigma_c}{\sigma_t} = \frac{12{\cdot}7891}{5{\cdot}5338} = 2{\cdot}3111$$

$$V_c = \frac{\pi d^2}{4} h = 2{\cdot}1715 \times 10^{-5}\ m^3$$

It follows that

$$P_f = 1 - \exp\left(-1{\cdot}4899 \times 10^{-6}\ \sigma^{6{\cdot}6723}\right)$$

APPENDIX C

NUMERICAL CALCULATION OF THE PARAMETERS REQUIRED FOR STRESS INTEGRAL COMPUTATION

The failure probability of brittle component depends on the mean strength and the variability of strength of the material, the shape and size of the component, as well as the type and magnitude of the loads. All these effects are incorporated in the four-function Weibull equation (173).

$$P_f = 1 - \exp\left[-\left(\frac{1}{m}!\right)^m \left(\frac{\sigma_{nom}}{\bar{\sigma}_{fv}}\right)^m \left(\frac{V_B}{v}\right) \Sigma(V) \right]$$

Where

m is the Weibull modulus.

σ_{nom} is the nominal stress.

$\bar{\sigma}_{fv}$ is the mean tensile fracture of unit volume of the material.

$\Sigma(V)$ is the stress-volume integral.

V_B is the volume of the disc.

$$V_B = \frac{\pi d^2}{4} t = 1{\cdot}964 \times 10^{-6}$$

An alternative approach is possible in which it is assumed that all fracture begins on the surface of the stressed body. With this assumption the general form of the four-function Weibull equation becomes

$$P_f = 1 - \exp\left[-\left(\frac{1}{m}!\right)^m \left(\frac{\sigma_{nom}}{\bar{\sigma}_{fa}}\right)^m \left(\frac{A_B}{a}\right) \Sigma(A) \right]$$

Where

$\bar{\sigma}_{fa}$ is the mean tensile fracture stress of unit surface area of the material.

$\Sigma(A)$ is the stress-area integral.

A_B is the total surface of the disc.

$A_B = 1{\cdot}296 \times 10^{-3}$

With third point bending, $m = 3$

$$\sigma(A) = \frac{1}{4} \times \frac{1}{(m+1)^2} \left(1 + \frac{bm}{b+d}\right) \cdot 4n + 2(m+1)(1-2n)$$

$$\sigma(A) = 5 \cdot 1395$$

$$A = 2L(b+d) = 5 \cdot 52 \times 10^{-3}$$

$$\bar{\sigma}_{fa} = \bar{\sigma}_{nom} \left[\frac{A\sigma(A)}{a}\right]^{1/m} = 3 \cdot 2445$$

APPENDIX D

STRESS INTEGRAL FOR A BRAZILIAN DISC

The output files which contain the principal stresses and model geometry data for a Brazilian disc using the finite element package (PAFEC 75 - Level 6.1) were modified by inputting the Weibull modulus (m), step function [$H(\sigma)$], disc thickness (t), and material constant (k).

From Appendix B :

$$H(\sigma) = 2.3111$$

The material constant k is computed from (171)

$$\frac{\sigma_B}{\sigma_t} = \left(\frac{1}{2}\right)^{1/k}$$

Where

σ_B is the mean fracture strength in equibiaxial stress state.

σ_t is the mean fracture strength in uniaxial tension.

Hence

$$\frac{4{\cdot}9425}{5{\cdot}5338} = \left(\frac{1}{2}\right)^{1/k} \text{ or } \quad k = 6{\cdot}1395$$

A post-processing computer code was used to access these files. Each averaged stress was divided by the appropriate value of the step function $H(\sigma)$, raised to the exponent k and multiplied by the Jacobian D to determine the stress at the Gauss point.

$$\sigma_{Gauss} = \left[\frac{\sigma_{ave}}{H(\sigma)}\right]^k \cdot D$$

The Gaussian stress was then substituted in

$$I_V = \sum_{n=1}^{N} \sum_{j=1}^{4} \sum_{i=1}^{2} \left(\sigma_{Gauss}\right)^{m/k} \cdot t$$

A similar procedure was followed for the stress-area integral except that the Gaussian stress was not multiplied by the disc thickness.

$$I_a = \sum_{n=1}^{N} \sum_{j=1}^{4} \sum_{i=1}^{2} \left(\sigma_{Gauss}\right)^{m/k}$$

Where

i is the number of Gaussian stresses.

j is the sampling points.

N is the number of elements.

t is the disc thickness.

A flow chart for the procedure to be used is shown in Fig. D.1. The ouput of the programme, when run with the above data :

$$I_v = 4.7224 \times 10^{20}$$

$$I_a = 1.1806 \times 10^{23}$$

Because the stress analysis was performed on a quarter disc, the stress-volume integral is

$$\Sigma(V) = \frac{4 I_v}{V_B \bar{\sigma}_{nom}^{m}}$$

and the stress-area integral is

$$\Sigma(A) = \frac{4 I_a}{A_B \bar{\sigma}_{nom}^{m}}$$

Where

V_B is the volume of the disc.

A_B is the surface of the disc.

$\bar{\sigma}_{nom}$ is the mean value of the nominal failure stress.

m is the Weibull modulus.

The failure probability of the Brazilian disc test can now be written as

$$P_f = 1 - \exp\left[-\left(\frac{1}{m}!\right)^{m} \left(\frac{\sigma_{nom}}{\bar{\sigma}_{fv}}\right)^{m} \left(\frac{V_B}{V}\right) \Sigma(V) \right]$$

$$P_f = 1 - \exp\left[-1{\cdot}035\ \sigma_{nom}^{6{\cdot}6723} \right]$$

If the flaws were assumed surface-distributed :

$$P_f = 1 - \exp\left[-\left(\frac{1}{m}!\right)^{m} \left(\frac{\sigma_{nom}}{\bar{\sigma}_{fa}}\right)^{m} \left(\frac{A_B}{a}\right) \Sigma(A) \right]$$

$$P_f = 1 - \exp\left[-4{\cdot}906 \times 10^{-4}\ \sigma^{6{\cdot}6723} \right]$$

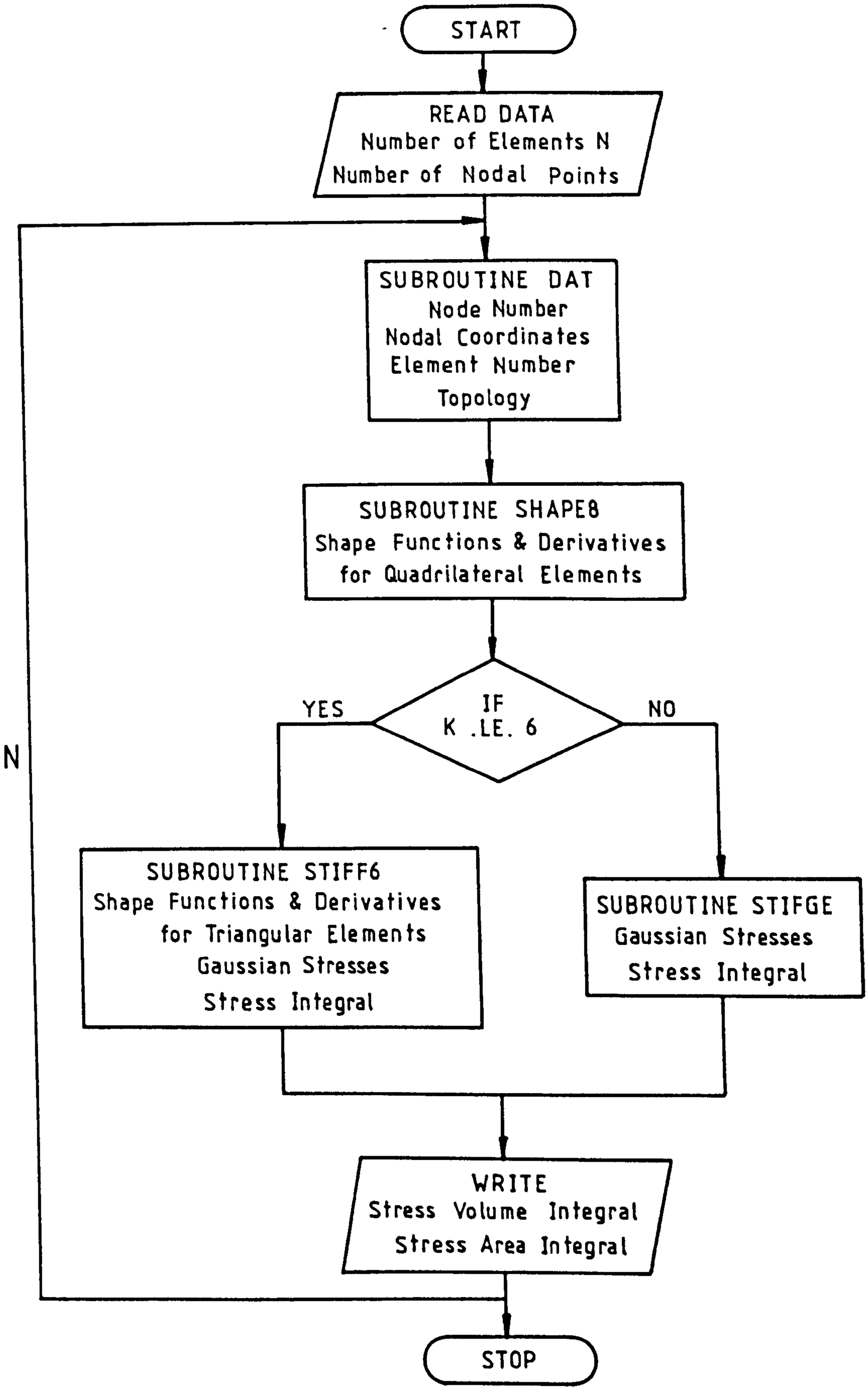

FIG. D.1 FLOW CHART OF THE METHOD OF COMPUTING STRESS INTEGRAL

APPENDIX E

DERIVATION OF THE LOAD FACTOR K_v

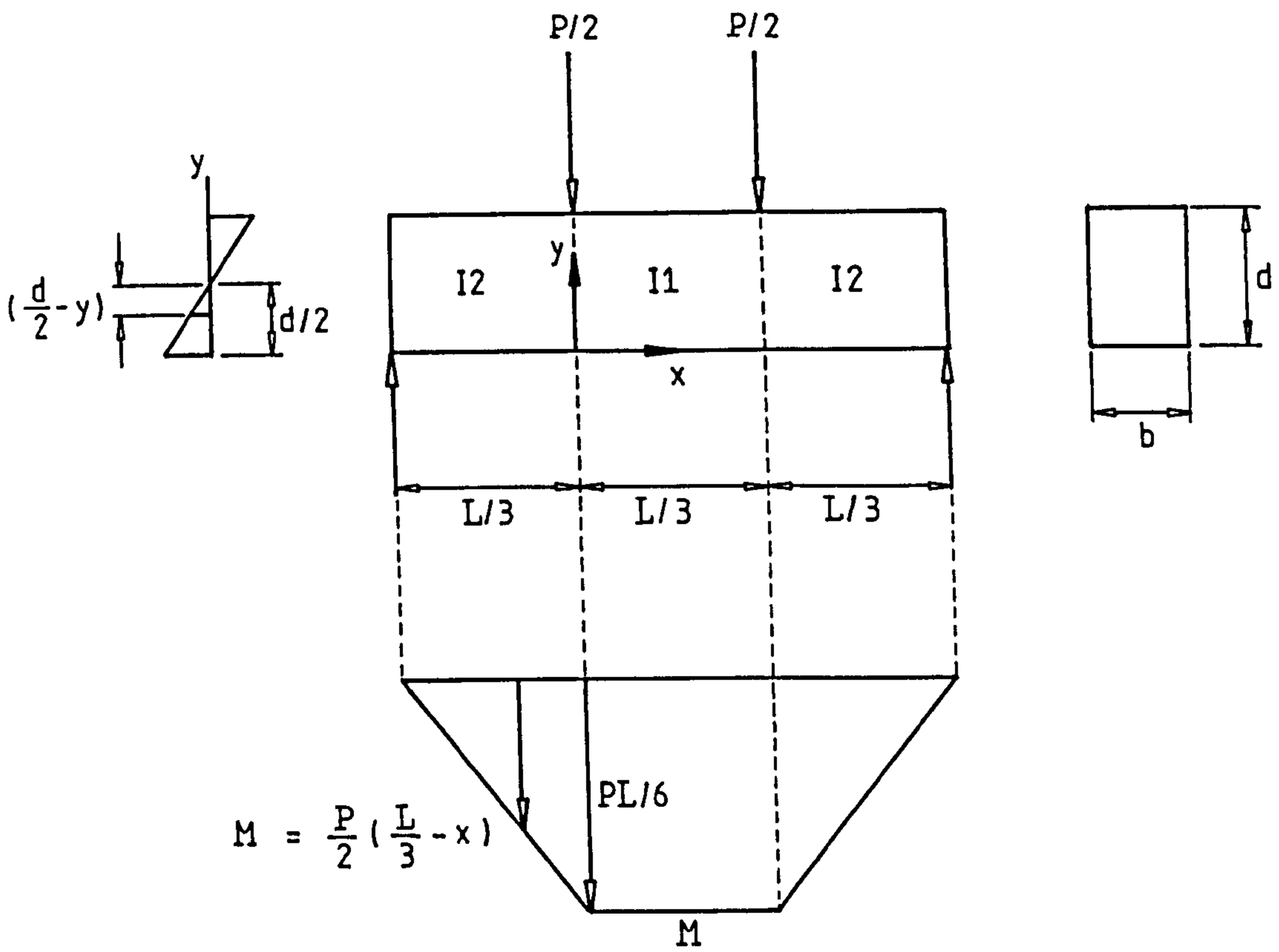

The Weibull distribution function relates the cumulative probability of failure (P_f) to the volume (V) under the tensile stress(σ) with two parameters, the Weibull modulus (m), and a normalizing constant (σ_o) as follows

$$P_f = 1 - \exp\left[- \int_V \left(\frac{\sigma}{\sigma_o}\right)^m dV \right] = 1 - \exp\left[- I_{total} \right]$$

Where $I_{total} = I_1 + 2I_2$

The bending stress is obtained from simple beam theory :

$$\sigma = \frac{M}{I} \cdot c = \frac{M}{I}\left(\frac{d}{2} - y\right)$$

Where

I is the moment of inertia of the section of the beam with respect to the neutral axis.

c is the distance from the neutral axis.

For $L/3 \geqslant x > 0$

$$M = PL/6 \qquad V = bdL/3$$

$$\sigma = PL/6I(d/2 - y) \qquad dV = bdyL/3$$

The maximum stress σ_{max} occurs at $y = 0$

$$\sigma_{max} = PLd/12I$$

Hence

$$\frac{\sigma}{\sigma_{max}} = \frac{PL}{6I}\left(\frac{d}{2} - y\right)\cdot\frac{12I}{PLd} = 1 - \frac{2y}{d}$$

$$I_1 = \int_V \left(\frac{\sigma}{\sigma_o}\right)^m dV = \left(\frac{\sigma_{max}}{\sigma_o}\right)^m \int_V \left(\frac{\sigma}{\sigma_{max}}\right)^m dV = \left(\frac{\sigma_{max}}{\sigma_o}\right)^m \int_V \left(1 - \frac{2y}{d}\right)^m dV$$

$$= \frac{bL}{3}\left(\frac{\sigma_{max}}{\sigma_o}\right)^m \int_0^{d/2} \left(1 - \frac{2y}{d}\right)^m dy$$

Through the change of variable

$$u = 1 - (2y/d)$$

I_1 becomes

$$I_1 = -\frac{bdL}{6}\left(\frac{\sigma_{max}}{\sigma_o}\right)^m \int_1^0 u^m du = \frac{bdL}{6(m+1)}\left(\frac{\sigma_{max}}{\sigma_o}\right)^m$$

For $0 > x \geqslant -L/3$

$$M = P/2(L/3 - x) \qquad V = bdL/3$$

$$\sigma = P/2I(L/3 - x)(d/2 - y) \qquad dV = bdydx$$

$$\frac{\sigma}{\sigma_{max}} = \frac{P}{2I}\left(\frac{L}{3} - x\right)\left(\frac{d}{2} - y\right)\frac{12I}{PLd} = \left(1 - \frac{3x}{L}\right)\left(1 - \frac{2y}{d}\right)$$

$$I_2 = \int_V \left(\frac{\sigma}{\sigma_o}\right)^m dV = \left(\frac{\sigma_{max}}{\sigma_o}\right)^m \int_V \left(\frac{\sigma}{\sigma_{max}}\right)^m dV$$

$$= \left(\frac{\sigma_{max}}{\sigma_o}\right)^m \int_0^{d/2} \int_0^{L/3} \left(1 - \frac{3x}{L}\right)^m \left(1 - \frac{2y}{d}\right)^m b\, dx\, dy$$

$$= b\left(\frac{\sigma_{max}}{\sigma_o}\right)^m \int_0^{d/2} \int_0^{L/3} \left(1 - \frac{3x}{L}\right)^m \left(1 - \frac{2y}{d}\right)^m dx\, dy$$

With the change of variables

$$u = 1 - (3x/L)$$

and

$$v = 1 - (2y/d)$$

I_2 is transformed into

$$I_2 = \frac{bdL}{6}\left(\frac{\sigma_{max}}{\sigma_o}\right)^m \int_1^0 \int_1^0 u^m v^m \, du \, dv$$

$$= \frac{bdL}{6}\left(\frac{\sigma_{max}}{\sigma_o}\right) \frac{1}{(m+1)^2}$$

The risk of fracture is finally obtained :

$$I_{total} = I_1 + 2I_2 = bdL\frac{m+3}{6(m+1)^2}\left(\frac{\sigma_{max}}{\sigma_o}\right)^m$$

and

$$P_f = 1 - \exp\left[-I_{total}\right] = 1 - \exp\left[-V\frac{m+3}{6(m+1)^2}\left(\frac{\sigma_{max}}{\sigma_o}\right)^m\right]$$

Hence the load factor

$$K_v = m+3 \;/\; \left[6(m+1)^2\right]$$

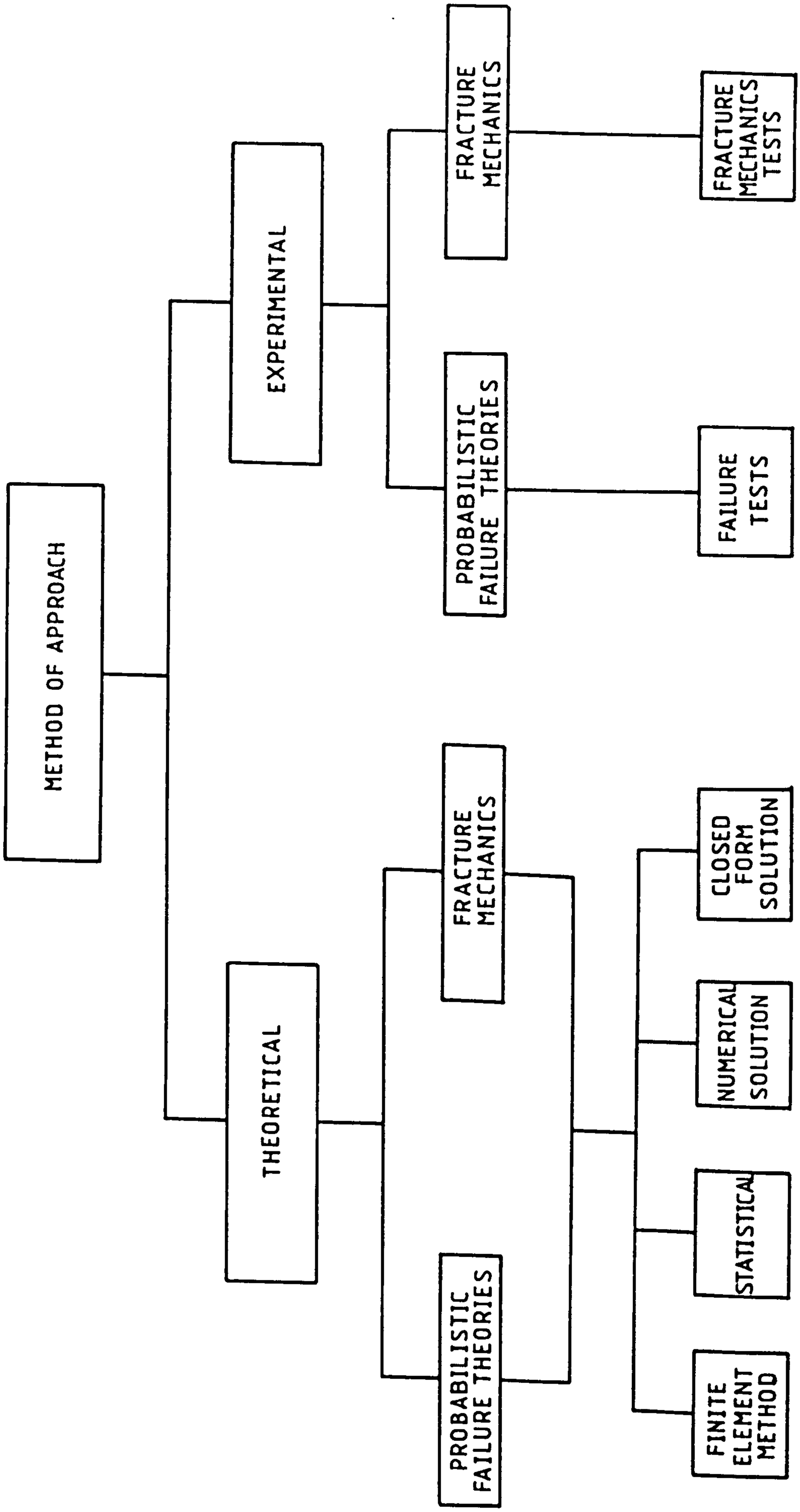

FIG. 1.1 BLOCK DIAGRAM SUMMARIZING THE METHOD OF APPROACH

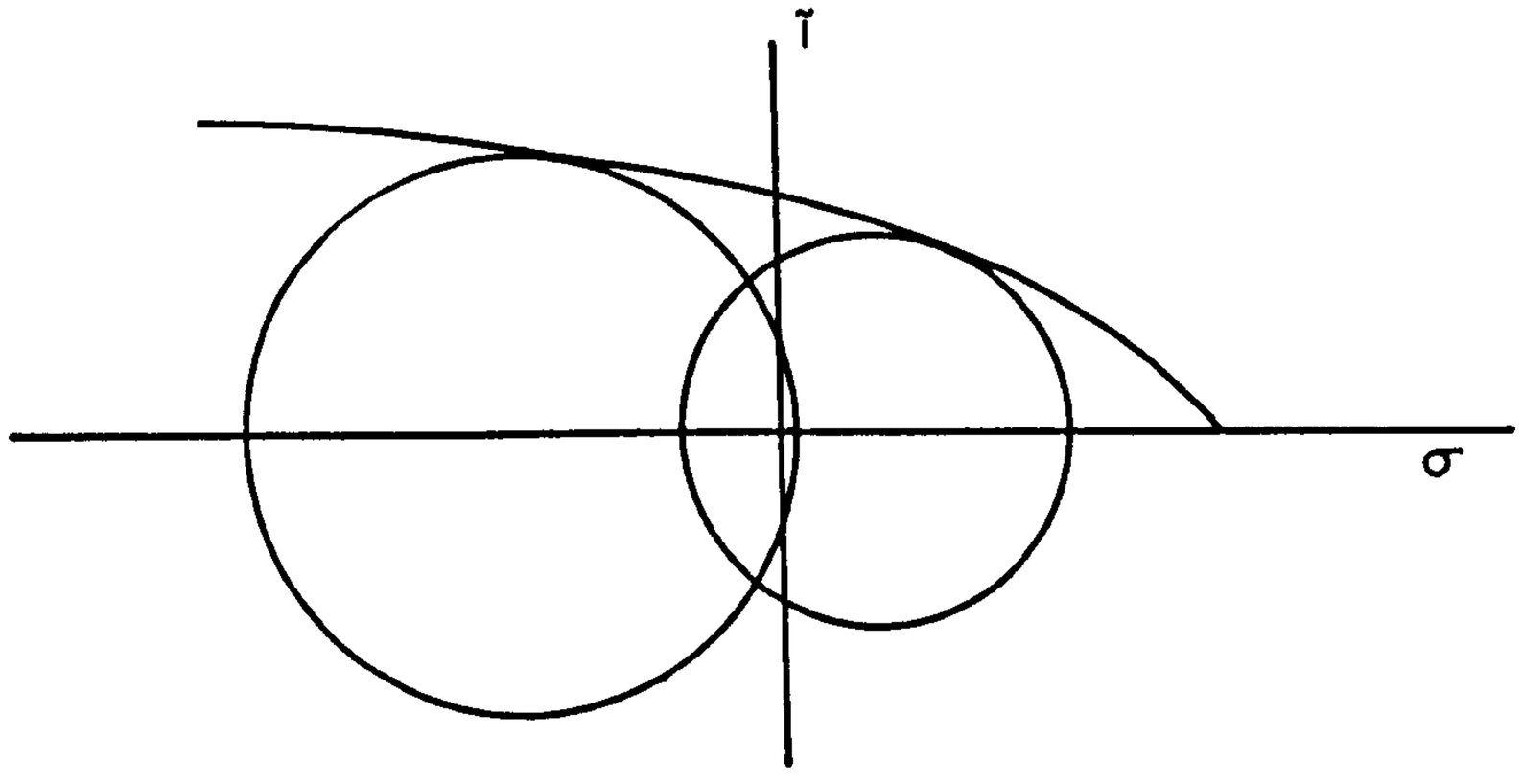

FIG. 2.1 MOHR STRENGTH ENVELOPE

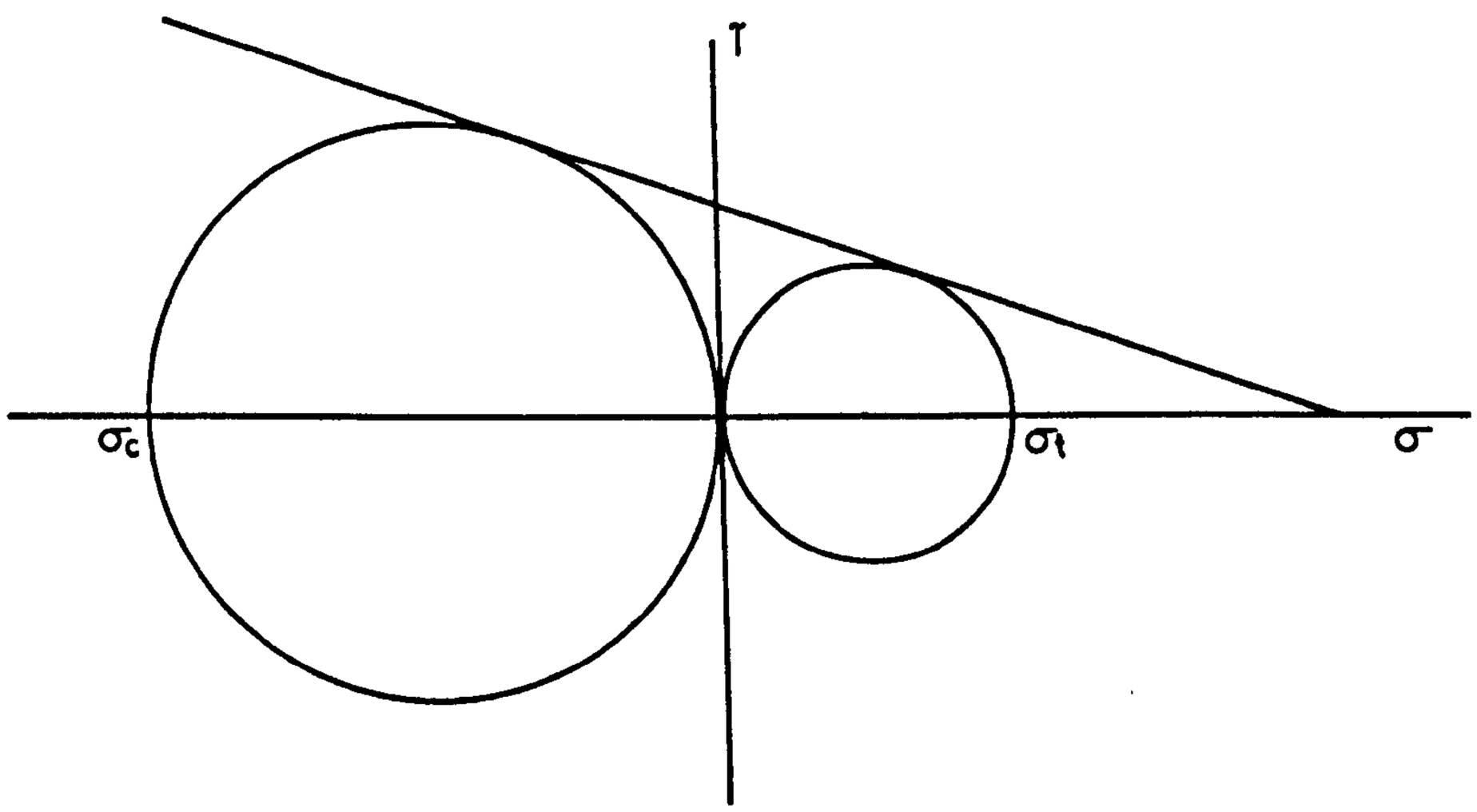

FIG. 2.2 SIMPLIFIED MOHR STRENGTH ENVELOPE

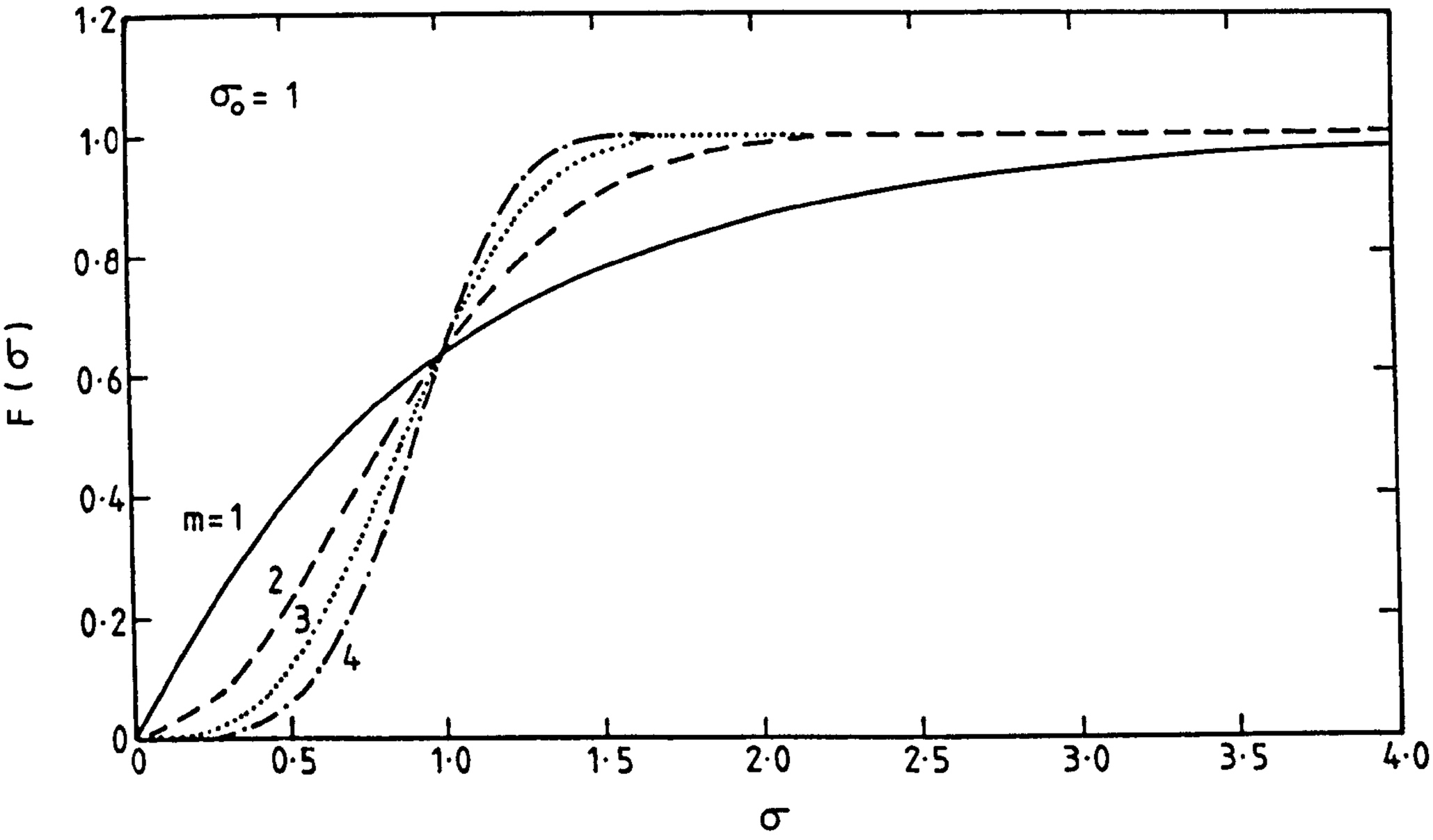

FIG. 2.3 CALCULATED WEIBULL CDF CURVES WITH
(a) INCREASING WEIBULL MODULI
(b) INCREASING SCALE PARAMETERS

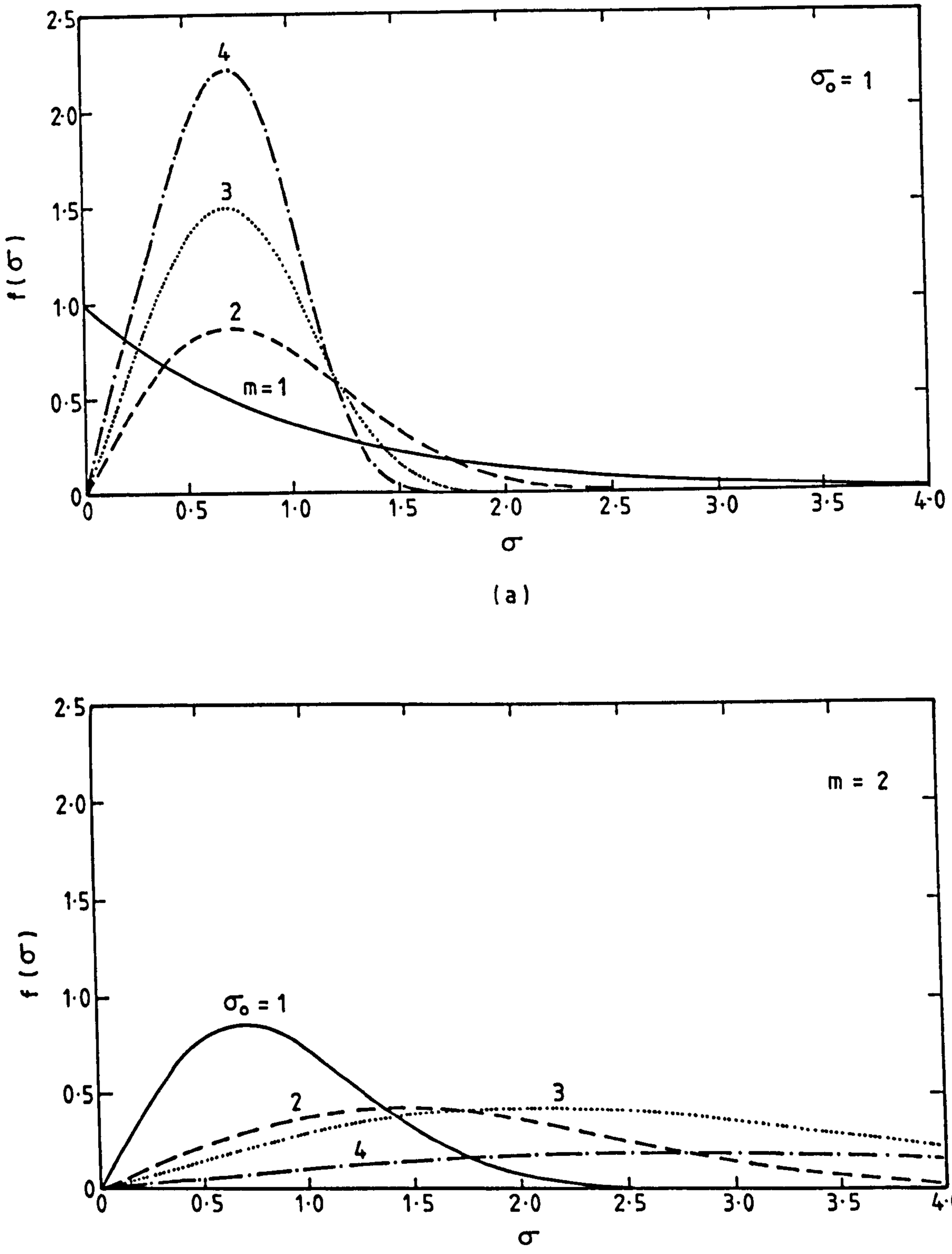

FIG. 2.4 CALCULATED WEIBULL PDF CURVES WITH
(a) INCREASING WEIBULL MODULI
(b) INCREASING SCALE PARAMETERS

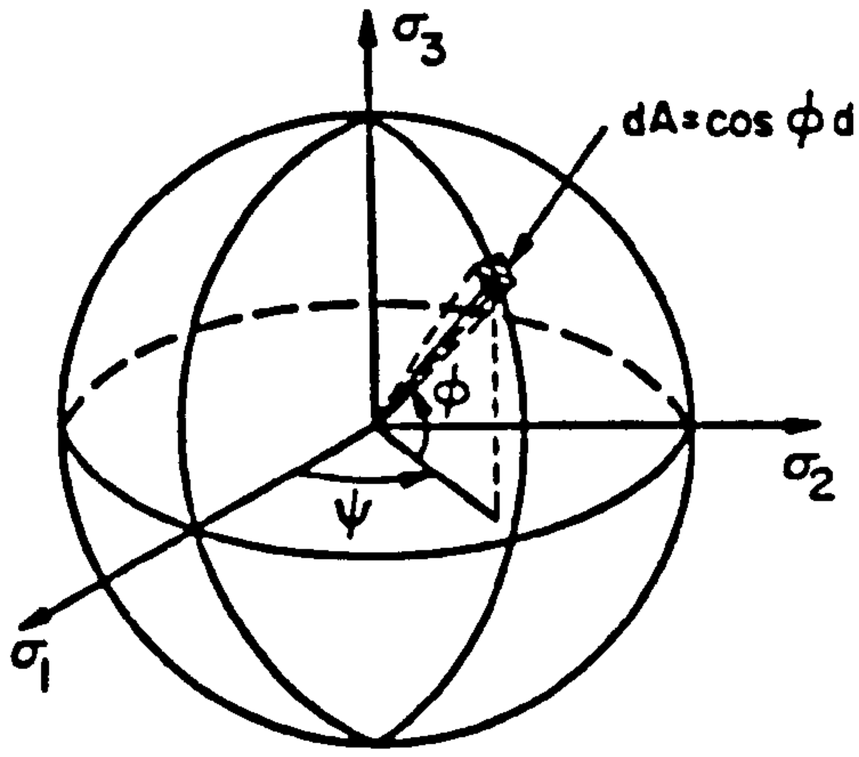

FIG. 2.5(a) GEOMETRIC VARIABLES DESCRIBING LOCATION ON UNIT SPHERE

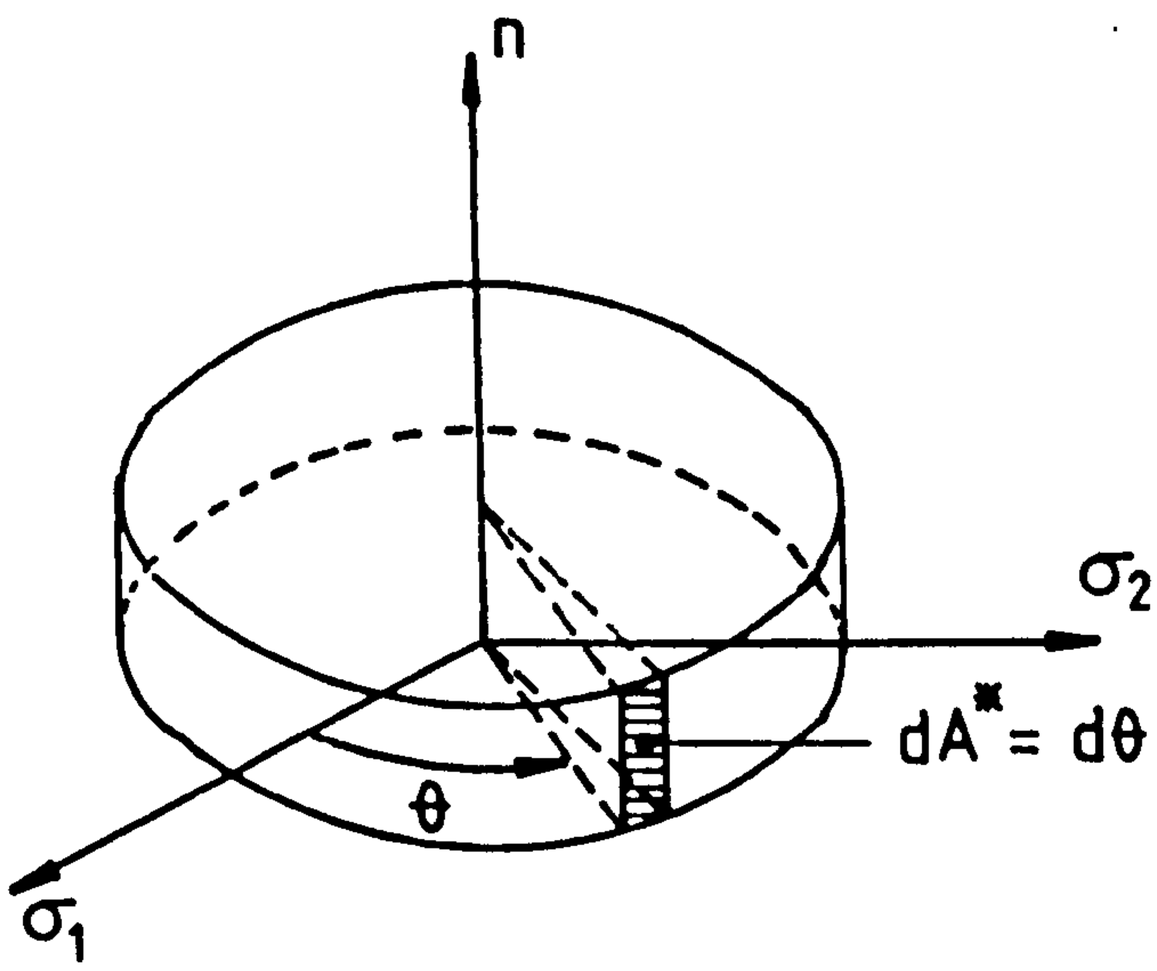

FIG. 2.5(b) GEOMETRIC VARIABLES DESCRIBING LOCATION ON UNIT DISC

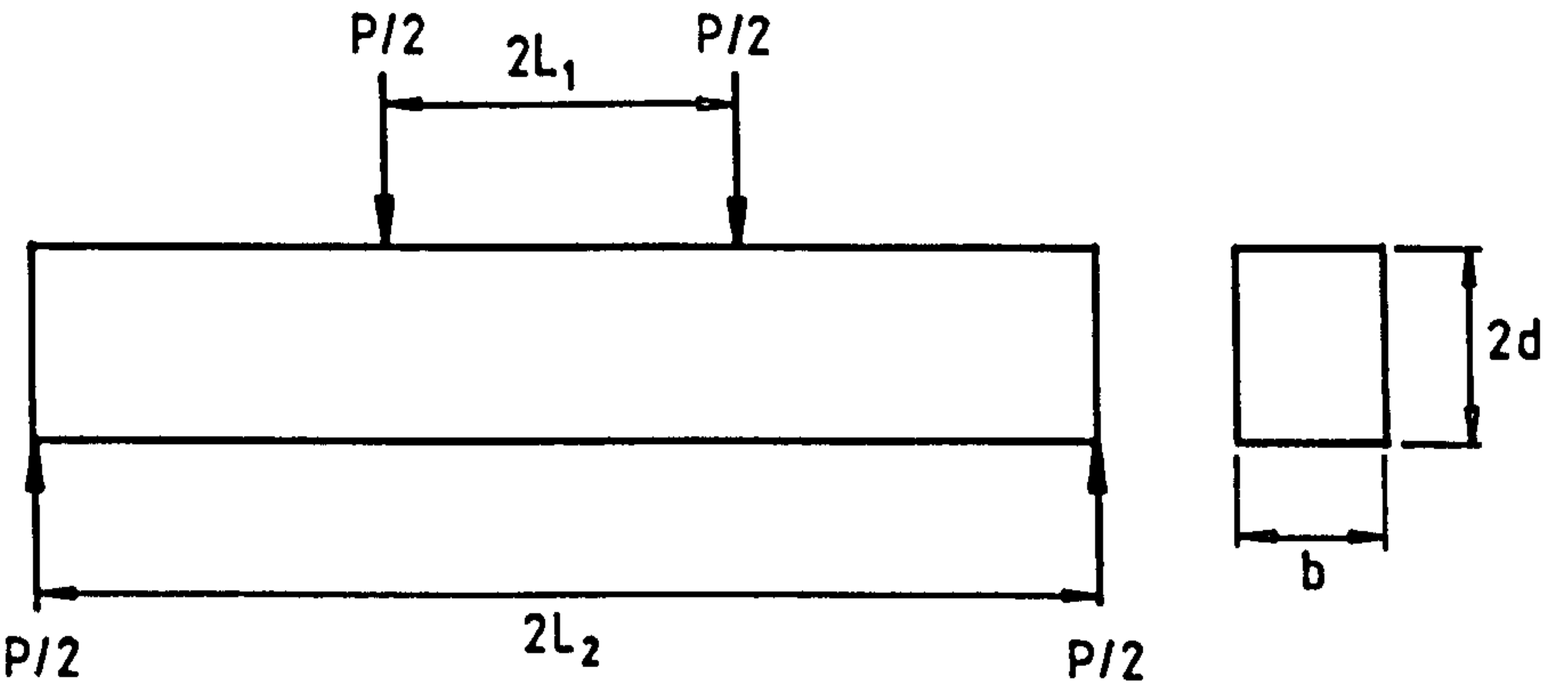

FIG. 2.6 FOUR-POINT BEND TEST

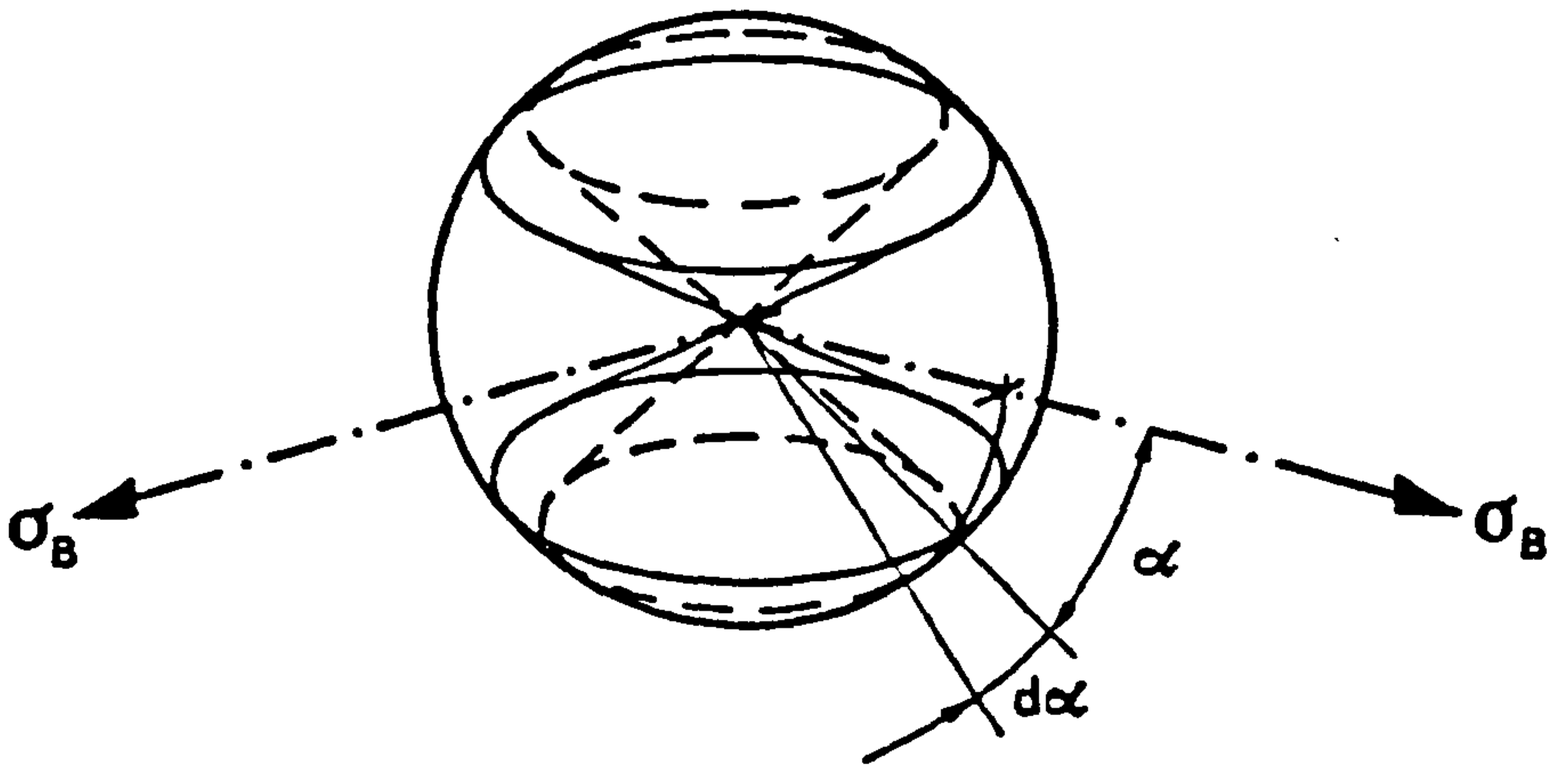

FIG. 2.7 FLAW ORIENTATION IN EQUIBIAXIAL TENSION

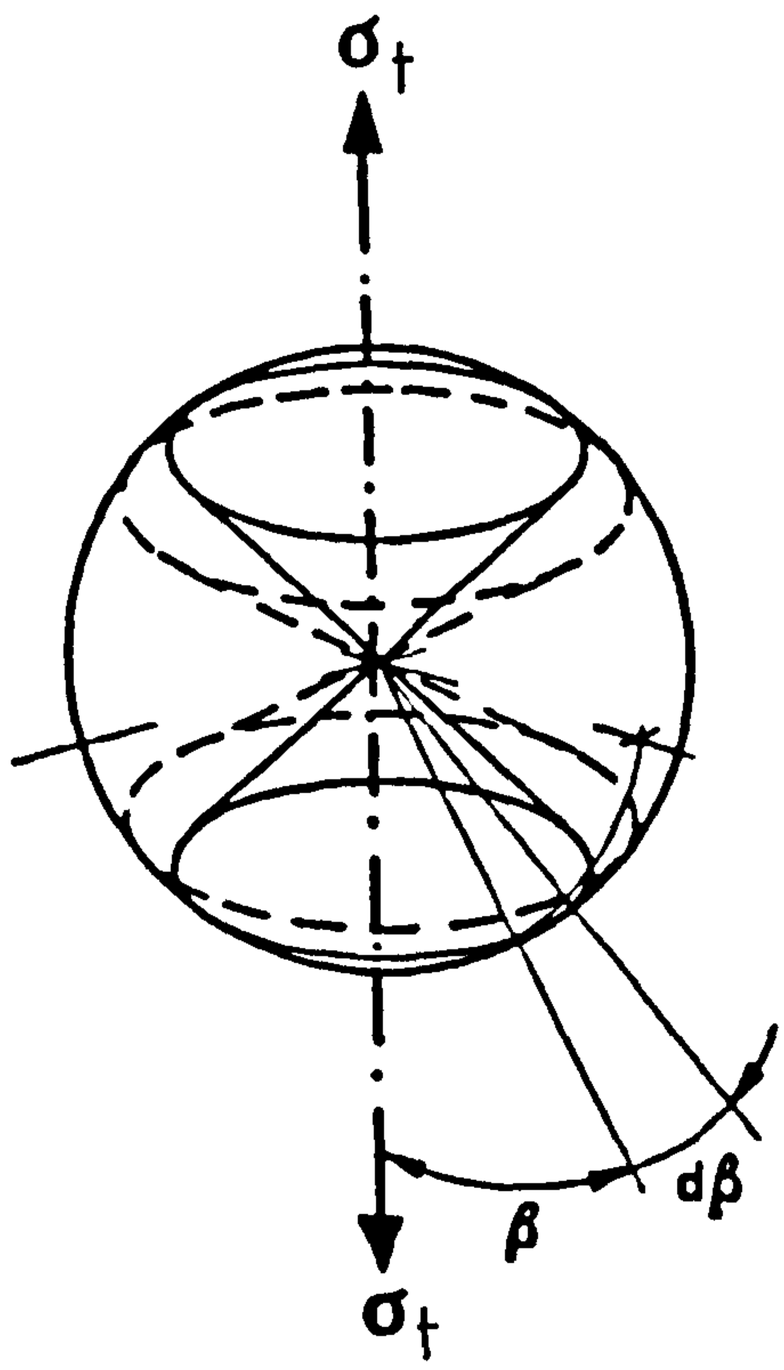

FIG. 2.8 FLAW ORIENTATION IN UNIAXIAL TENSION

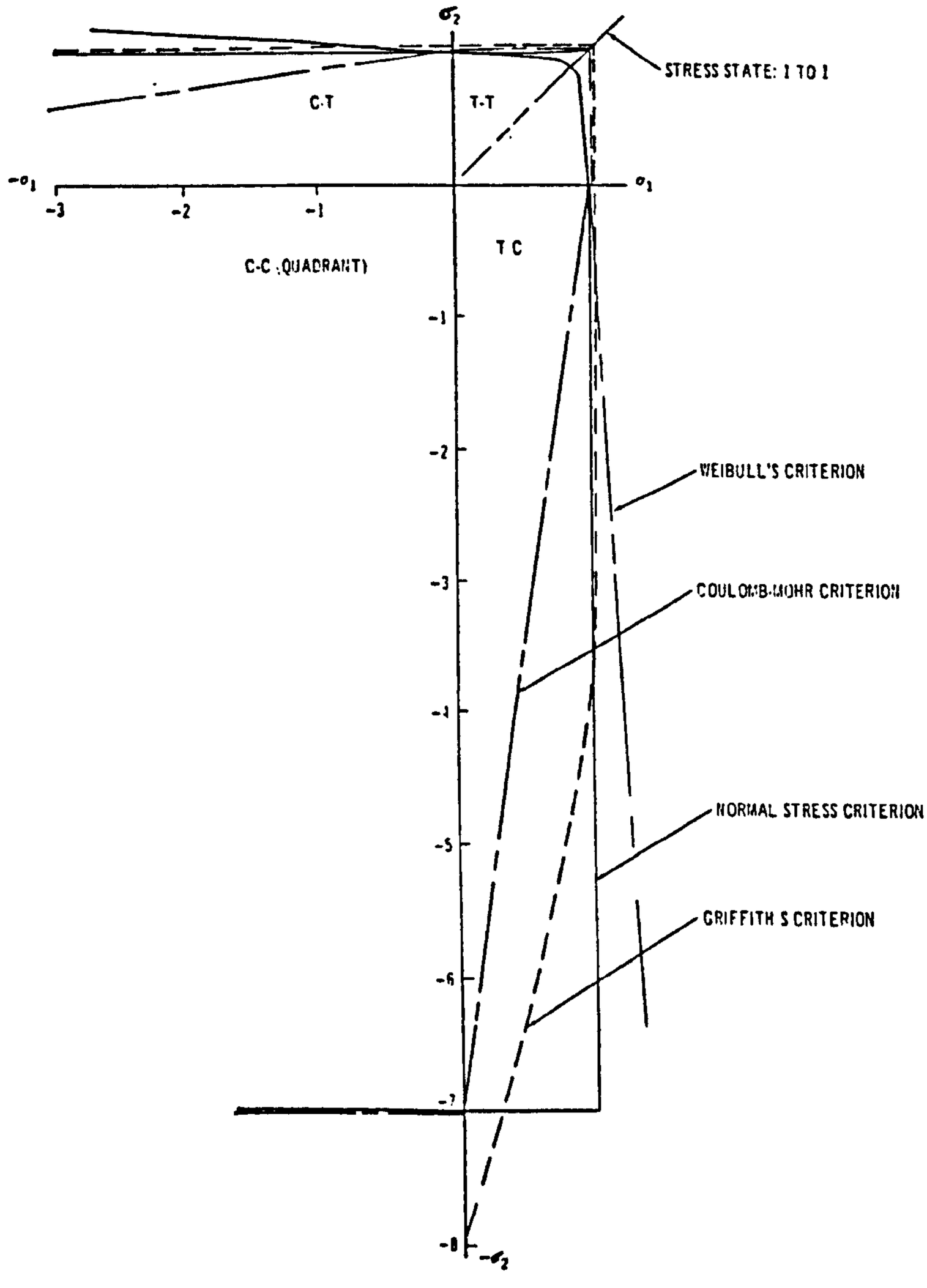

FIG. 2.9 COMPARISON OF FAILURE THEORIES FOR A BRITTLE MATERIAL WITH A COMPRESSIVE/TENSILE STRENGTH RATIO = 7

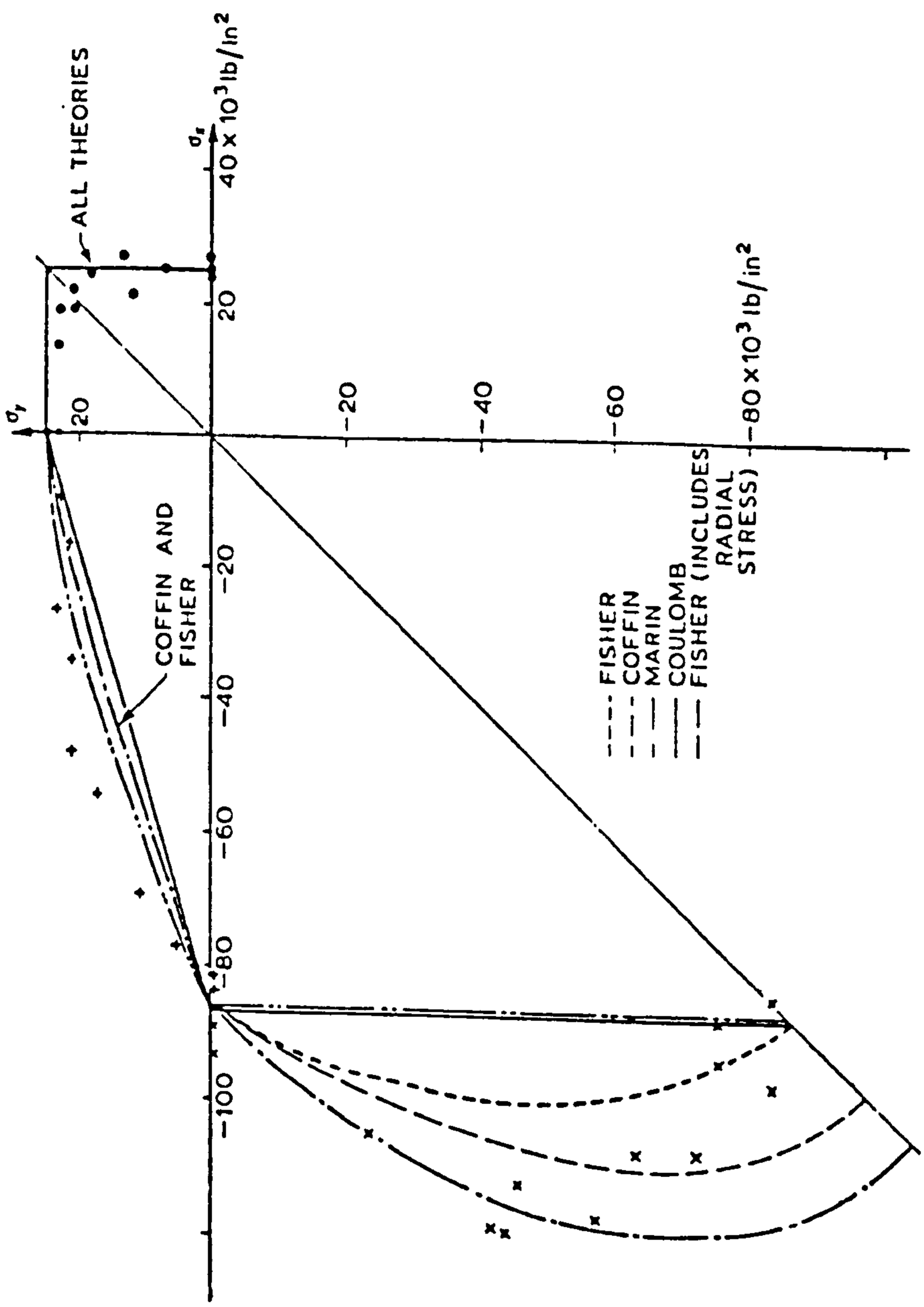

FIG. 2.10 COMPARISON OF FAILURE THEORIES WITH EXPERIMENTAL DATA ON CAST IRON
COMPRESSIVE / TENSILE STRENGTH RATIO = 3

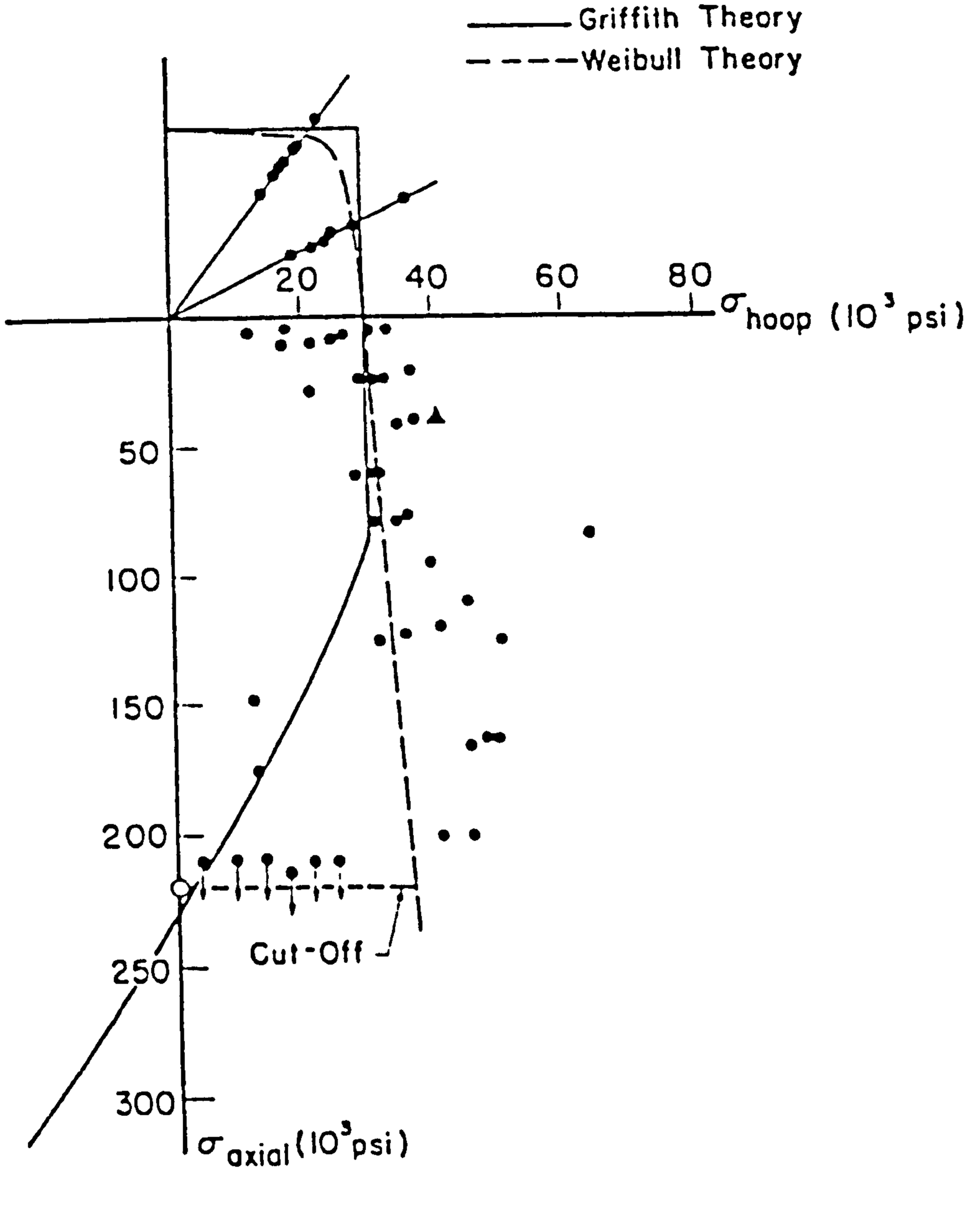

FIG. 2.11 COMPARISON OF FAILURE THEORIES WITH EXPERIMENTAL DATA ON CERAMICS. COMPRESSIVE/TENSILE STRENGTH RATIO = 7·5

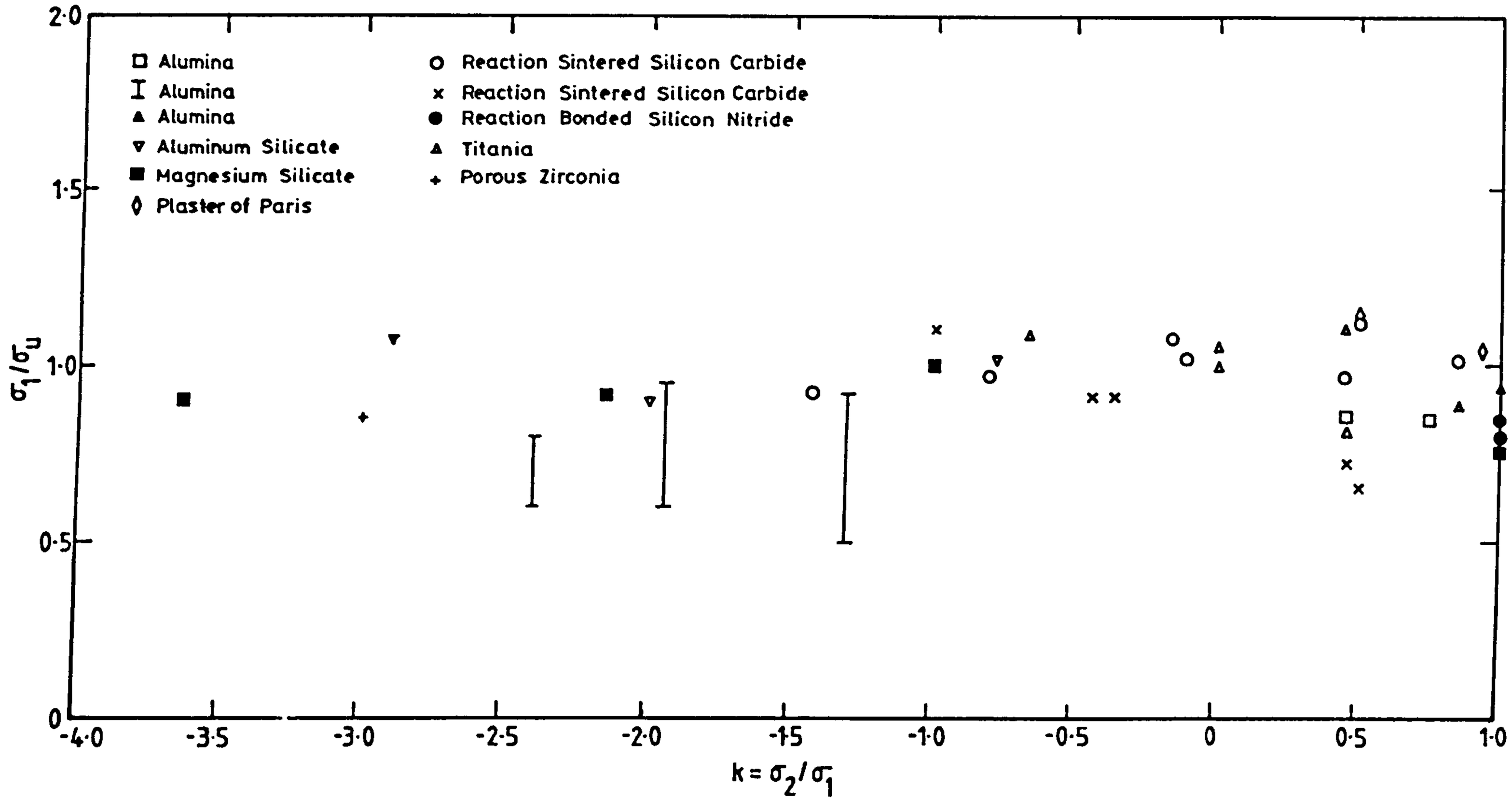

FIG.2.12 BIAXIAL STRENGTH VALUES FOR SPECIMENS FREE OF LARGE DOMINANT FLAWS. After Duckworth and Rosenfield (168)

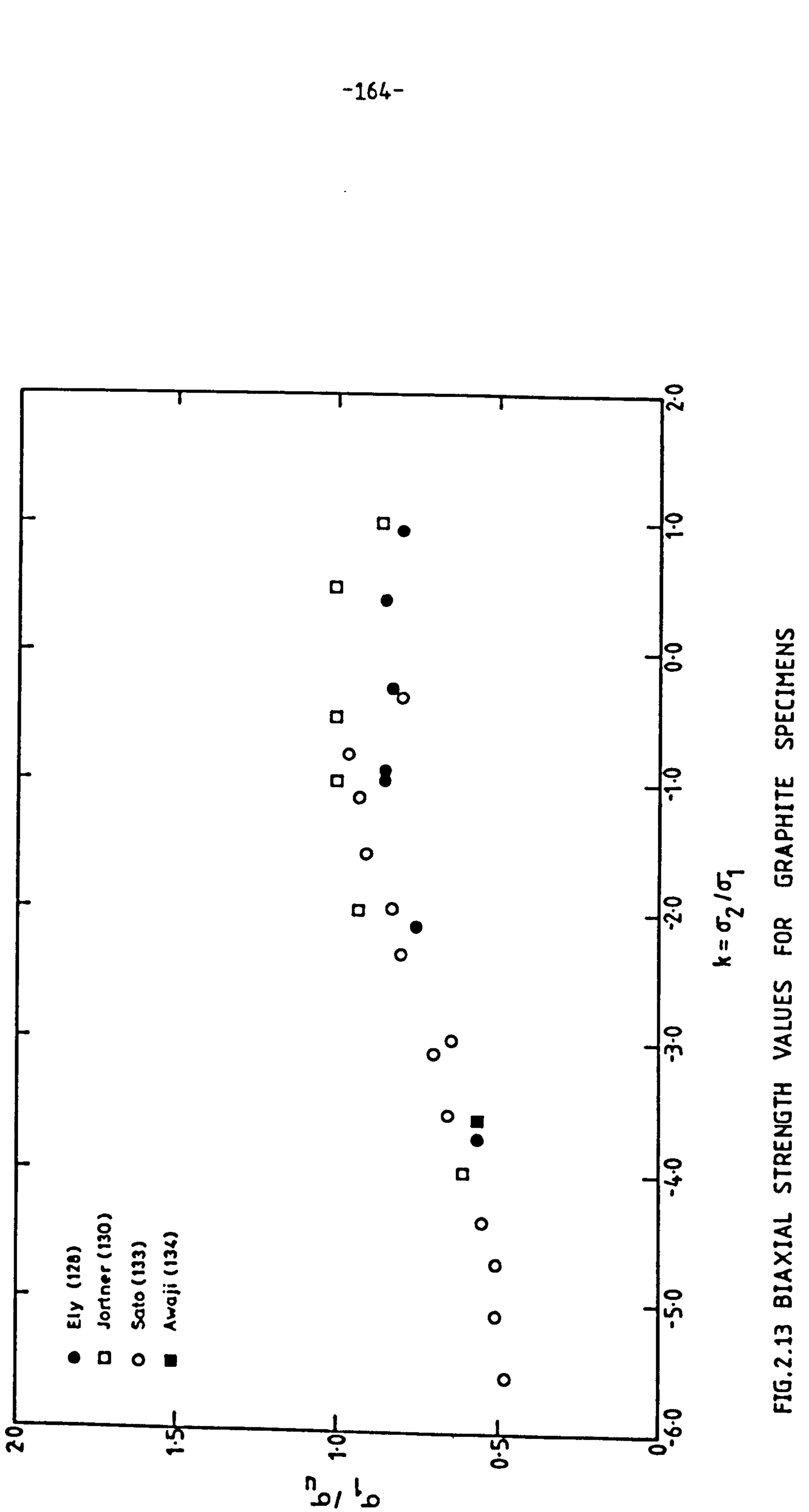

FIG.2.13 BIAXIAL STRENGTH VALUES FOR GRAPHITE SPECIMENS

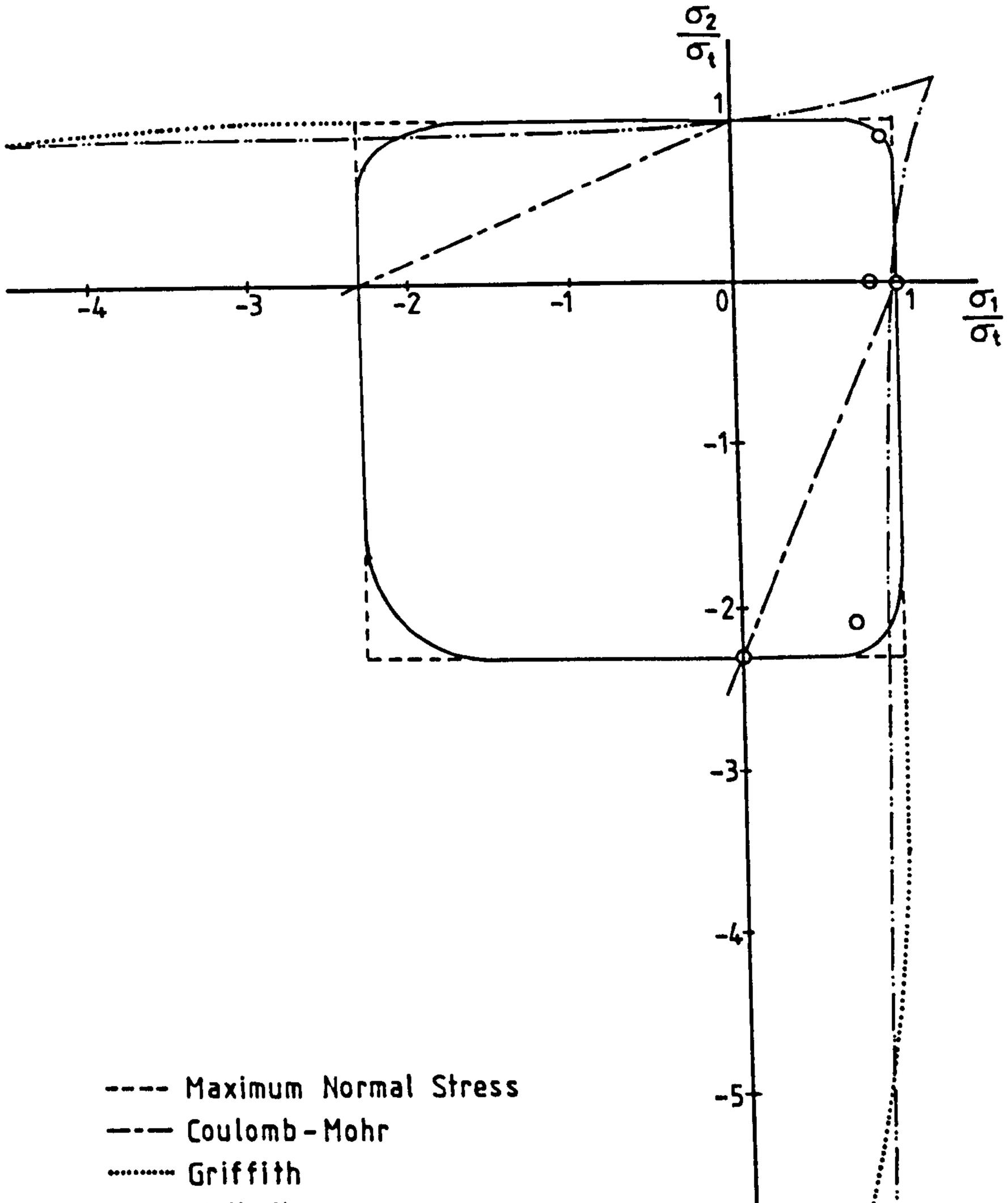

FIG. 3.1 COMPARISON OF FAILURE CRITERIA WITH EXPERIMENTAL RESULTS FOR HERCULITE LX PLASTER

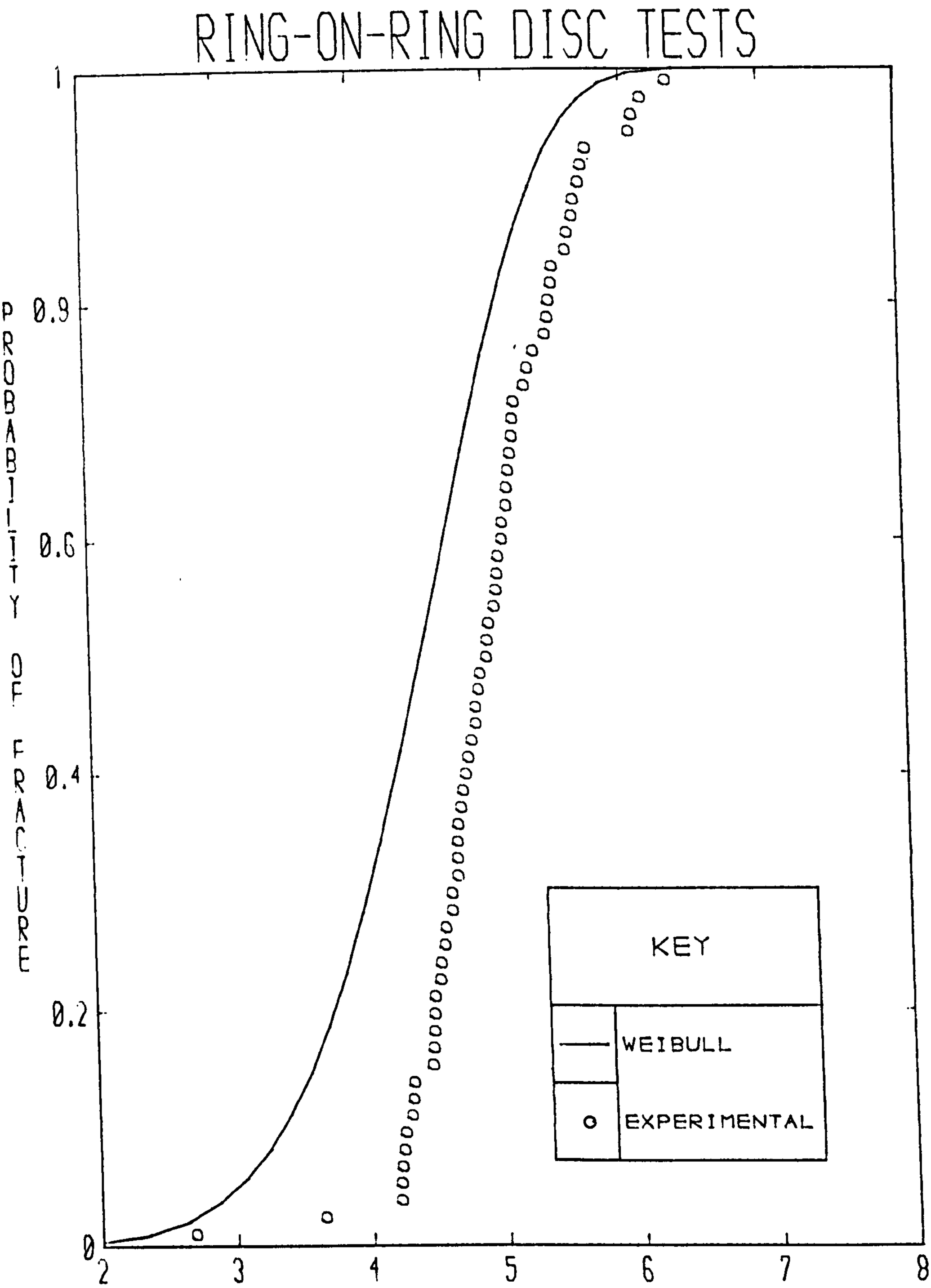

FIG. 3.2 COMPARISON BETWEEN WEIBULL THEORY AND EXPERIMENT

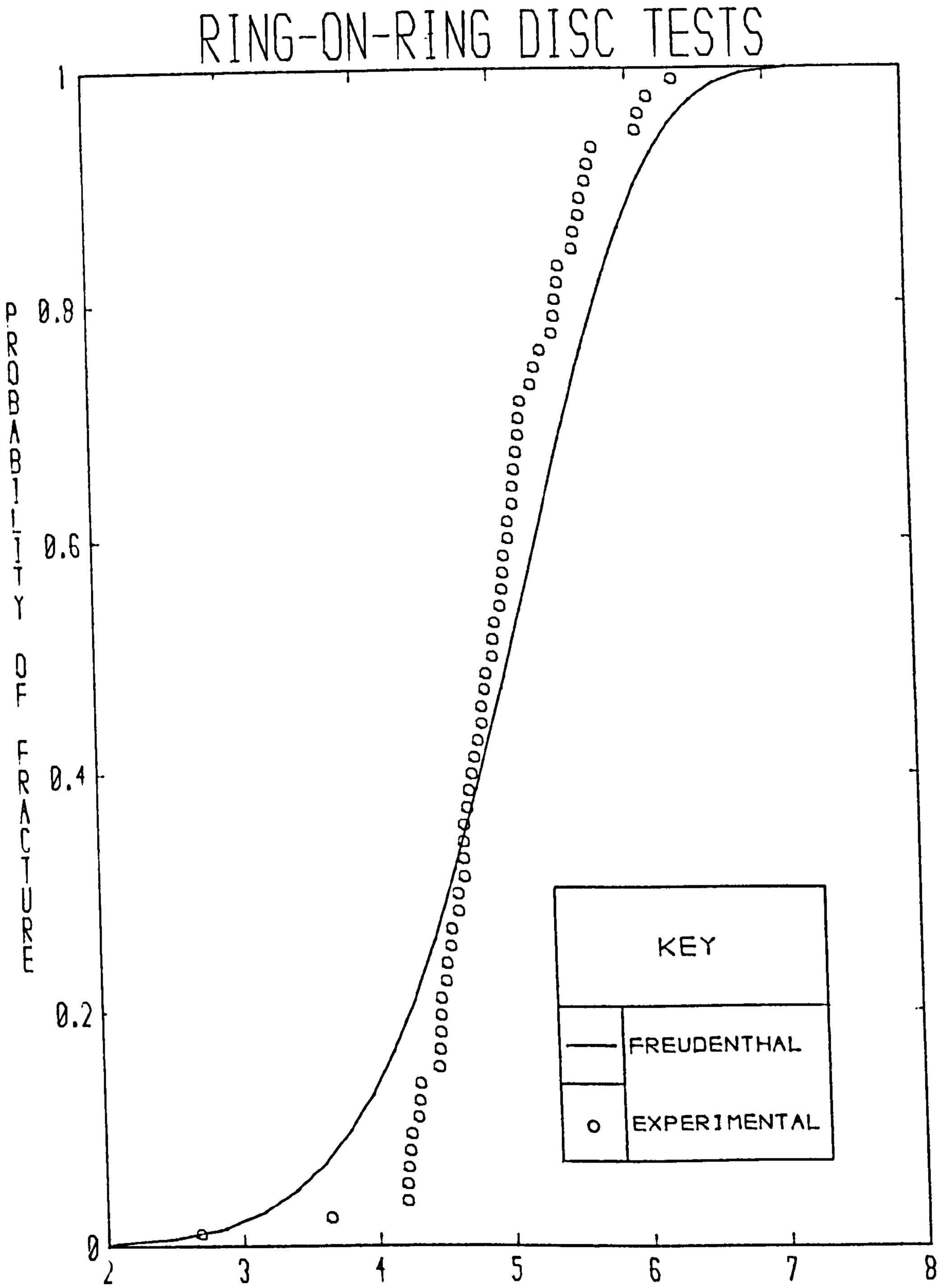

FIG. 3.3 FREUDENTHAL THEORY COMPARED TO EXPERIMENT

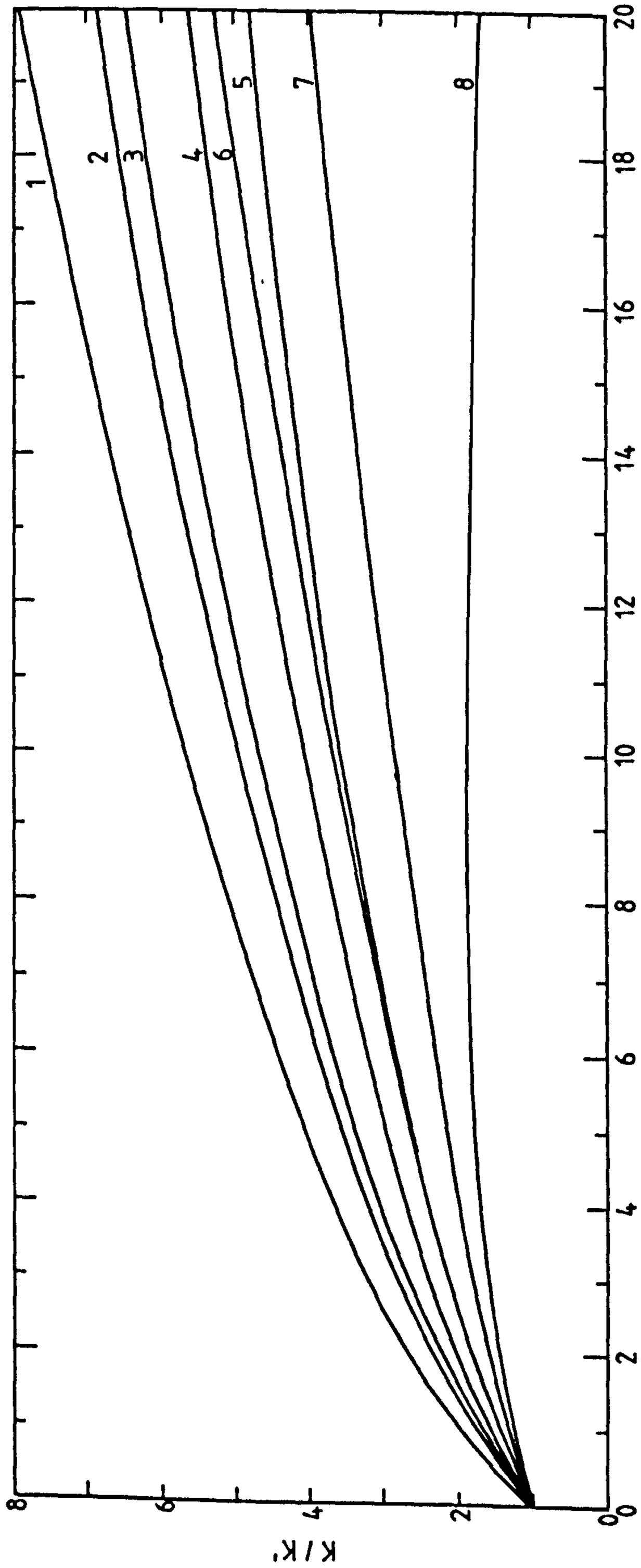

FIG. 3.4 RELATION BETWEEN UNIAXIAL AND EQUIBIAXIAL FRACTURE STATISTICS FOR VARIOUS THEORIES. After S. B. Batdorf (172)

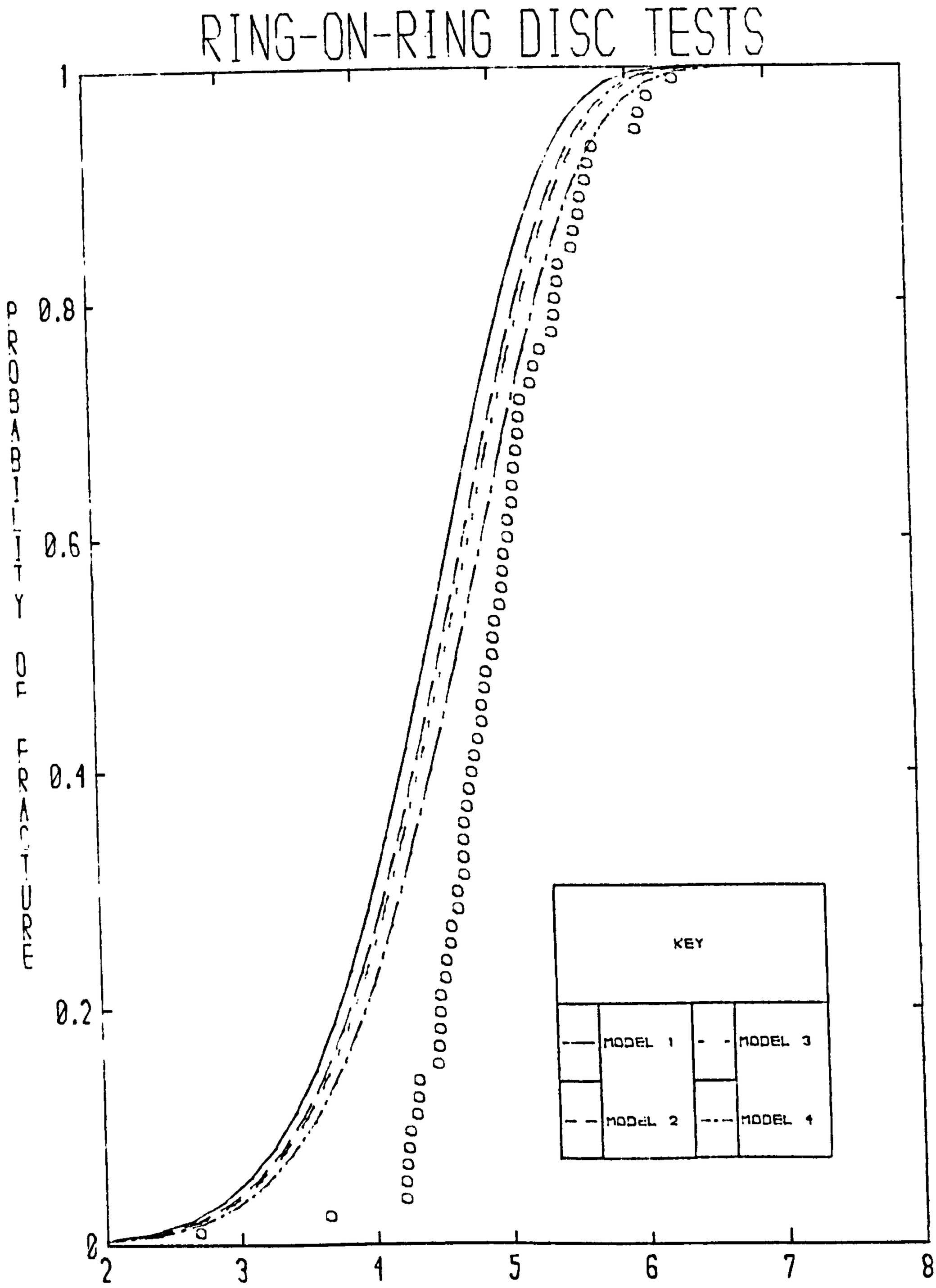

FIG. 3.5 FAILURE PROBABILITY CURVES FITTED TO EXPERIMENT. MODELS 1-4
(Model 1 : Normal Stress Criterion
Model 2 : Griffith Cracks
Model 3 : Penny-shaped Cracks
Model 4 : Strain-Energy Release-Rate Criterion. Griffith Cracks)

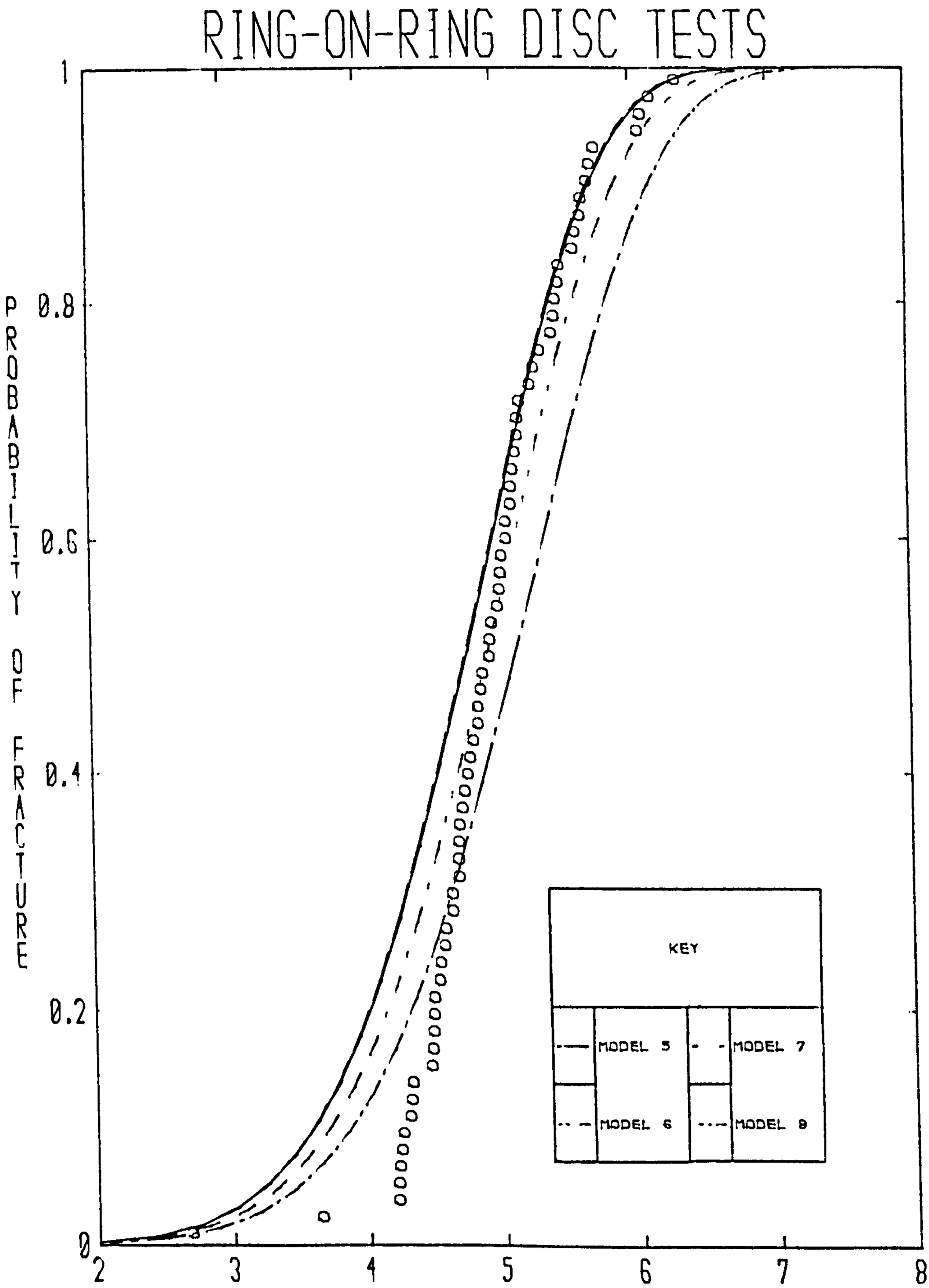

FIG. 3.6 FAILURE PROBABILITY CURVES FITTED TO EXPERIMENT . MODELS 5-8
(Model 5 : Strain - Energy Release - Rate Criterion . Penny - shaped Cracks
Model 6 : Energy Density Criterion . Griffith Cracks
Model 7 : Energy Density Criterion . Penny - shaped Cracks
Model 8 : Erdogan and Sih Criterion . Closed Cracks)

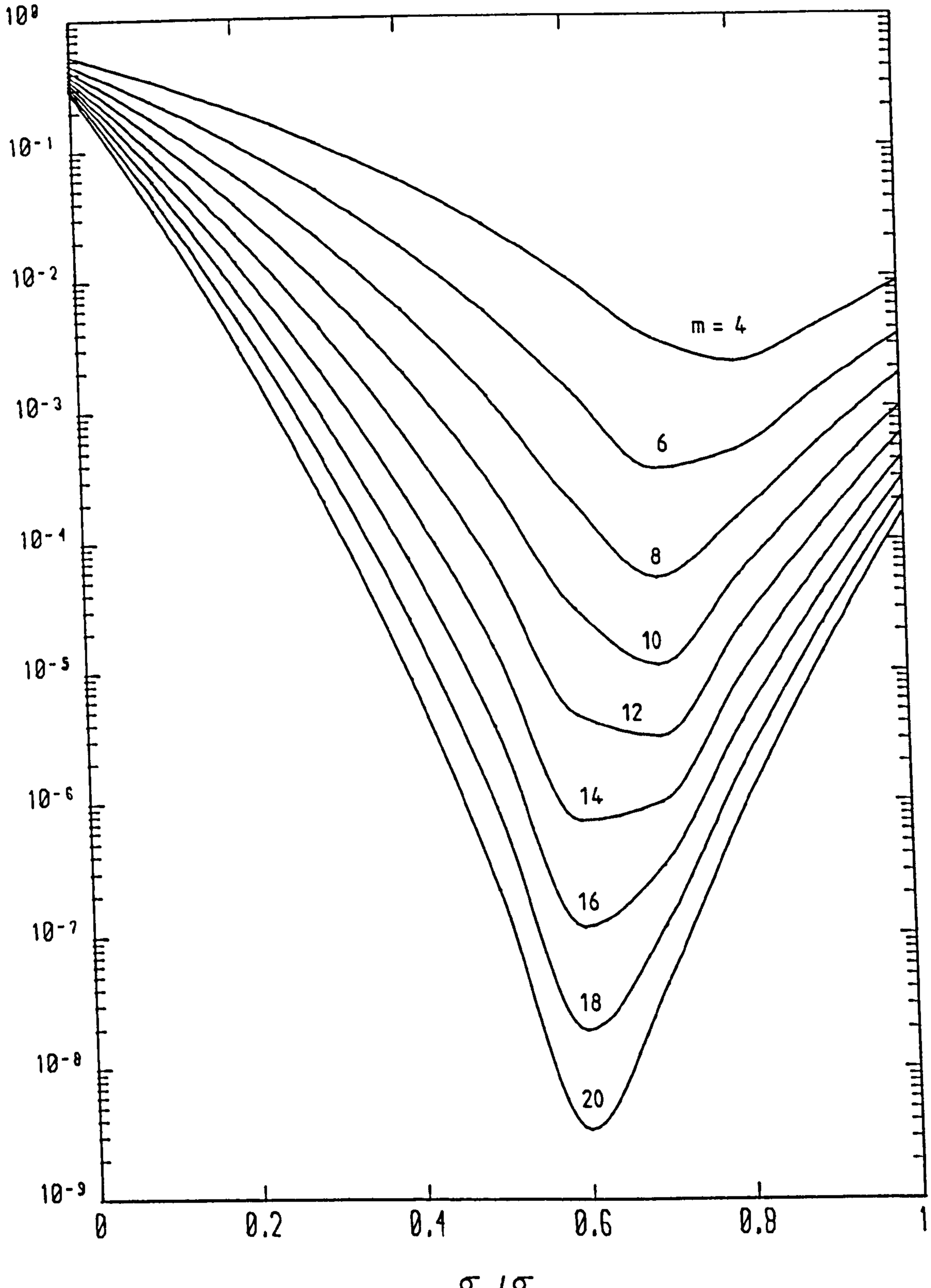

FIG. 3.7 PLOT OF PARAMETER I_B AS A FUNCTION OF σ_U/σ_B FOR SEVERAL VALUES OF WEIBULL MODULUS m

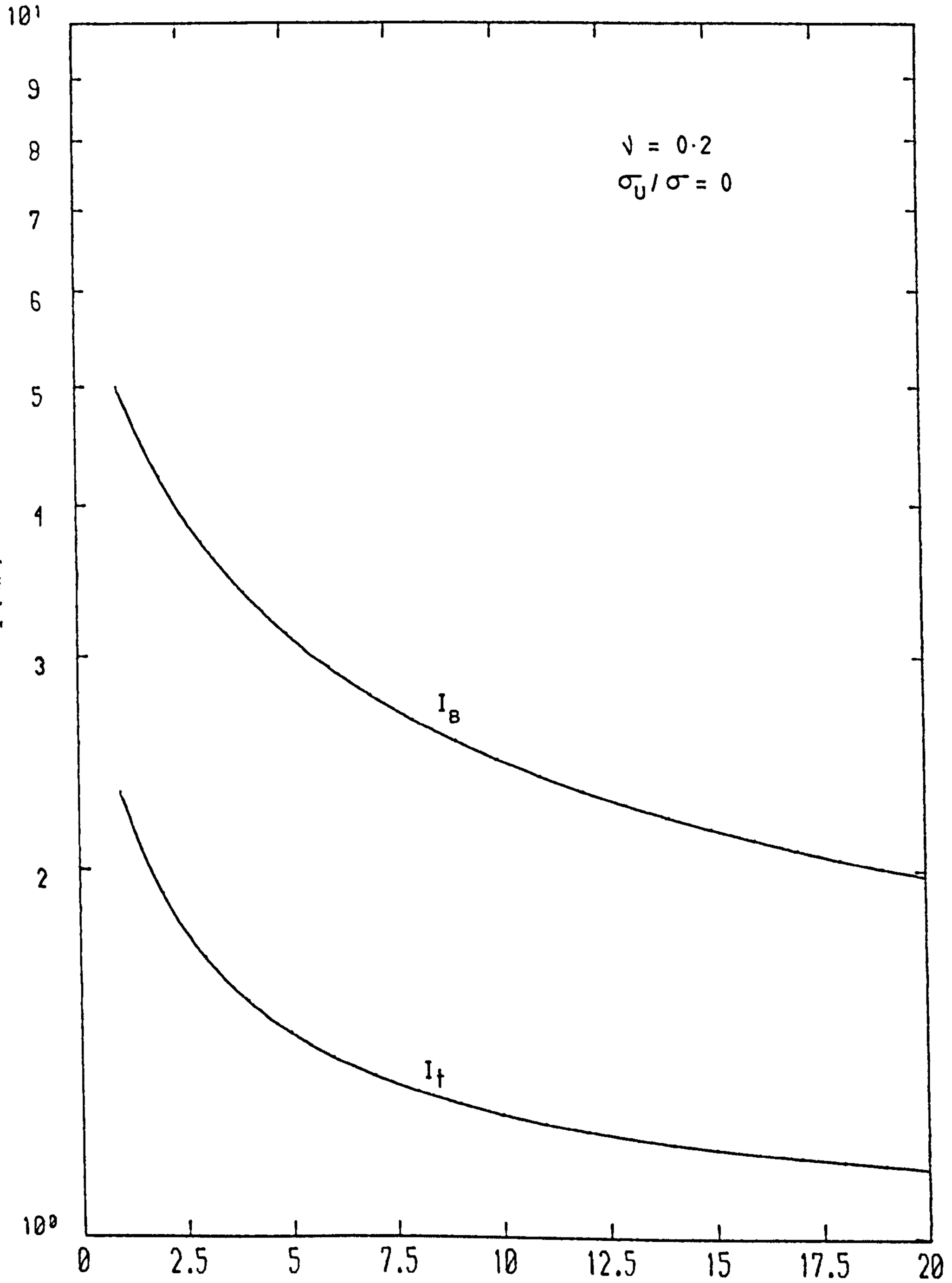

FIG. 3.8 PLOT OF I_B AND I_f AS A FUNCTION OF WEIBULL MODULUS m

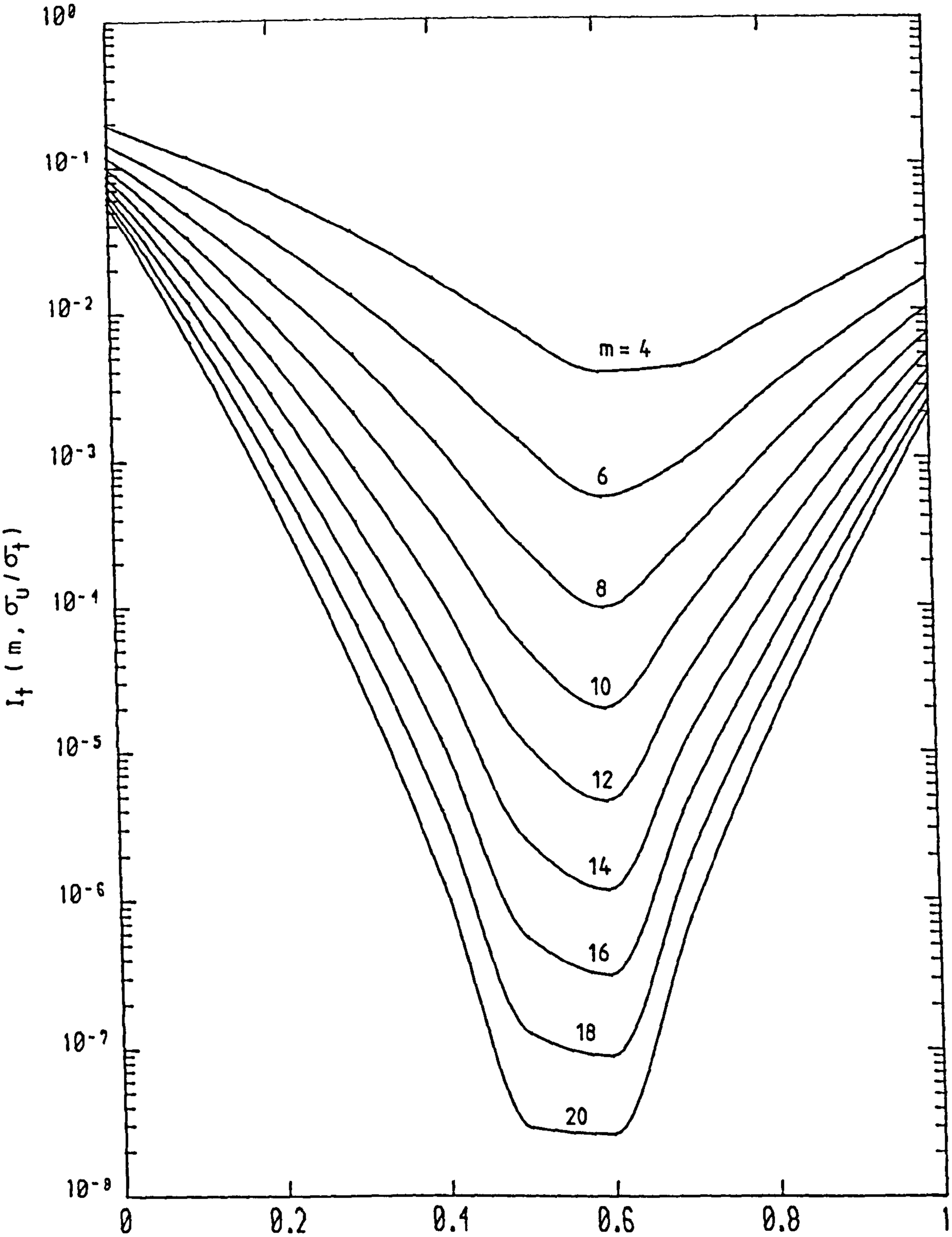

FIG. 3.9 PLOT OF PARAMETER I_f AS A FUNCTION OF σ_u/σ_f FOR SEVERAL VALUES OF WEIBULL MODULUS m

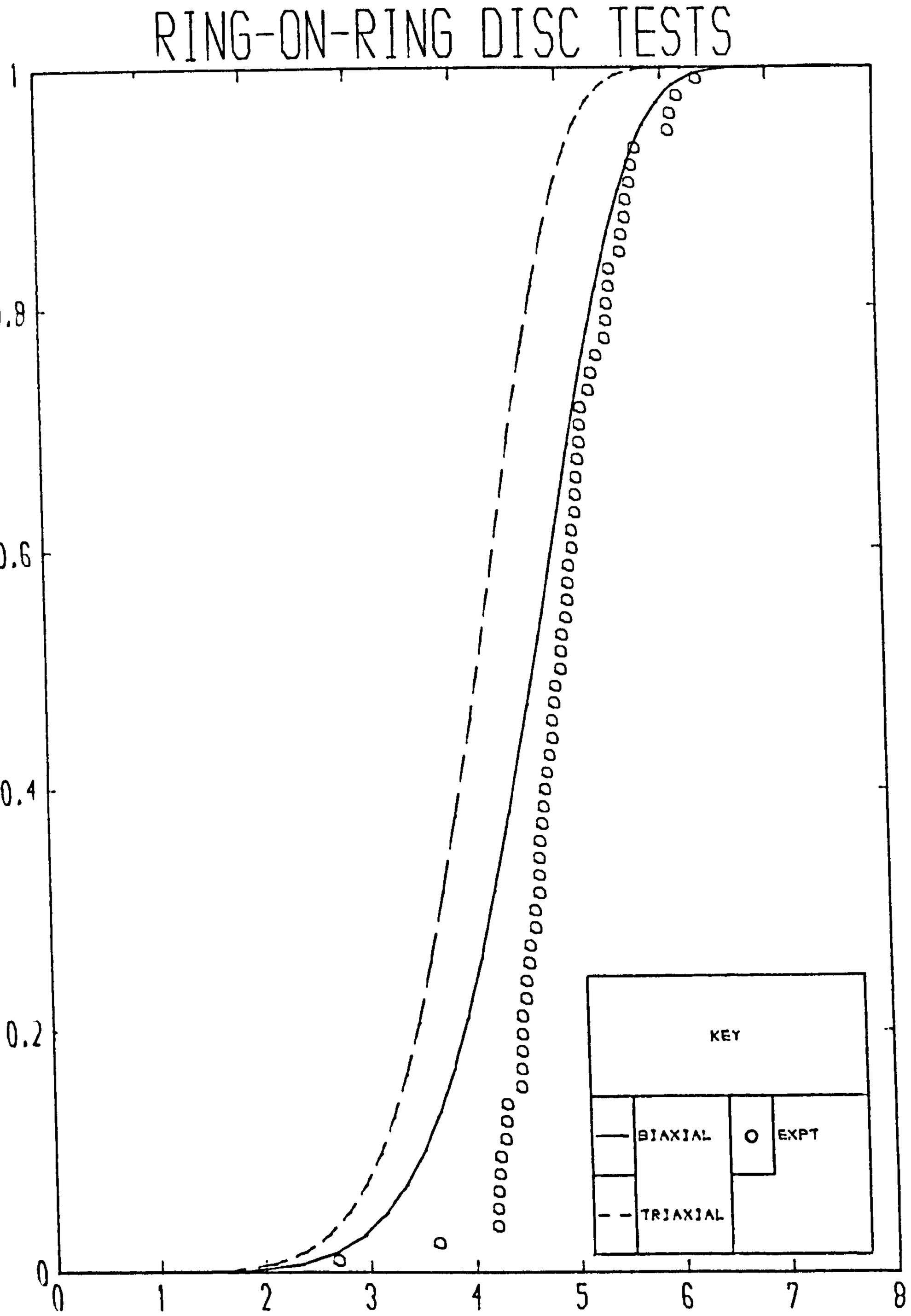

FIG. 3.10 EVANS THEORY COMPARED TO EXPERIMENT. ALSO SHOWN IS EQUITRIAXIAL STRENGTH PREDICTED BY THE SAME THEORY

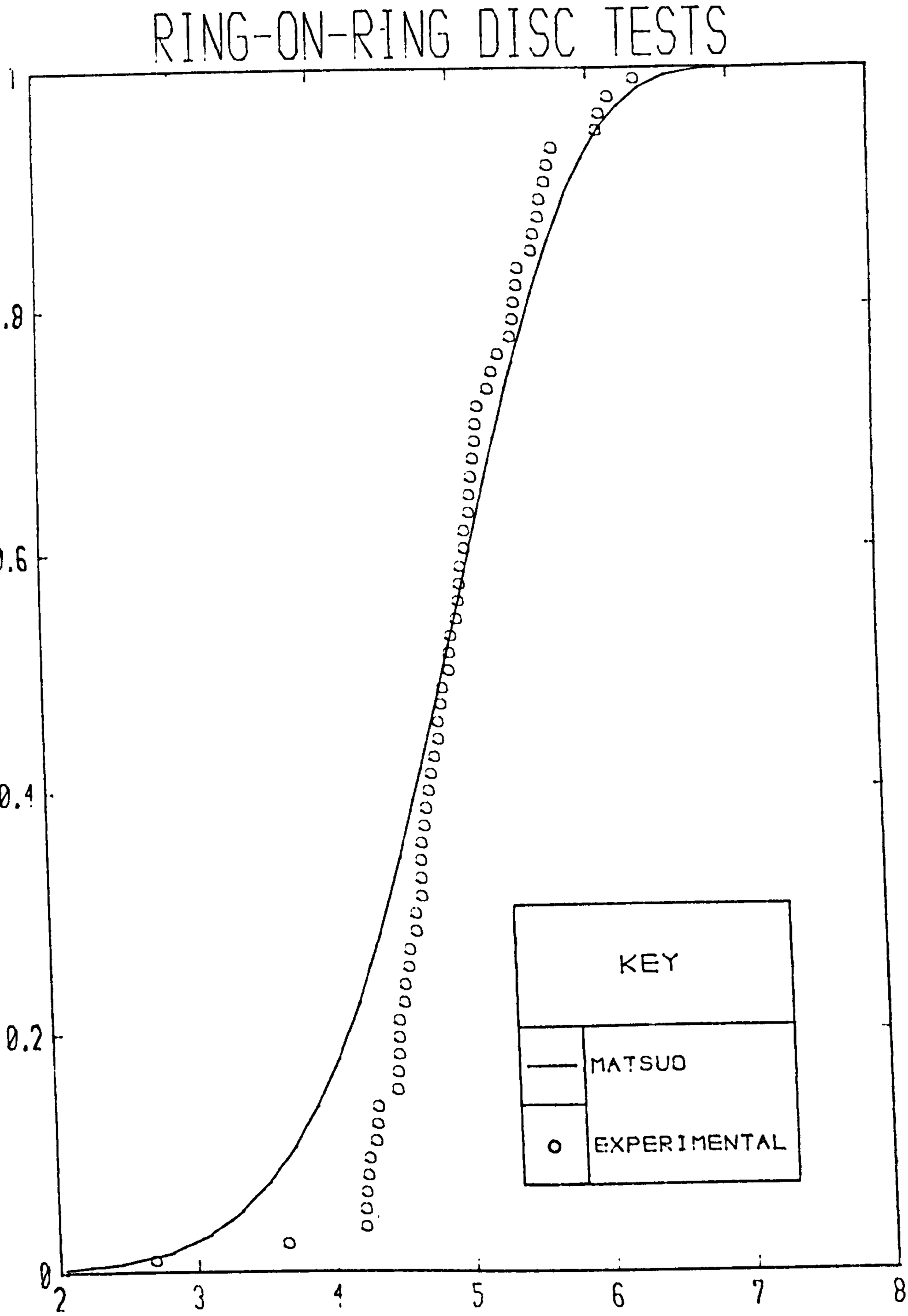

FIG. 3.11 MATSUO THEORY COMPARED TO EXPERIMENT

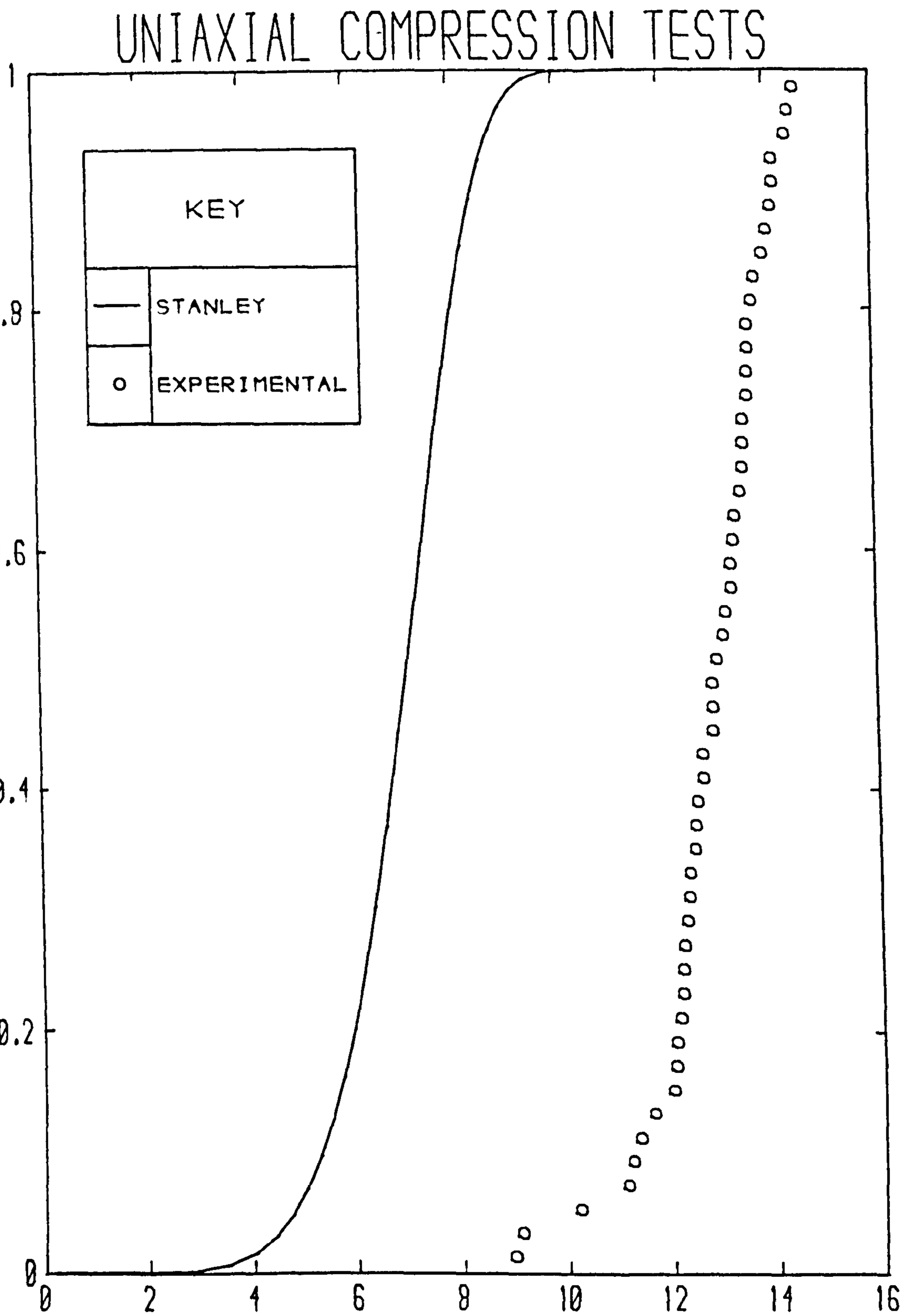

FIG. 3.12 STANLEY THEORY COMPARED TO EXPERIMENT

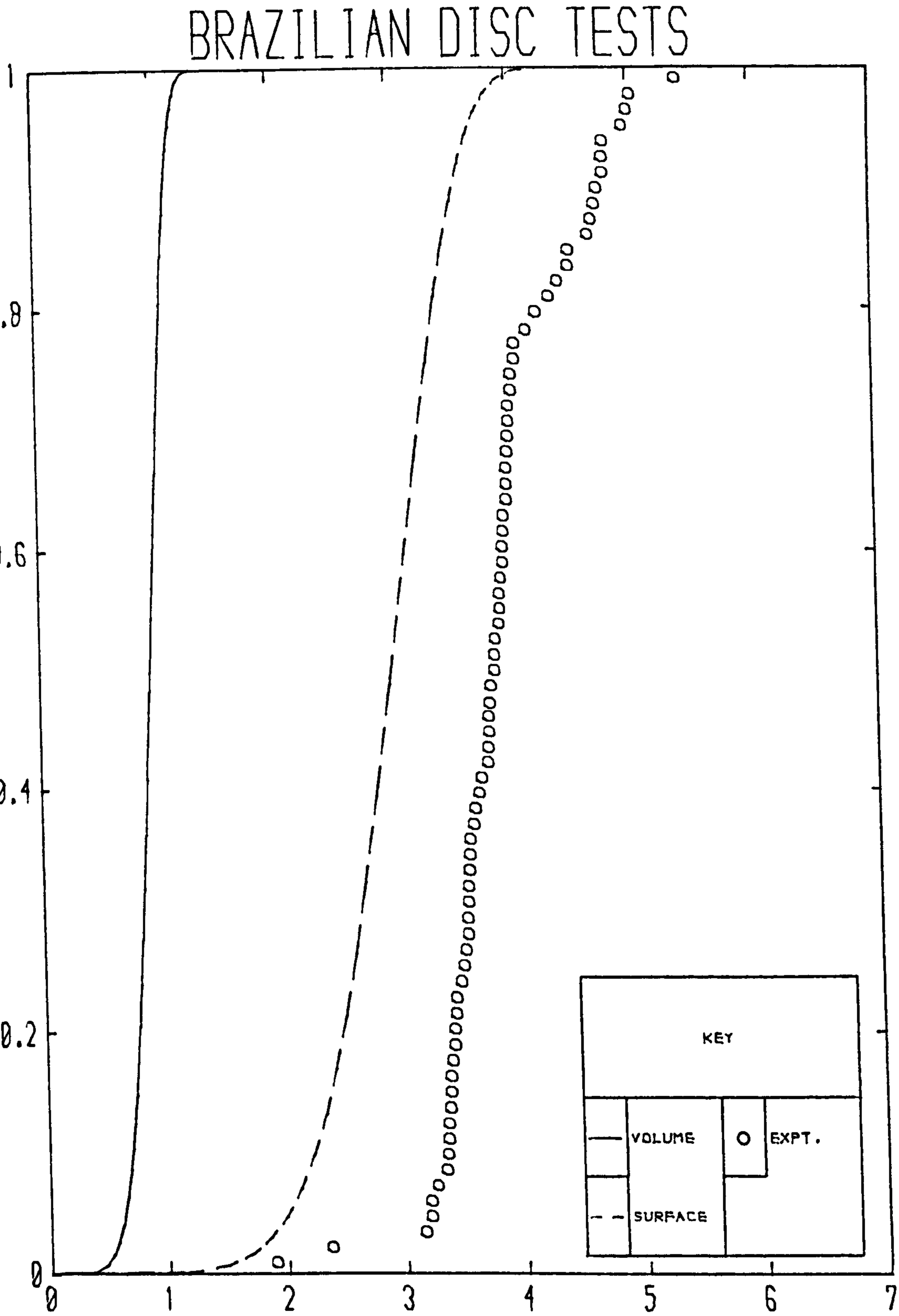

FIG. 3.13 FAILURE PROBABILITY DUE TO VOLUME AND SURFACE DEFECTS FOR BRAZILIAN DISCS

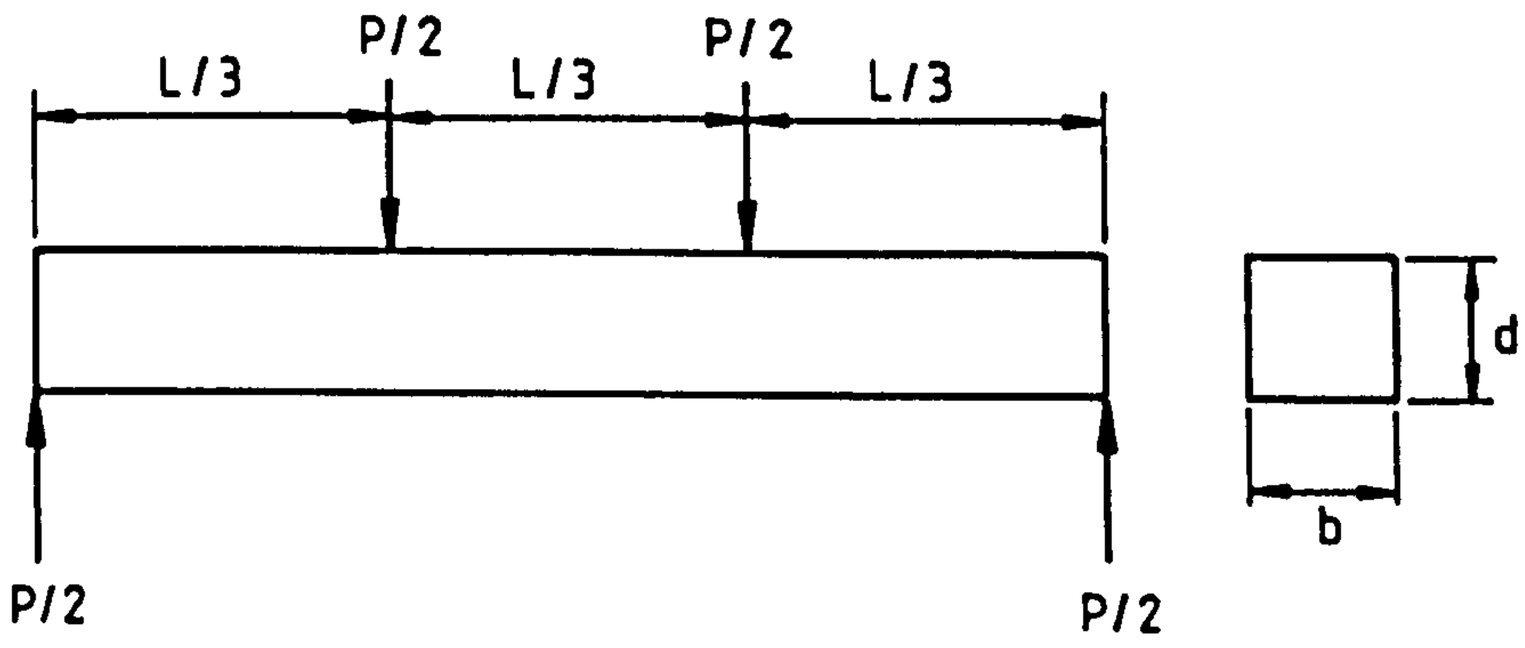

FIG. 3.14 FOUR-POINT BEND TEST

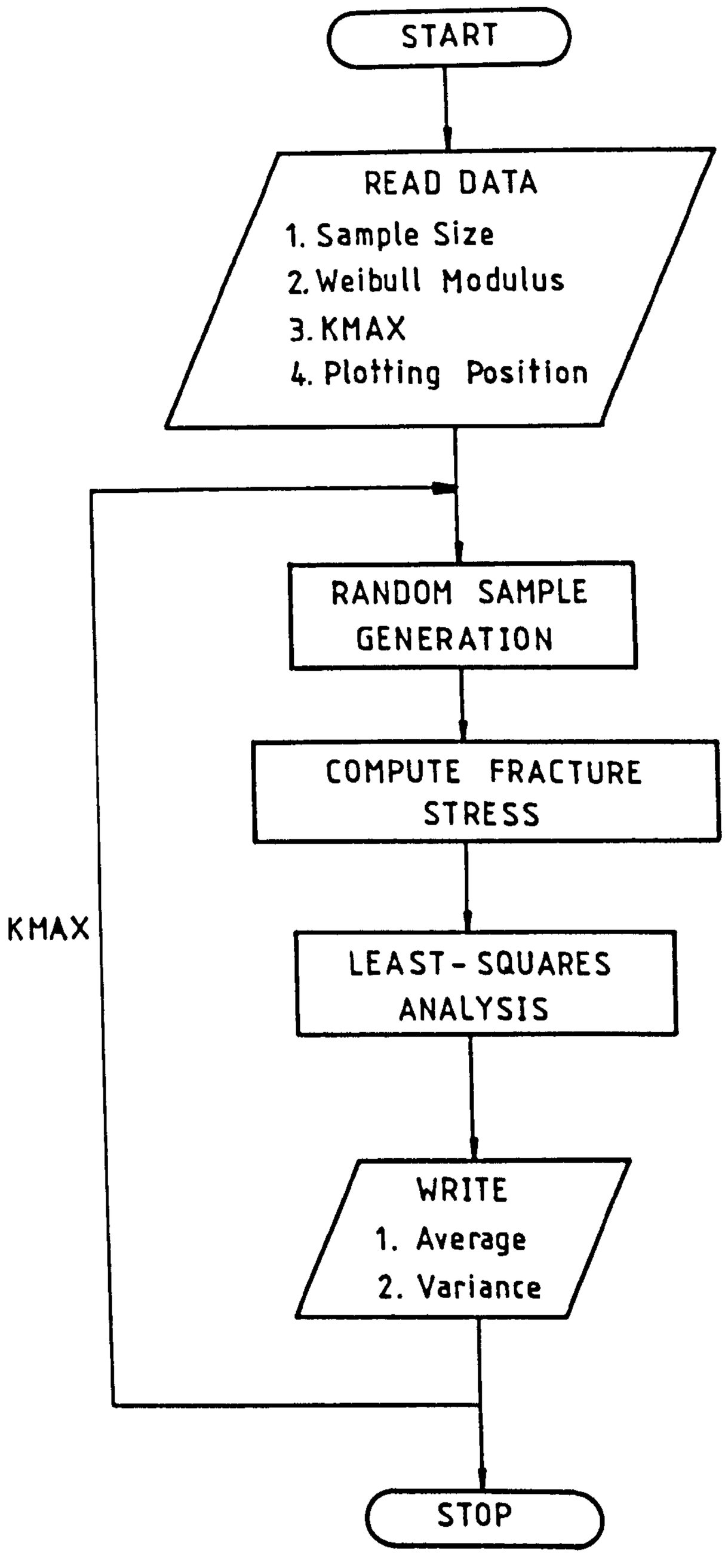

FIG.3.15 FLOW CHART FOR THE MONTE CARLO SIMULATION

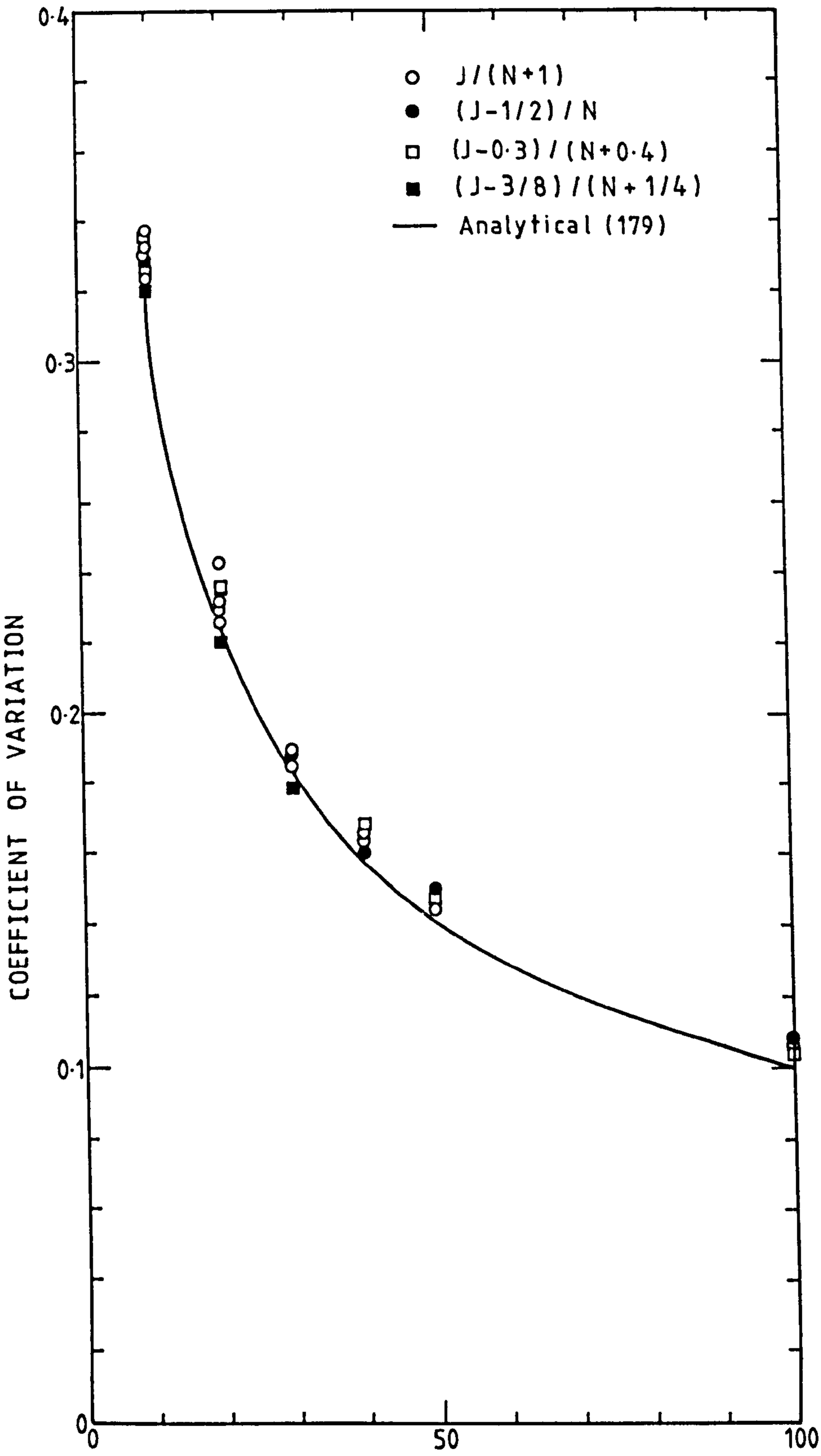

FIG. 3.16 COEFFICIENT OF VARIATION OF WEIBULL MODULUS AS A FUNCTION OF SAMPLE SIZE

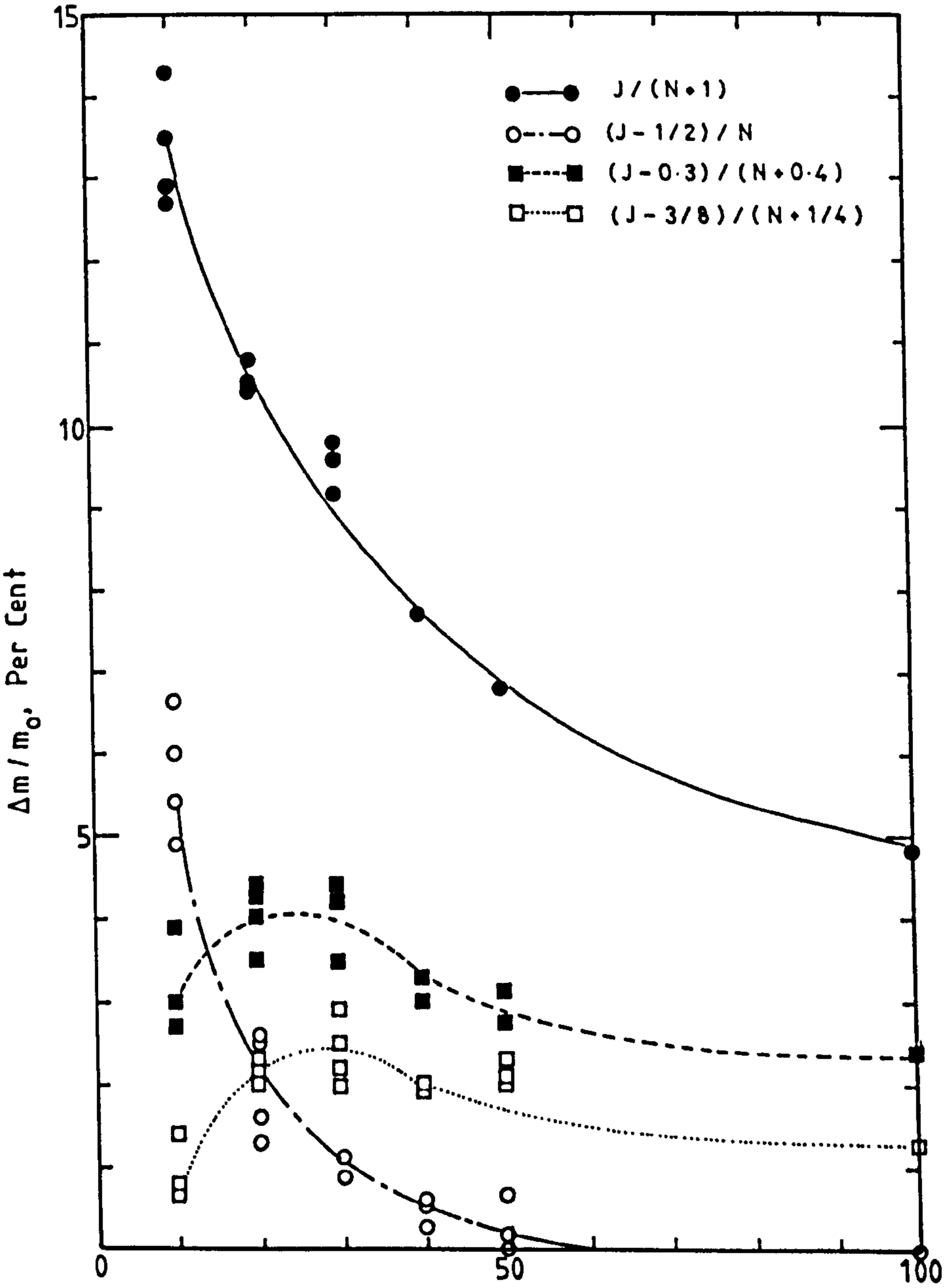

FIG. 3.17 VARIABILITY OF WEIBULL MODULUS WITH DIFFERENT PLOTTING POSITIONS AND SAMPLE SIZES

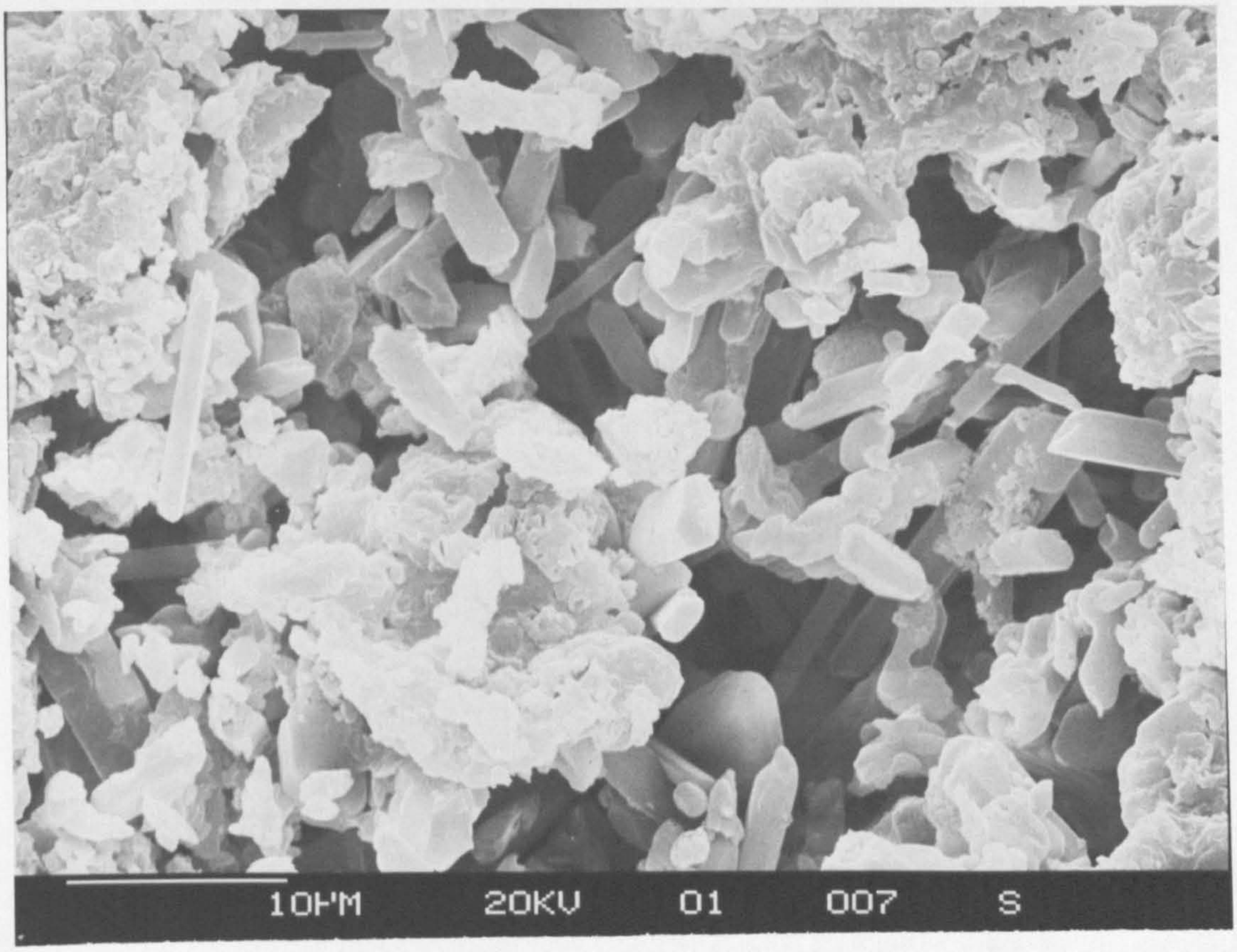

FIG. 4.1 SCANNING ELECTRON MICROGRAPH OF THE MICROSTRUCTURE OF UNIAXIAL COMPRESSION SPECIMEN AFTER CASTING; x 2000

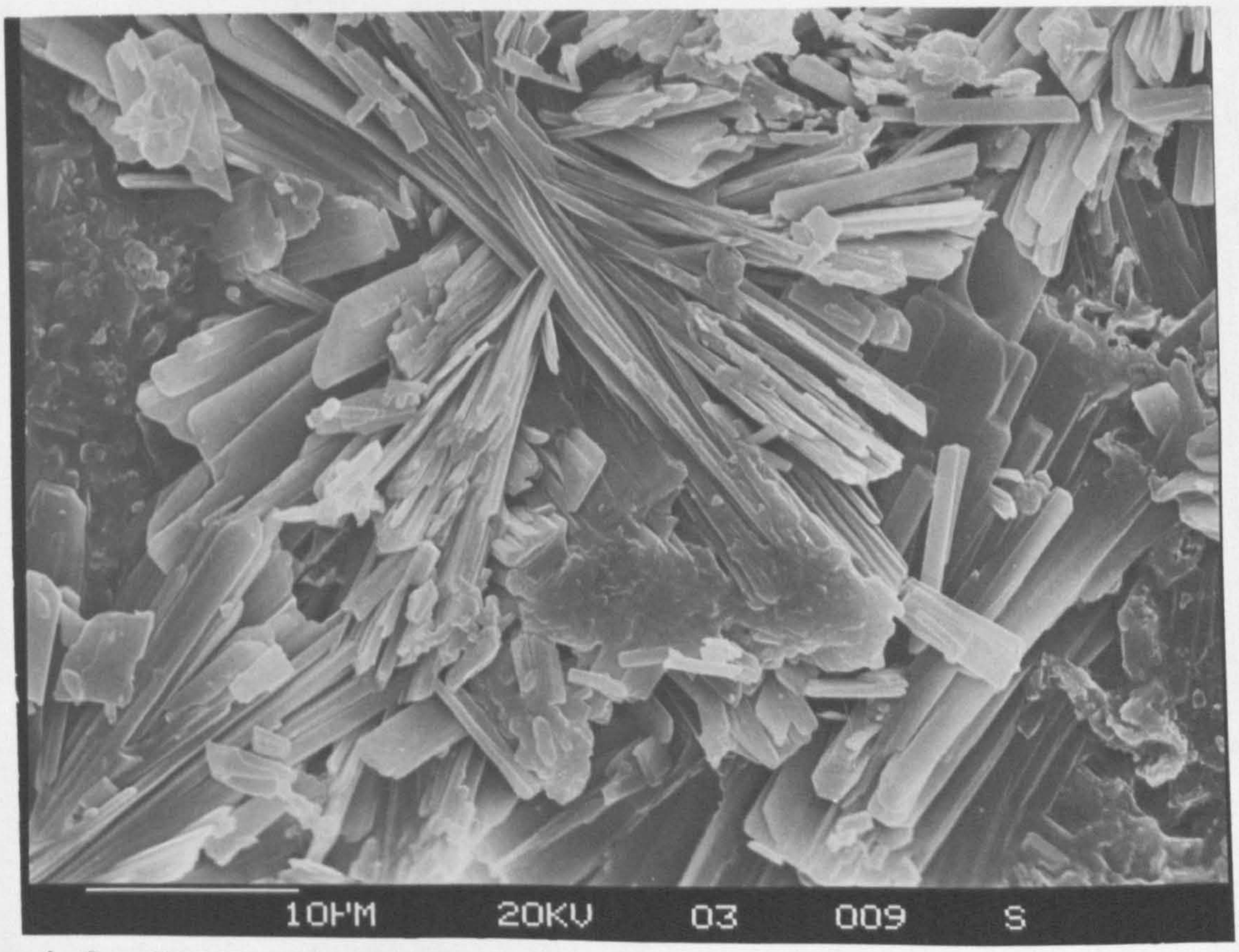

FIG. 4.2 SCANNING ELECTRON MICROGRAPH OF THE MICROSTRUCTURE OF DISC SPECIMEN AFTER CASTING; x 2000

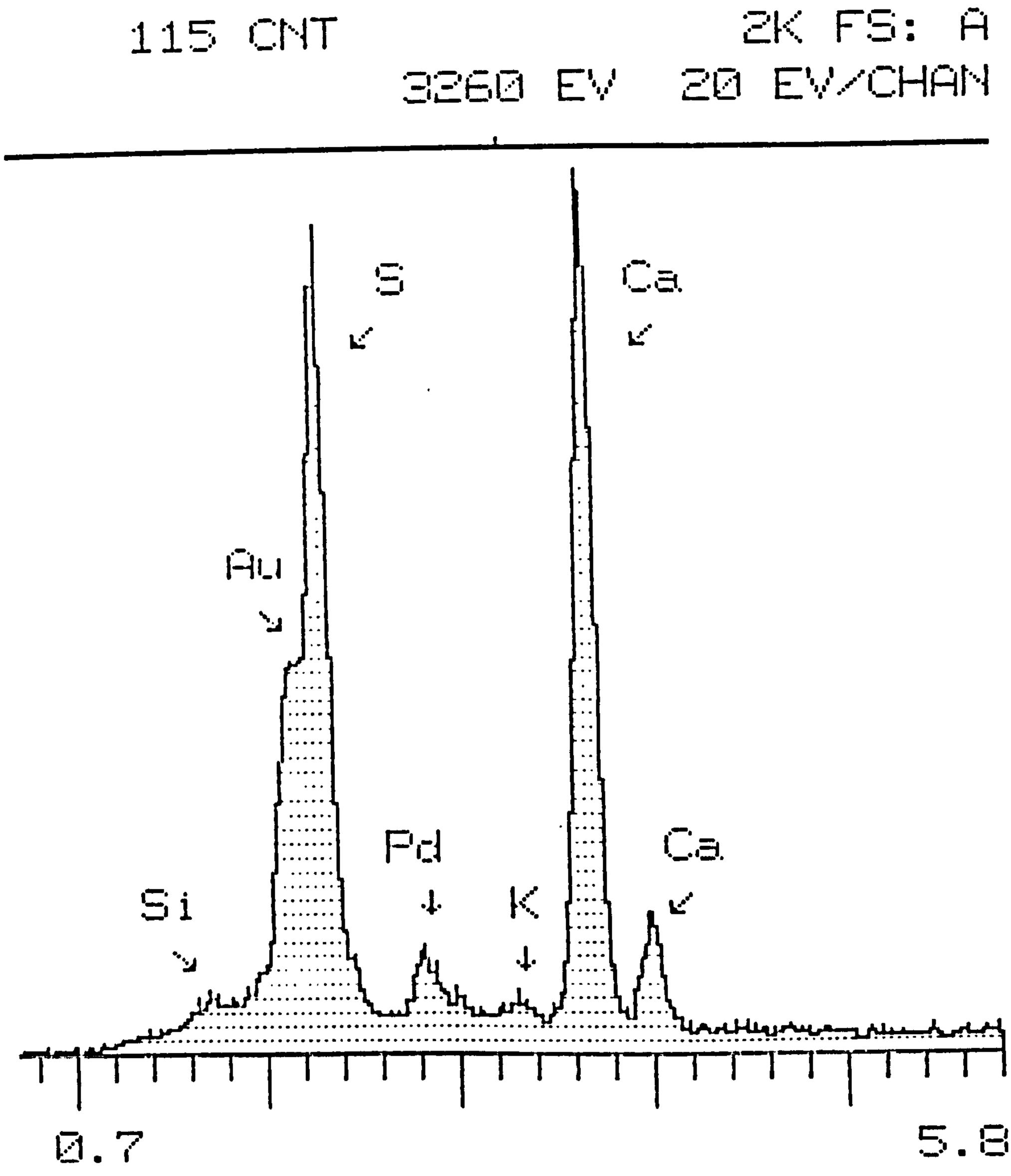

FIG. 4.3 ELEMENT DISTRIBUTION OF THE HERCULITE LX PLASTER

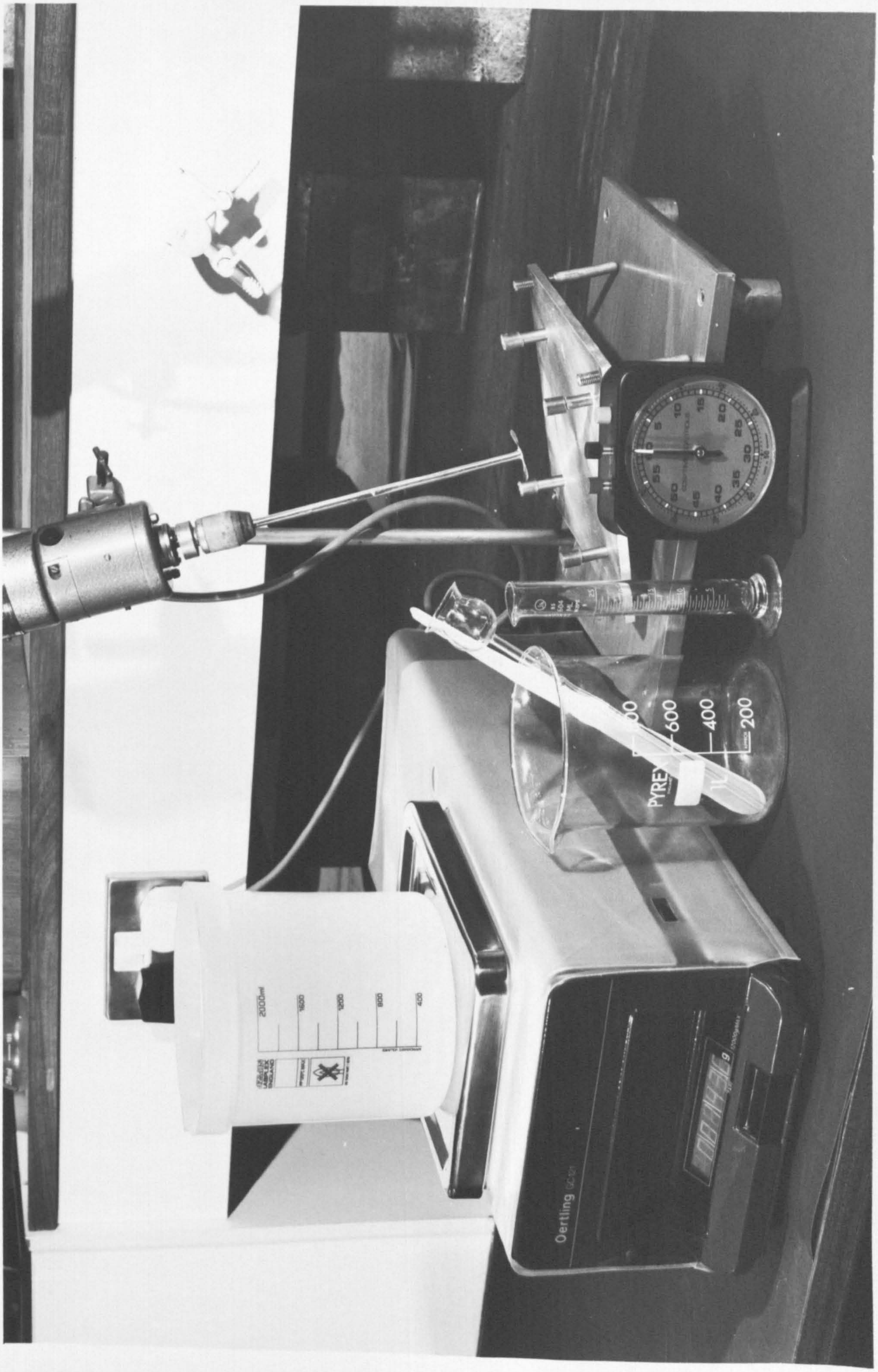

FIG. 4.4 MIXING APPARATUS

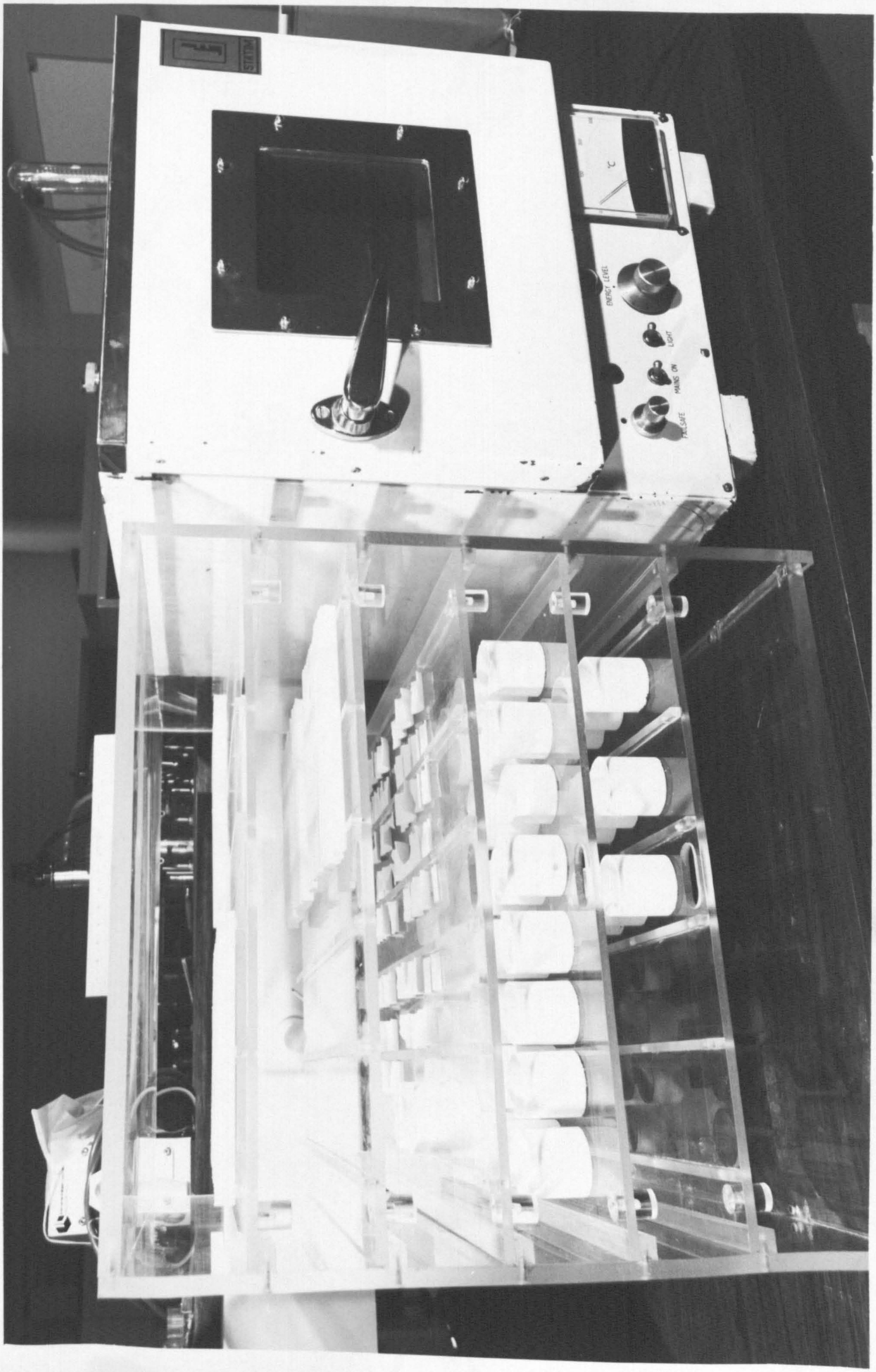

FIG. 4.5 DRYING CHAMBER AND CABINET

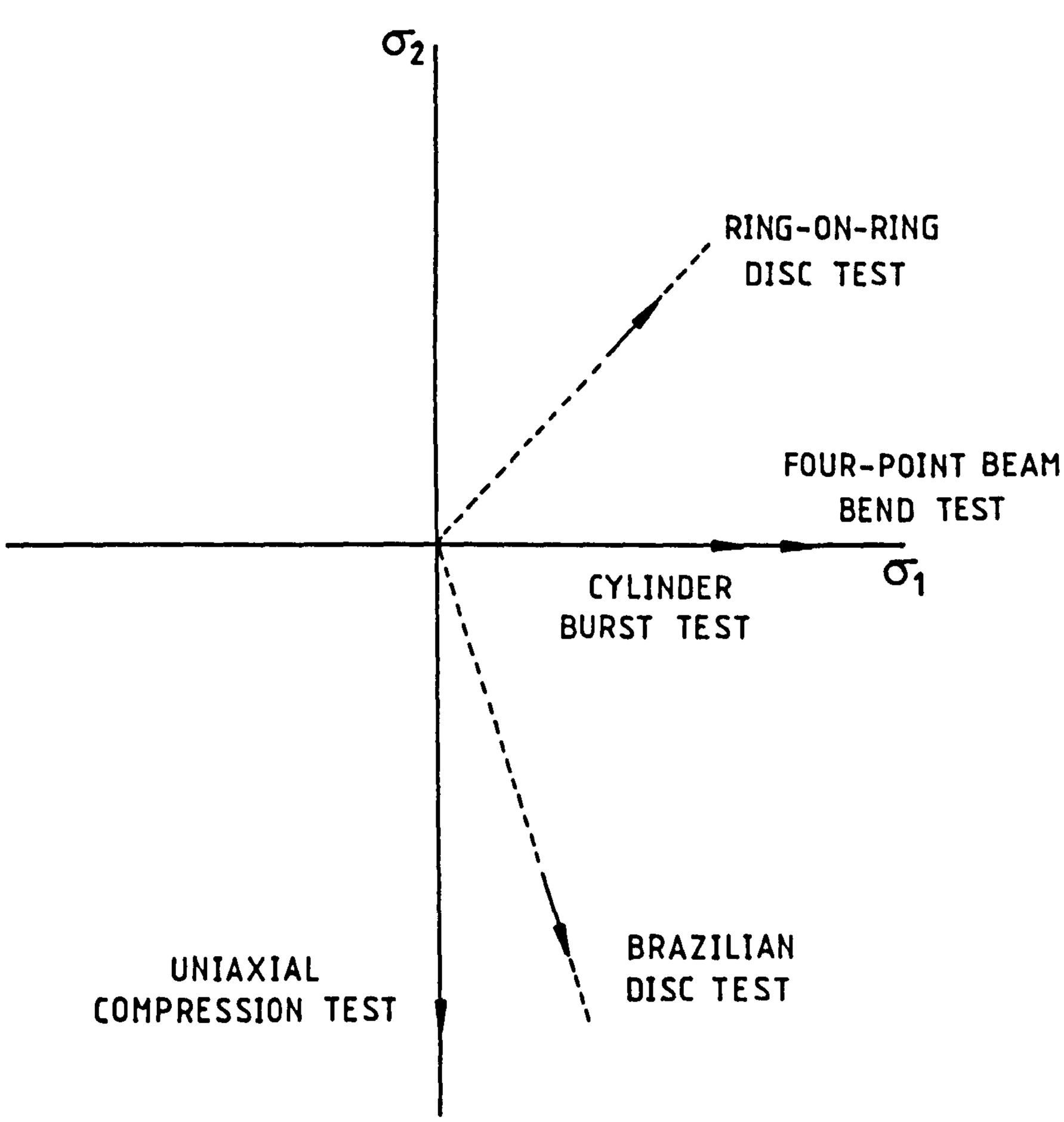

FIG. 4.6 ALLOCATION OF TESTS

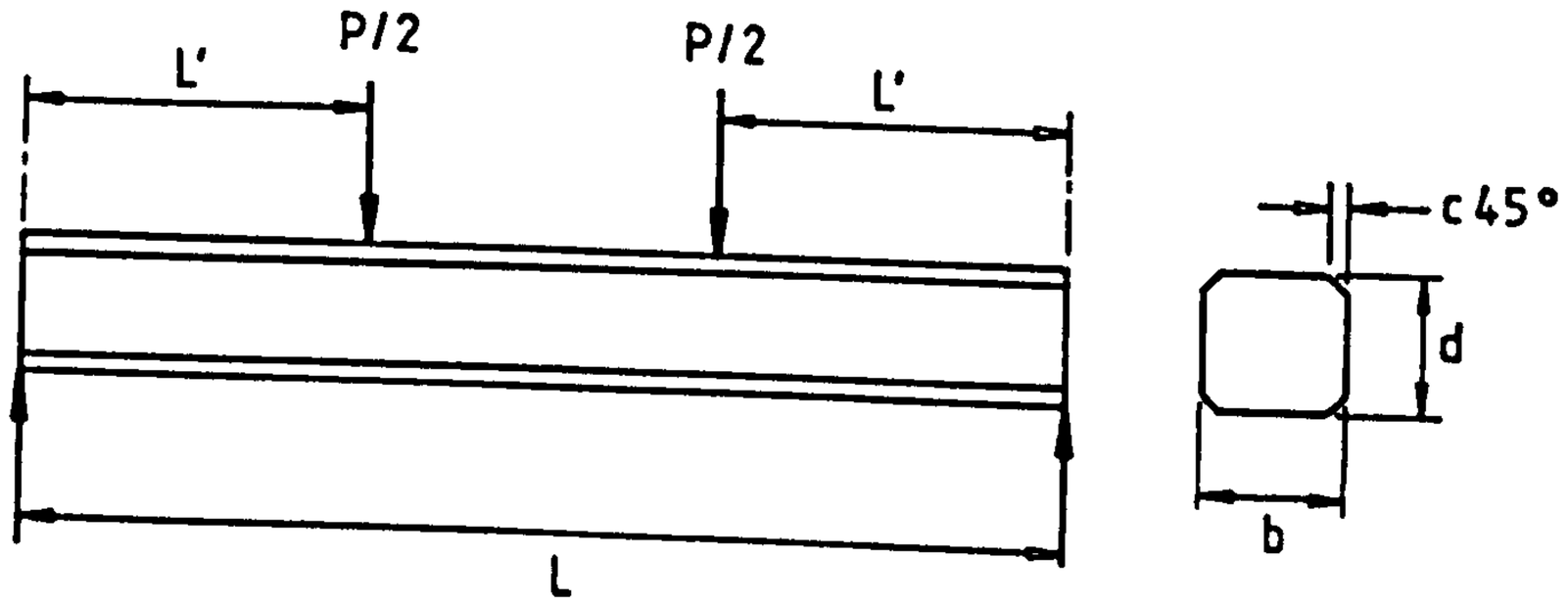

FIG. 4.7 SCHEMATIC DIAGRAM OF FOUR-POINT BENDING

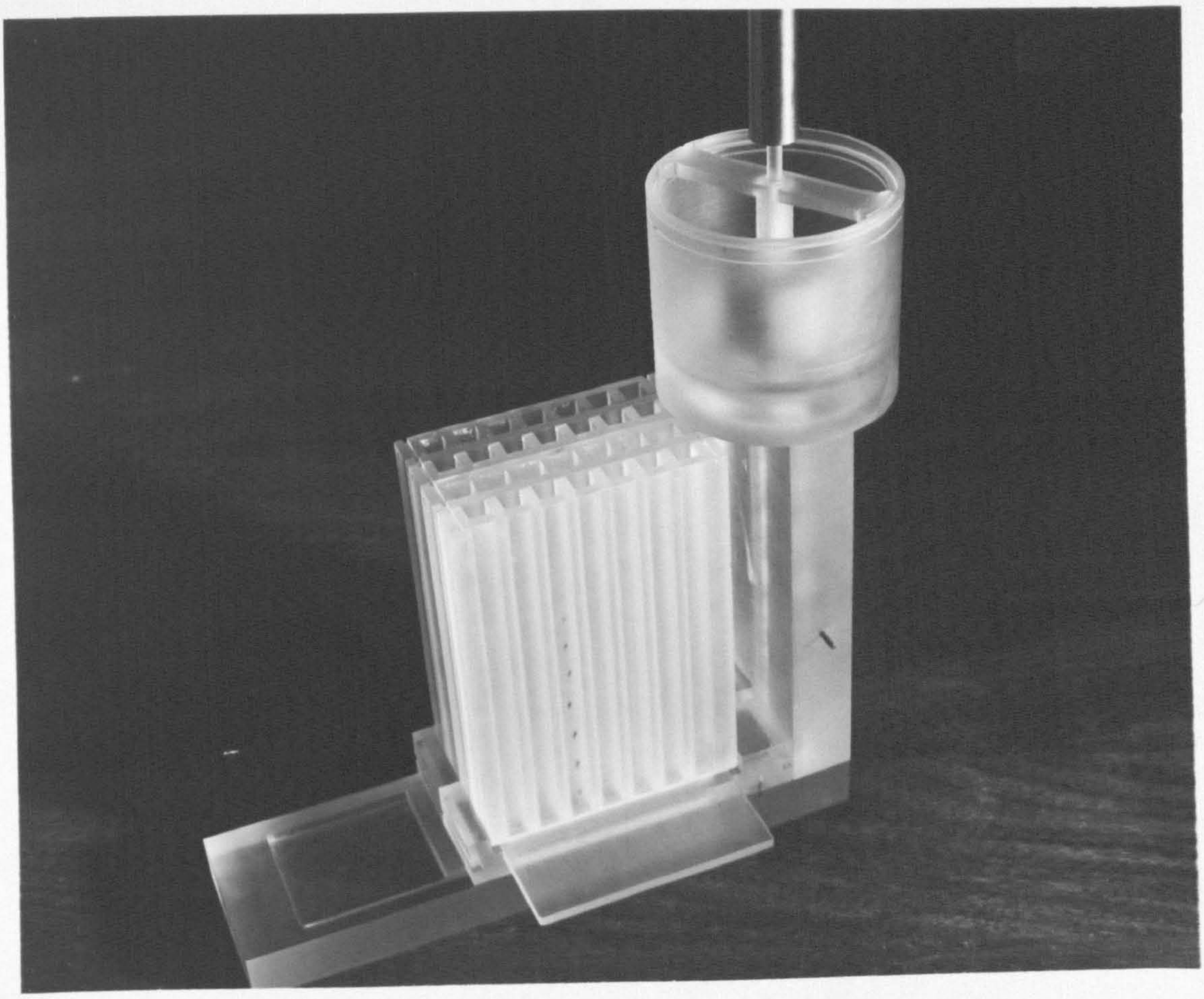

FIG. 4.8 BEAM MOULD ASSEMBLY

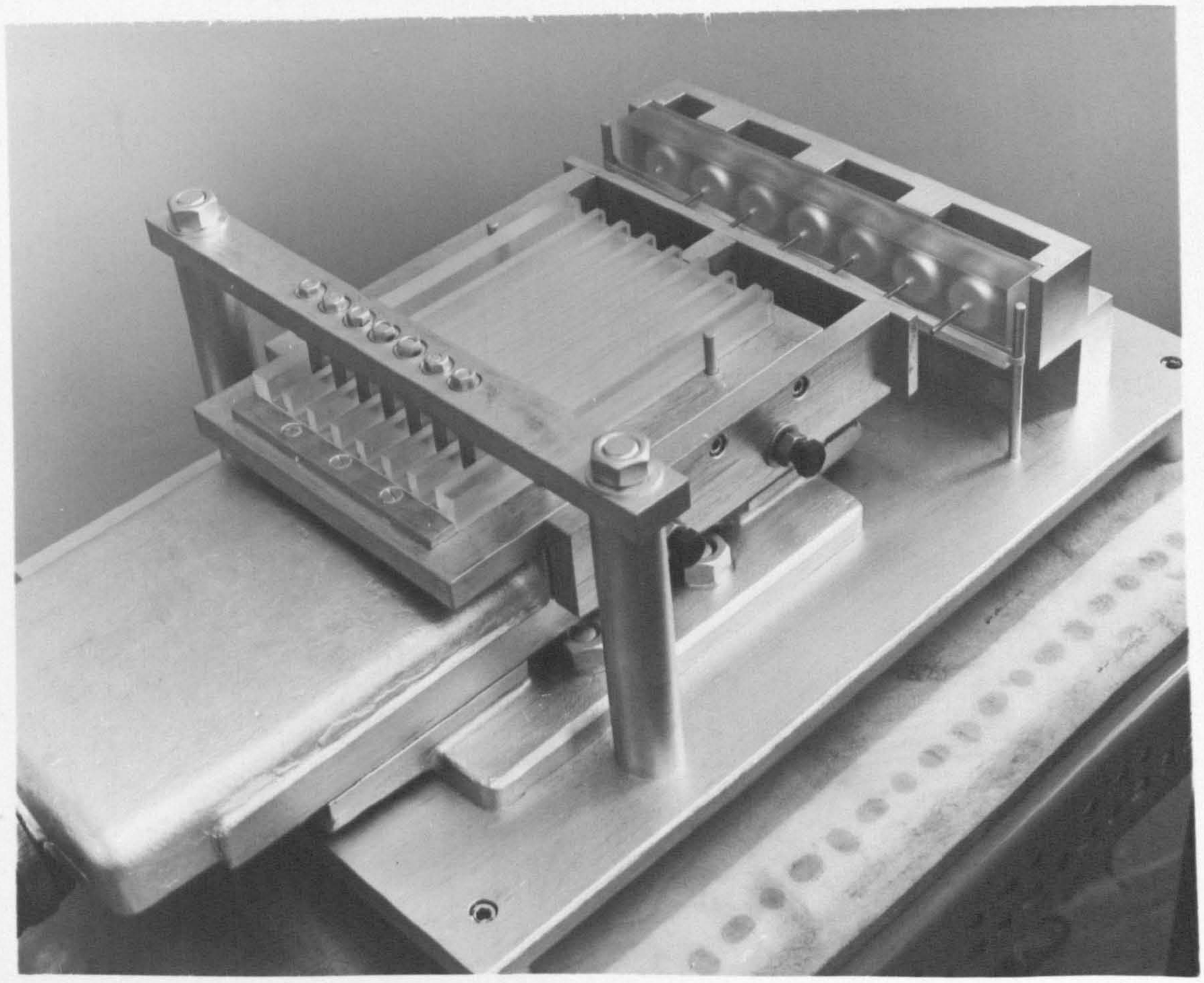

FIG. 4.9 BEAM AND DISC EXTRACTION DEVICE

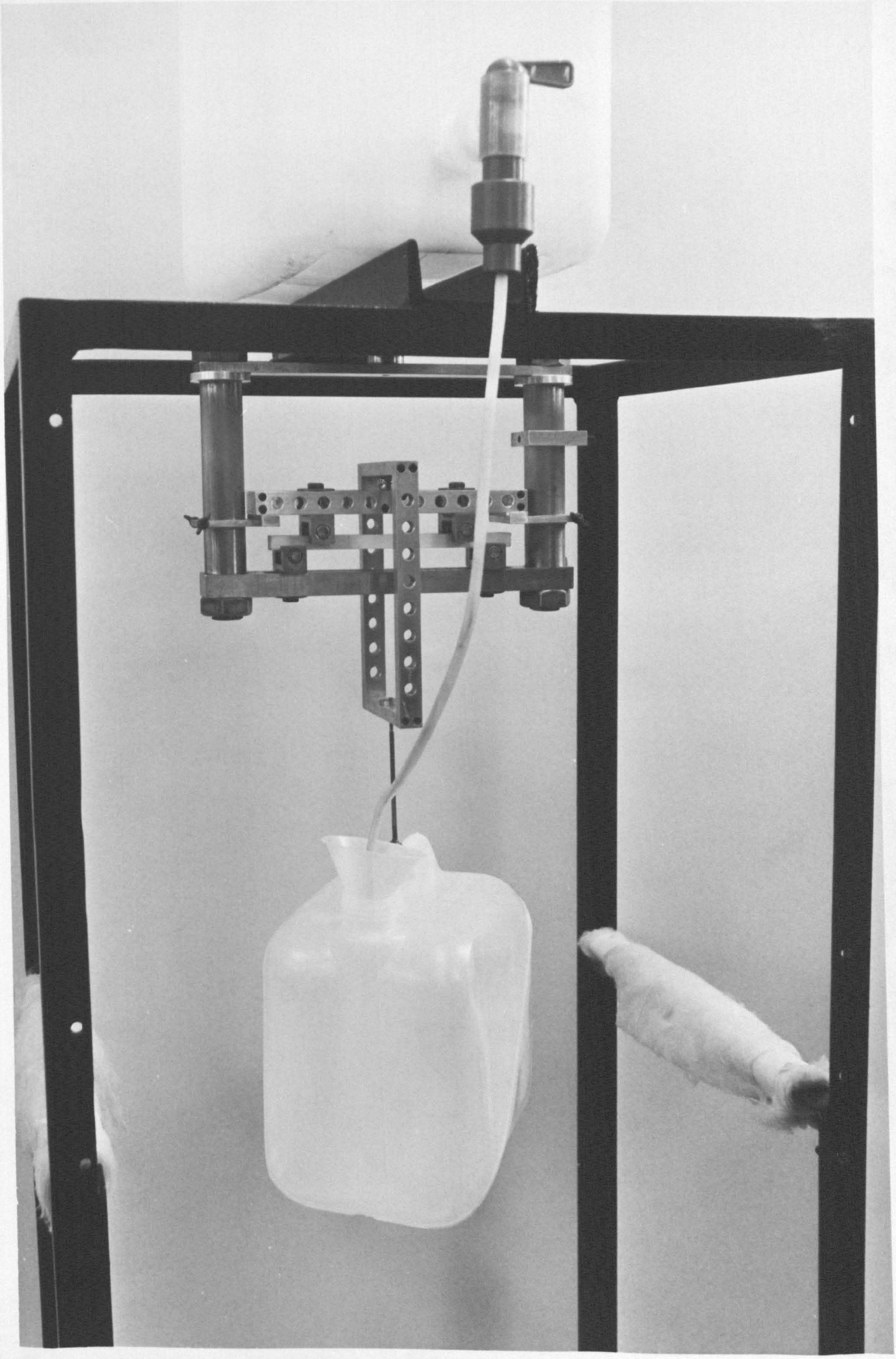

FIG. 4.1O FOUR-POINT BEAM BEND TEST MIXTURE

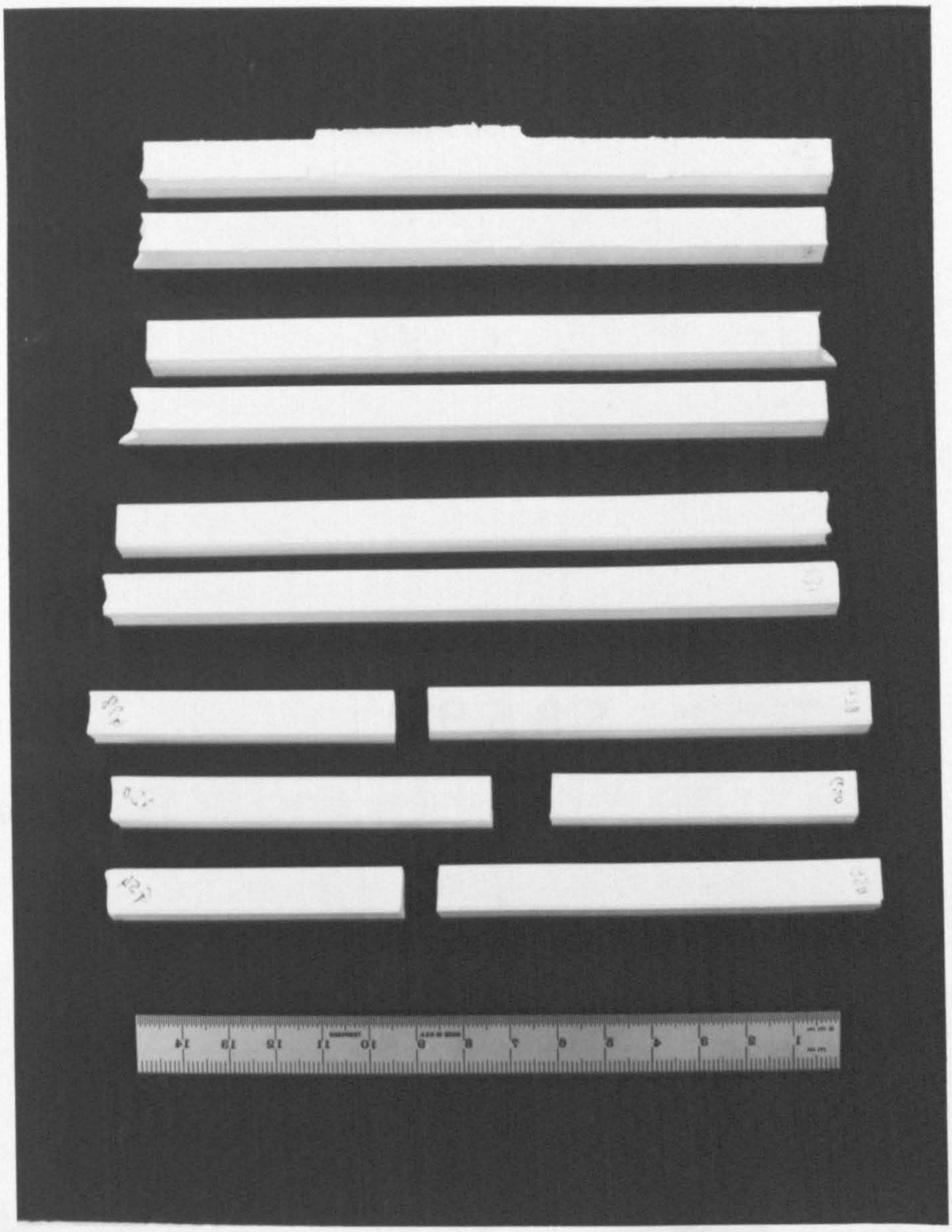

FIG. 4.11 VARIOUS BEAM SPECIMENS OBTAINED BEFORE AND AFTER TESTING

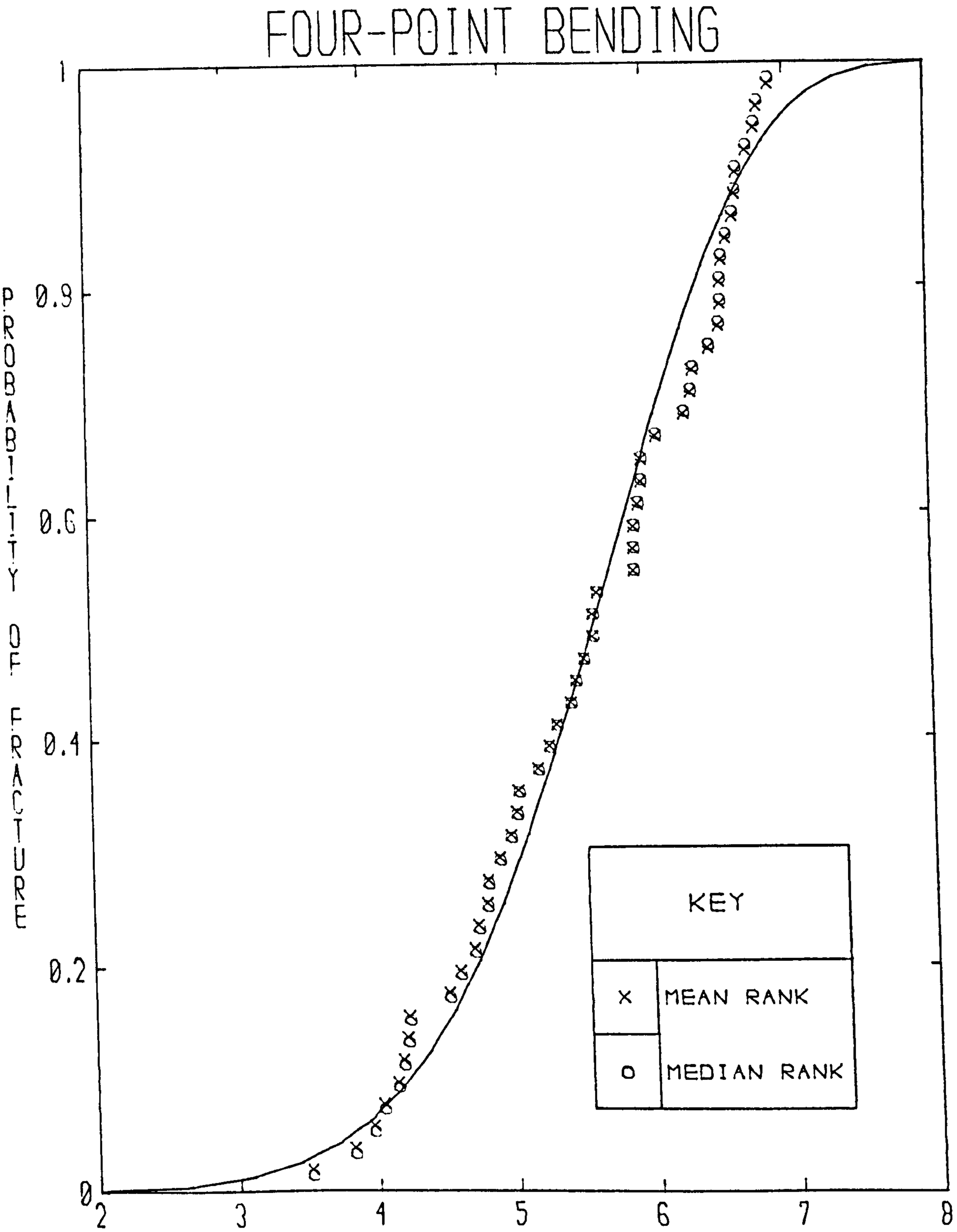

FIG. 4.12 THE CUMULATIVE DISTRIBUTION OF FRACTURE STRENGTHS OF 50 SPECIMENS TESTED IN FOUR-POINT BENDING

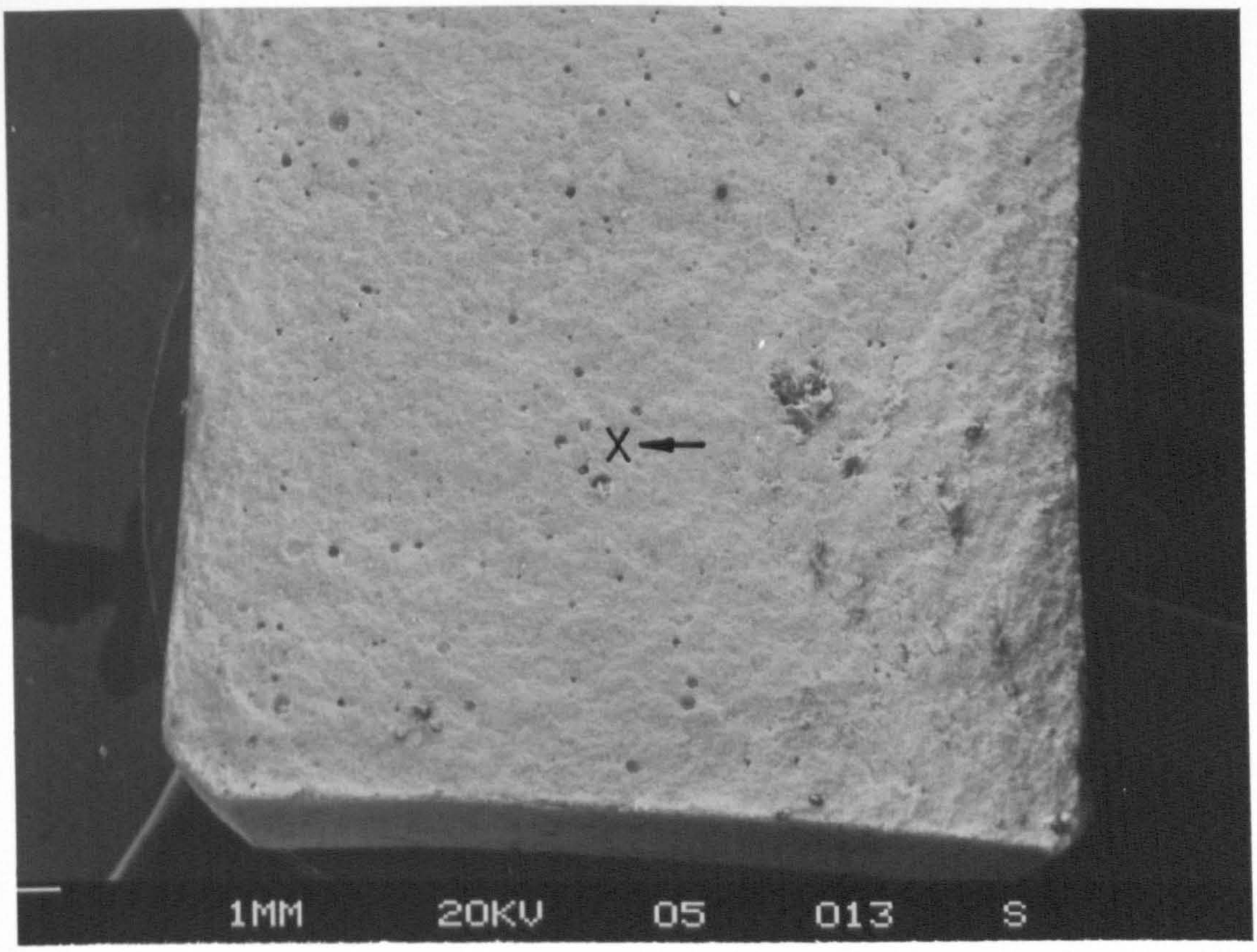

FIG. 4.13 A TYPICAL FRACTURE SURFACE OF A FOUR-POINT BEAM BEND TEST WITH POROSITY; x 6

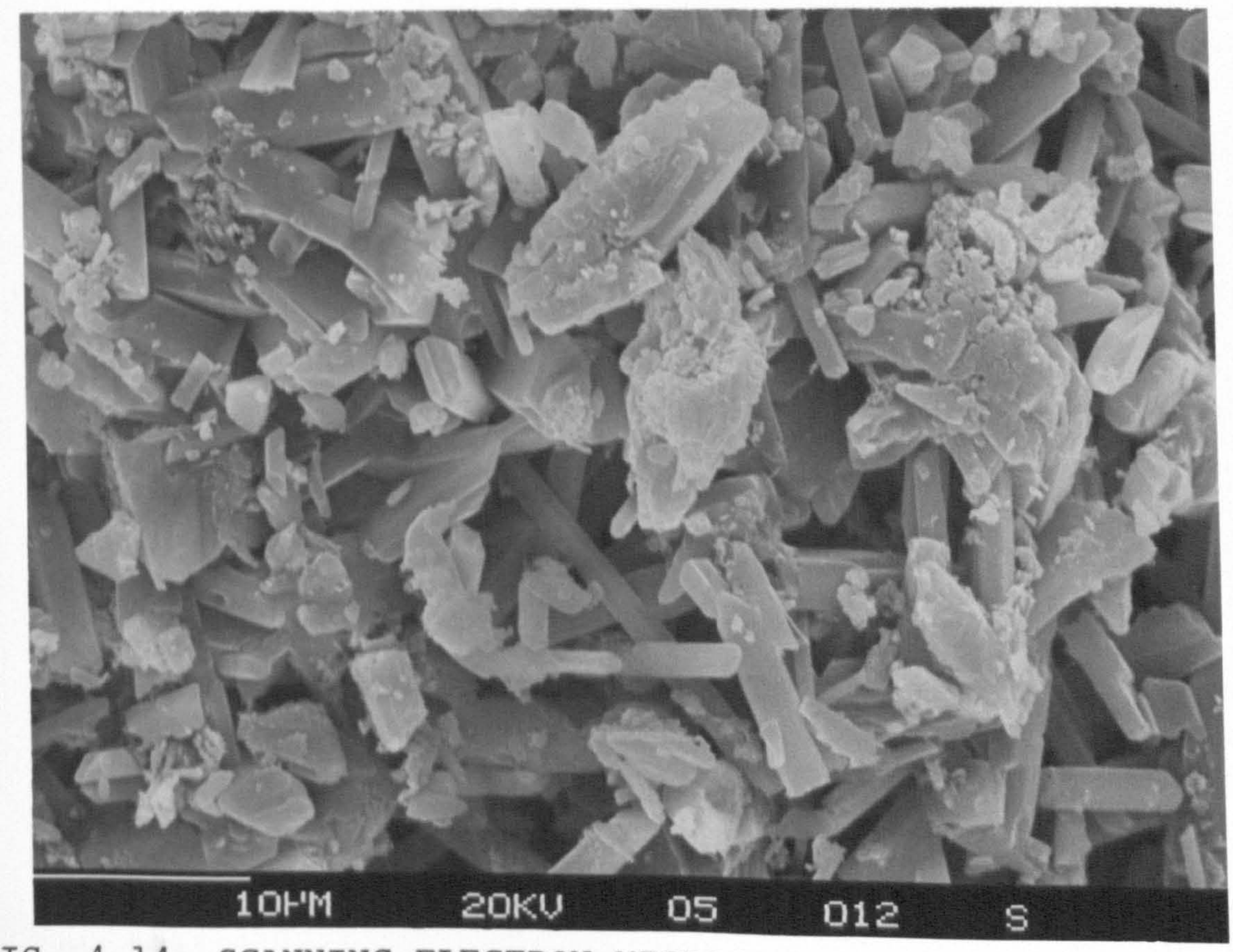

FIG. 4.14 SCANNING ELECTRON MICROGRAPH OF FRACTURE SURFACE OF A FOUR-POINT BEAM BEND TEST; x 2000

FIG. 4.15 CYLINDER BURST TEST ASSEMBLY

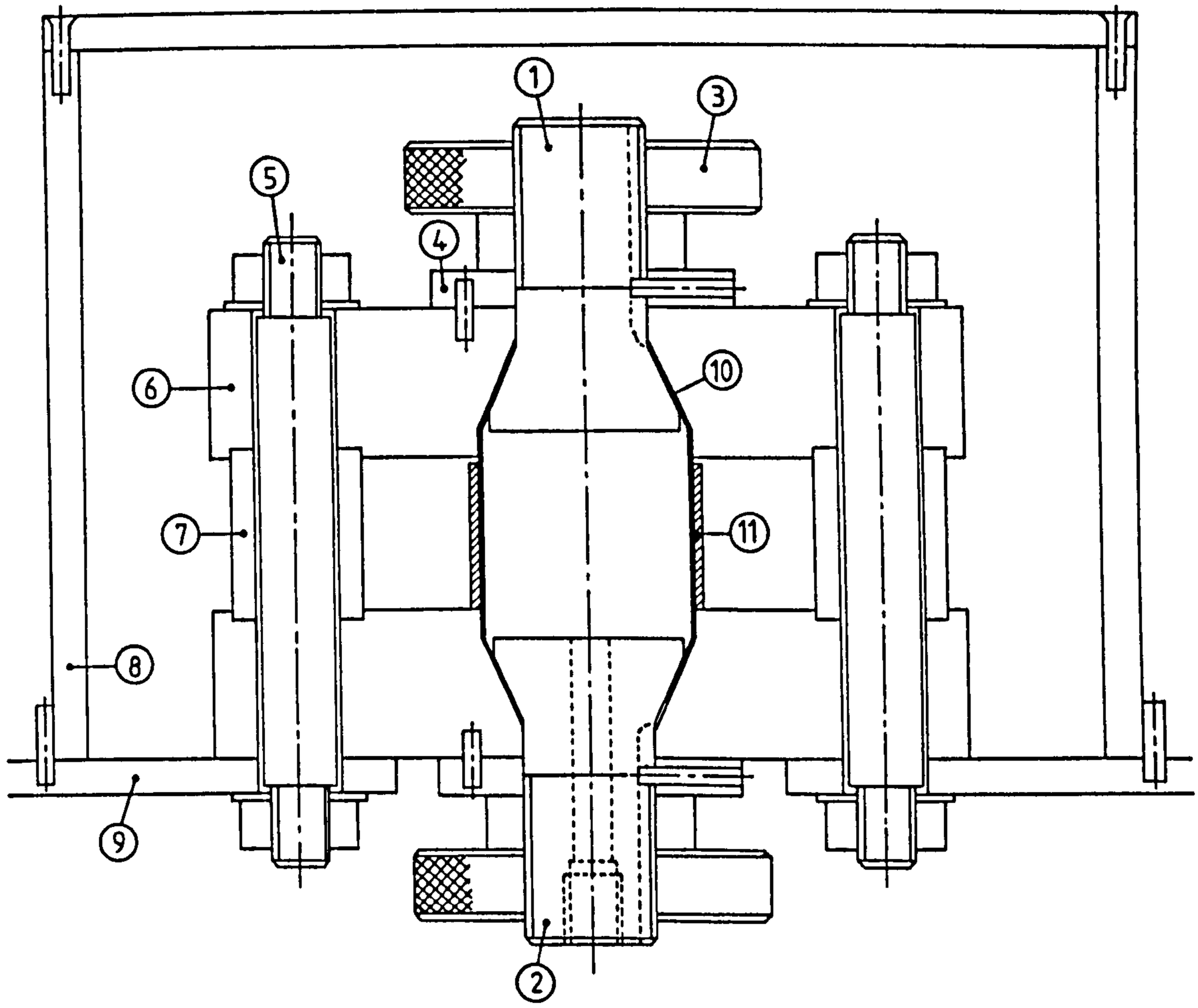

1. TOP CONICAL PLUG
2. BOTTOM CONICAL PLUG
3. CIRCULAR NUT
4. DISC
5. PILLAR
6. PLATE
7. SPACER BLOCK
8. COVER
9. BASE PLATE
10. RUBBER TUBE
11. SPECIMEN

FIG. 4.16 SCHEMATIC OF CYLINDER BURST TEST

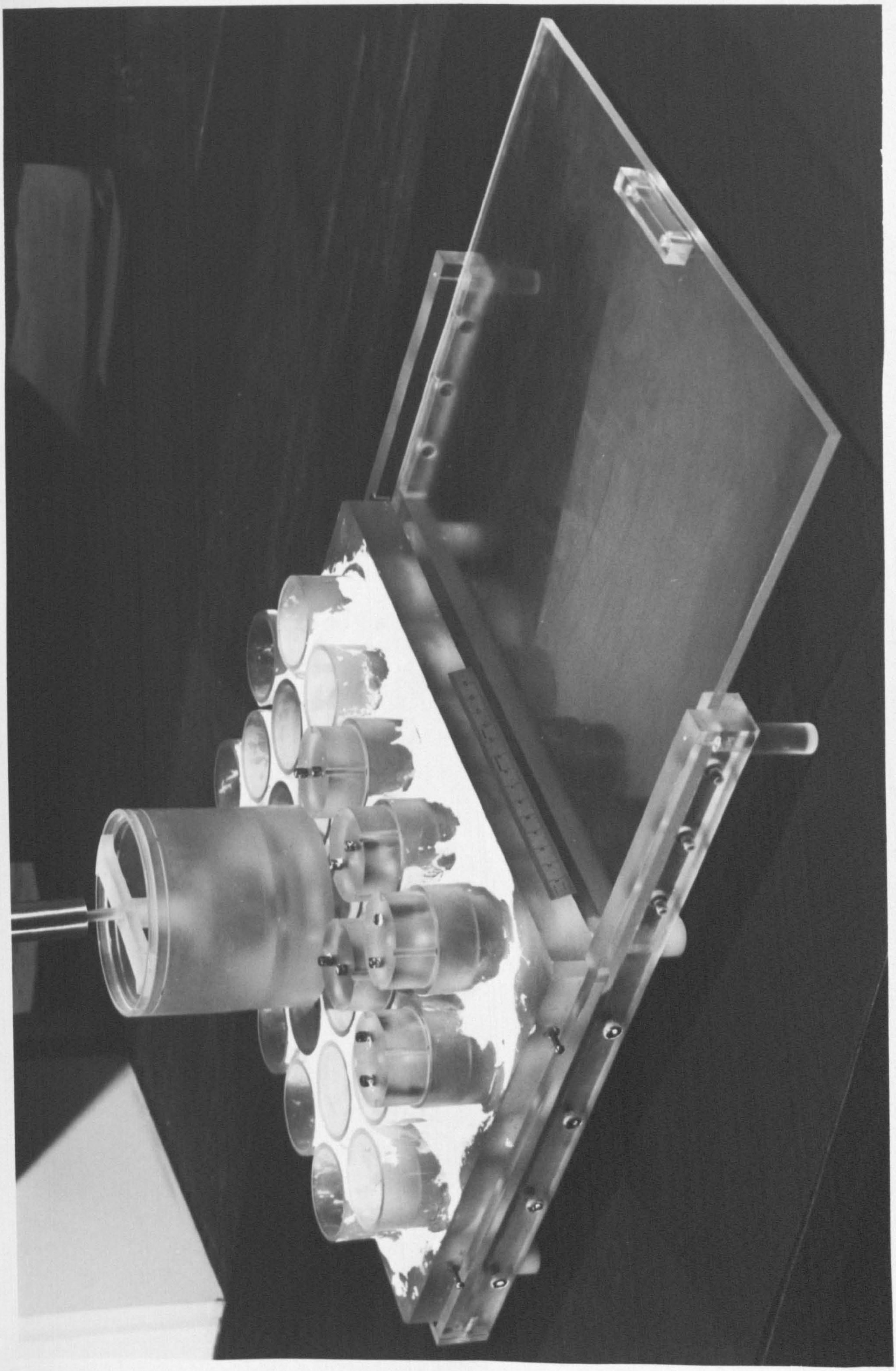

FIG. 4.17 CYLINDER MOULD ASSEMBLY

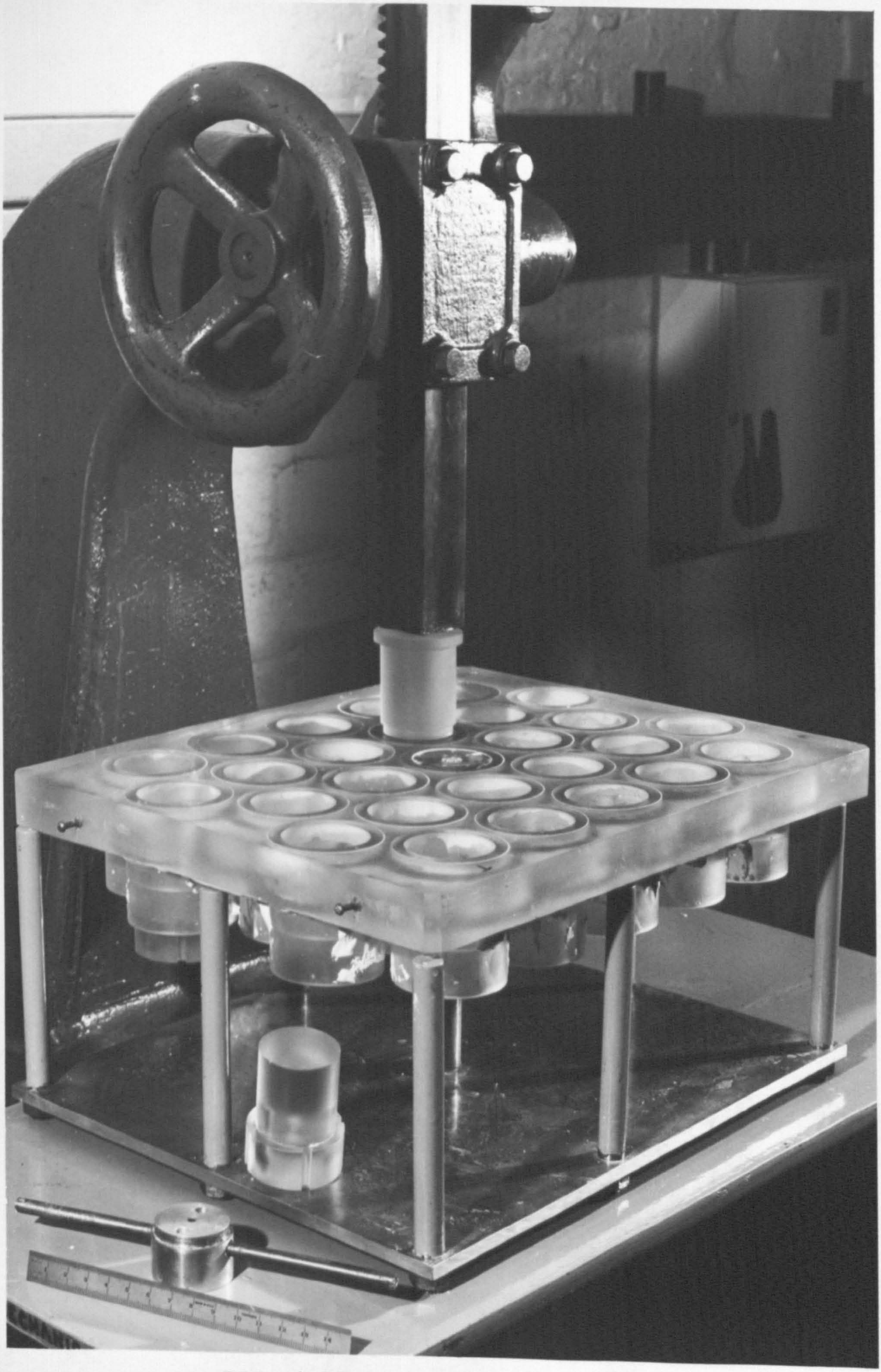

FIG. 4.18 CYLINDER EXTRACTION DEVICE

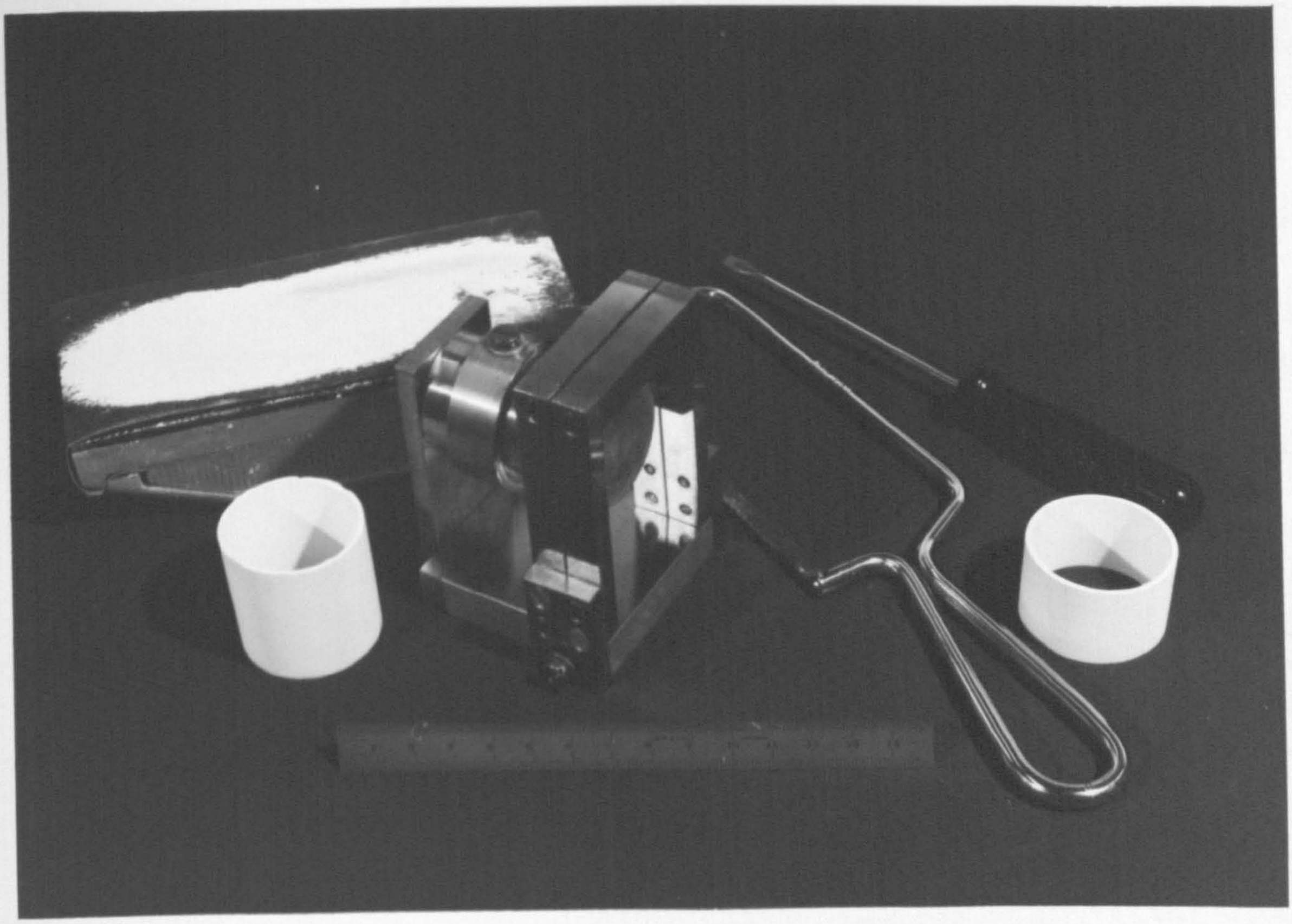

FIG. 4.19 DEVICE USED FOR PREPARATION OF THE CYLINDER

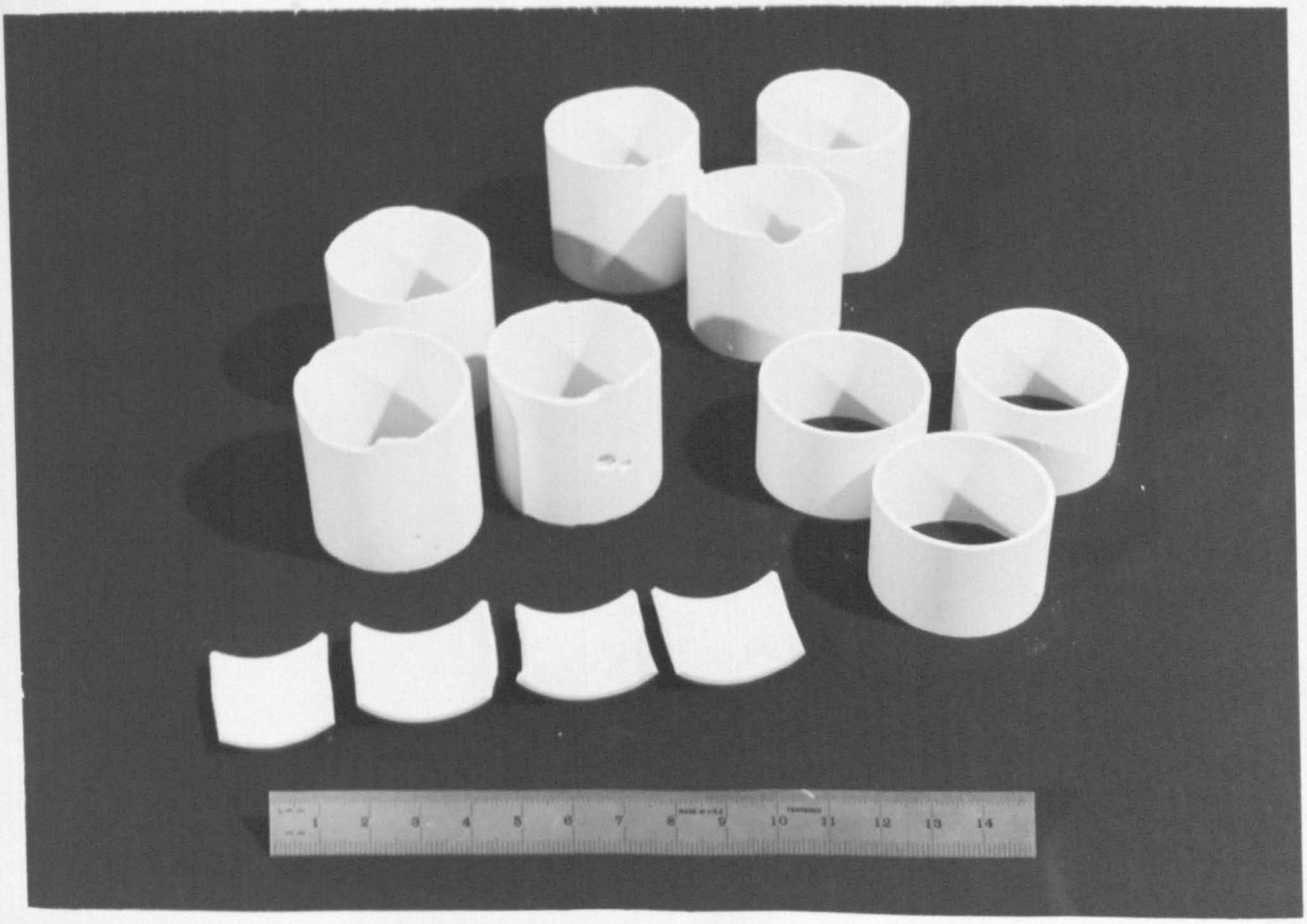

FIG. 4.20 VARIOUS CYLINDER SPECIMENS OBTAINED BEFORE AND AFTER TESTING

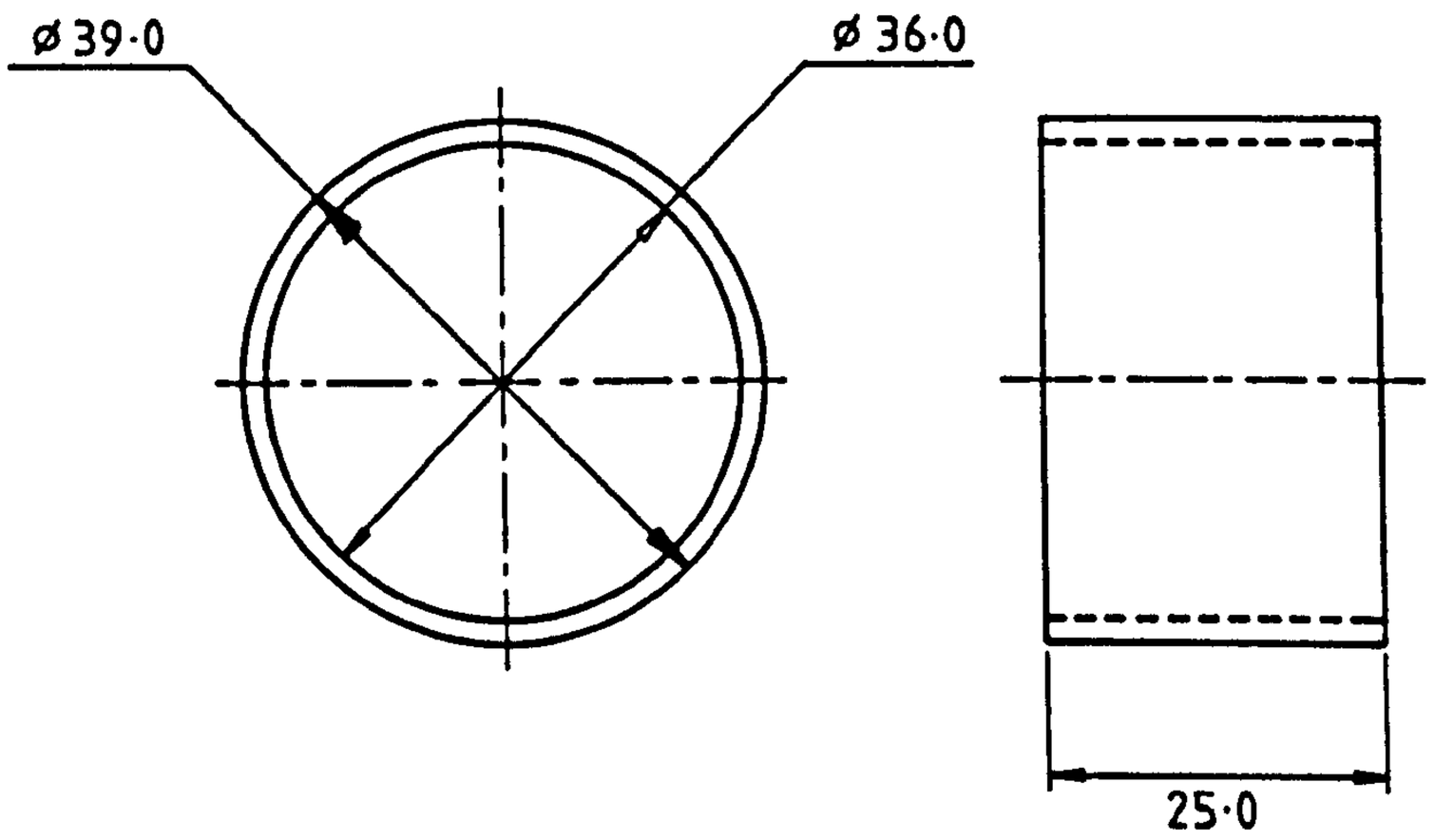

All dimensions in m.m

FIG. 4.21 SPECIMEN CONFIGURATION FOR CYLINDER BURST TEST

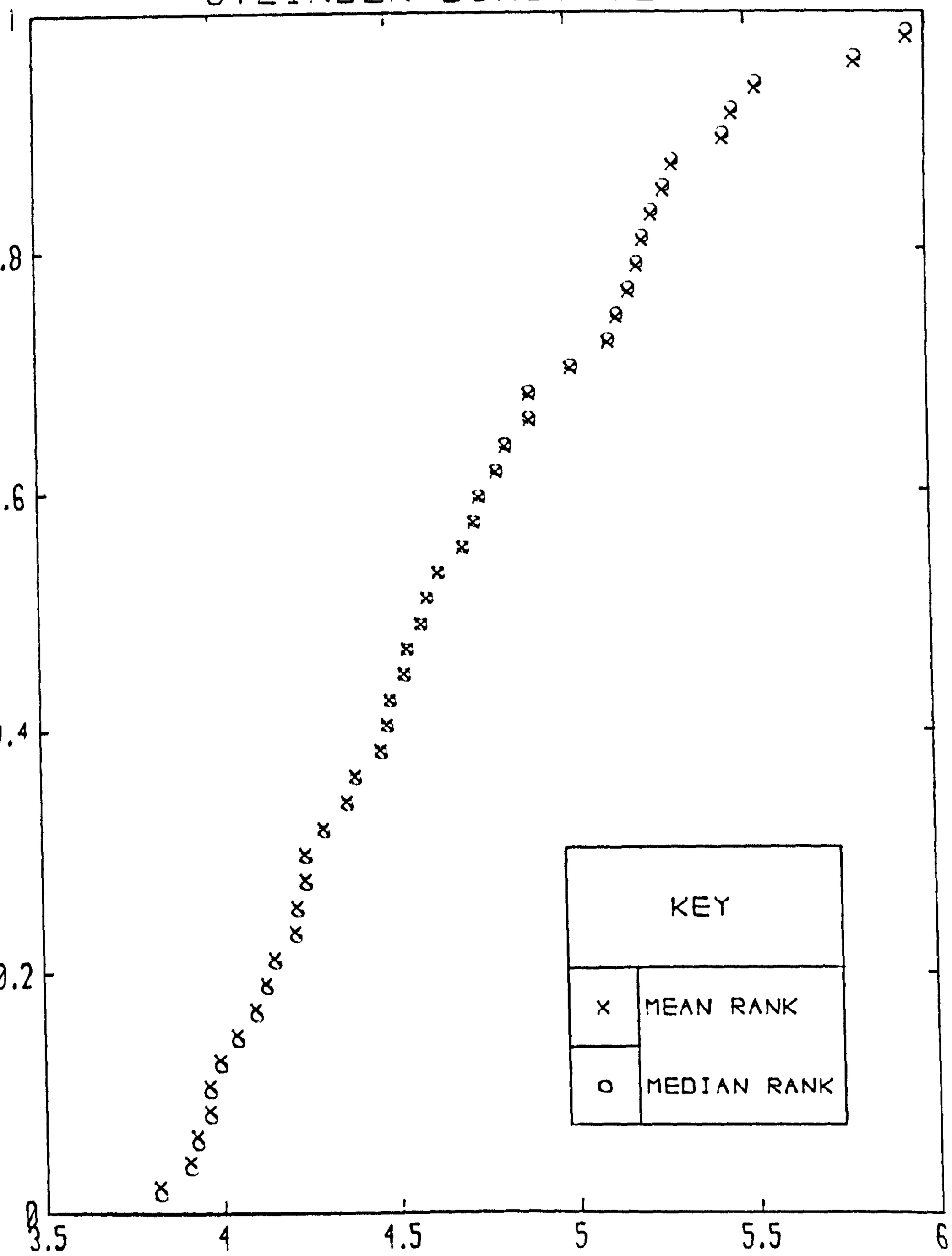

FIG. 4.22 THE CUMULATIVE DISTRIBUTION OF FRACTURE STRENGTHS OF 46 SPECIMENS TESTED IN CYLINDER BURST TEST

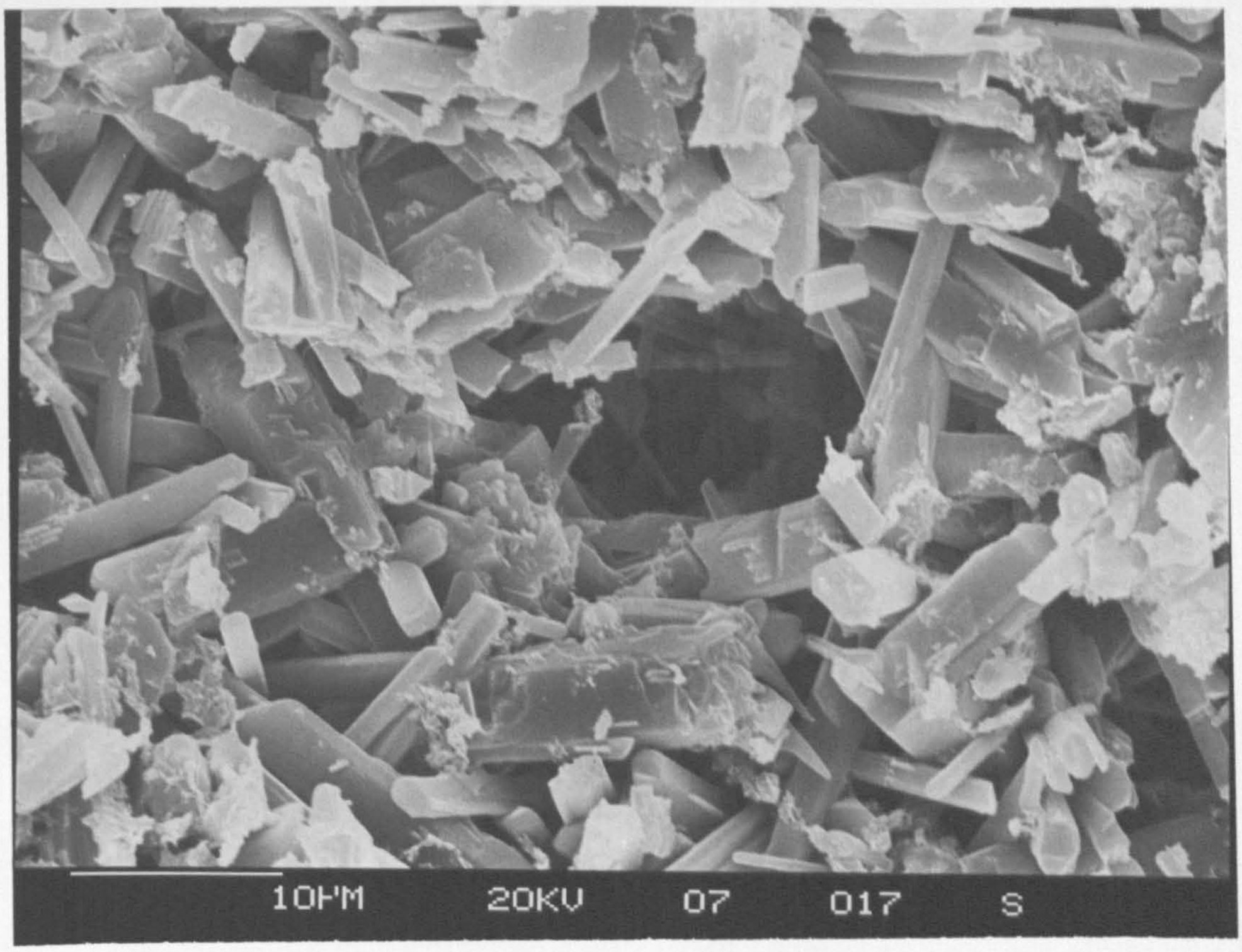

FIG. 4.23 SCANNING ELECTRON MICROGRAPH OF A FRACTURE SURFACE OF A CYLINDER BURST TEST; x 2000

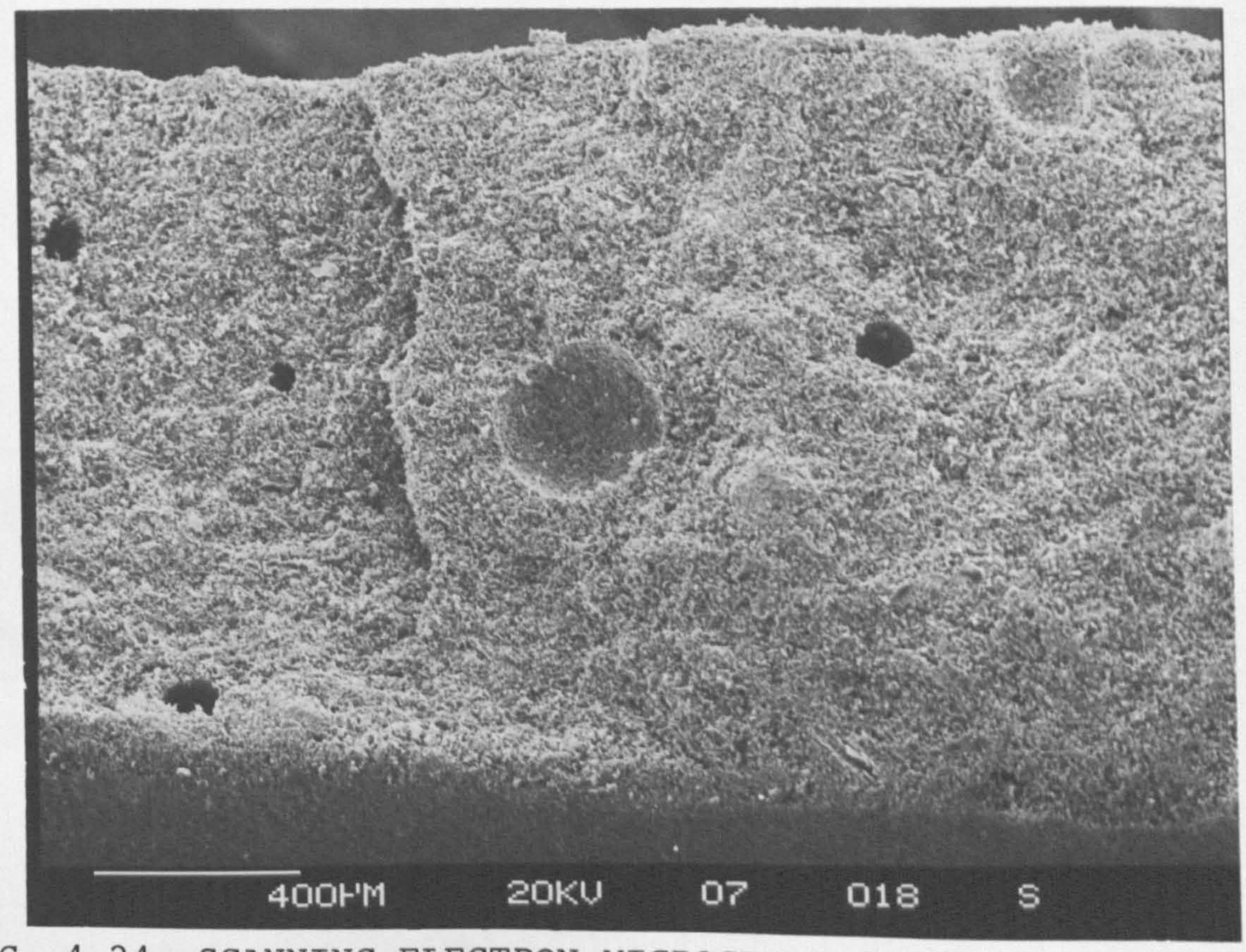

FIG. 4.24 SCANNING ELECTRON MICROGRAPH OF THE SAME FRACTURE SURFACE SHOWING THE DUAL PORE DISTRIBUTION; x 50

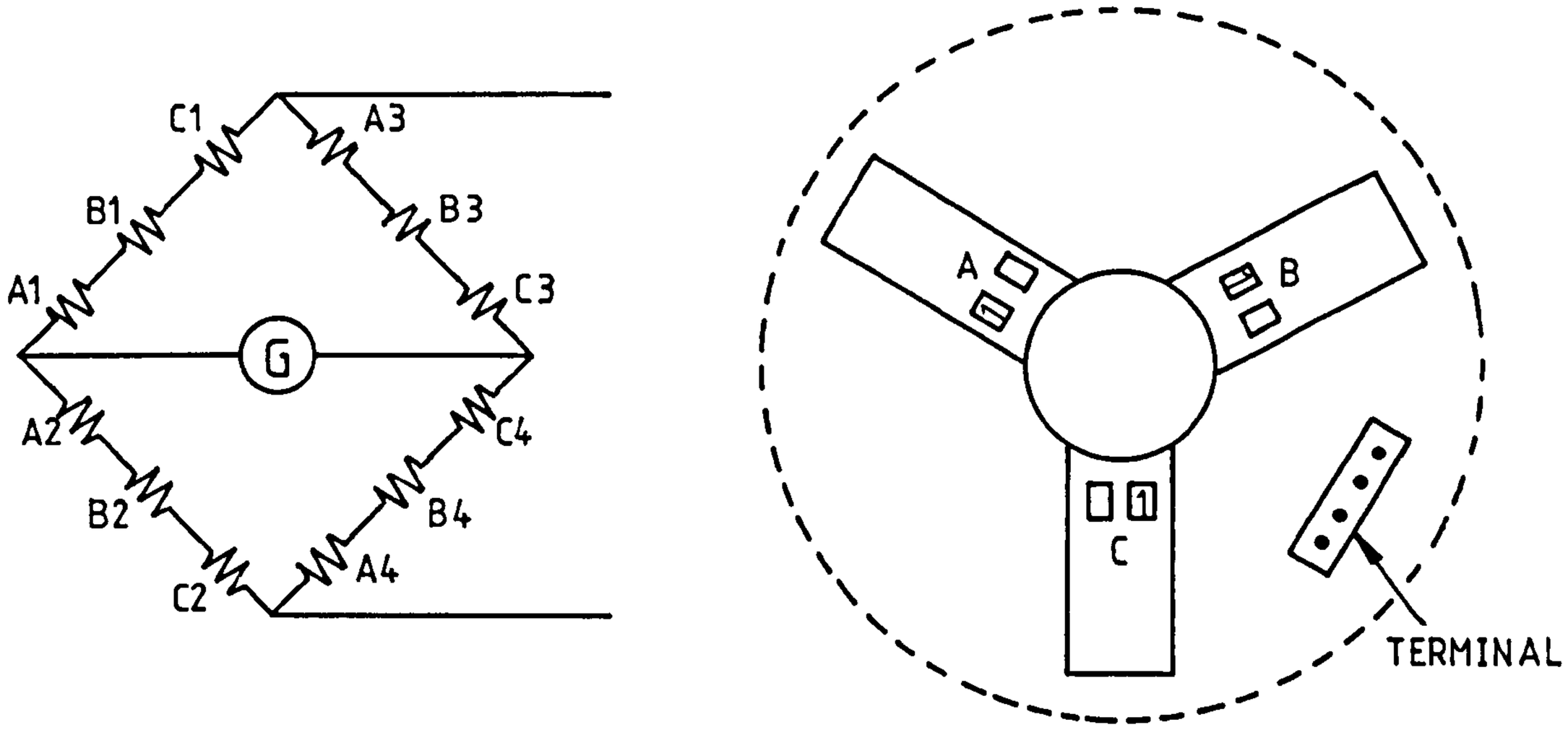

FIG. 4.25 THREE CANTILEVER BEAMS USING FULL BRIDGE

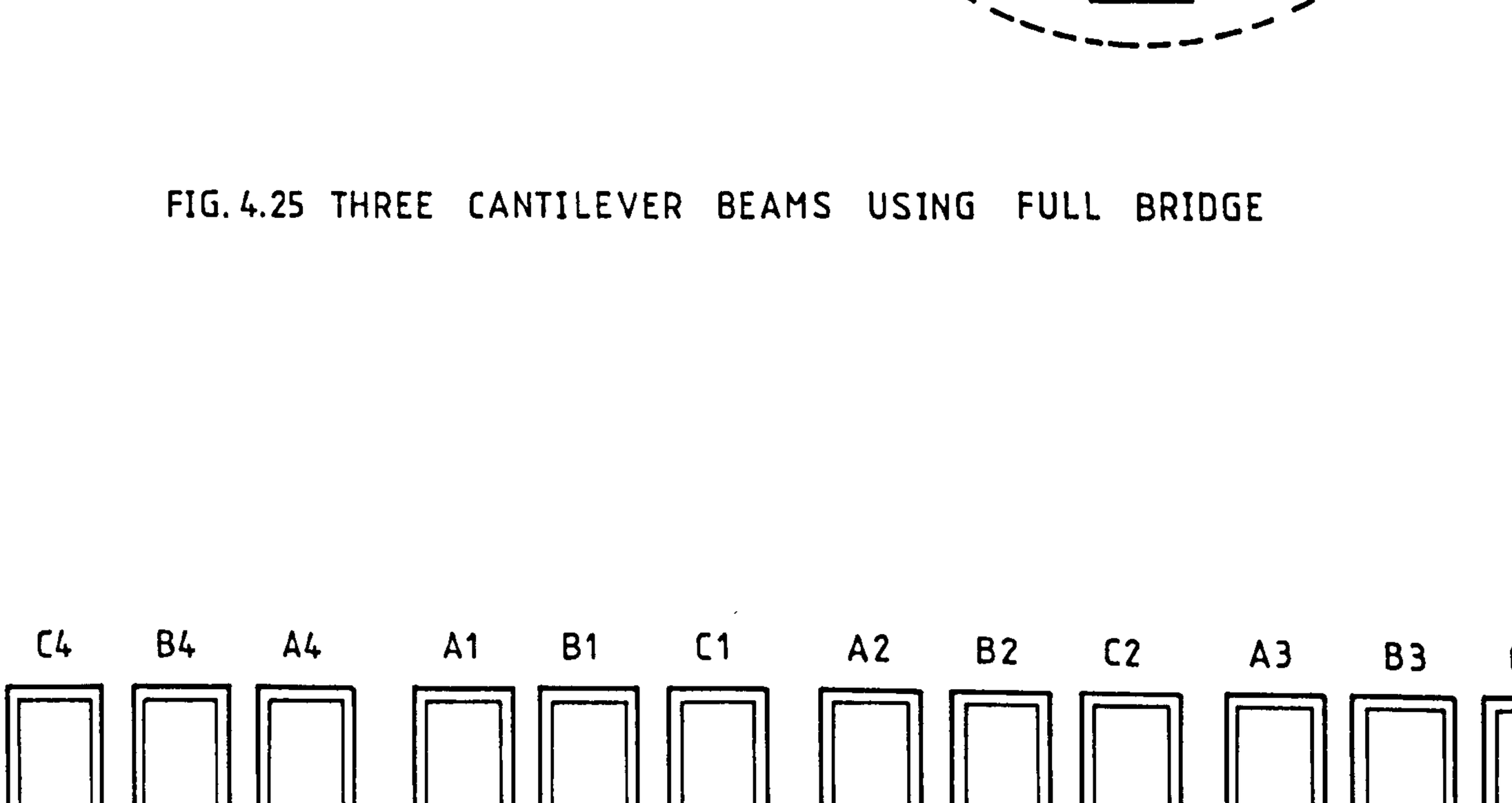

FIG. 4.26 FULL BRIDGE SYSTEM

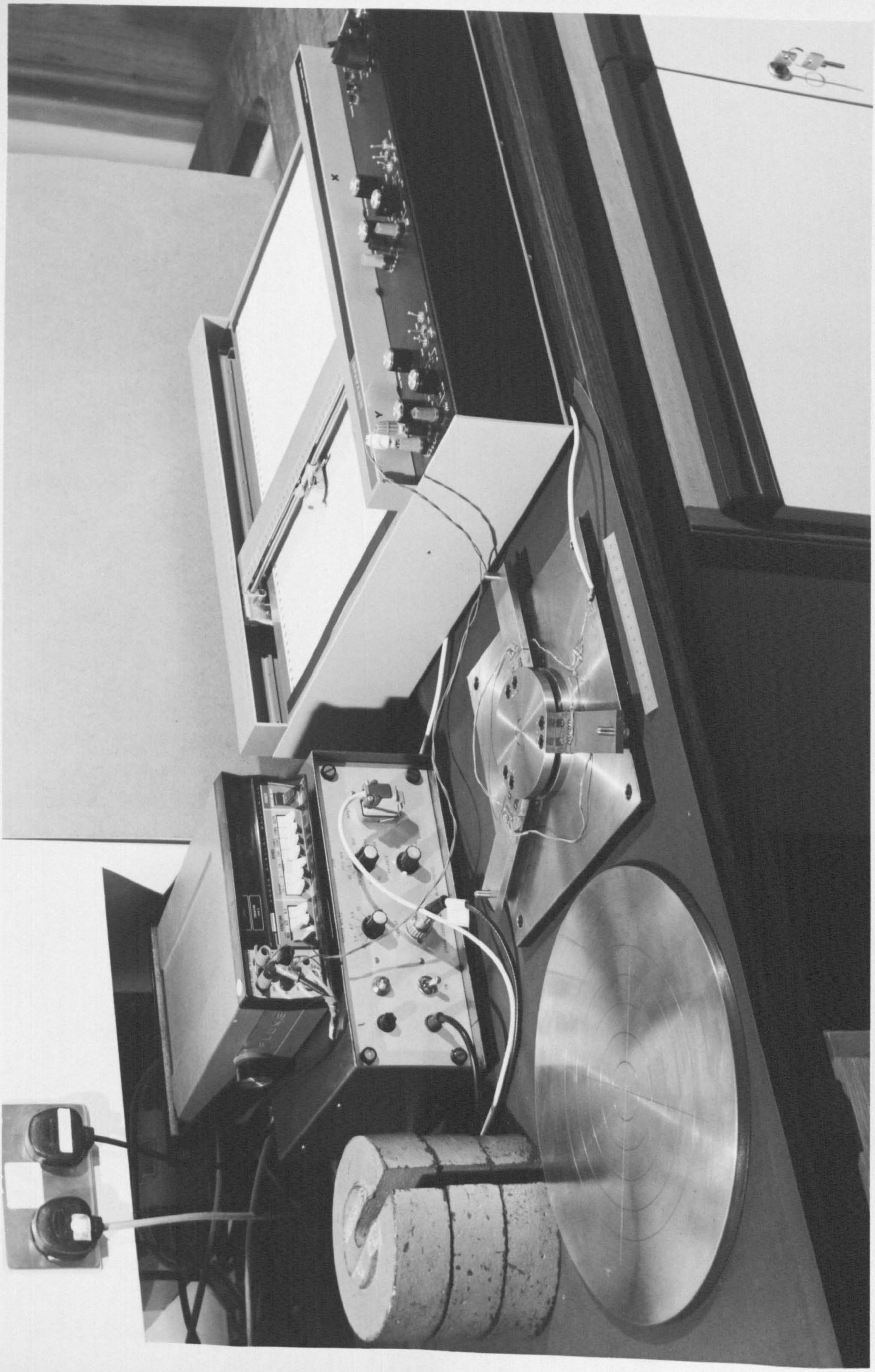

FIG. 4.27 LOAD CELL CALLIBRATION SET UP

FIG. 4.28 LOAD CELL MOUNTED ON TESTING MACHINE

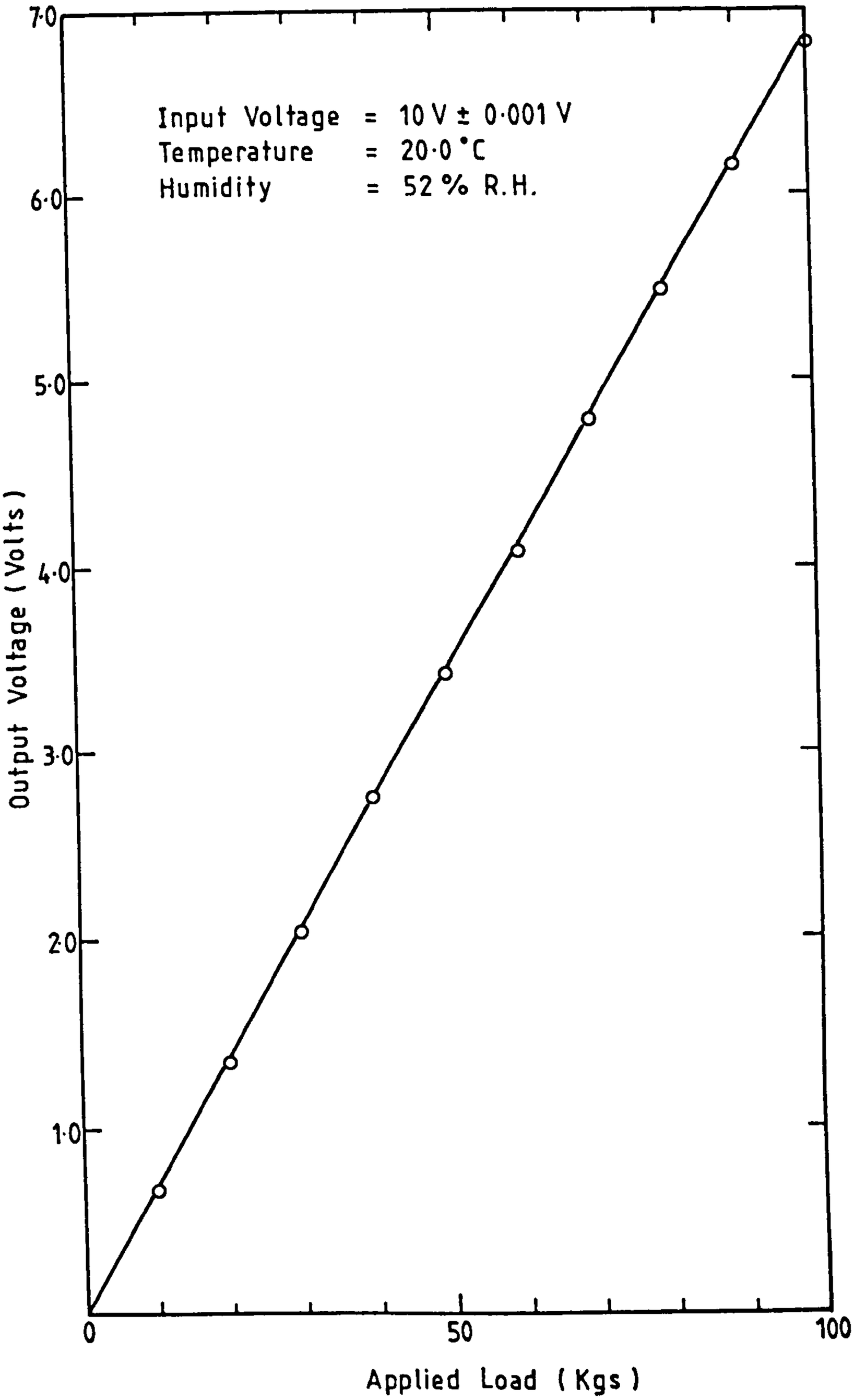

FIG.4.29 LOAD CELL CALIBRATION CURVE

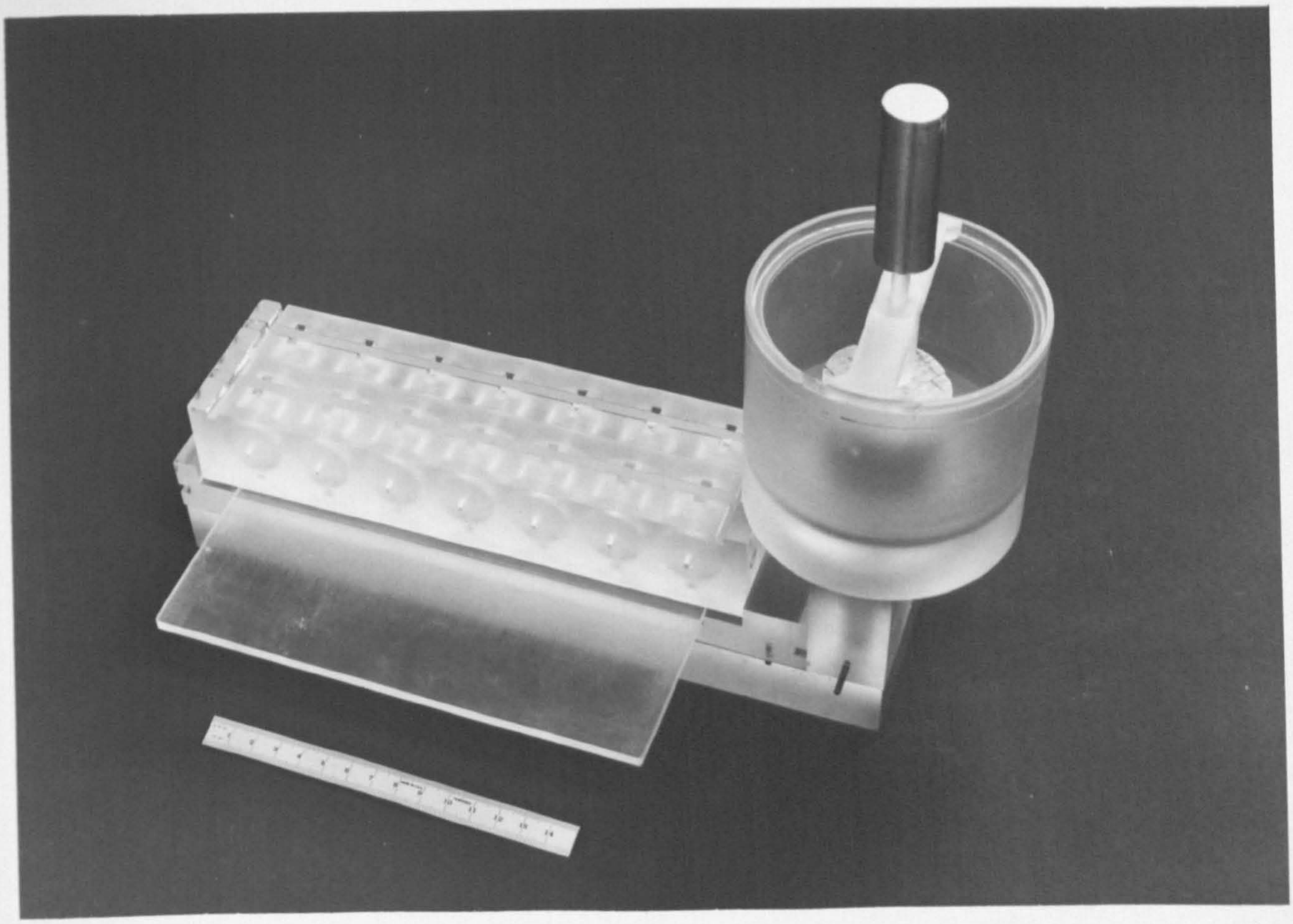

FIG. 4.30 DISC MOULD ASSEMBLY

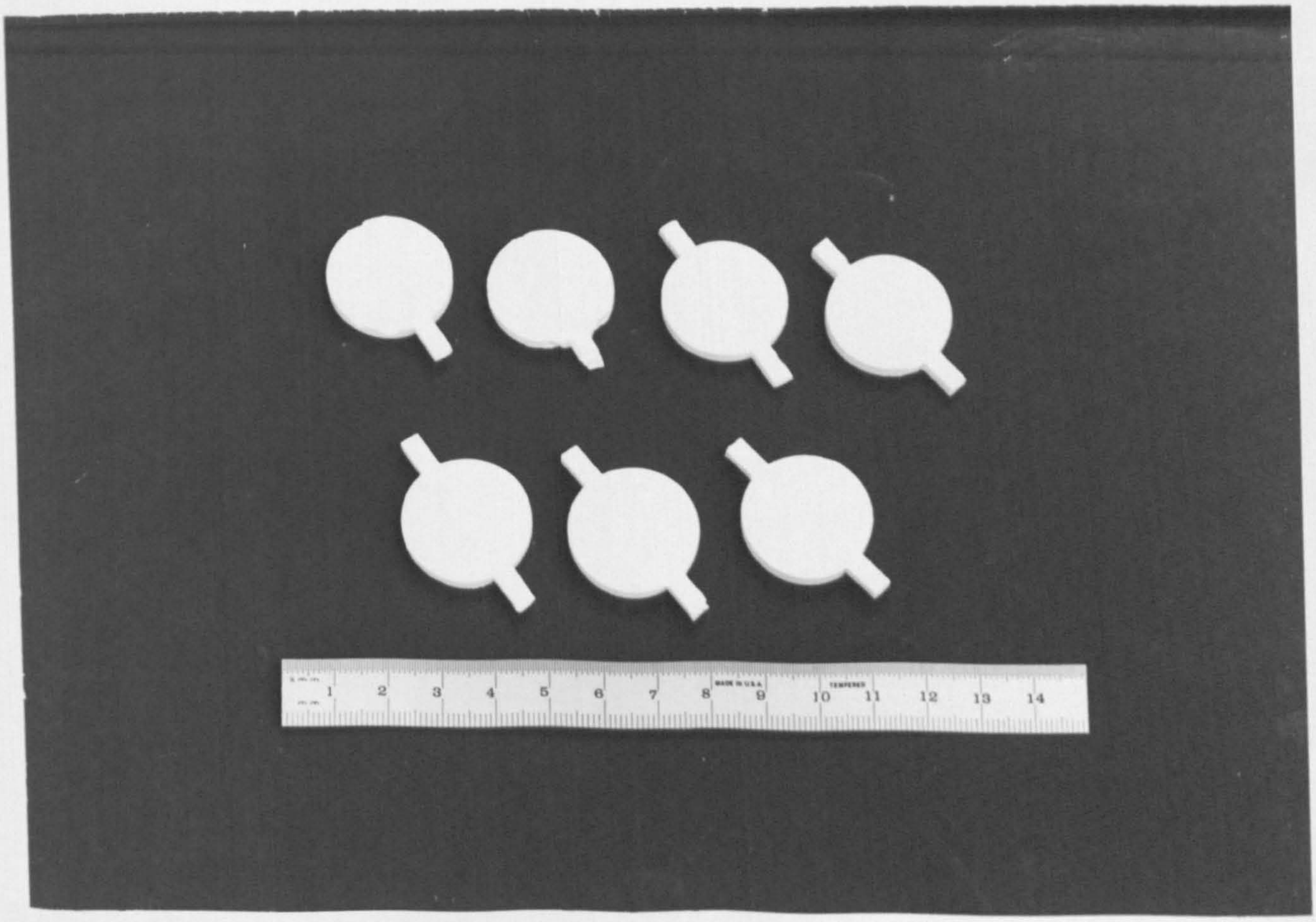

FIG. 4.31 VARIOUS DISC SPECIMENS OBTAINED BEFORE TESTING

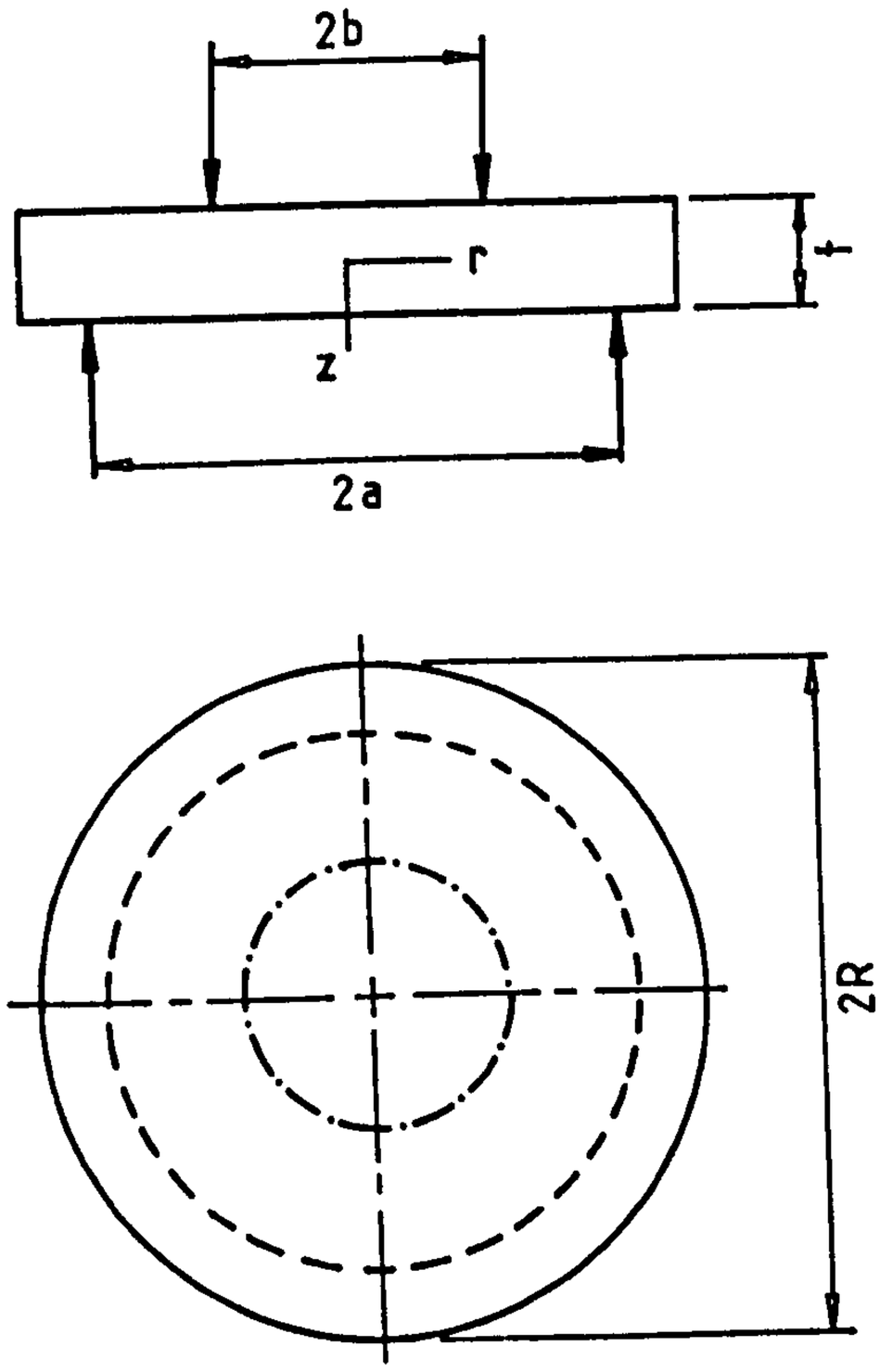

FIG. 4.32 SCHEMATIC DIAGRAM OF RING-ON-RING DISC TEST

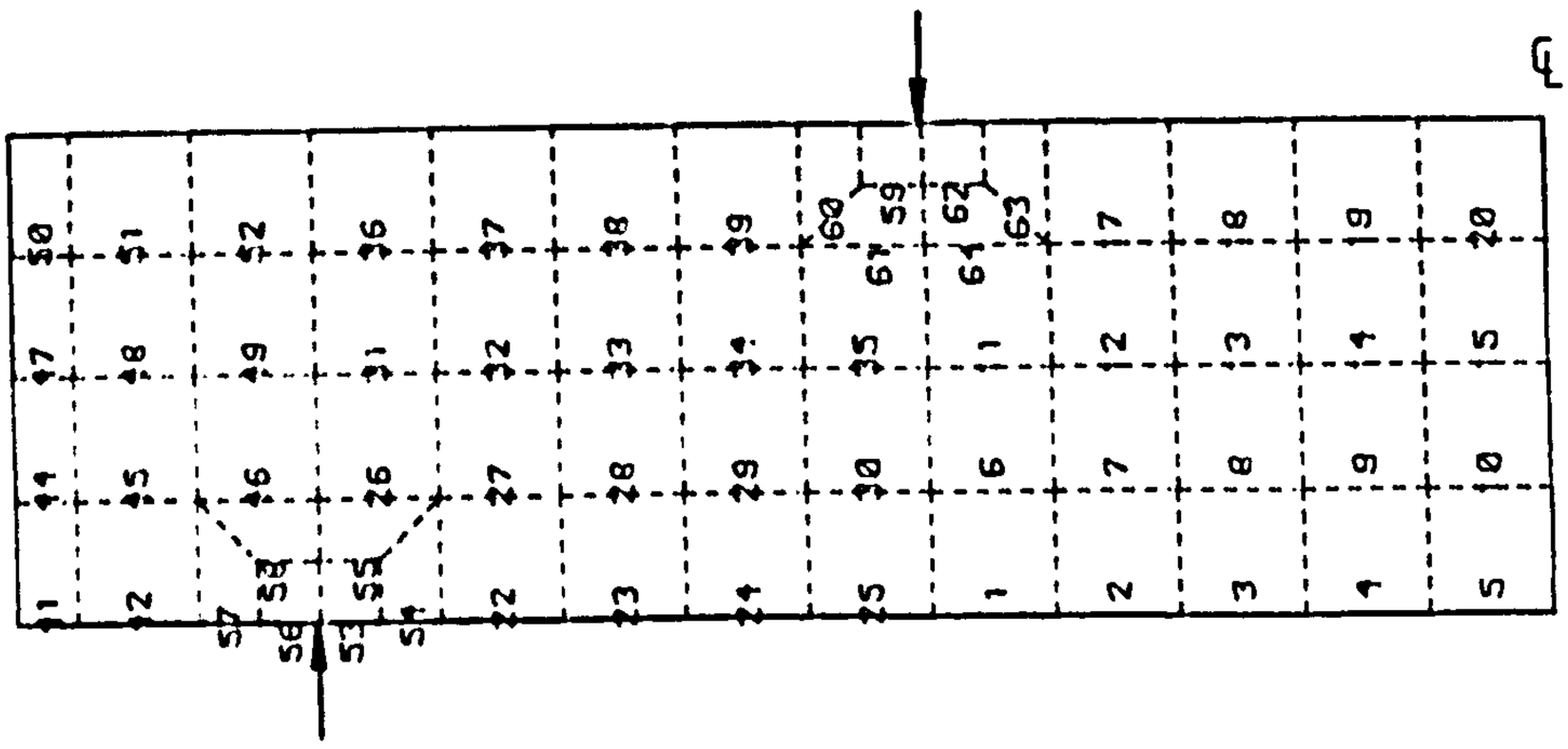

(a) Mesh with numbering elements

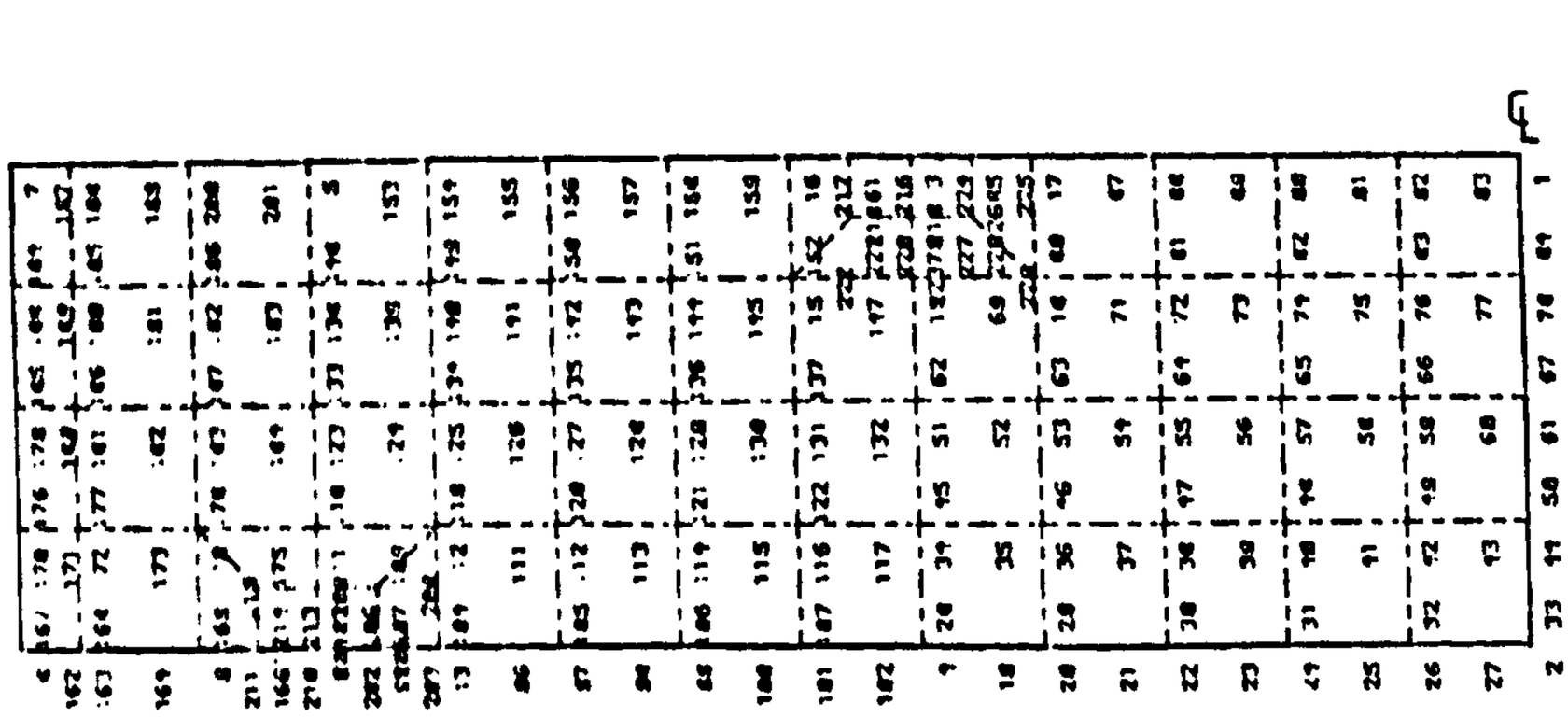

(b) Mesh with numbering nodes

FIG. 4.33 FIRST FINITE ELEMENT IDEALIZATION OF RING-ON-RING DISC

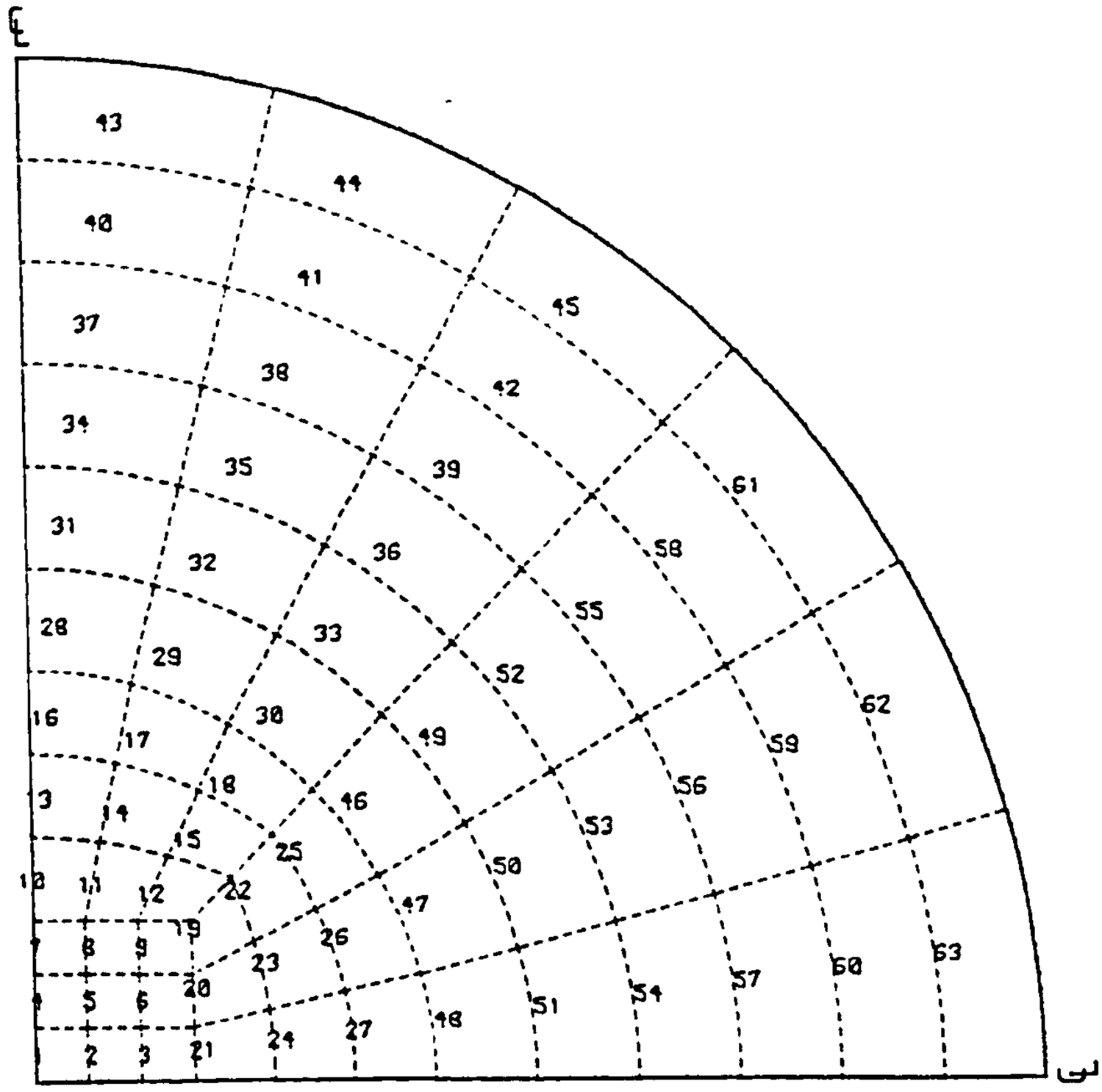

(a) Mesh with numbering elements

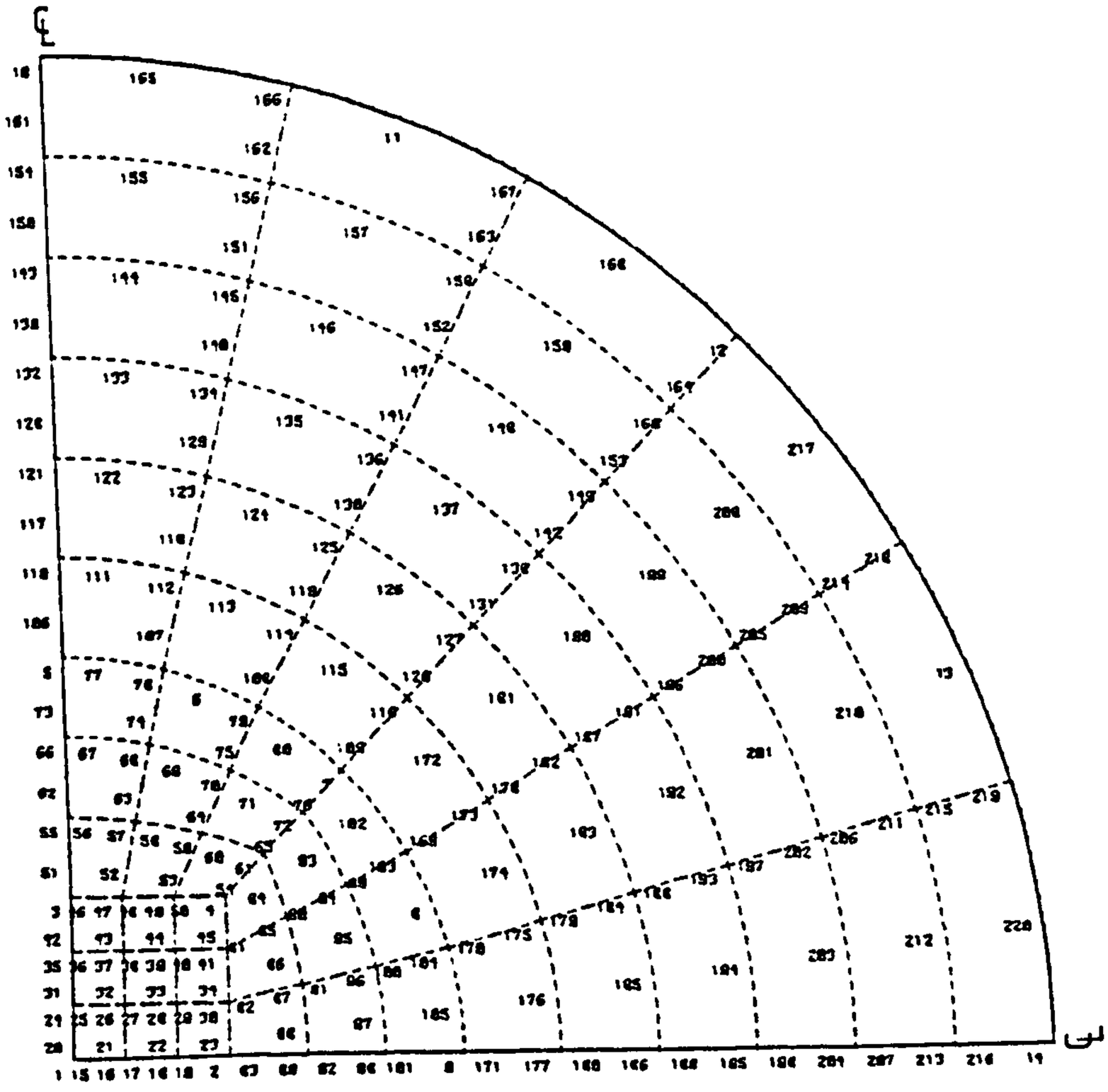

(b) Mesh with numbering nodes

FIG. 4.34 SECOND FINITE ELEMENT IDEALIZATION OF RING-ON-RING DISC

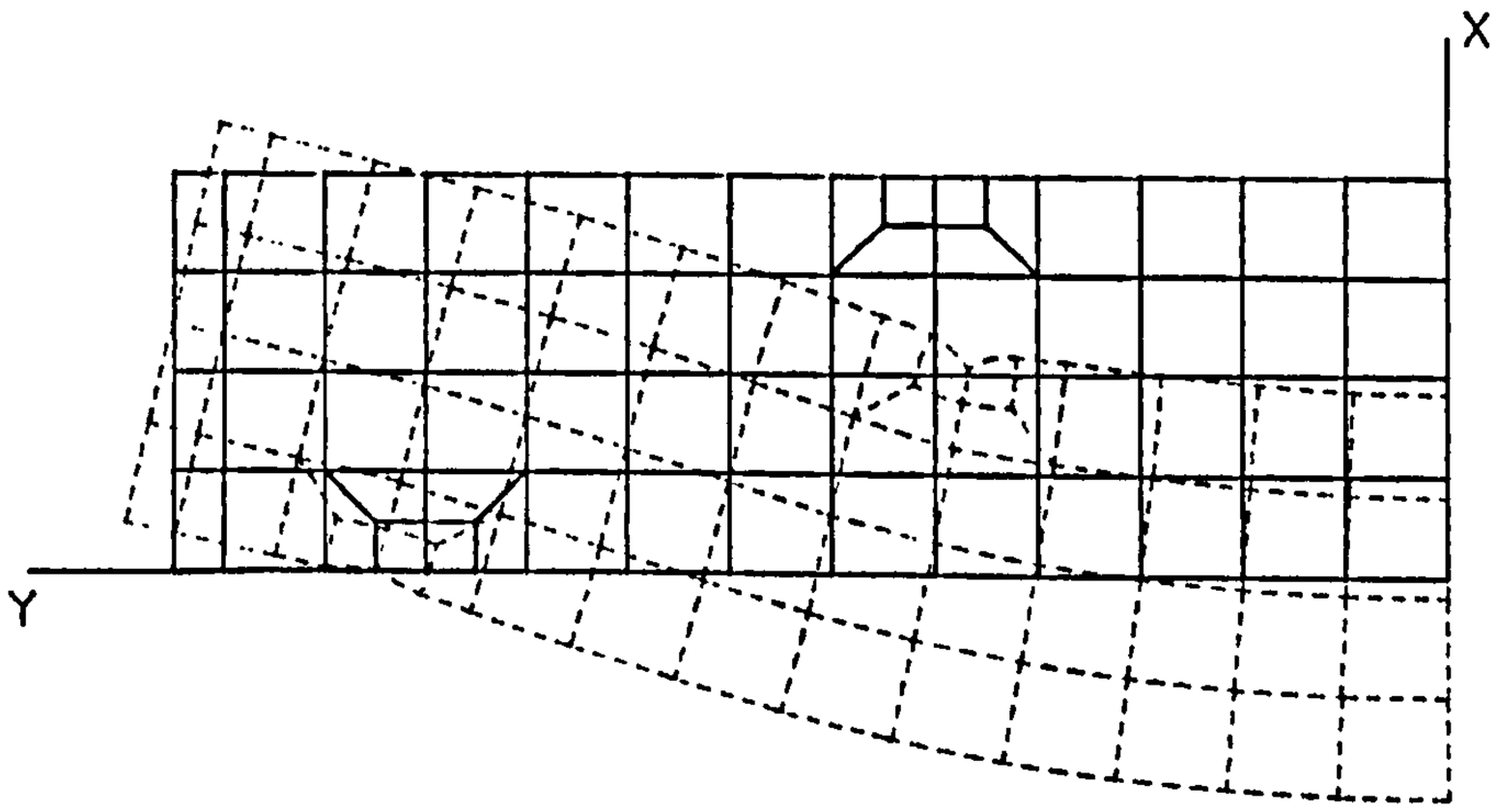

(a) First Idealization

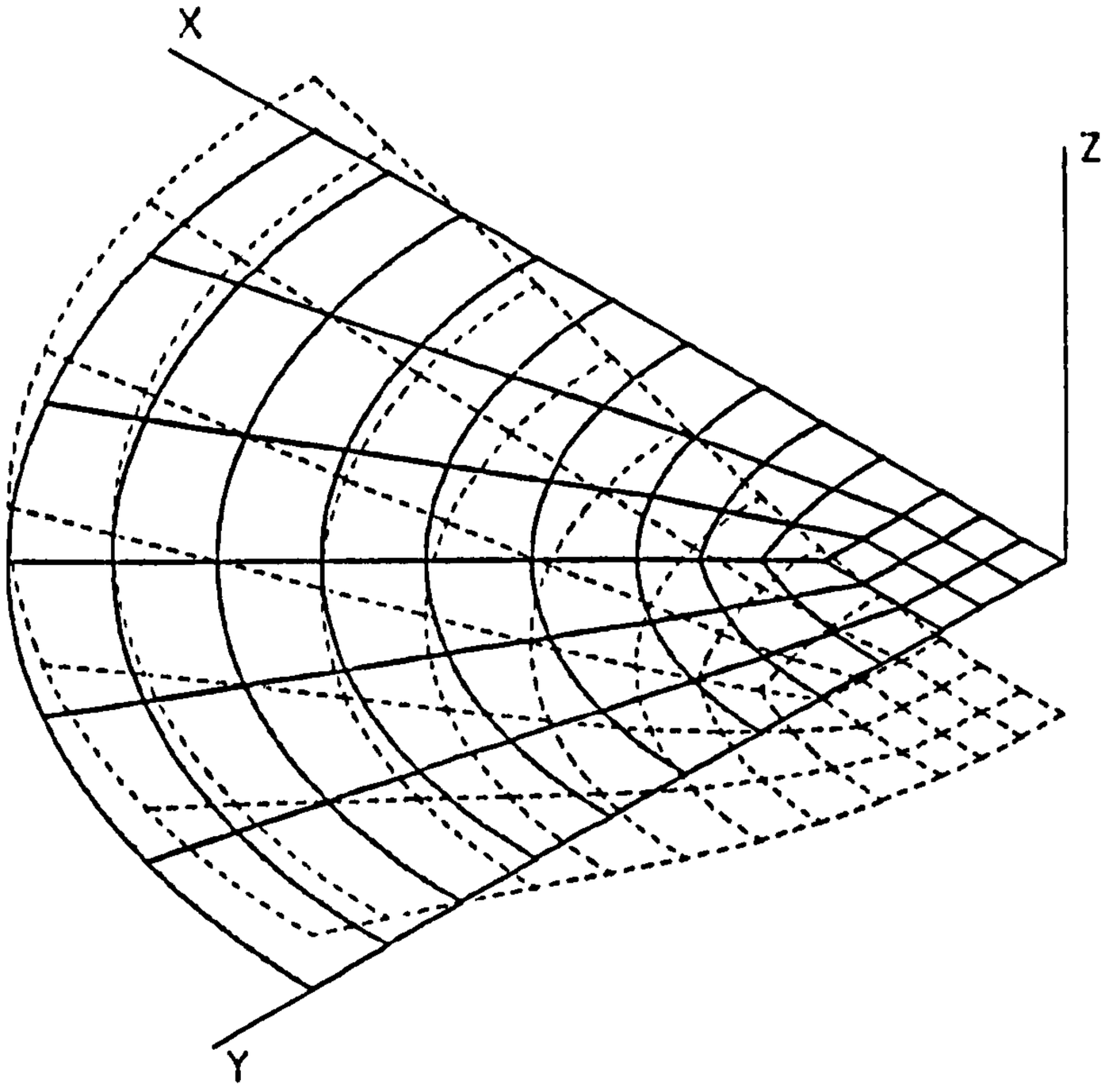

(b) Second Idealization

FIG. 4.35 MESH DISTORTION FOR RING-ON-RING DISC BENDING

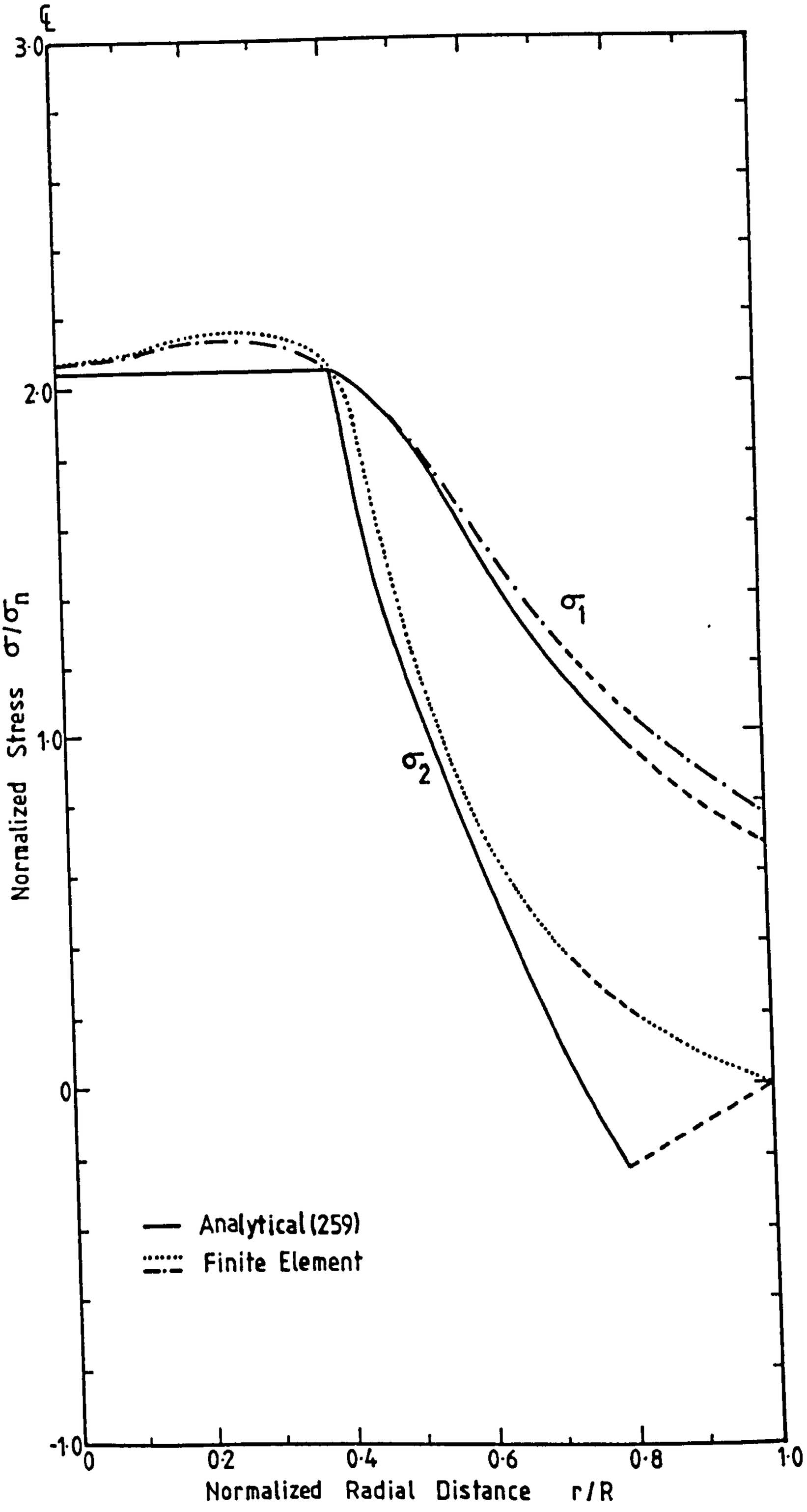

FIG. 4.36 STRESS DISTRIBUTION AT THE TENSILE FACE OF THE SPECIMEN IN THE RING ON RING DISC TEST

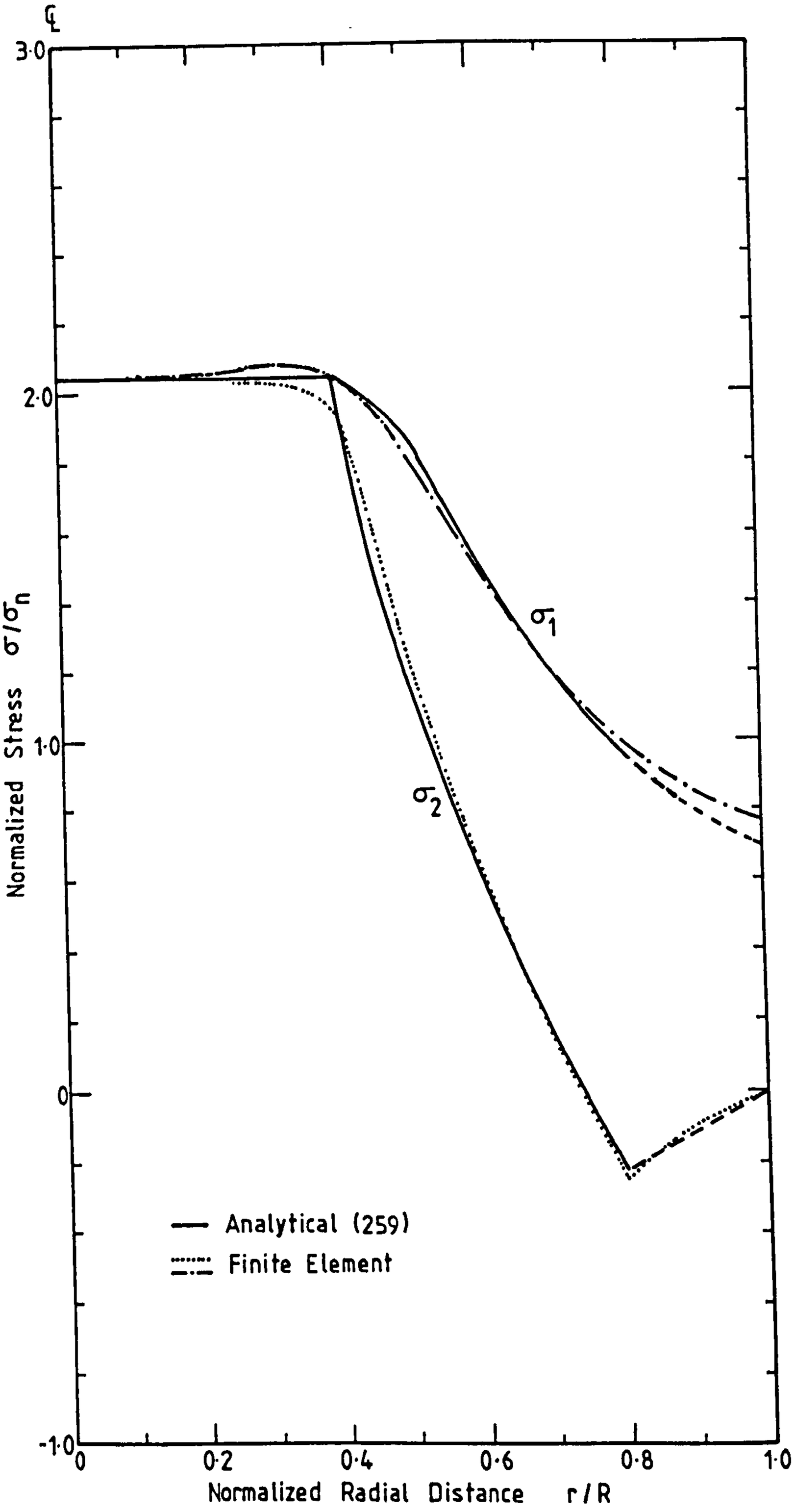

FIG. 4.37 STRESS DISTRIBUTION AT THE TENSILE FACE OF THE SPECIMEN IN THE RING ON RING DISC TEST

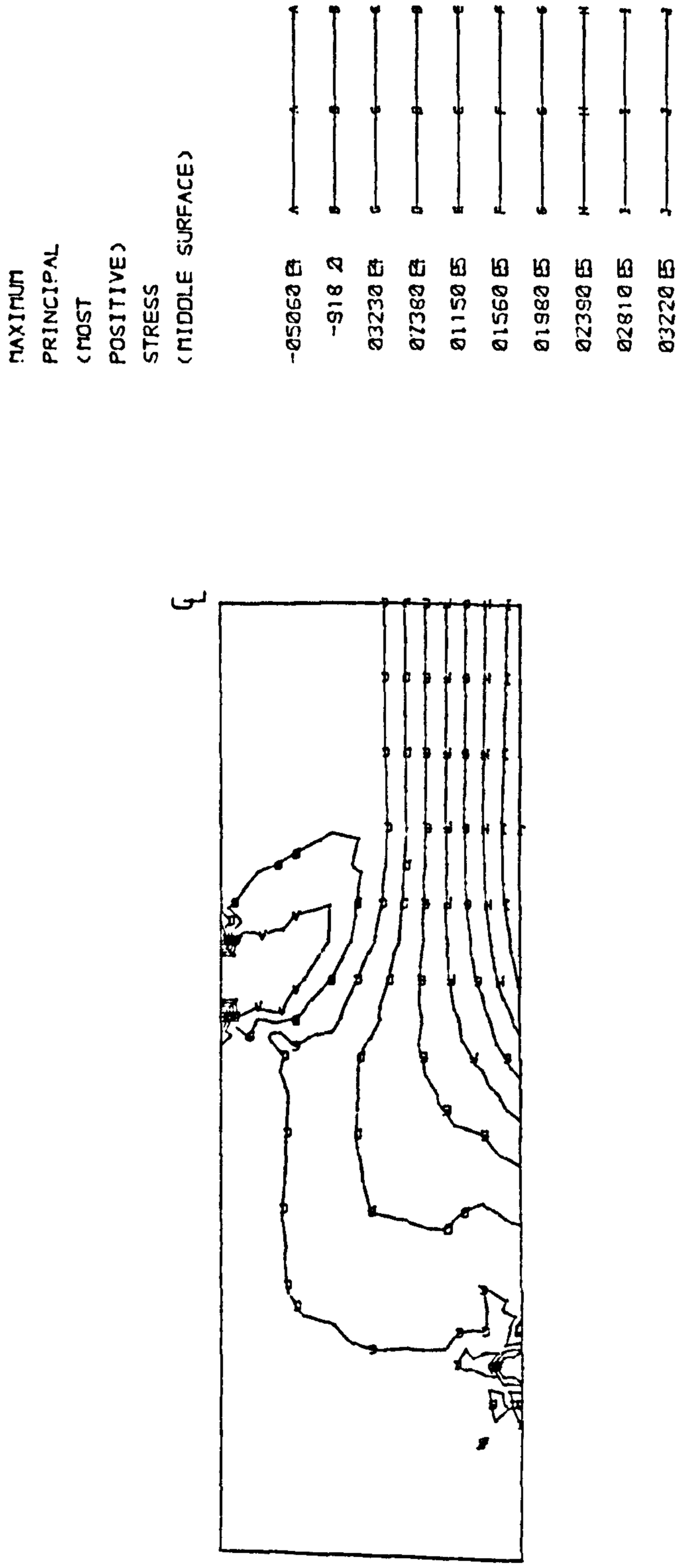

FIG. 4.38 MAXIMUM STRESS DISTRIBUTION IN RING-ON-RING DISC BENDING

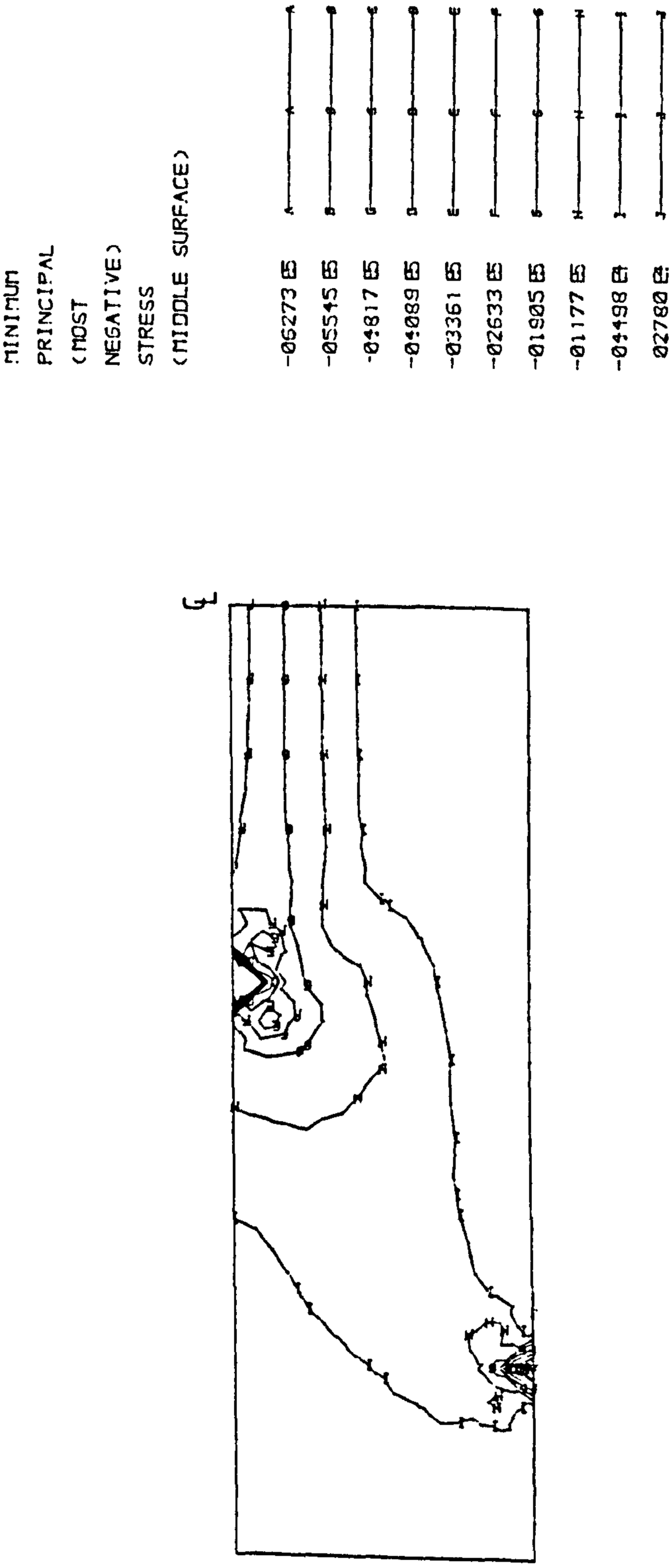

FIG.4.39 MINIMUM STRESS DISTRIBUTION IN RING-ON-RING DISC BENDING

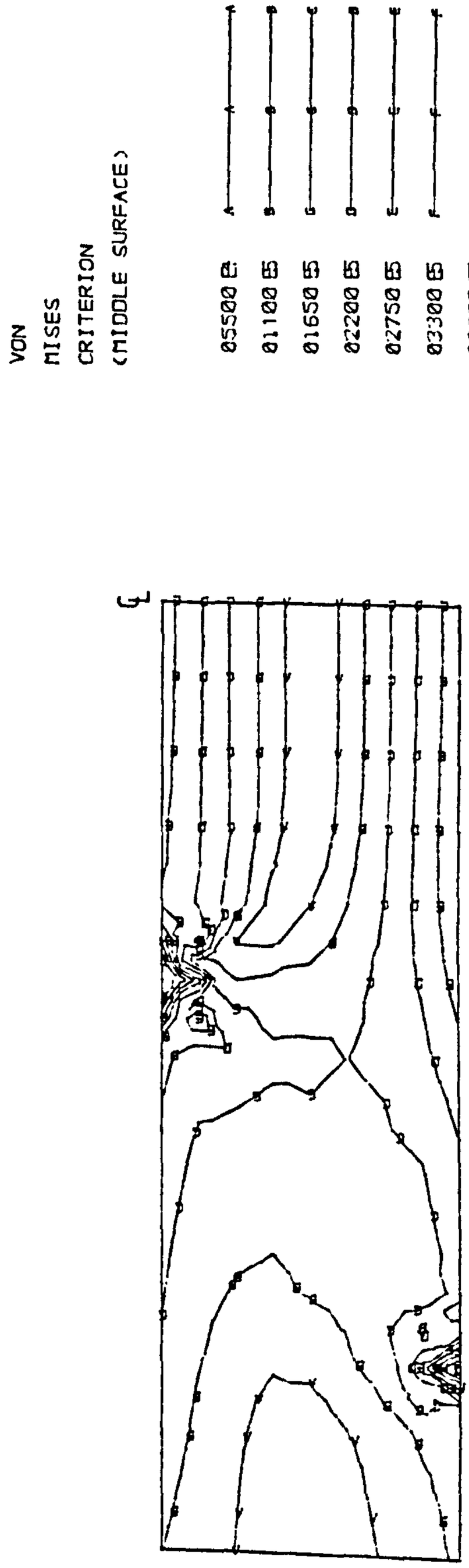

FIG. 4.40 EQUIVALENT STRESS DISTRIBUTION IN RING-ON-RING DISC BENDING

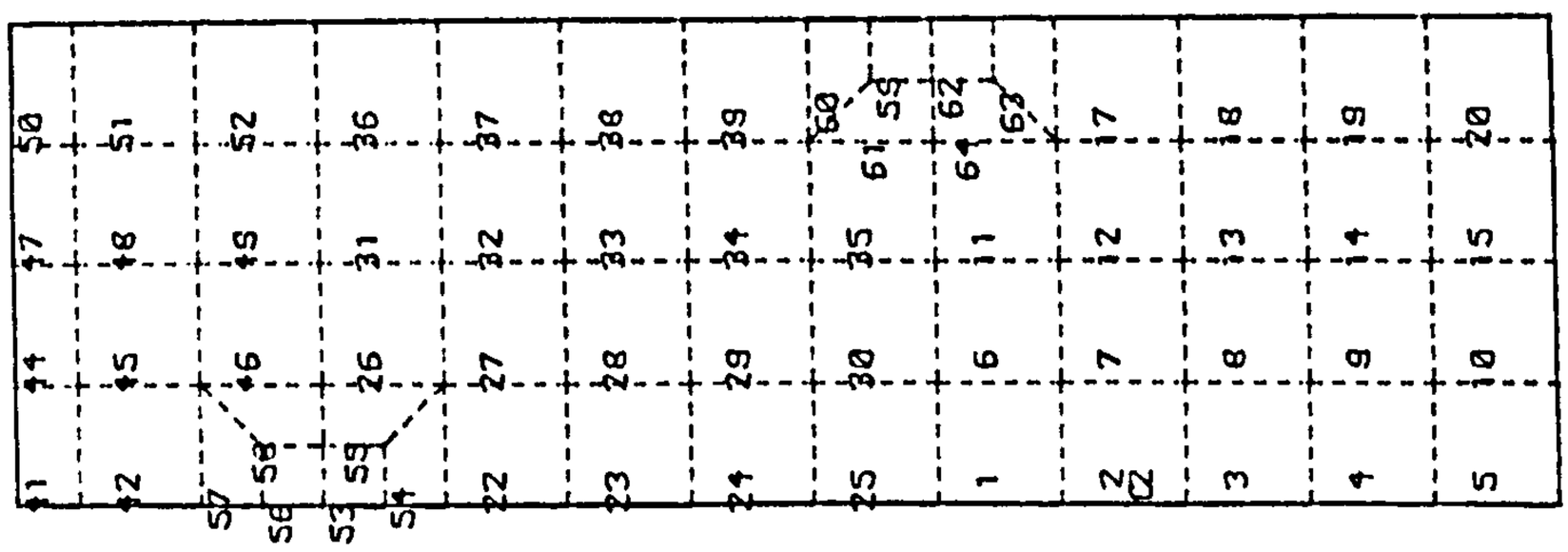

FIG.4.41 POSITIONAL FAILURE IN RING-ON-RING DISC BENDING

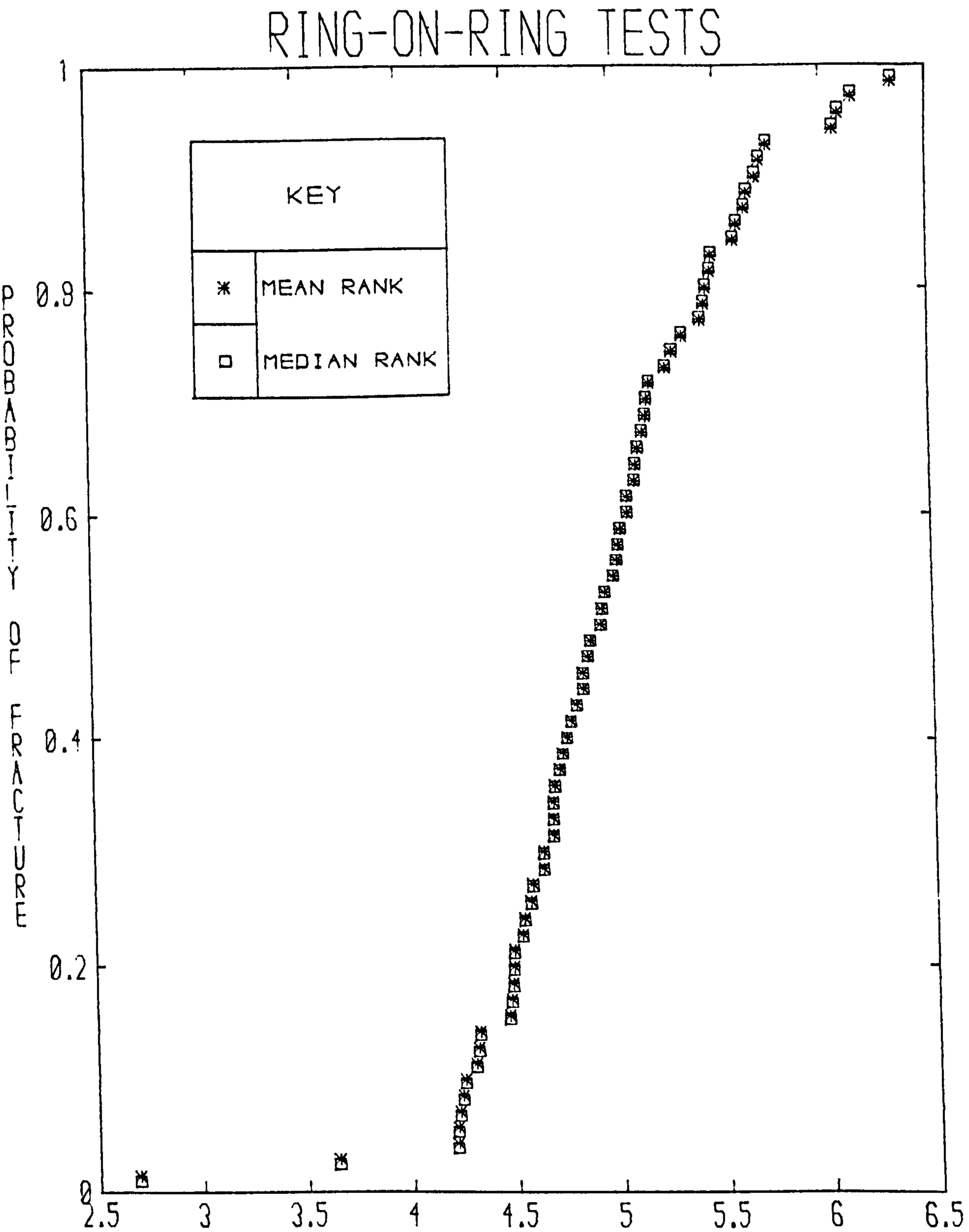

FIG. 4.42 THE CUMULATIVE DISTRIBUTION OF FRACTURE STRENGTHS OF 69 SPECIMENS TESTED IN RING-ON-RING DISC BENDING

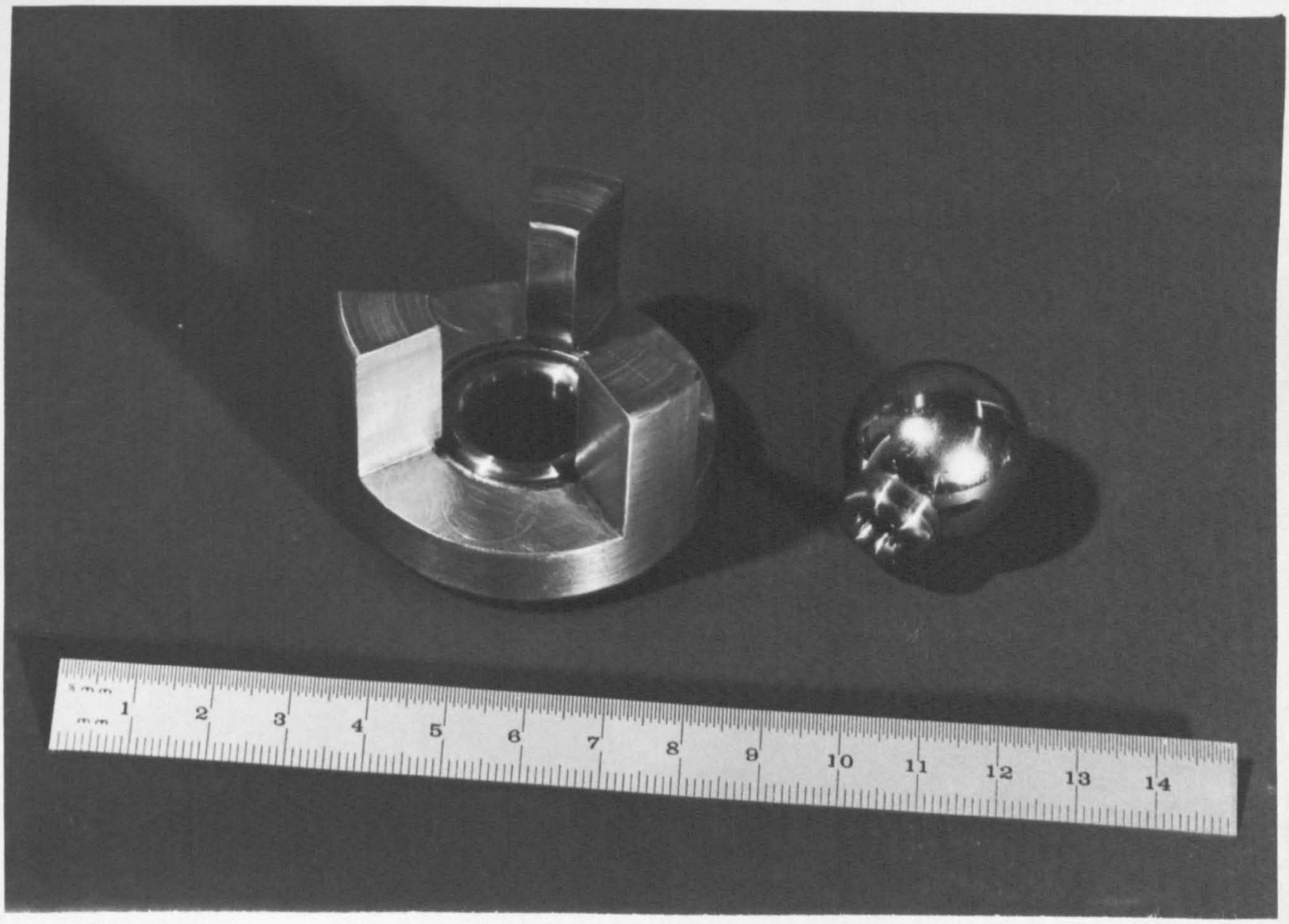

FIG. 4.43 RING-ON-RING LOADING JIG

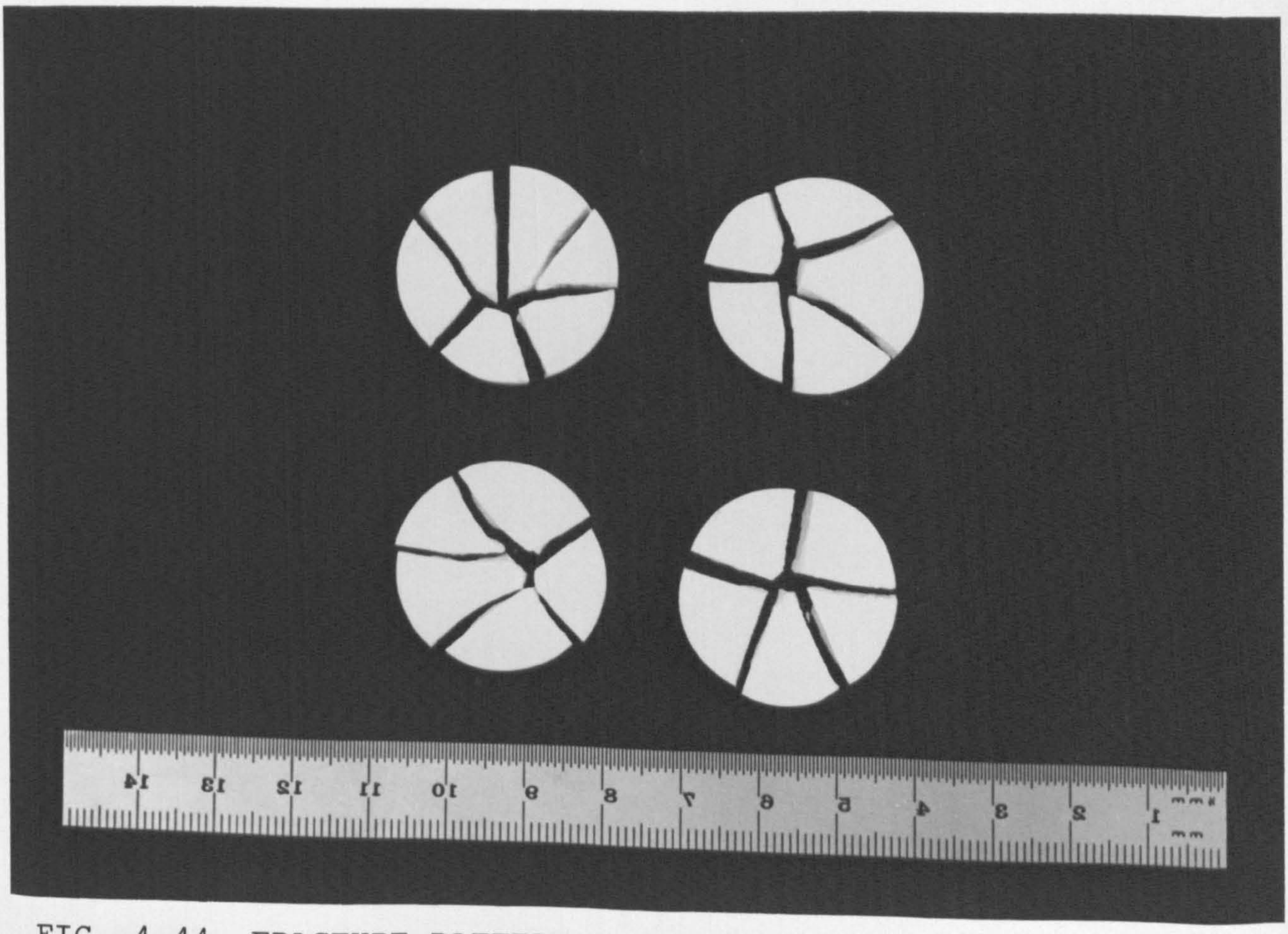

FIG. 4.44 FRACTURE PATTERN IN RING-ON-RING DISC TEST SPECIMEN

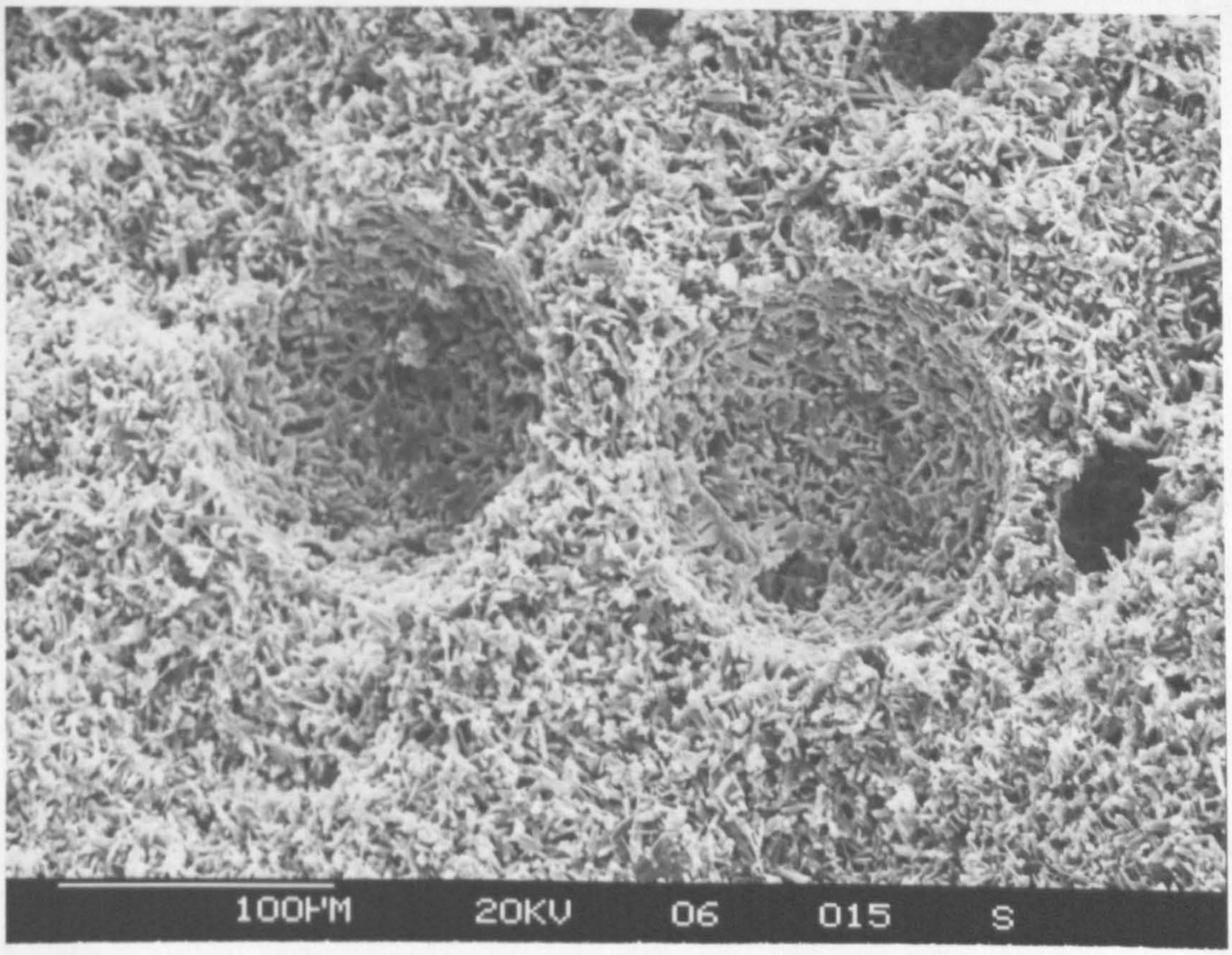

FIG. 4.45 SCANNING ELECTRON MICROGRAPH OF A FRACTURE SURFACE OF A RING-ON-RING DISC TEST SHOWING THE DUAL PORE DISTRIBUTION; x 250

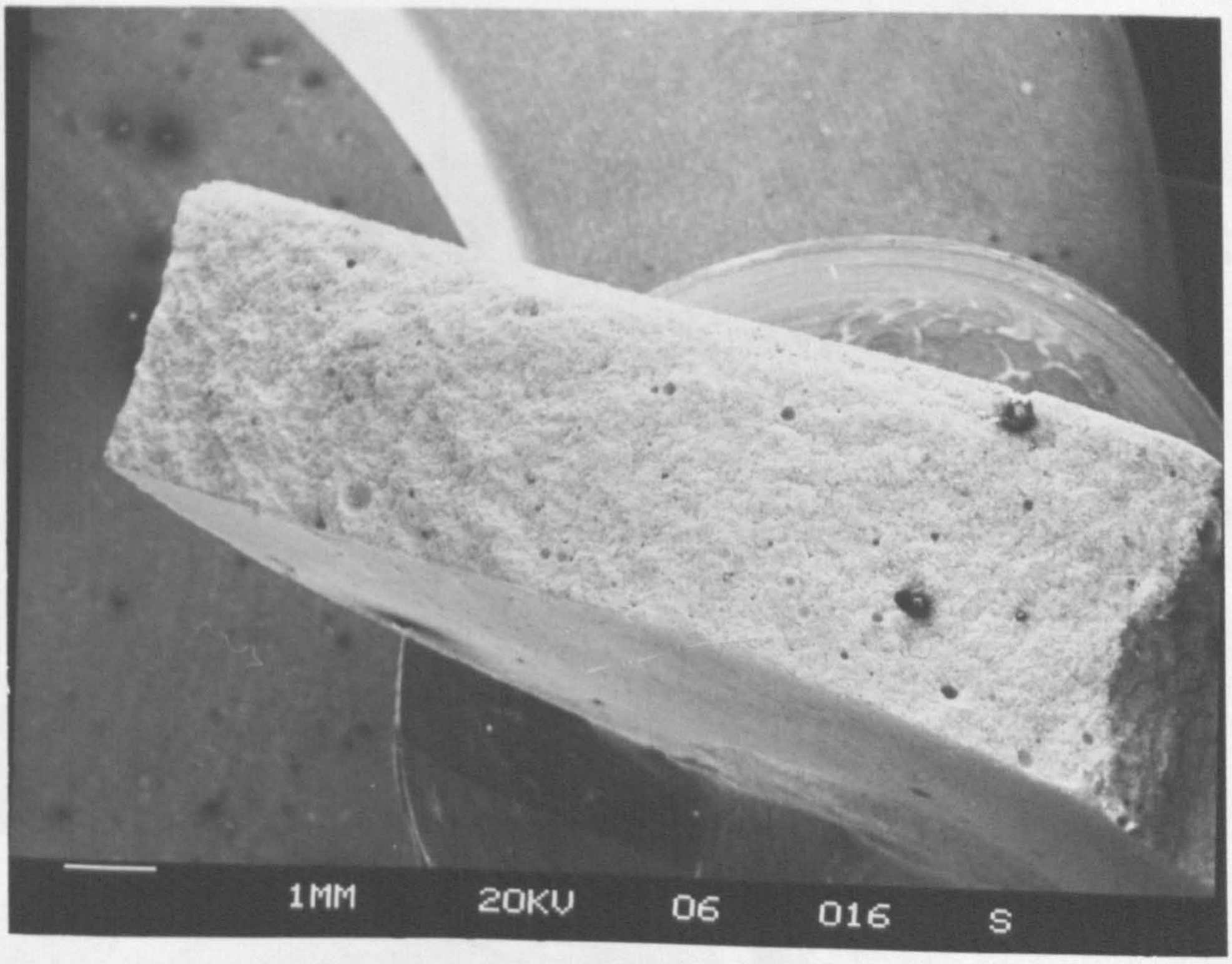

FIG. 4.46 SCANNING ELECTRON MICROGRAPH OF THE SAME FRACTURE SURFACE; x 7

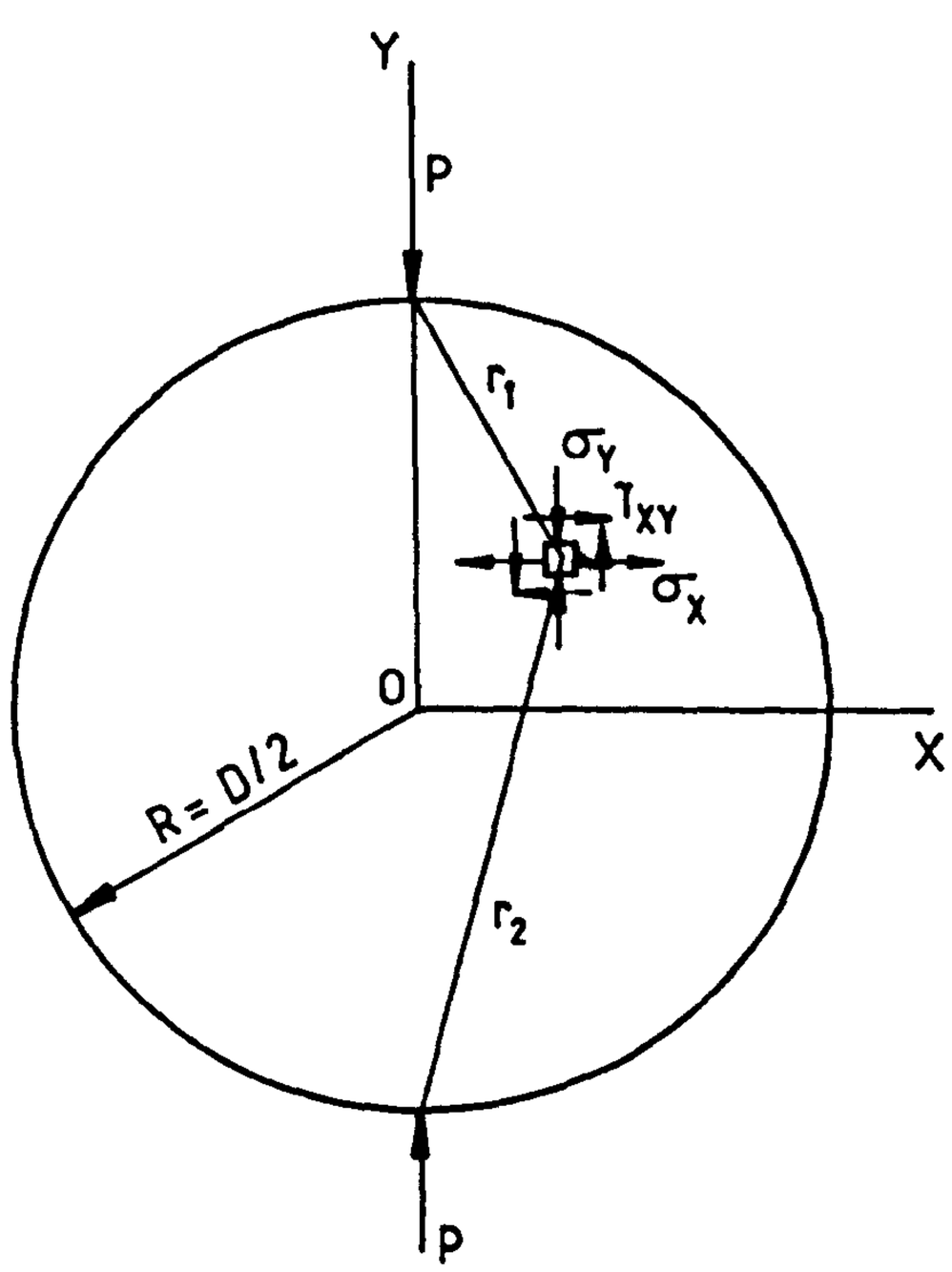

FIG. 4.47 IDEALIZED DIAMETRAL COMPRESSION TEST UNDER POINT LOAD

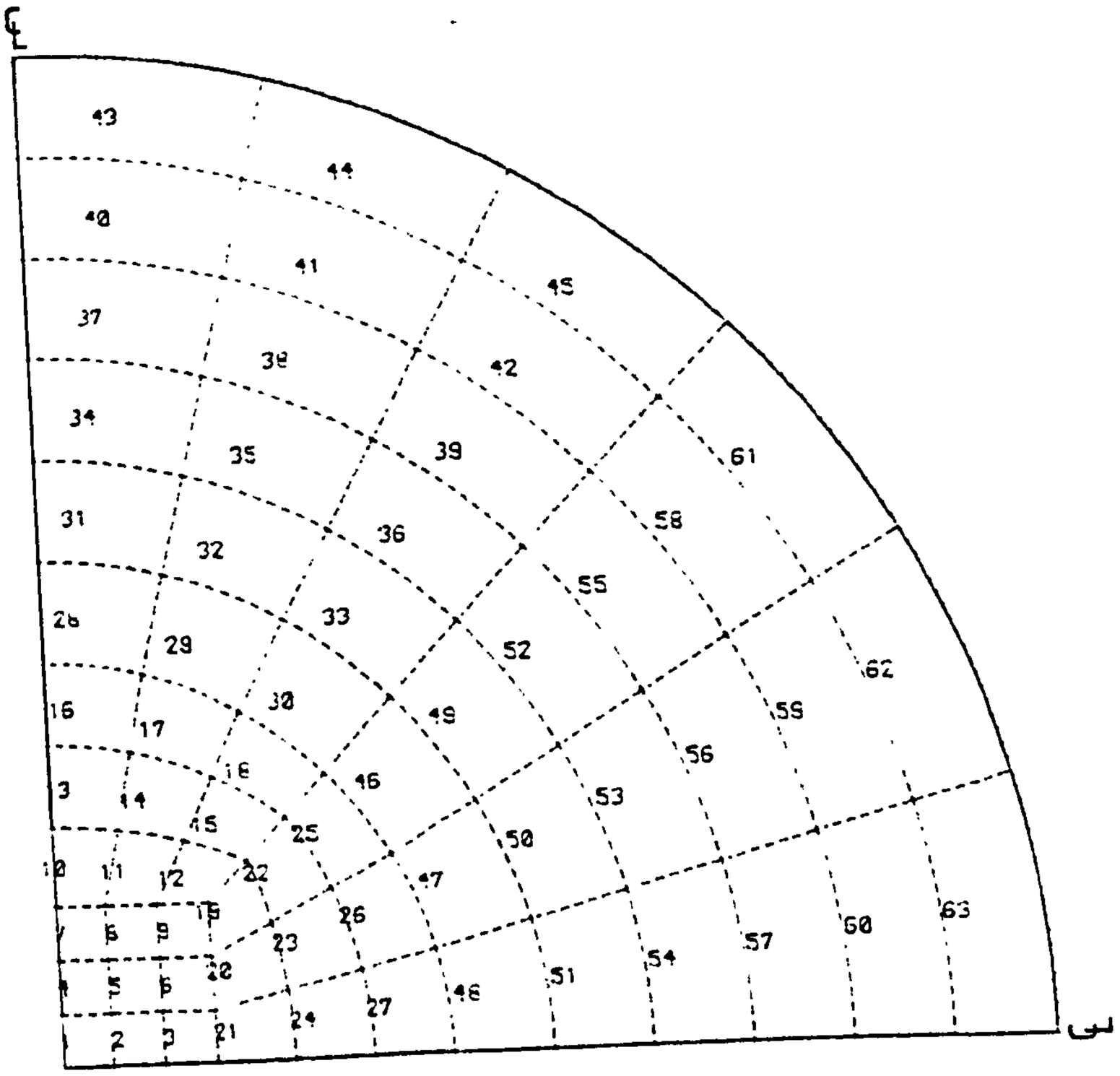

(a) Mesh with numbering elements

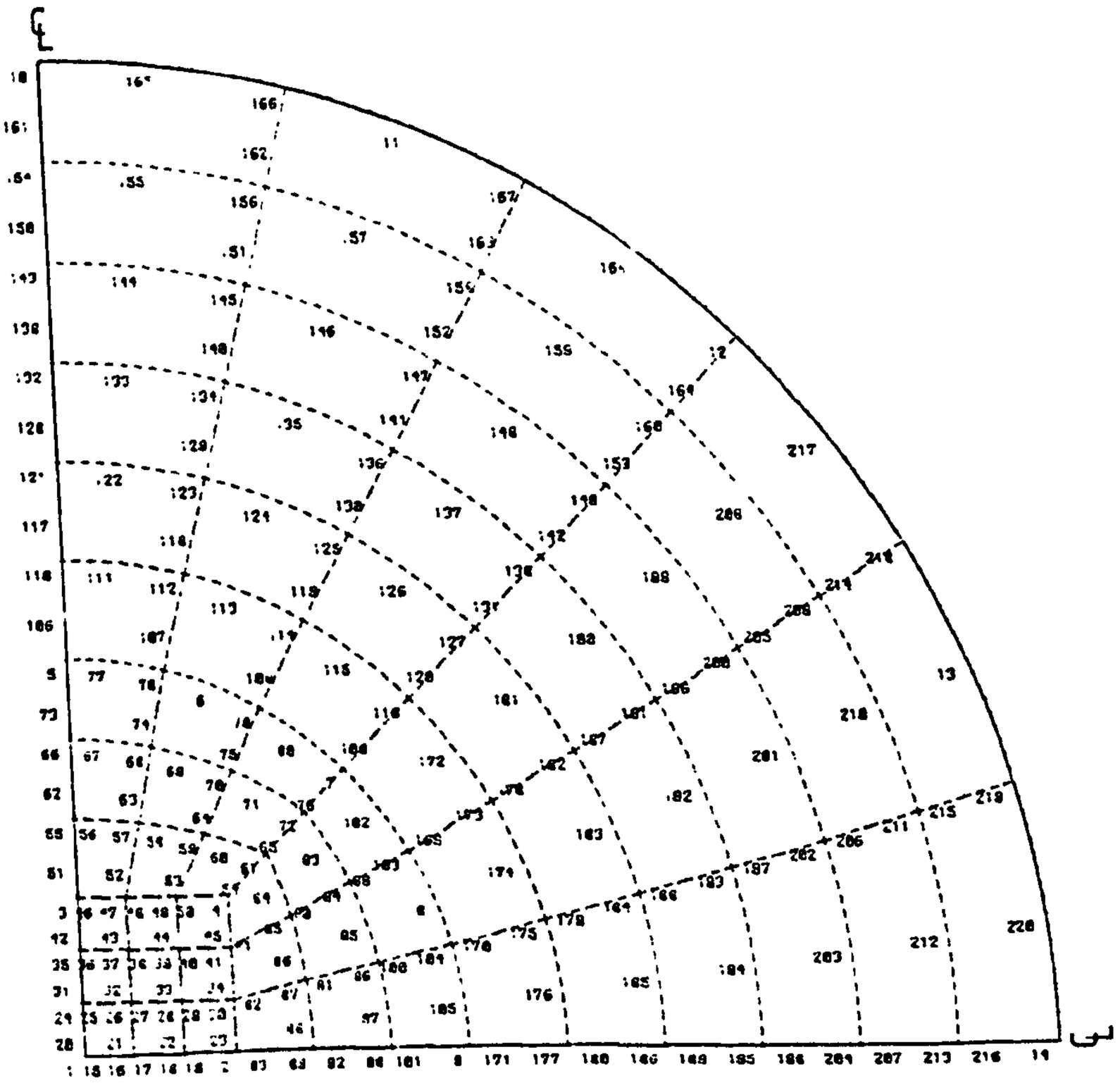

(b) Mesh with numbering nodes

FIG. 4.48 FIRST FINITE ELEMENT IDEALIZATION OF BRAZILIAN DISC

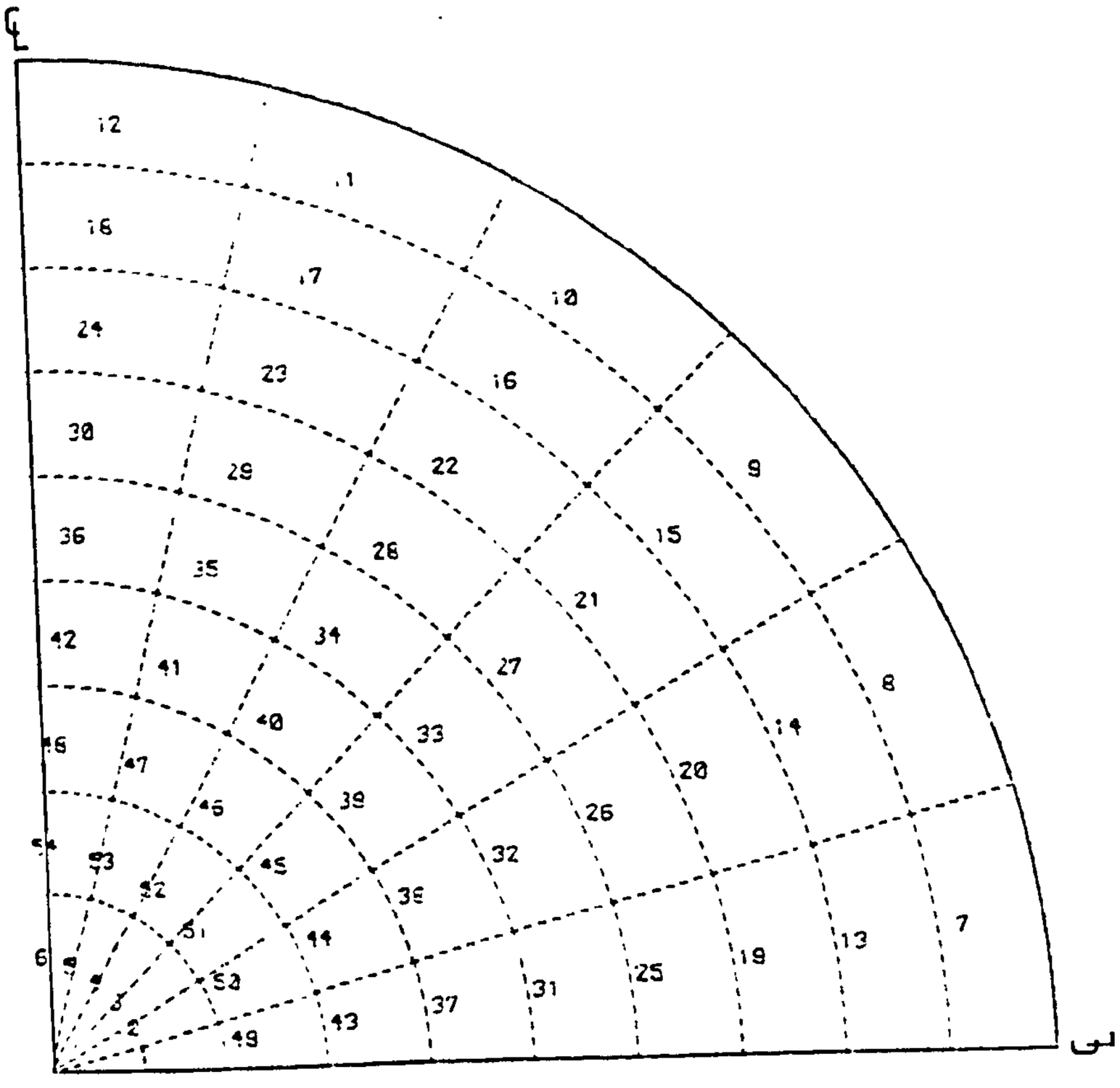

(a) Mesh with numbering elements

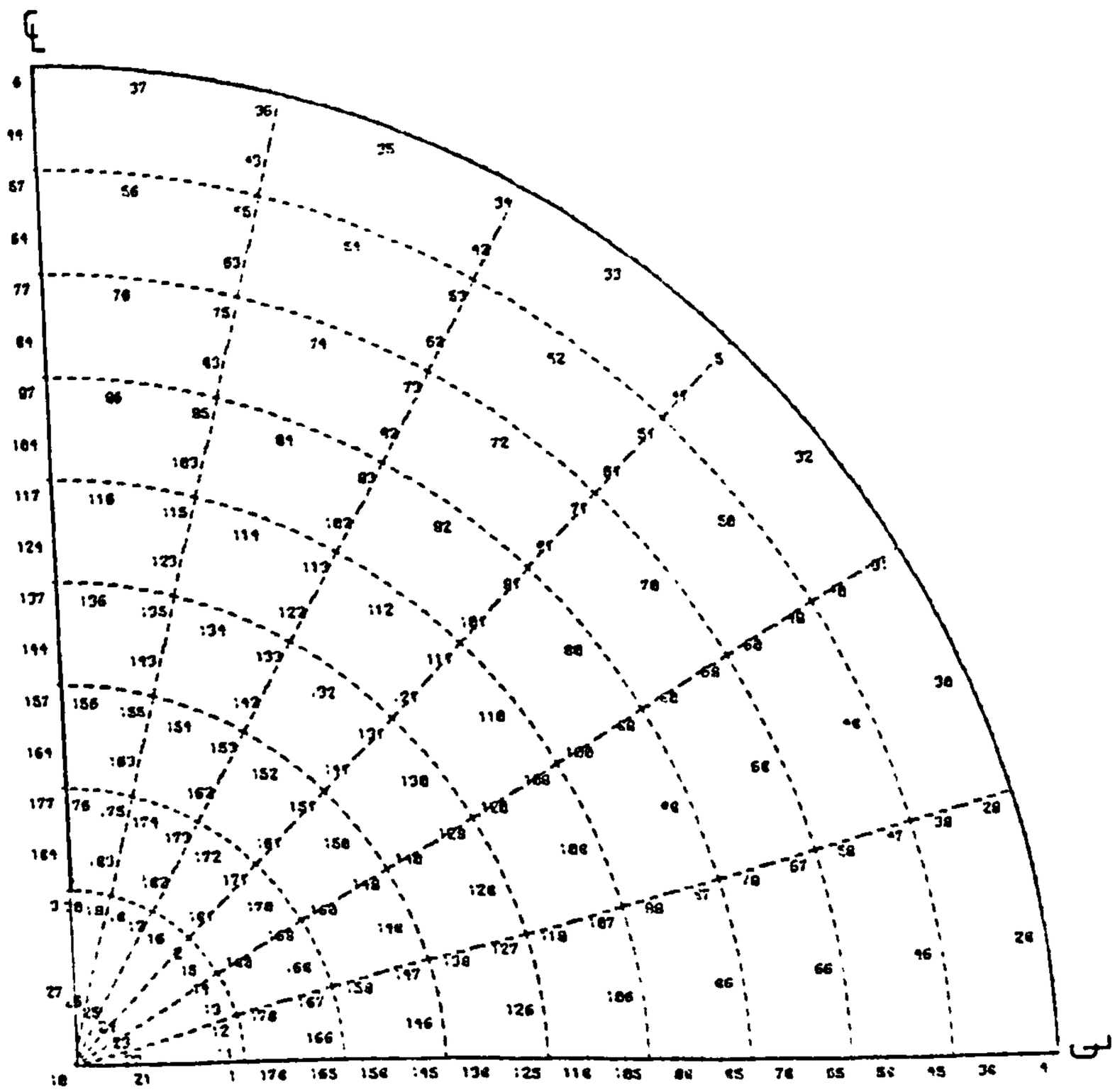

(b) Mesh with numbering nodes

FIG. 4.49 SECOND FINITE ELEMENT IDEALIZATION OF BRAZILIAN DISC

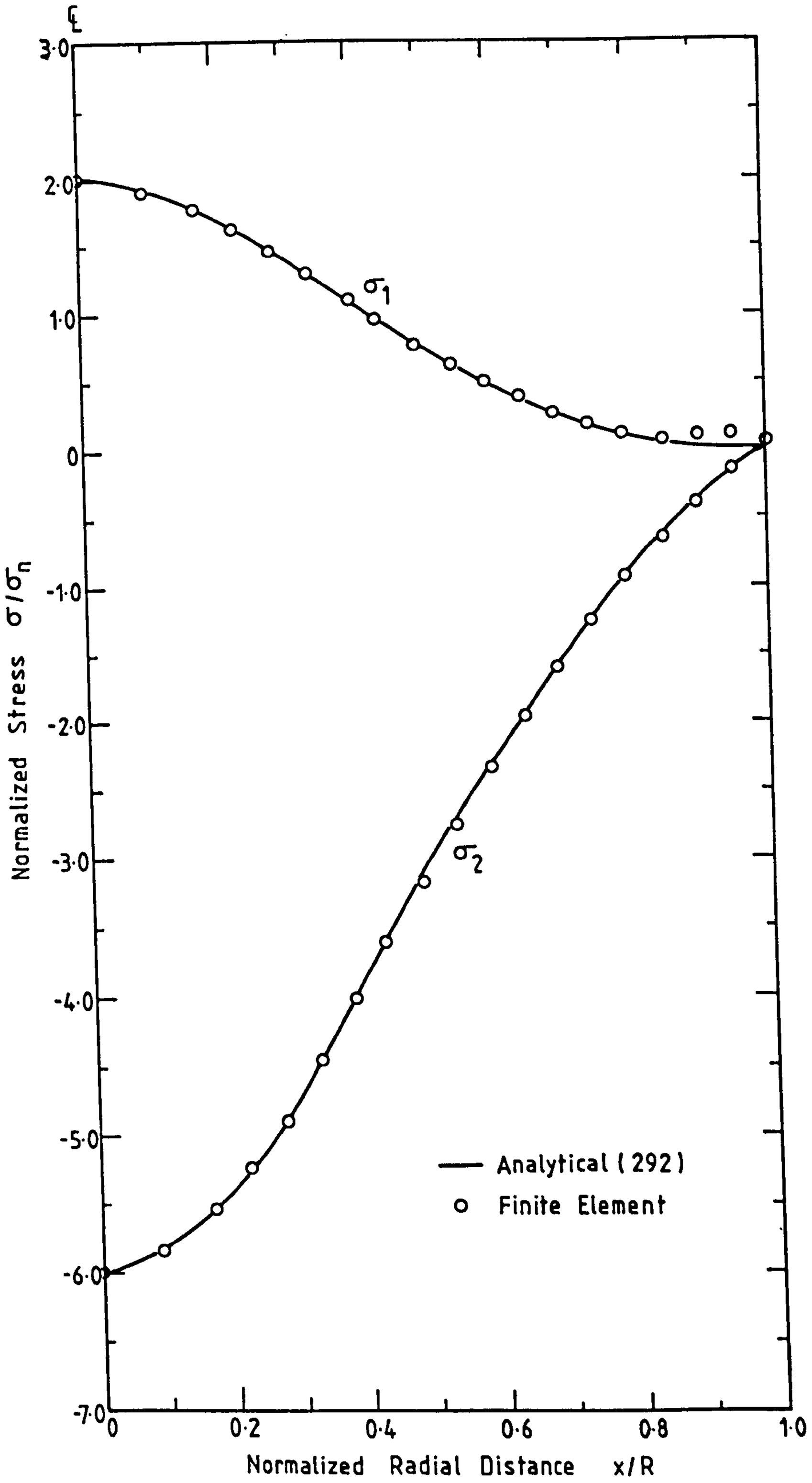

FIG. 4.50 PRINCIPAL STRESS DISTRIBUTION ACROSS HORIZONTAL DIAMETER FOR A BRAZILIAN DISC SUBJECTED TO POINT LOAD

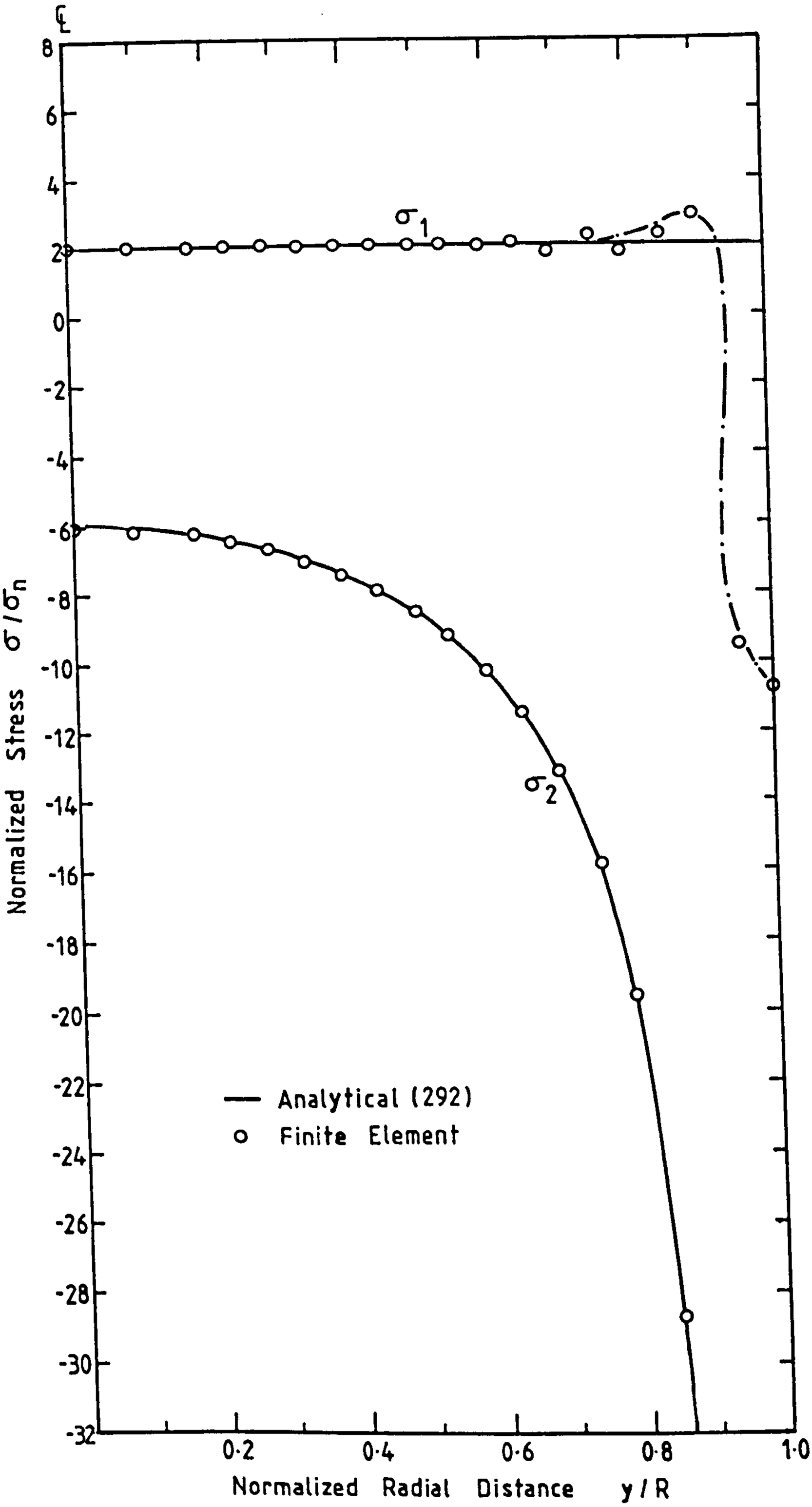

FIG. 4.51 PRINCIPAL STRESS DISTRIBUTION ACROSS VERTICAL DIAMETER FOR A BRAZILIAN DISC SUBJECTED TO POINT LOAD

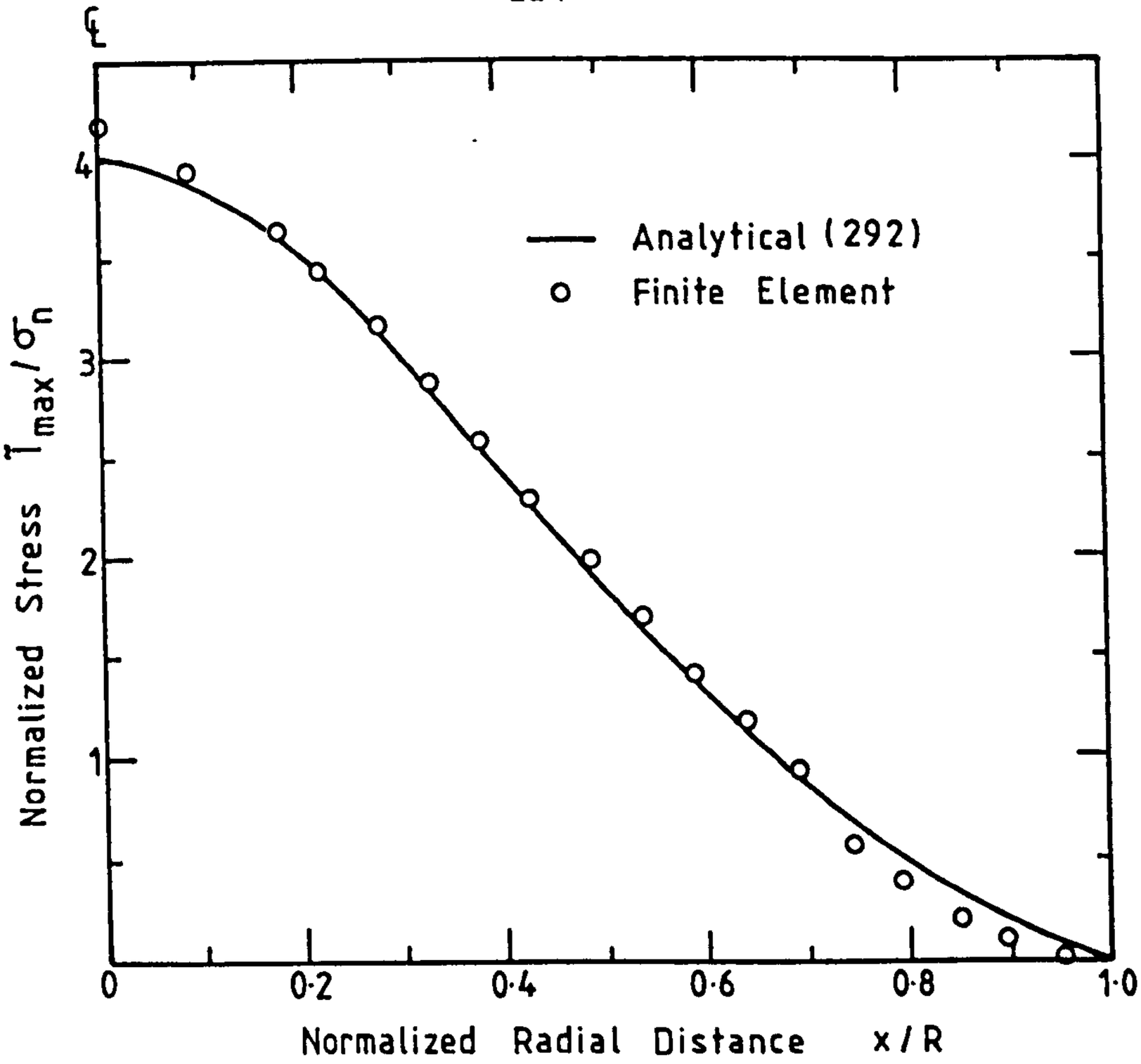

FIG. 4.52 SHEAR STRESS DISTRIBUTION ACROSS HORIZONTAL DIAMETER FOR A BRAZILIAN DISC SUBJECTED TO POINT LOAD

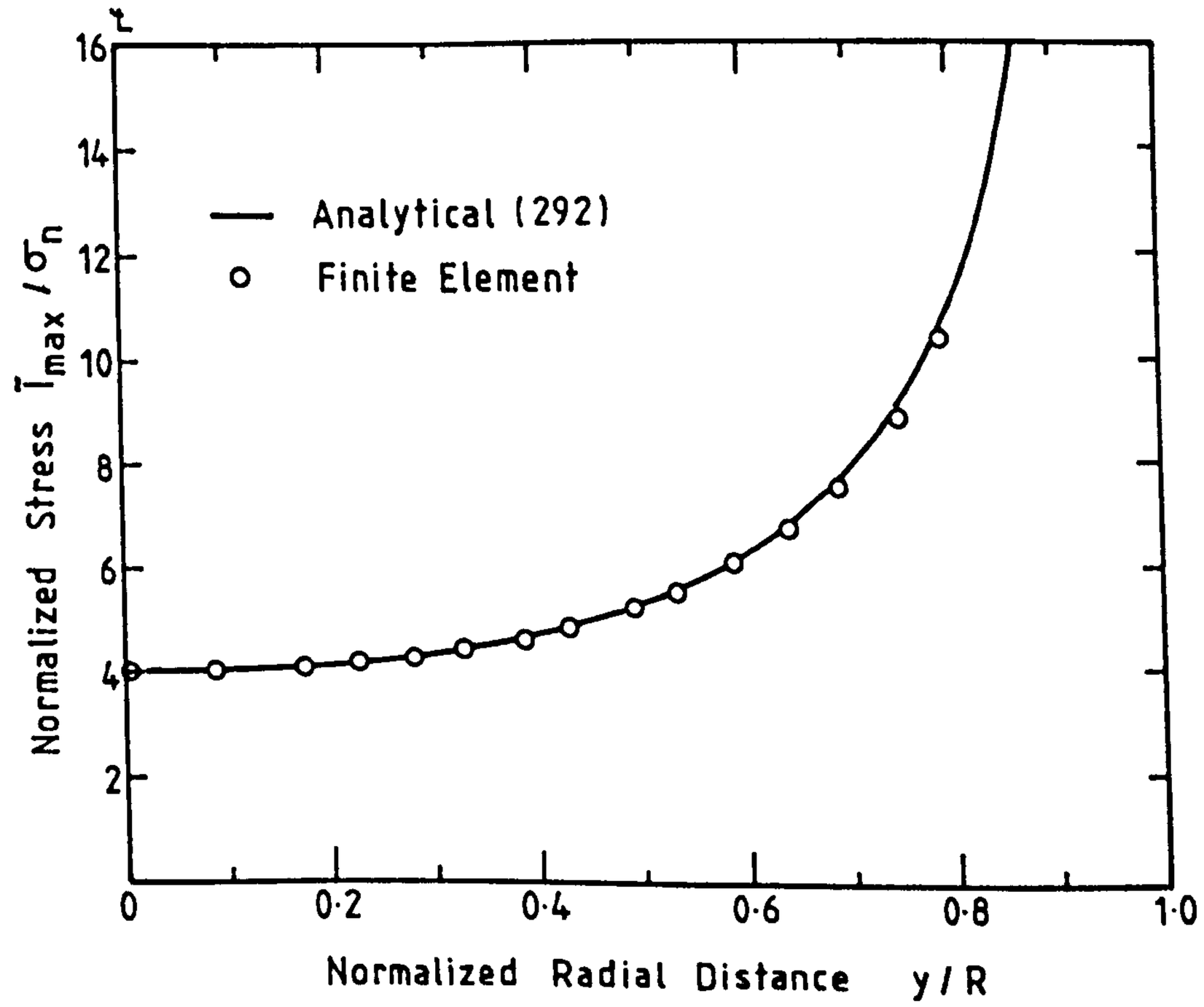

FIG. 4.53 SHEAR STRESS DISTRIBUTION ACROSS VERTICAL DIAMETER FOR A BRAZILIAN DISC SUBJECTED TO POINT LOAD

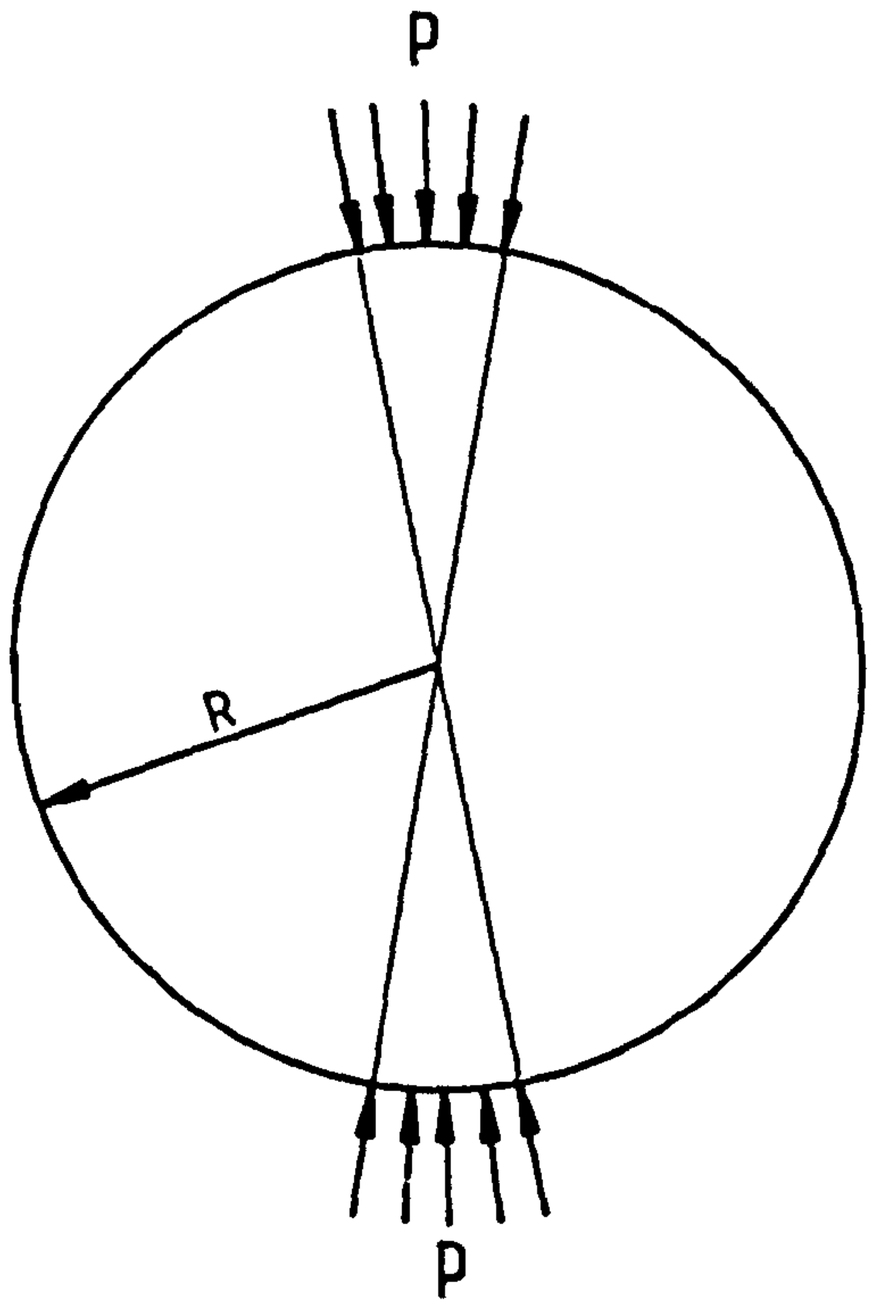

FIG.4.54 DIAMETRAL COMPRESSION TEST UNDER ARC LOAD

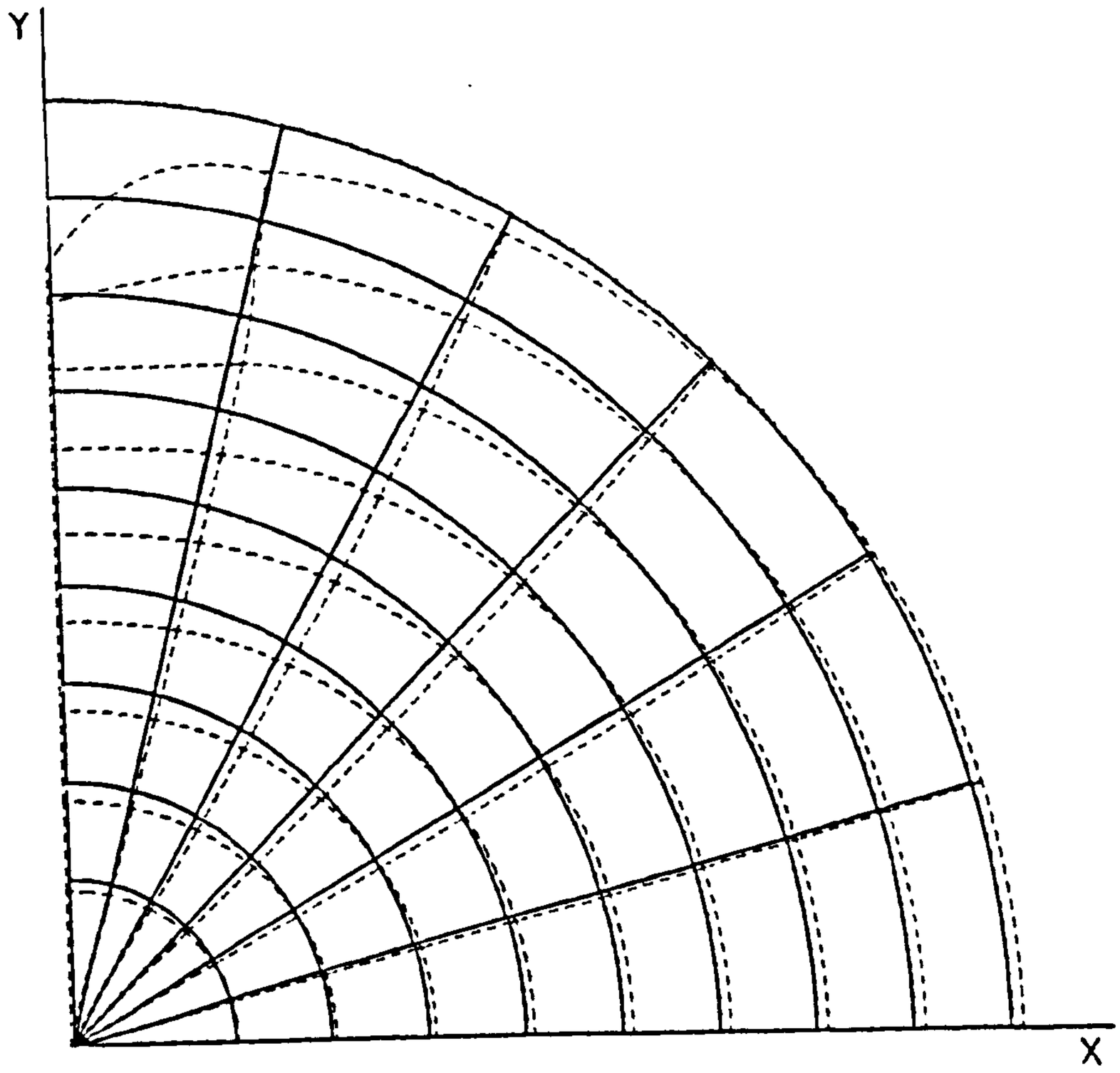

(a) Point Load

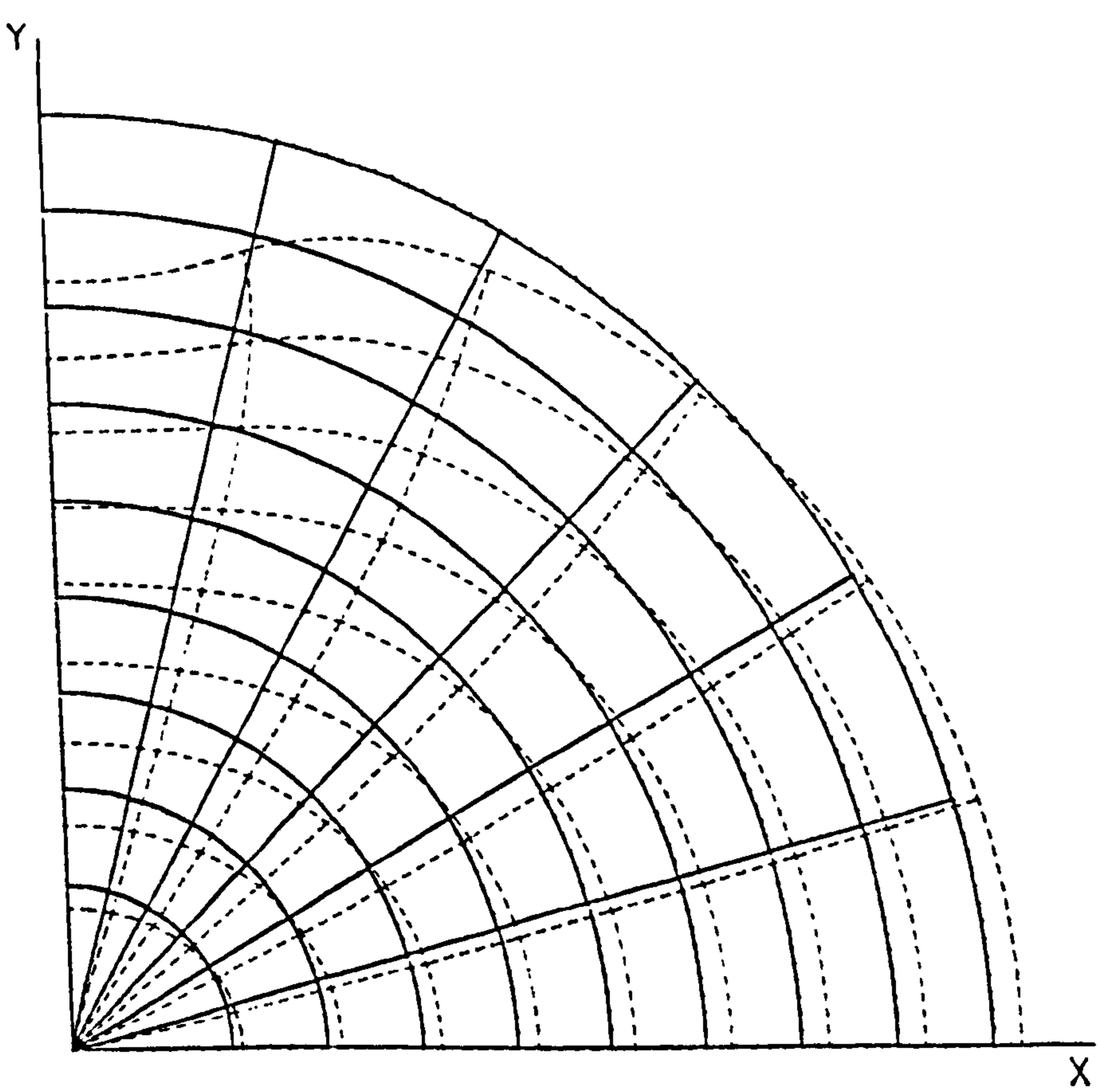

(b) Distributed Load

FIG. 4.55 MESH DISTORTION FOR BRAZILIAN DISC

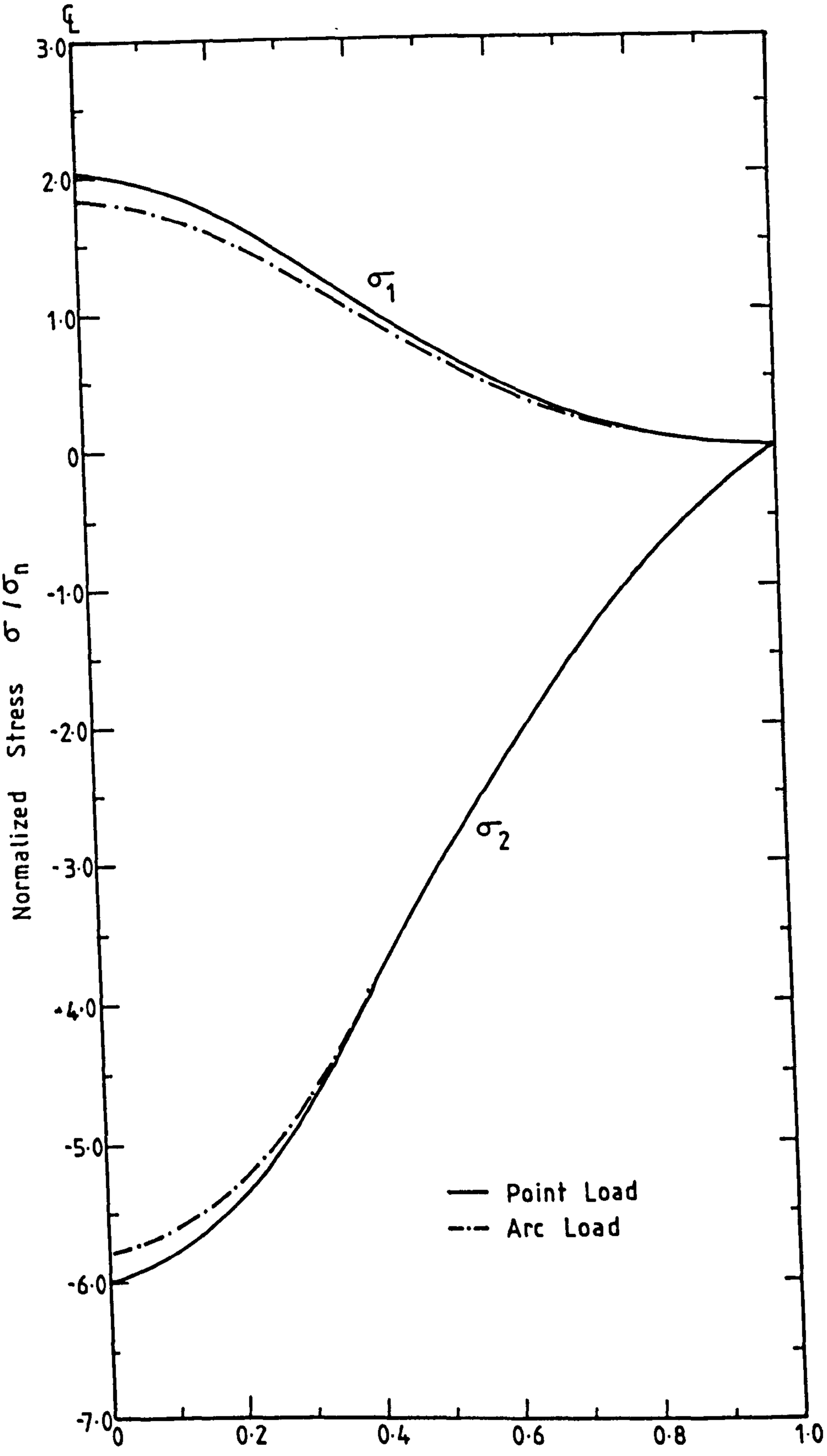

FIG. 4.56 COMPARISON OF PRINCIPAL STRESS DISTRIBUTIONS ACROSS HORIZONTAL DIAMETER FOR A BRAZILIAN DISC SUBJECTED TO POINT LOAD AND DISTRIBUTED LOAD

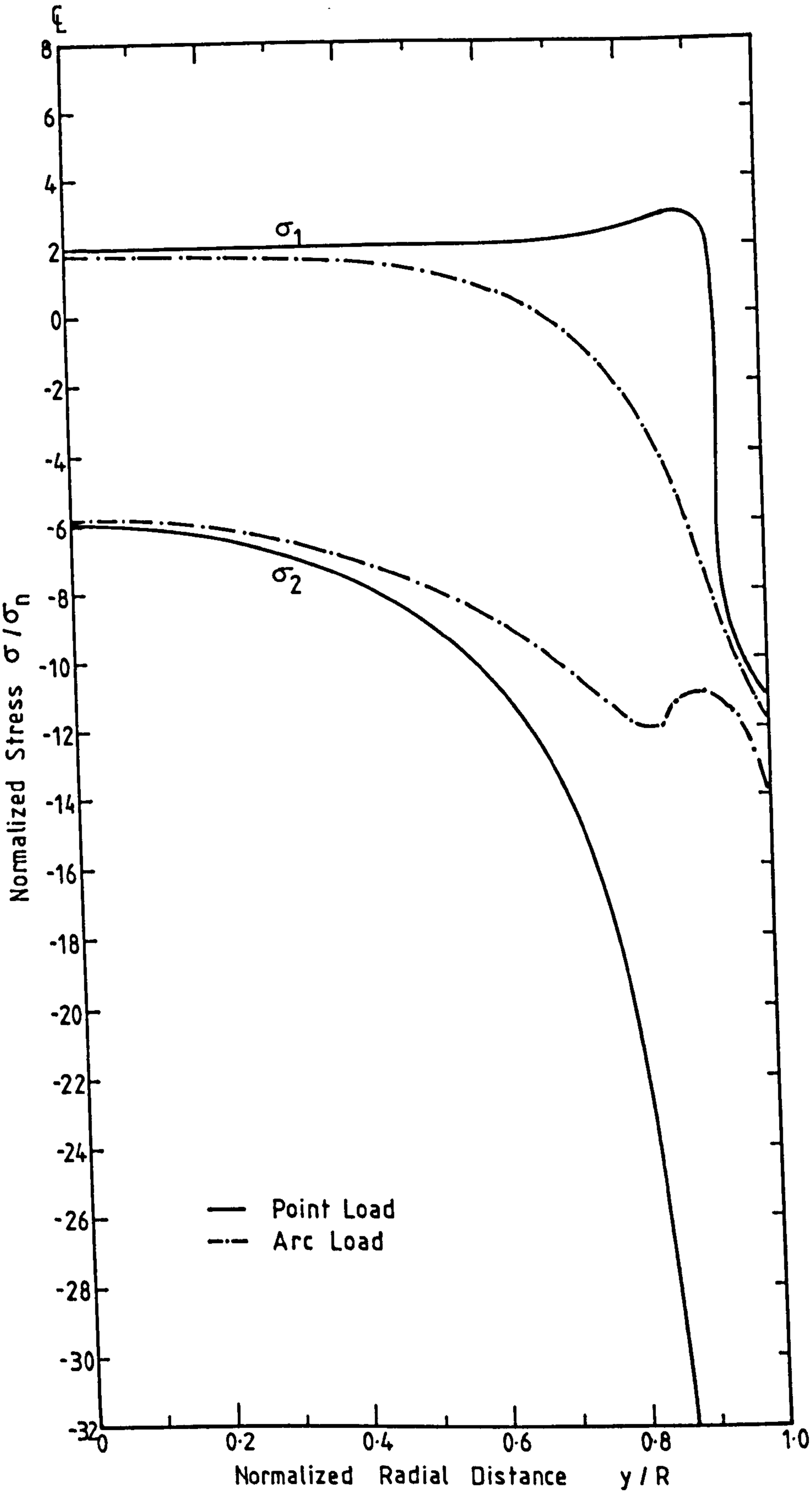

FIG. 4.57 COMPARISON OF PRINCIPAL STRESS DISTRIBUTIONS ACROSS VERTICAL DIAMETER FOR A BRAZILIAN DISC SUBJECTED TO POINT LOAD AND DISTRIBUTED LOAD

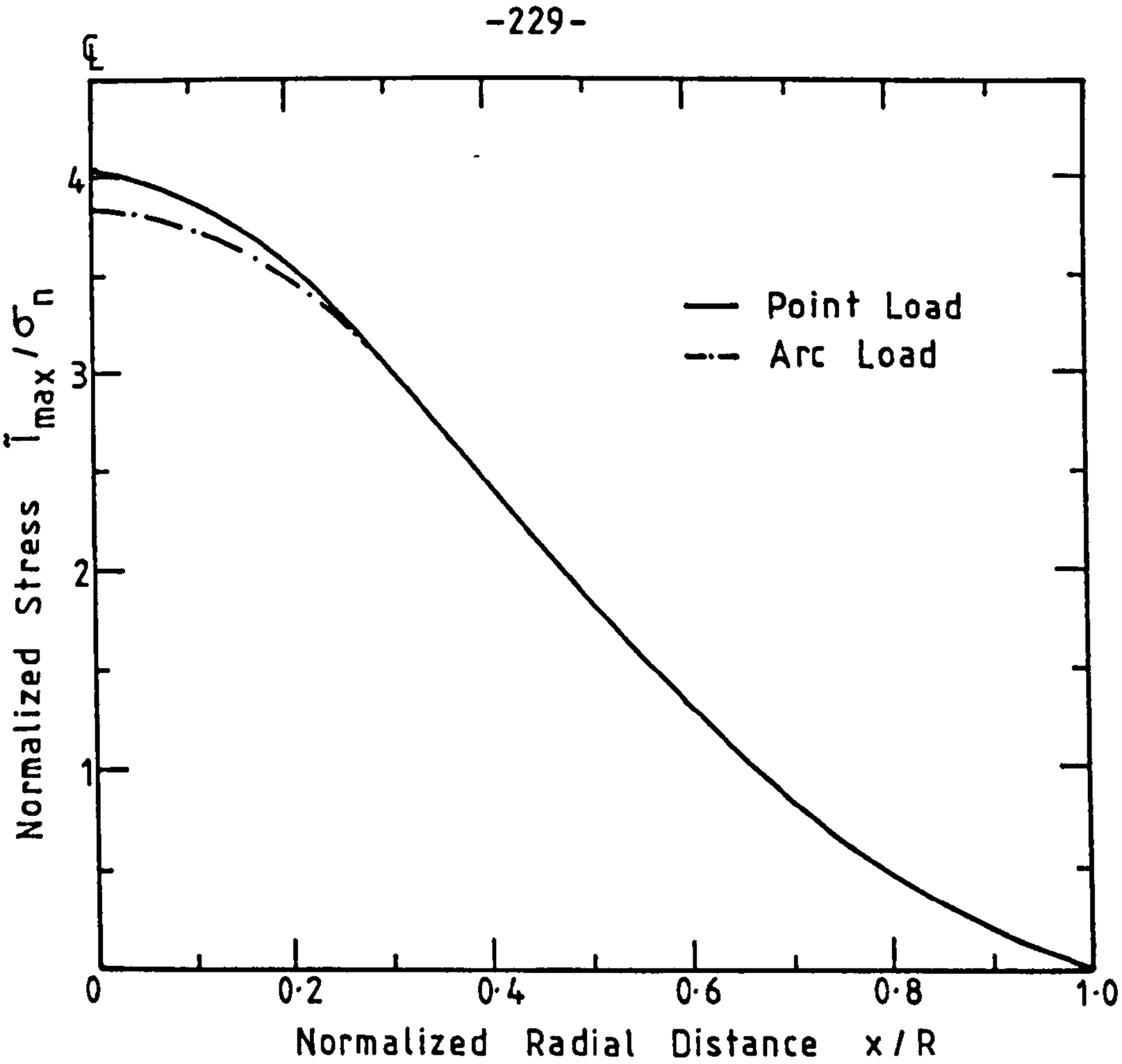

FIG. 4.58 COMPARISON OF SHEAR STRESS DISTRIBUTIONS ACROSS HORIZONTAL DIAMETER FOR A BRAZILIAN DISC SUBJECTED TO POINT LOAD AND DISTRIBUTED LOAD

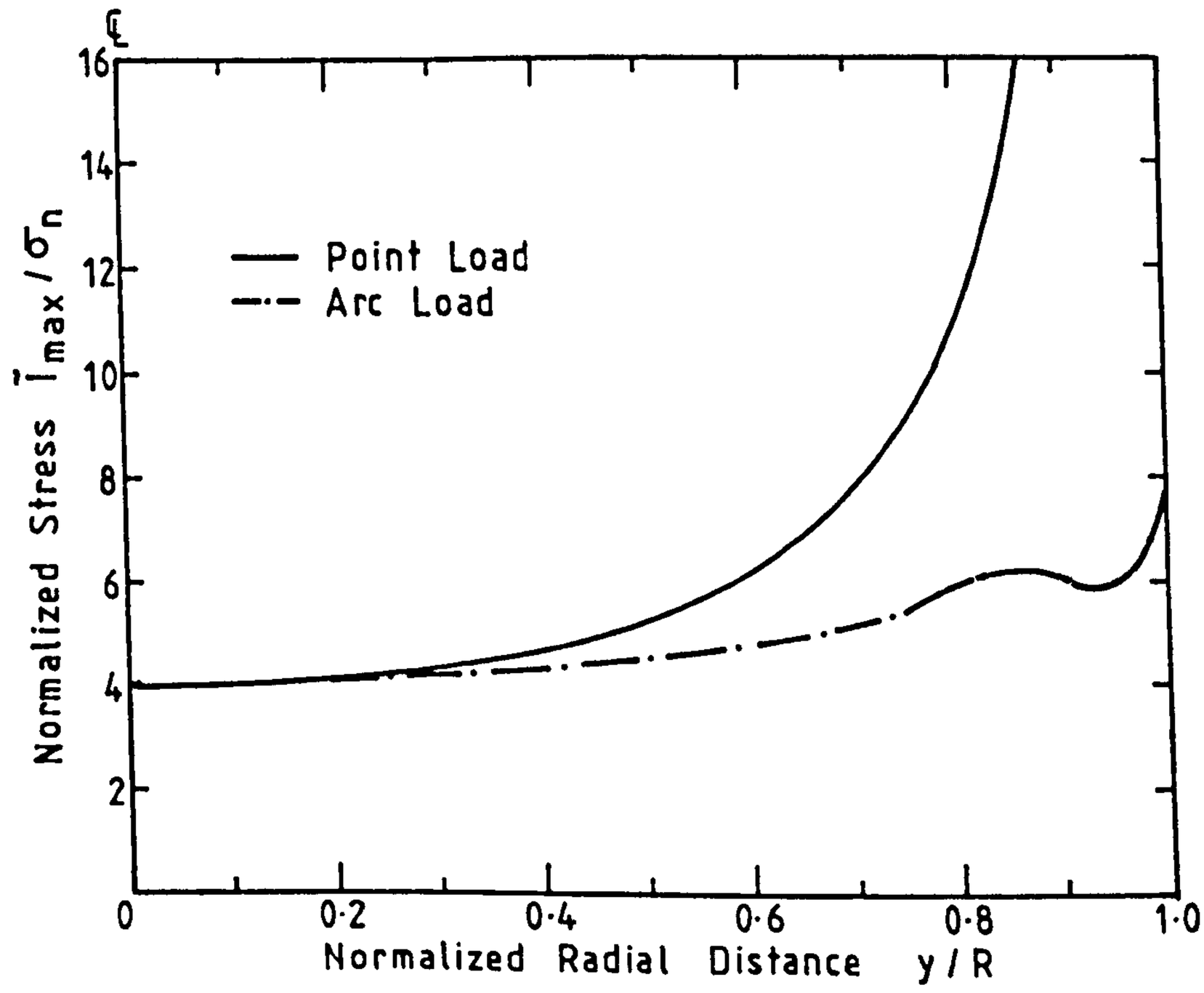

FIG. 4.59 COMPARISON OF SHEAR STRESS DISTRIBUTIONS ACROSS VERTICAL DIAMETER FOR A BRAZILIAN DISC SUBJECTED TO POINT LOAD AND DISTRIBUTED LOAD

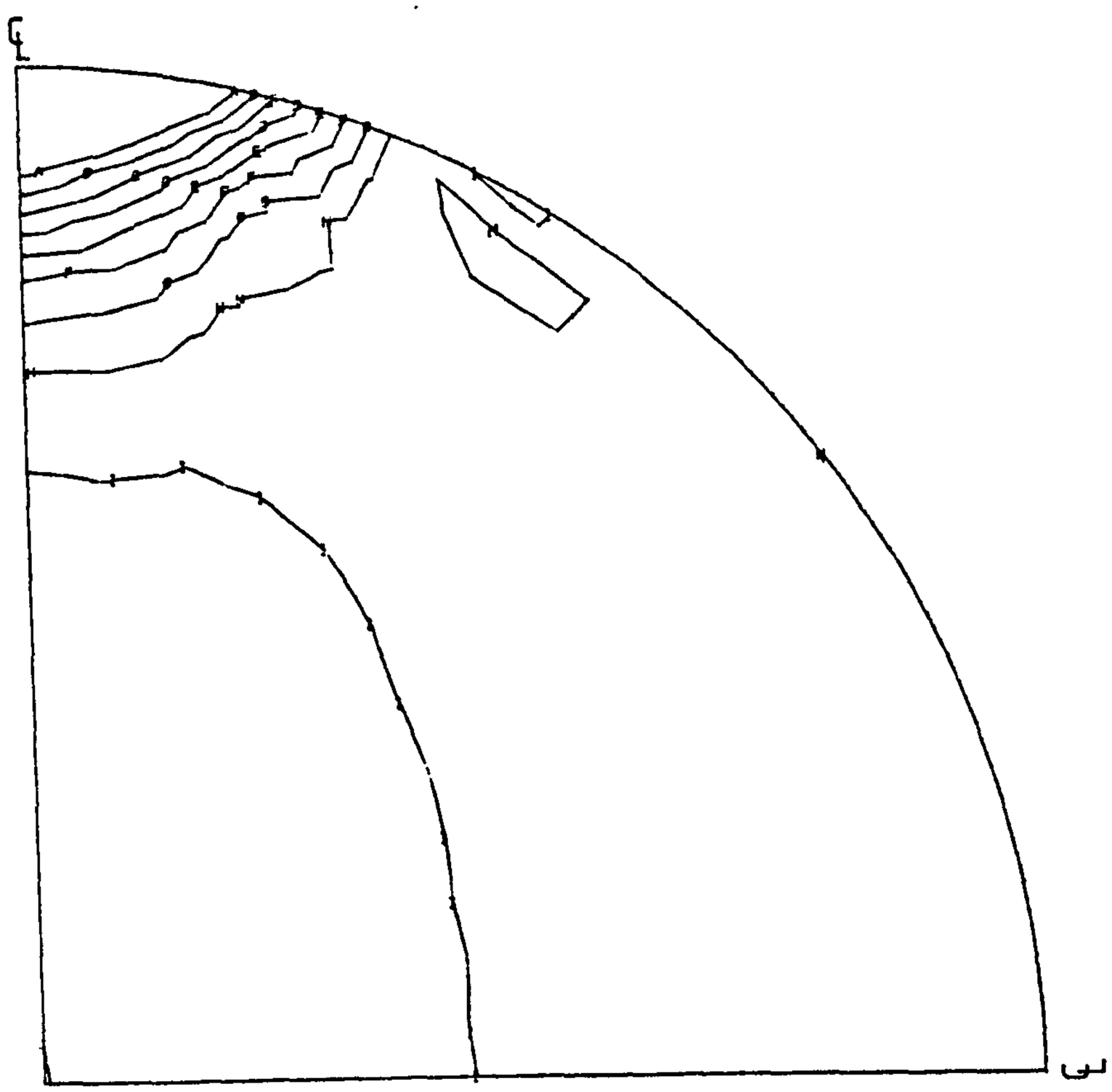

FIG. 4.60 MAXIMUM STRESS DISTRIBUTION IN BRAZILIAN DISC

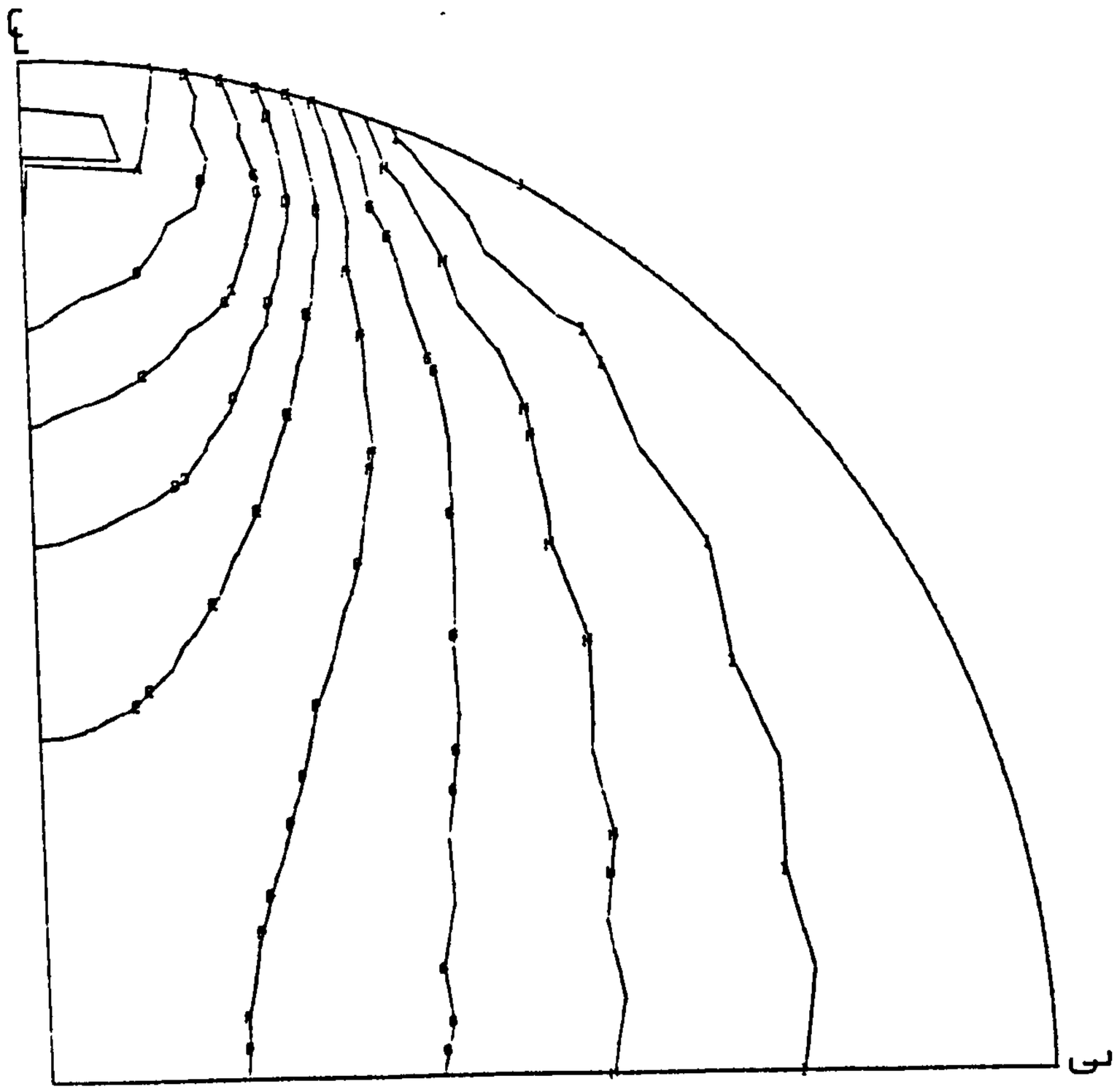

MINIMUM
PRINCIPAL
(MOST
NEGATIVE)
STRESS
(MIDDLE SURFACE)

-03828 E5
-03398 E5
-02969 E5
-02539 E5
-02109 E5
-01679 E5
-01250 E5
-03204 E4
-03907 E4
389 3

FIG.4.61 MINIMUM STRESS DISTRIBUTION IN BRAZILIAN DISC

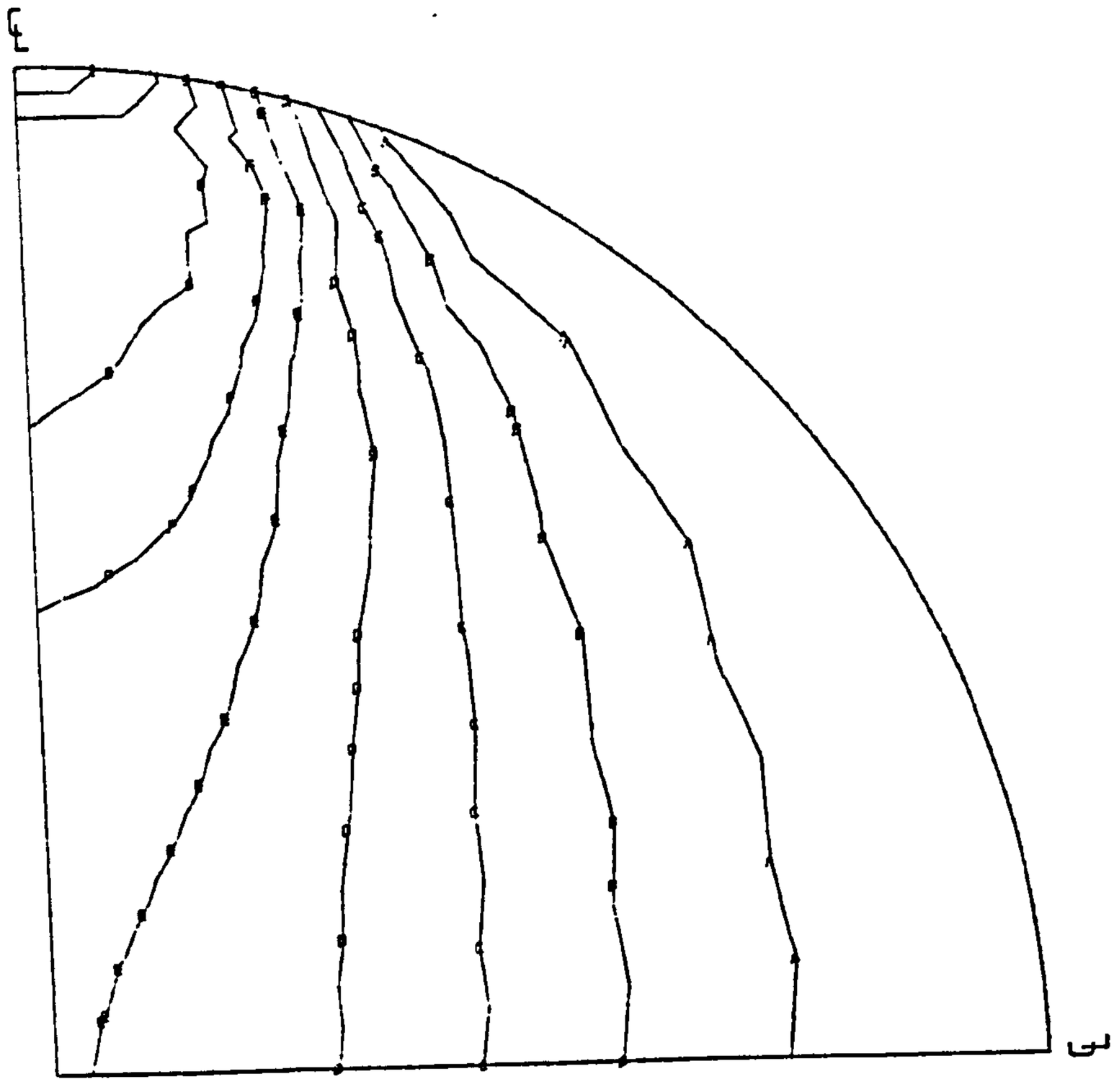

FIG. 4.62 EQUIVALENT STRESS DISTRIBUTION IN BRAZILIAN DISC

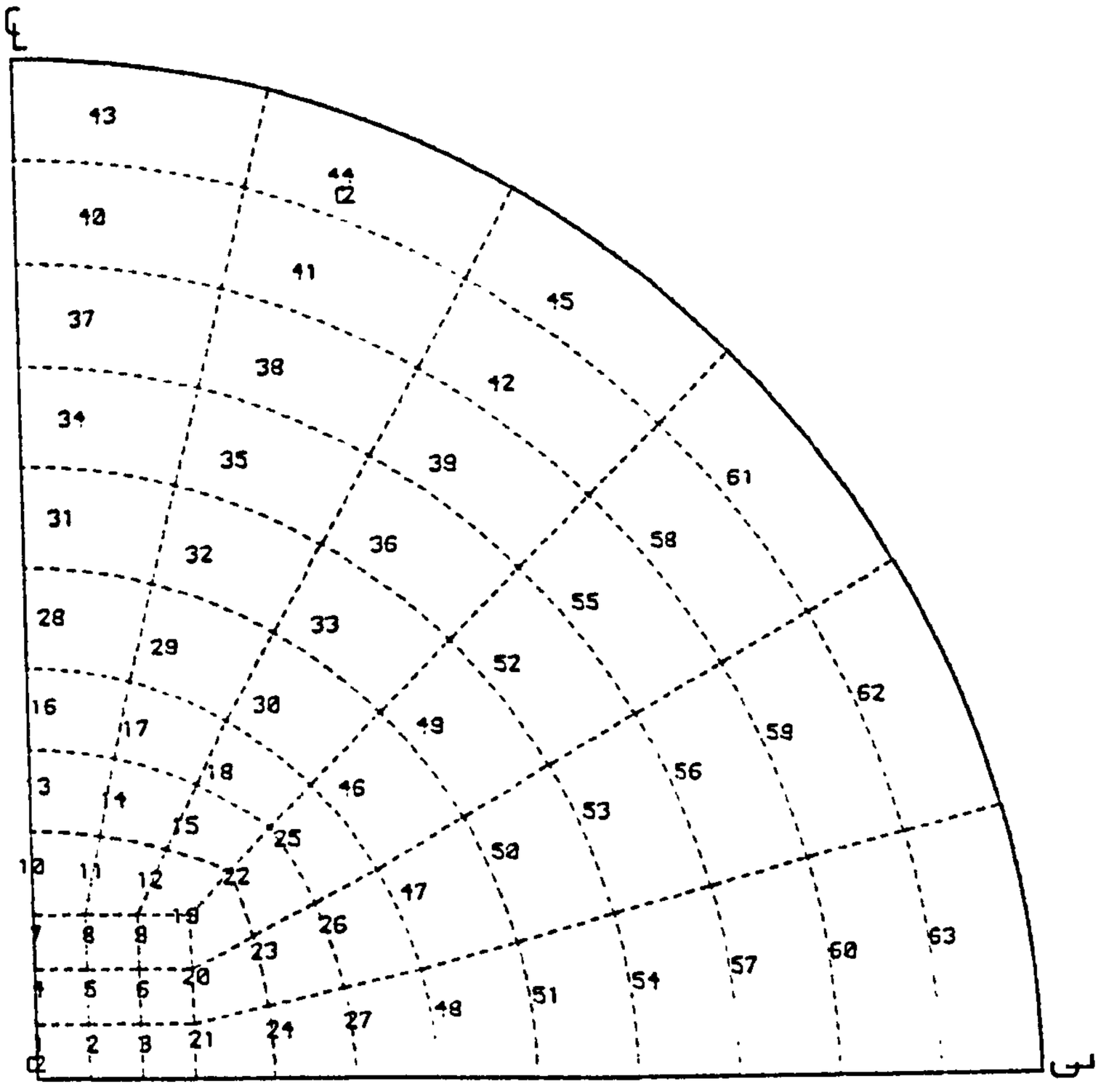

FIG. 4.63 POSITIONAL FAILURE IN BRAZILIAN DISC

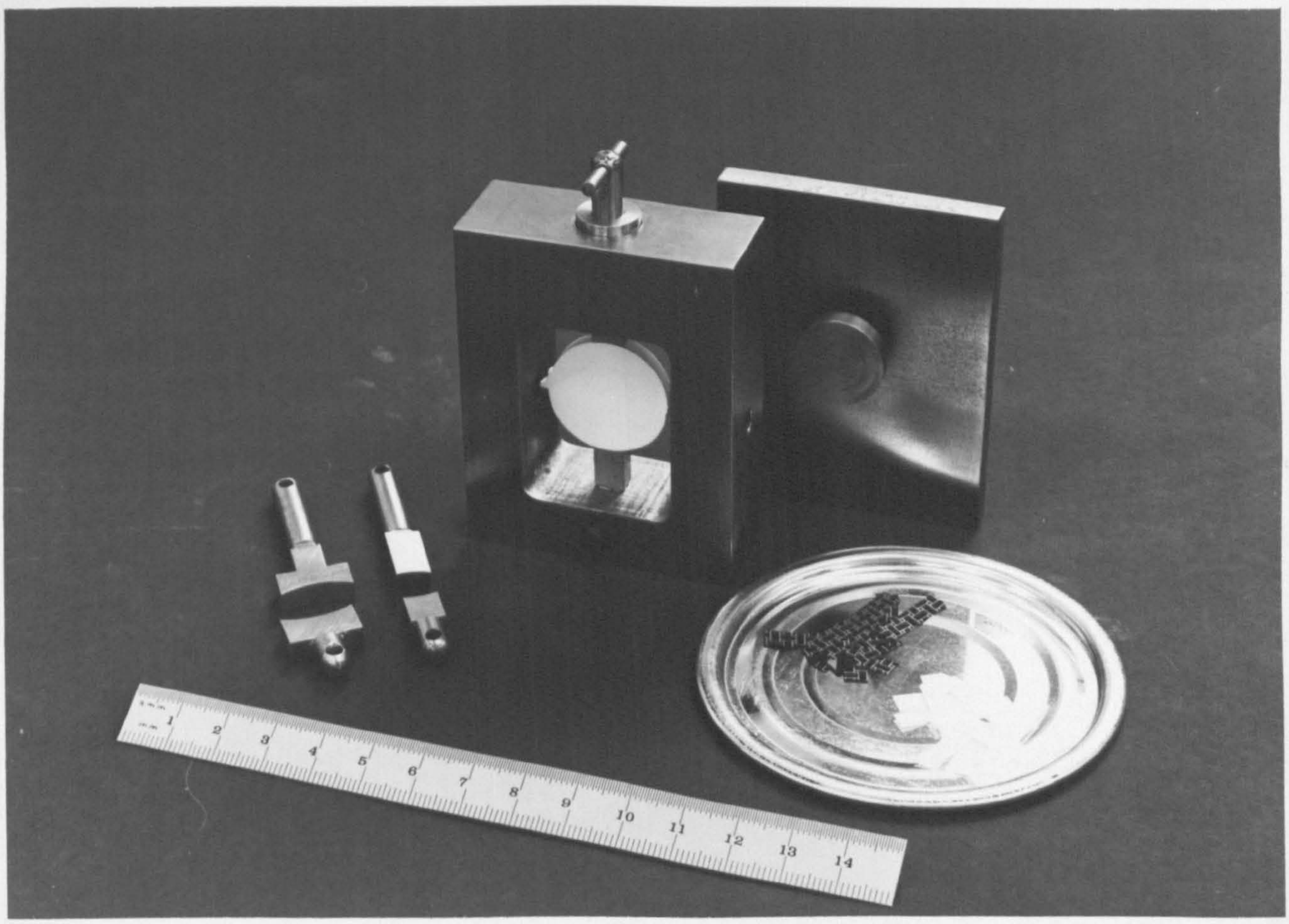

FIG. 4.64 BRAZILIAN DISC TEST ASSEMBLY

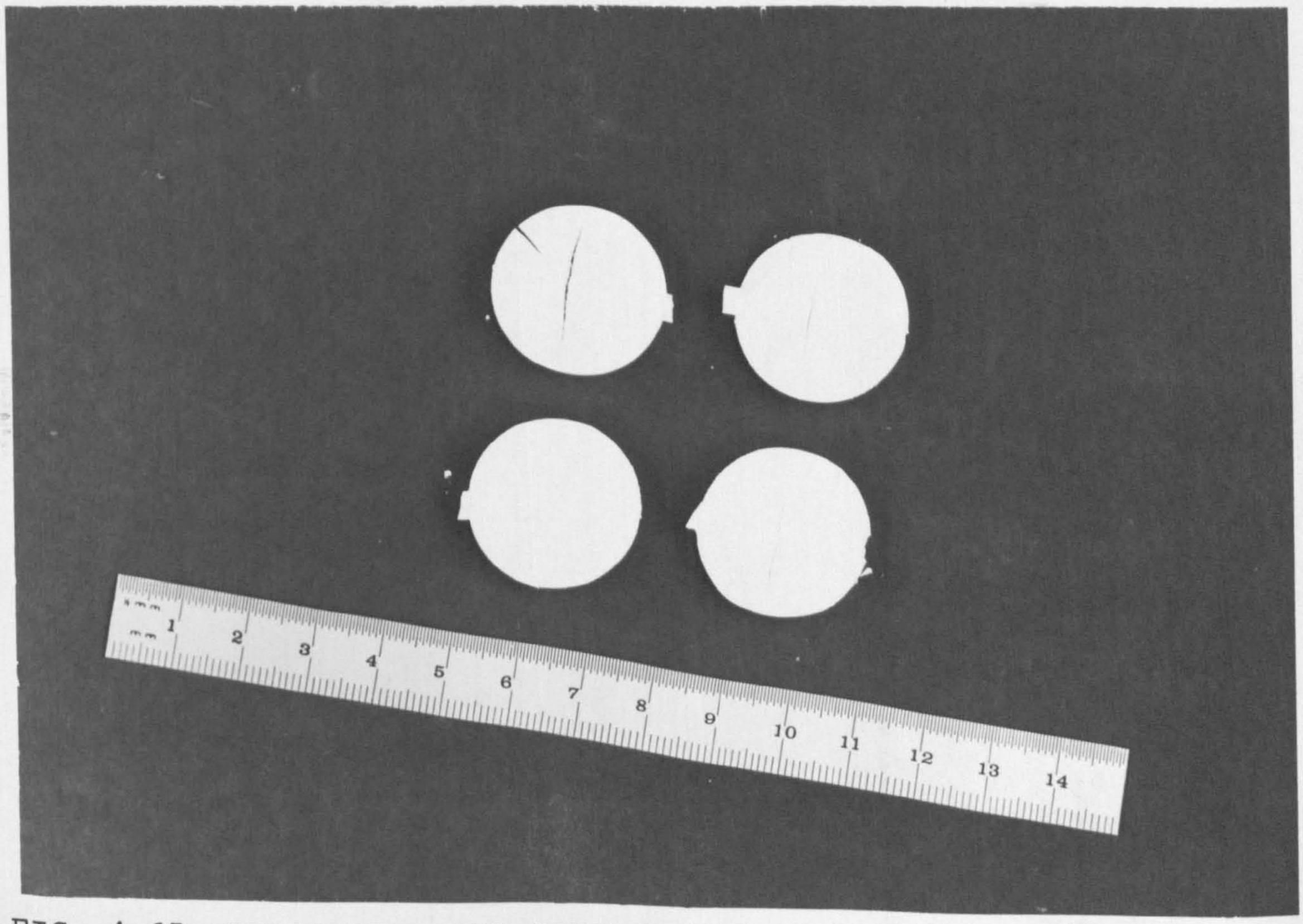

FIG. 4.65 FRACTURE MODES COMMONLY OBTAINED WITH THE BRAZILIAN DISC TEST

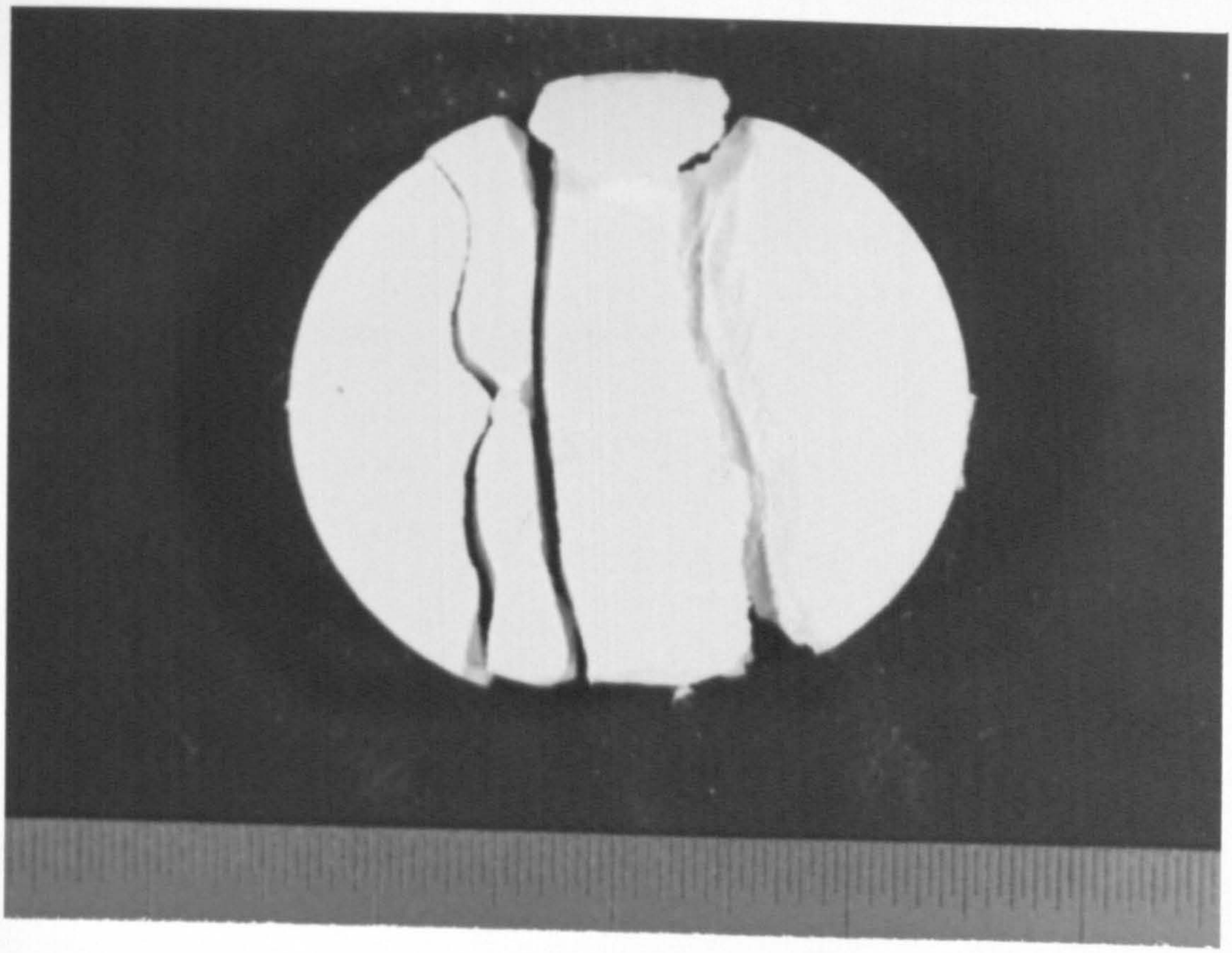

FIG. 4.66 TRIPLE-CLEFT FRACTURE OBSERVED IN BRAZILIAN DISC SPECIMEN

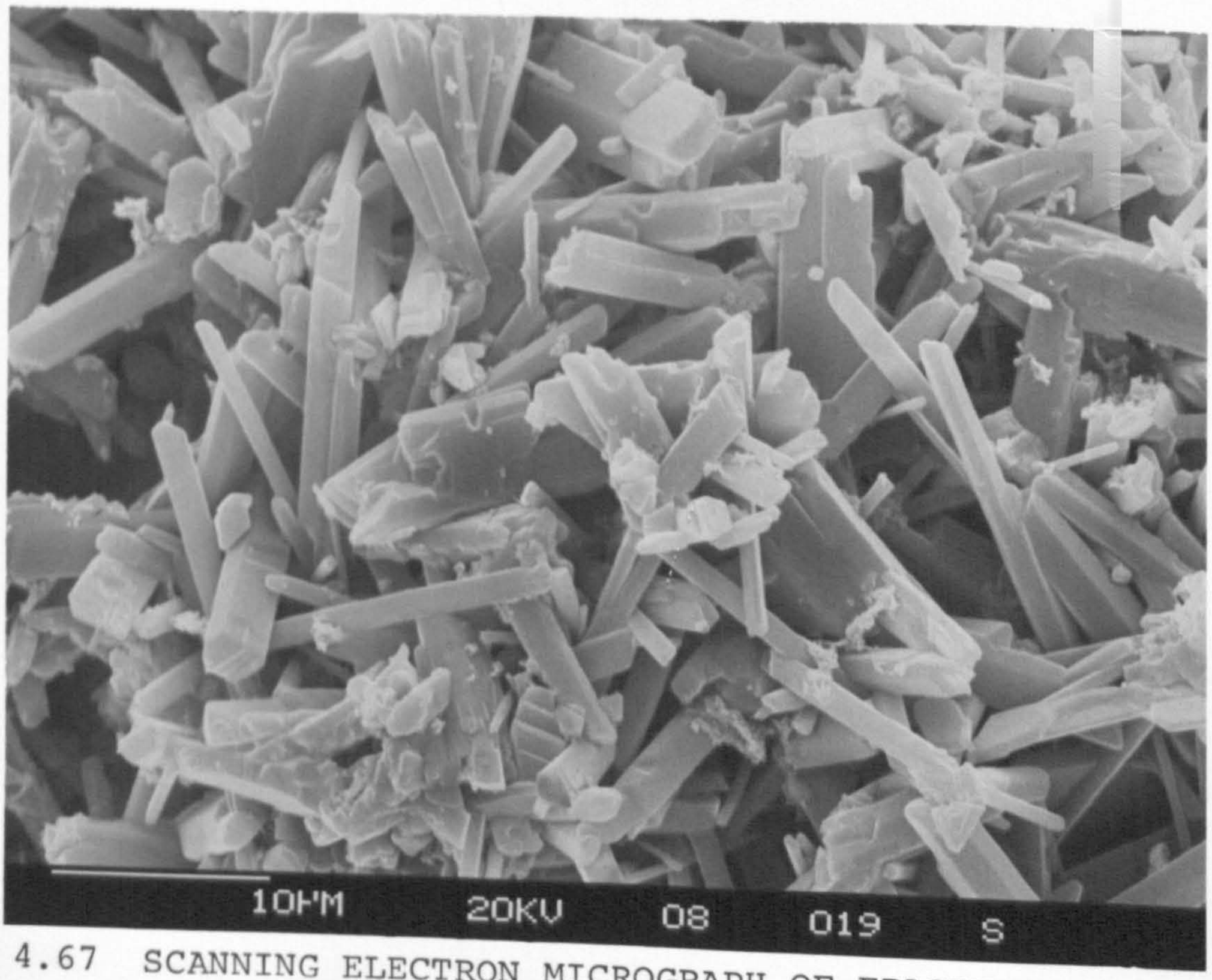

FIG. 4.67 SCANNING ELECTRON MICROGRAPH OF FRACTURE SURFACE OI A BRAZILIAN DISC TEST; x 2000

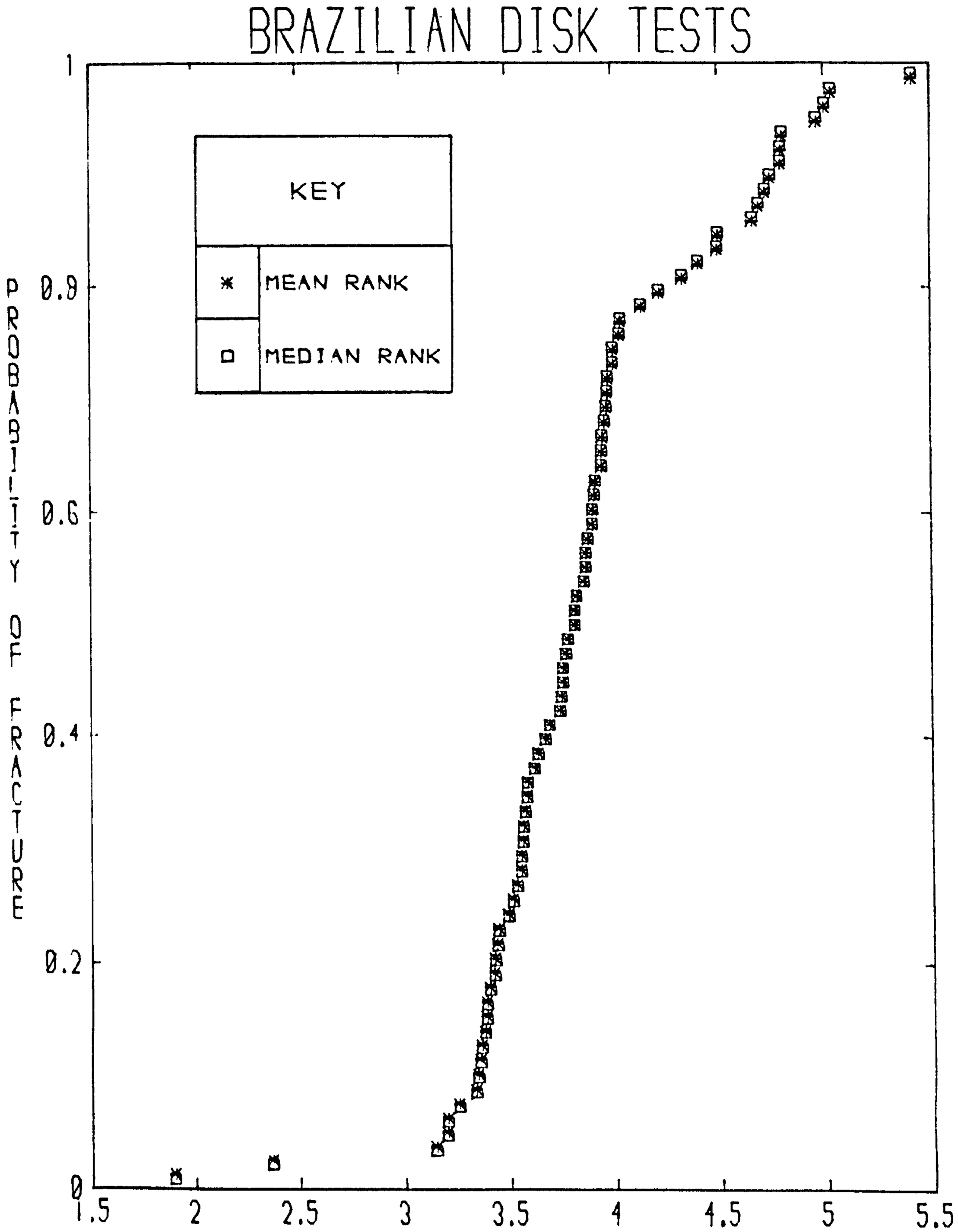

FIG. 4.68 THE CUMULATIVE DISTRIBUTION OF FRACTURE STRENGTHS OF 77 SPECIMENS TESTED IN BRAZILIAN DISC TEST

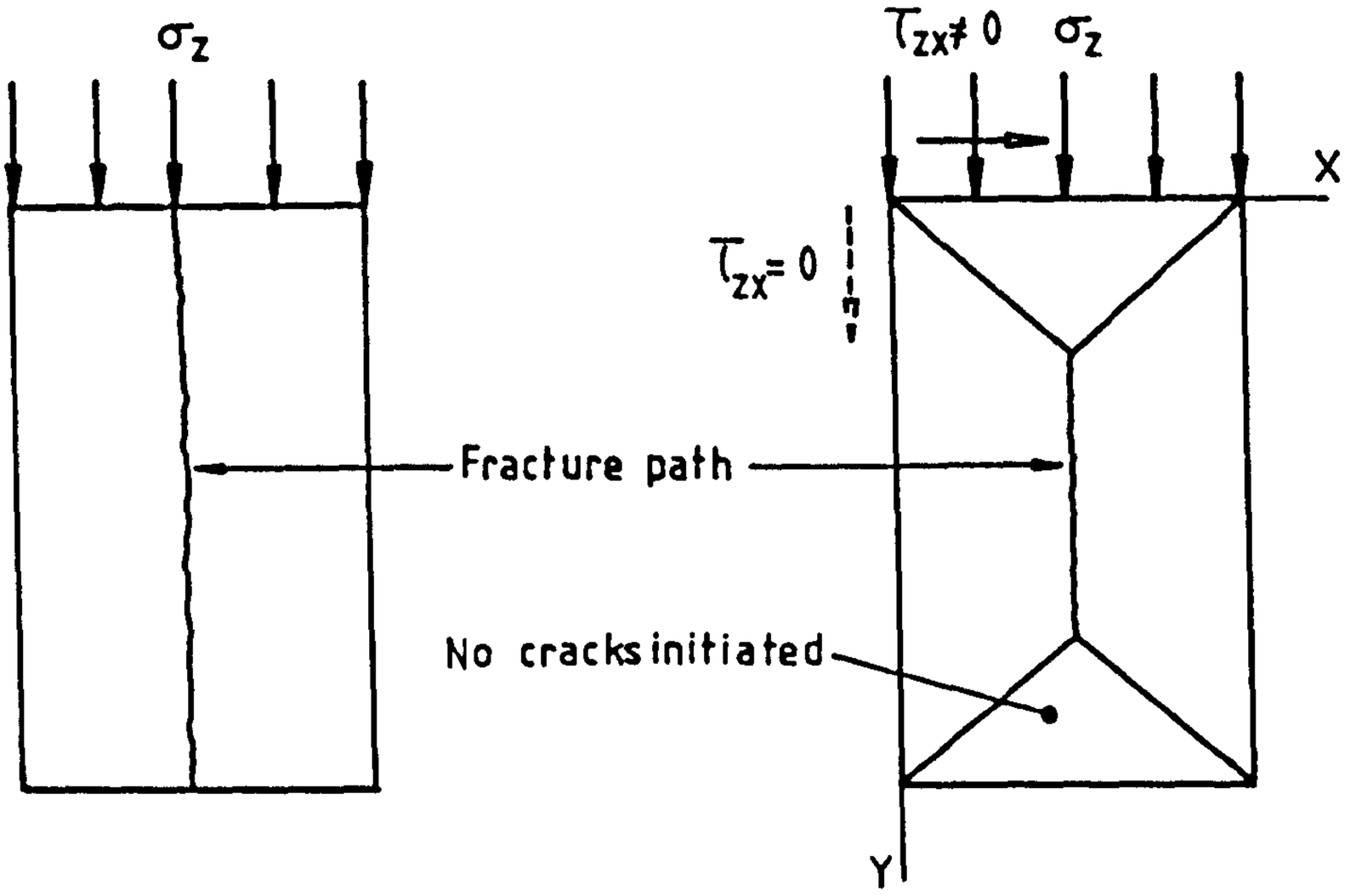

FIG. 4.69 CRACK PROPAGATION IN UNIAXIAL COMPRESSION OF BRITTLE MATERIAL WITH
(a) No friction at the end
(b) Friction at the end

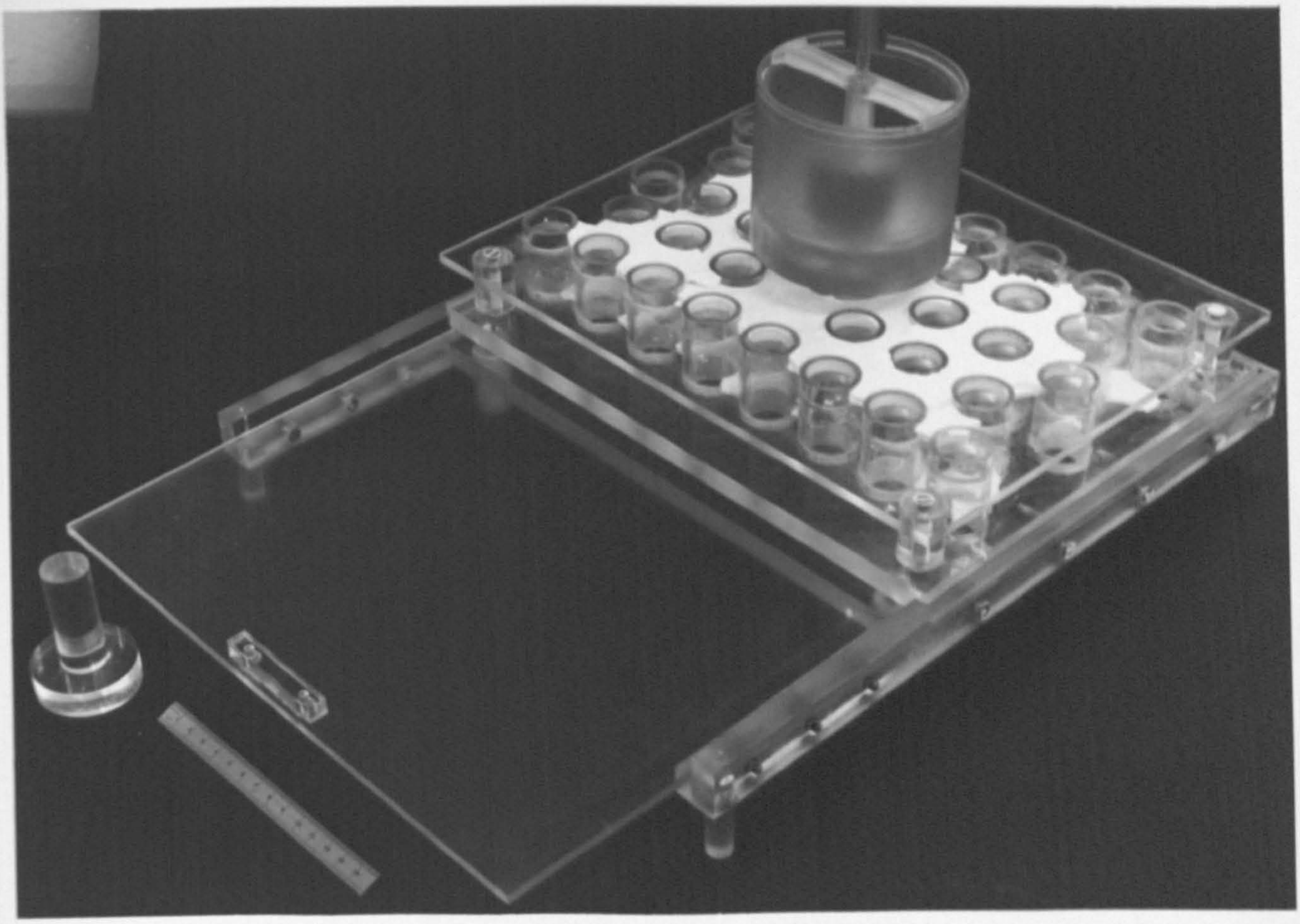

FIG. 4.7O SOLID CYLINDER MOULD ASSEMBLY

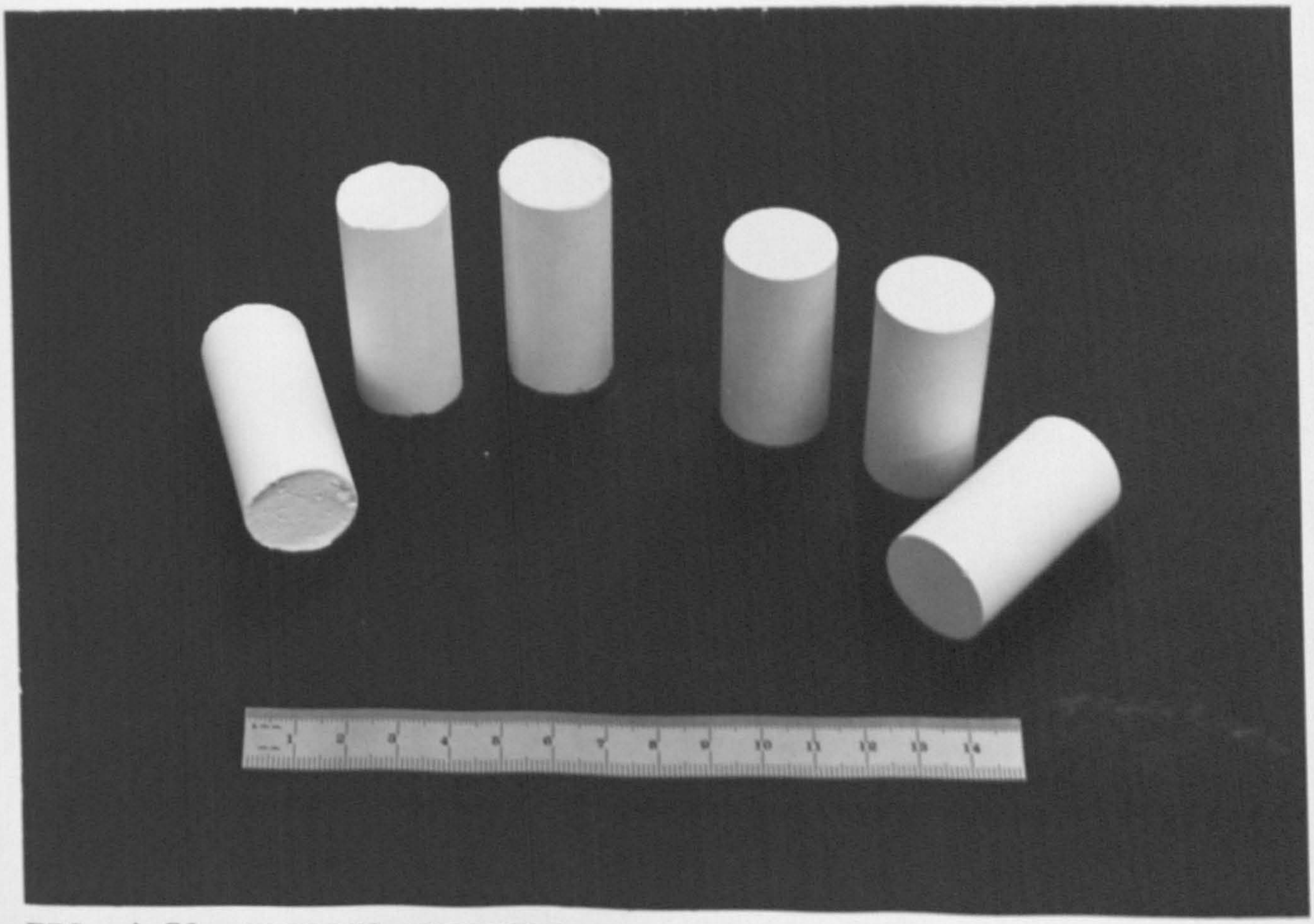

FIG. 4.71 VARIOUS UNIAXIAL COMPRESSION SPECIMENS AS CAST AND AFTER MACHINING

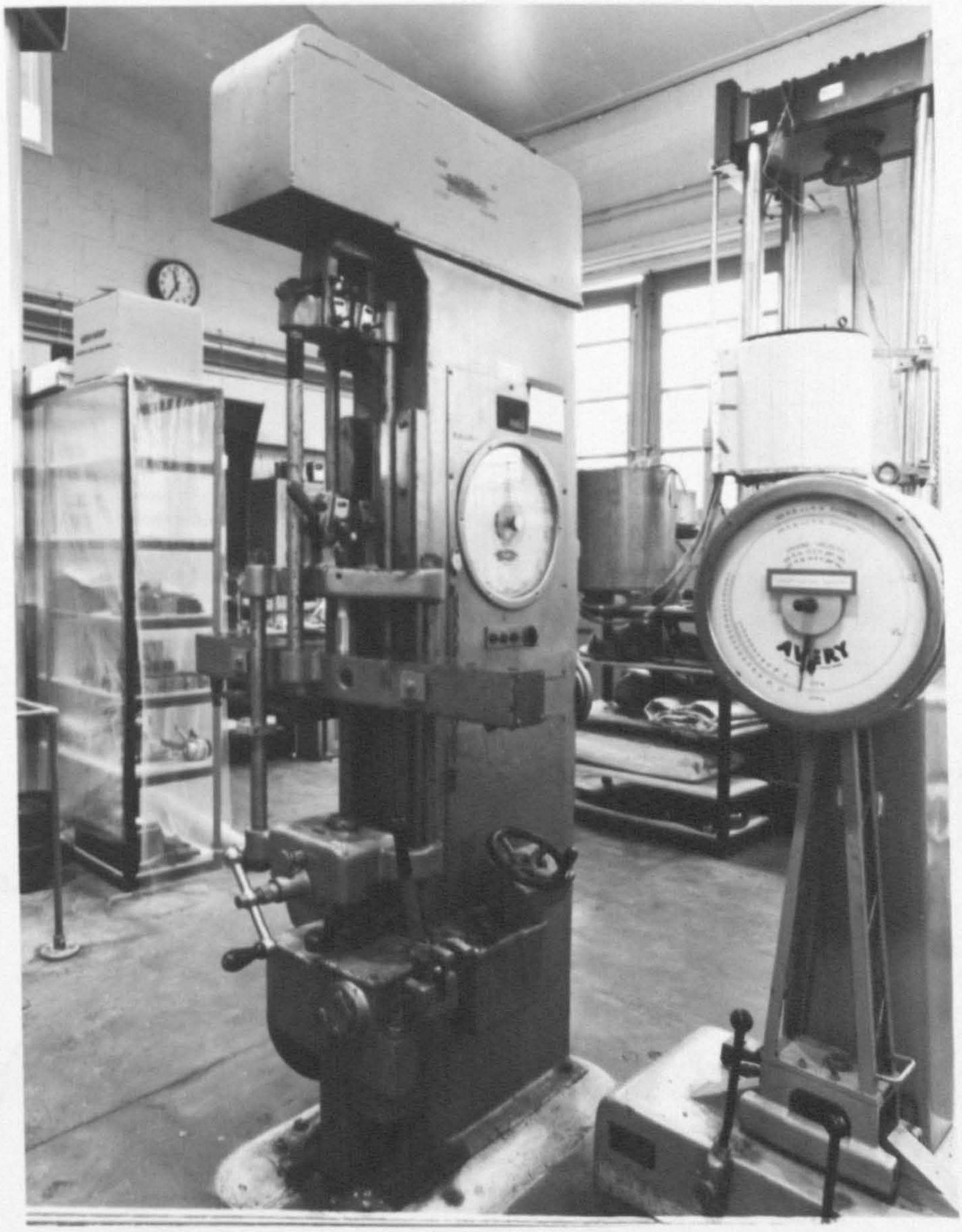

FIG. 4.72 SPECIMEN PLACED IN TESTING MACHINE, READY FOR TEST

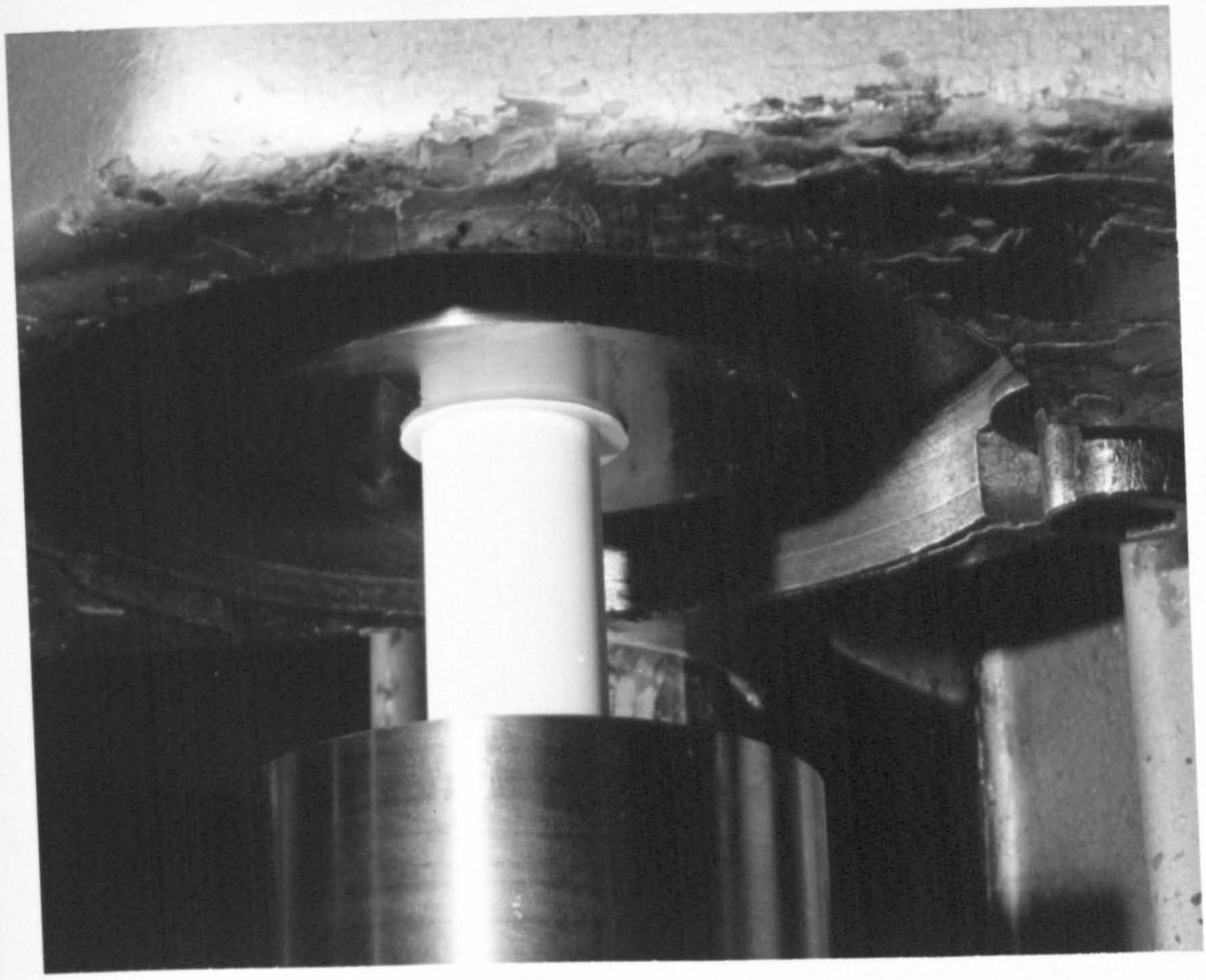

(a) Before testing

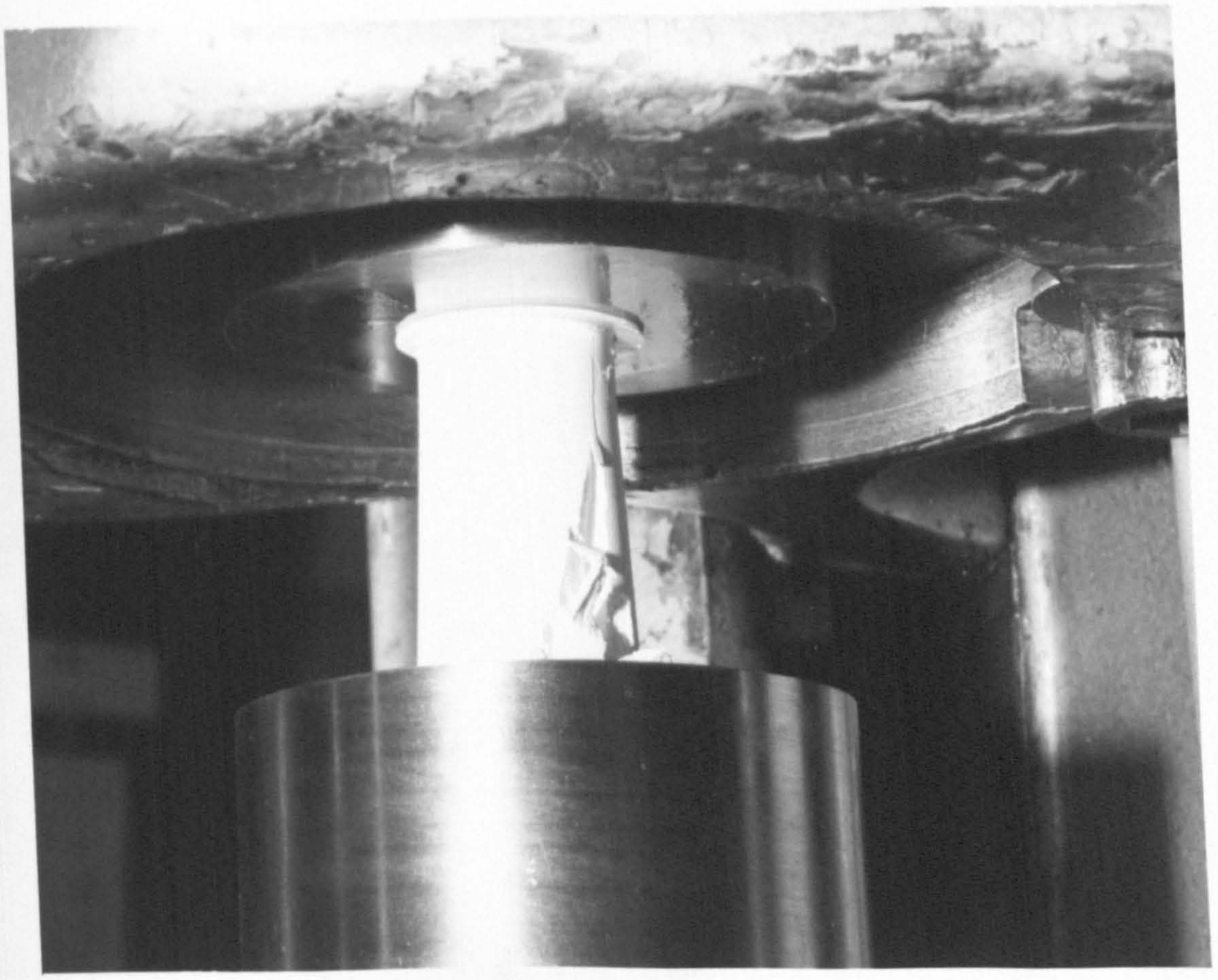

(b) After failure

FIG. 4.73 UNIAXIAL COMPRESSION TEST

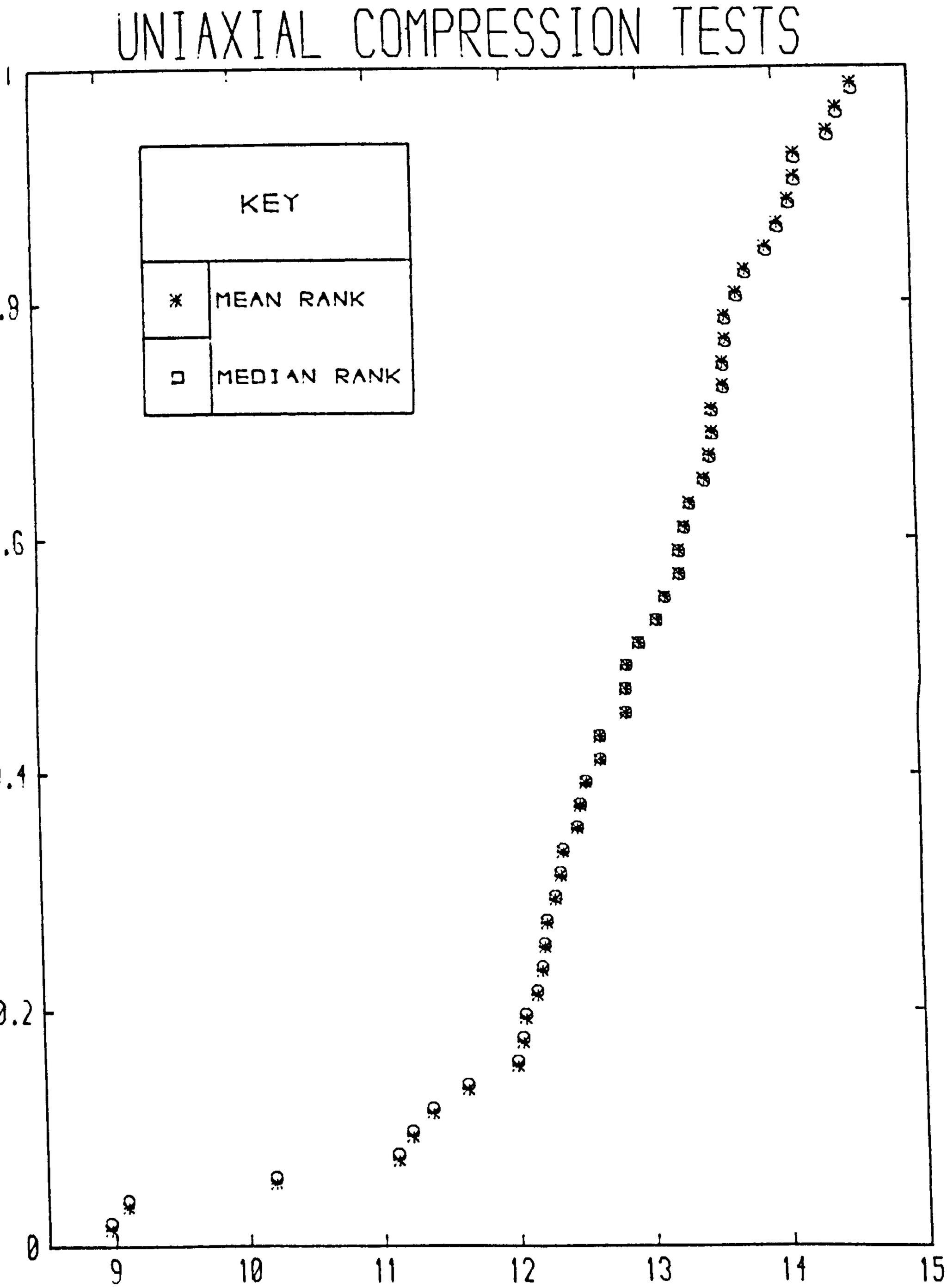

FIG. 4.74 THE CUMULATIVE DISTRIBUTION OF FRACTURE STRENGTHS OF 50 SPECIMENS TESTED IN UNIAXIAL COMPRESSION

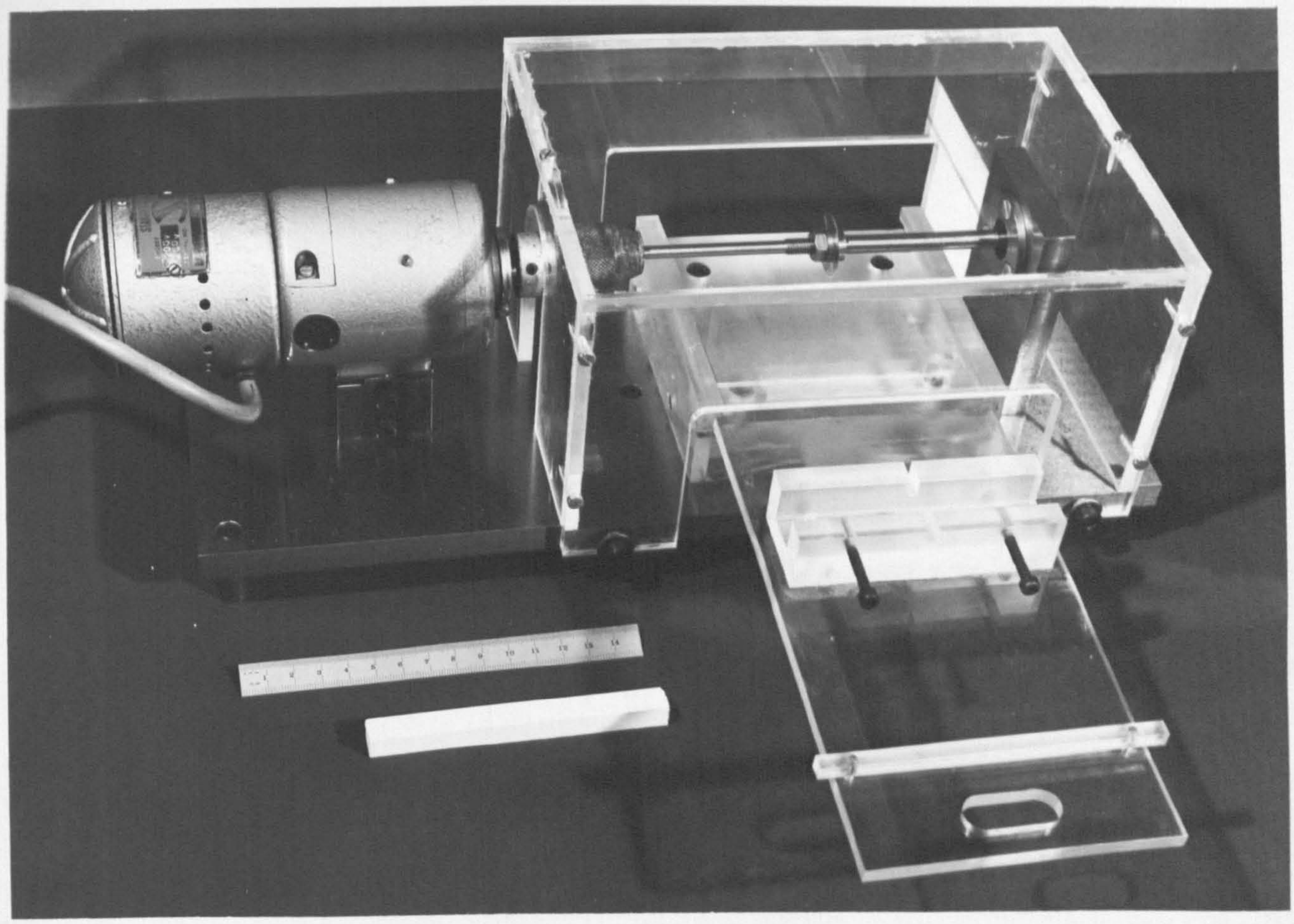

FIG. 4.75 SAW TABLE

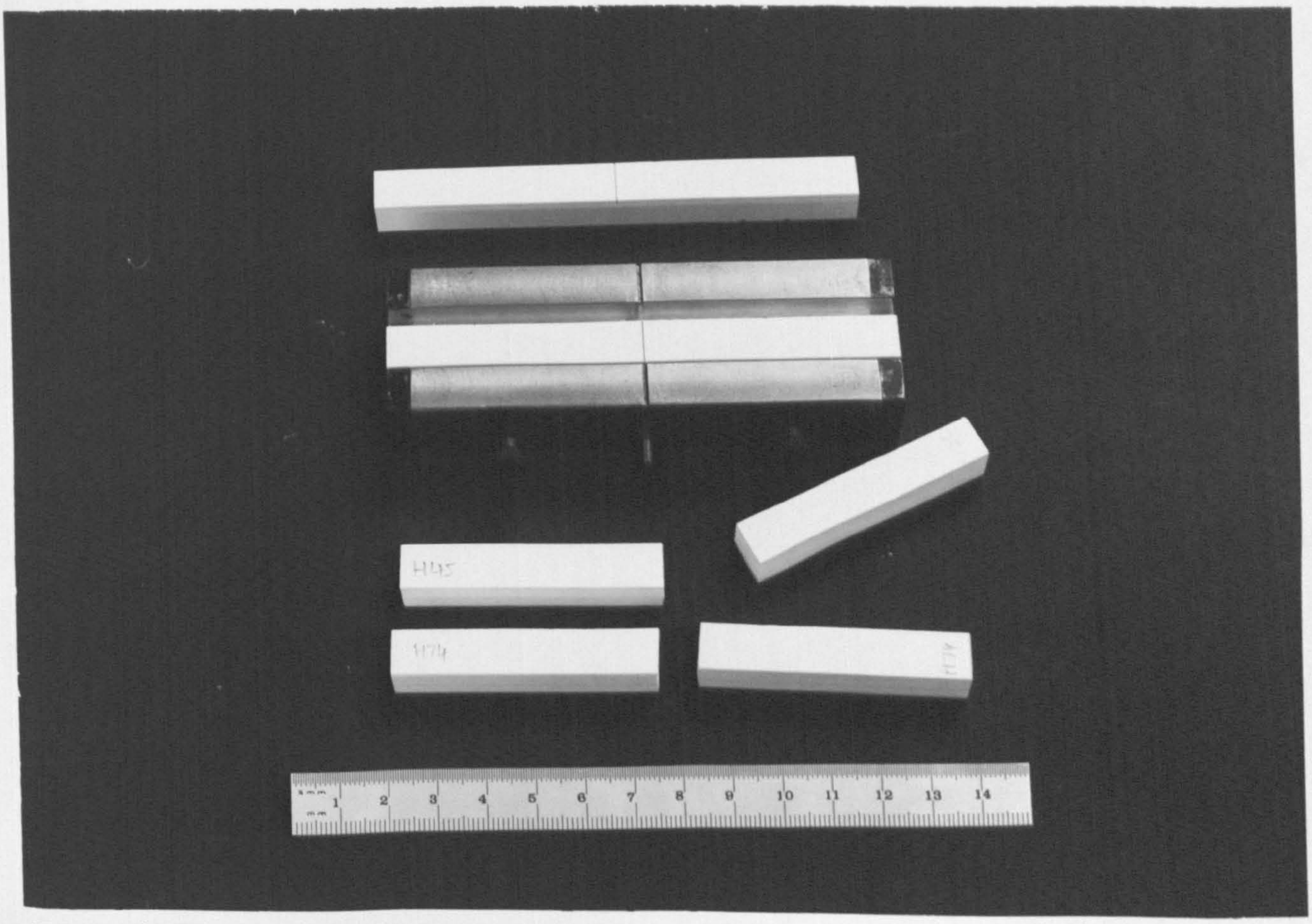

FIG. 4.76 DEVICE USED FOR PREPARATION OF THE THREE-POINT NOTCH BEND SPECIMEN

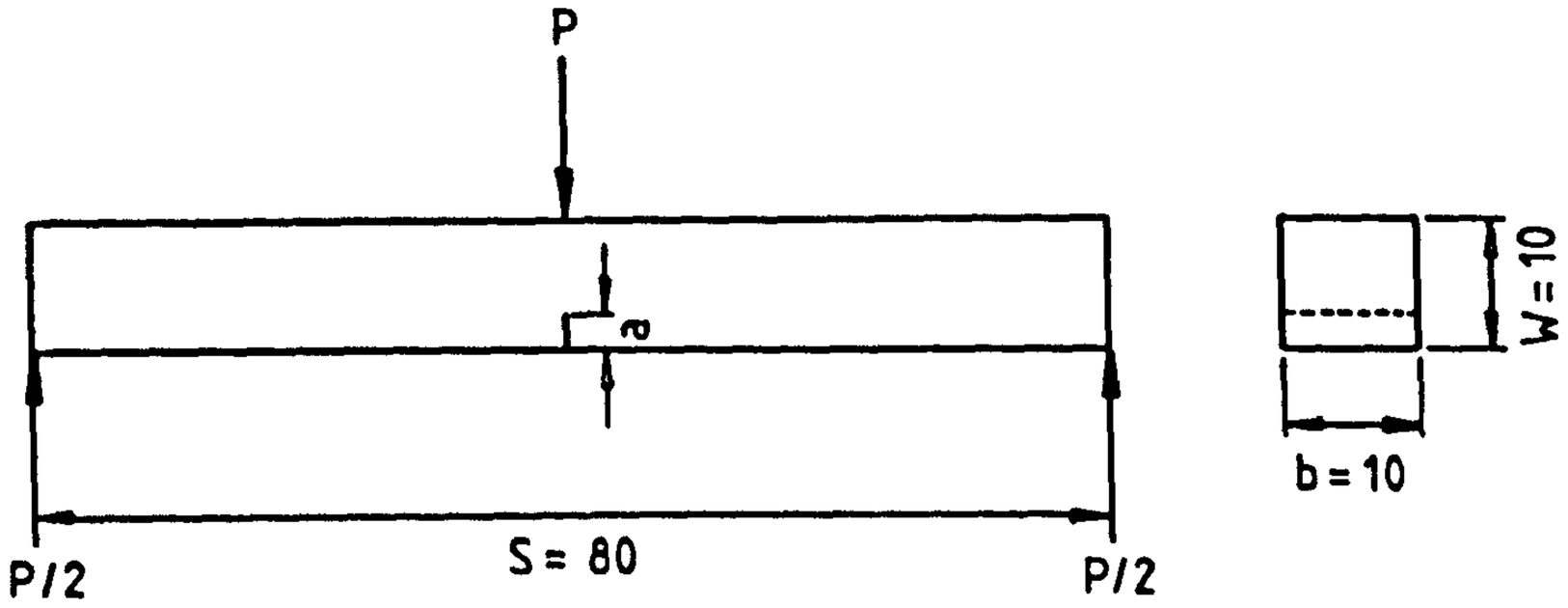

All dimensions in m.m

FIG. 4.77 TEST CONFIGURATION USED FOR MEASURING FRACTURE TOUGHNESS

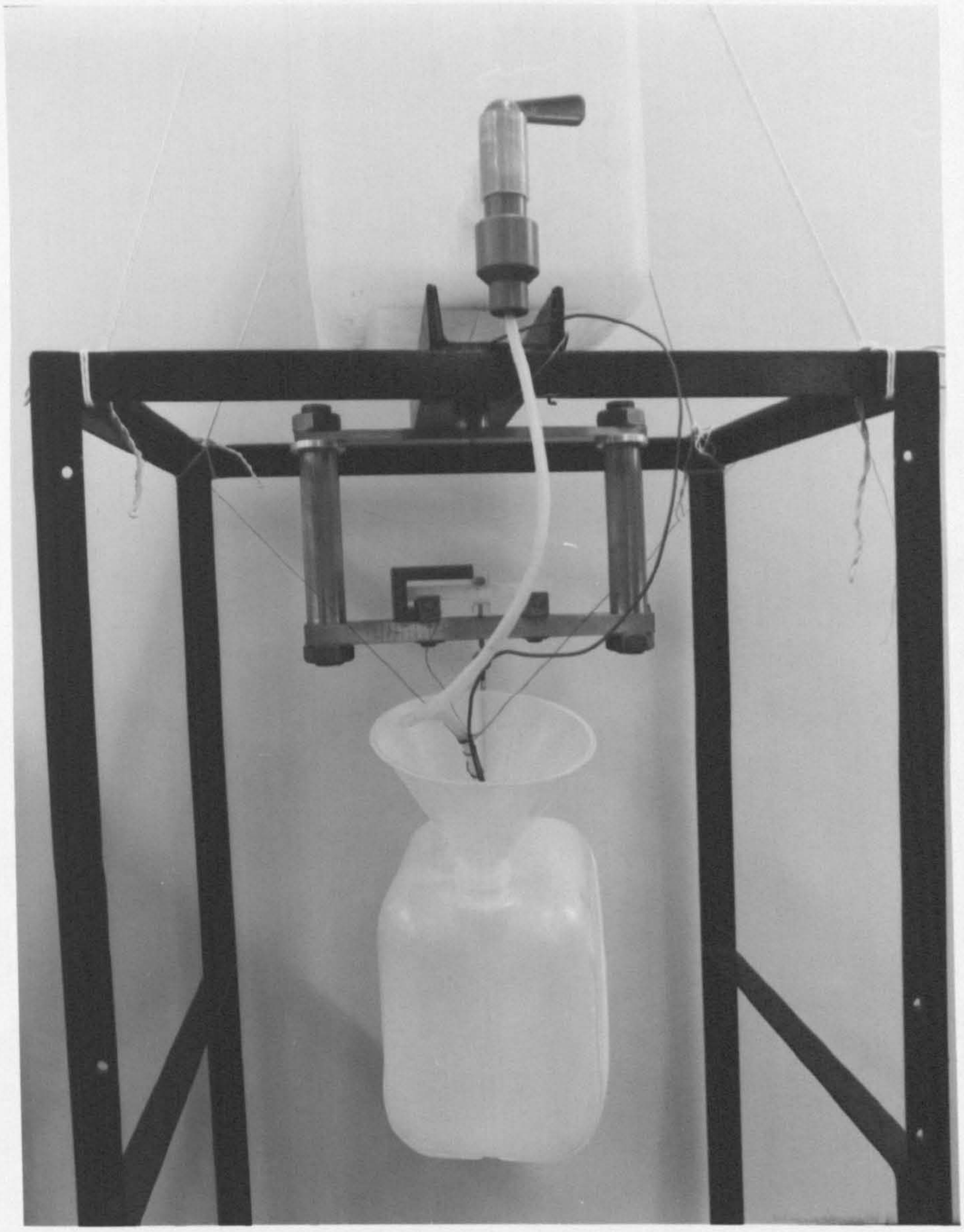

FIG. 4.78 THREE-POINT NOTCH BEND TEST FIXTURE

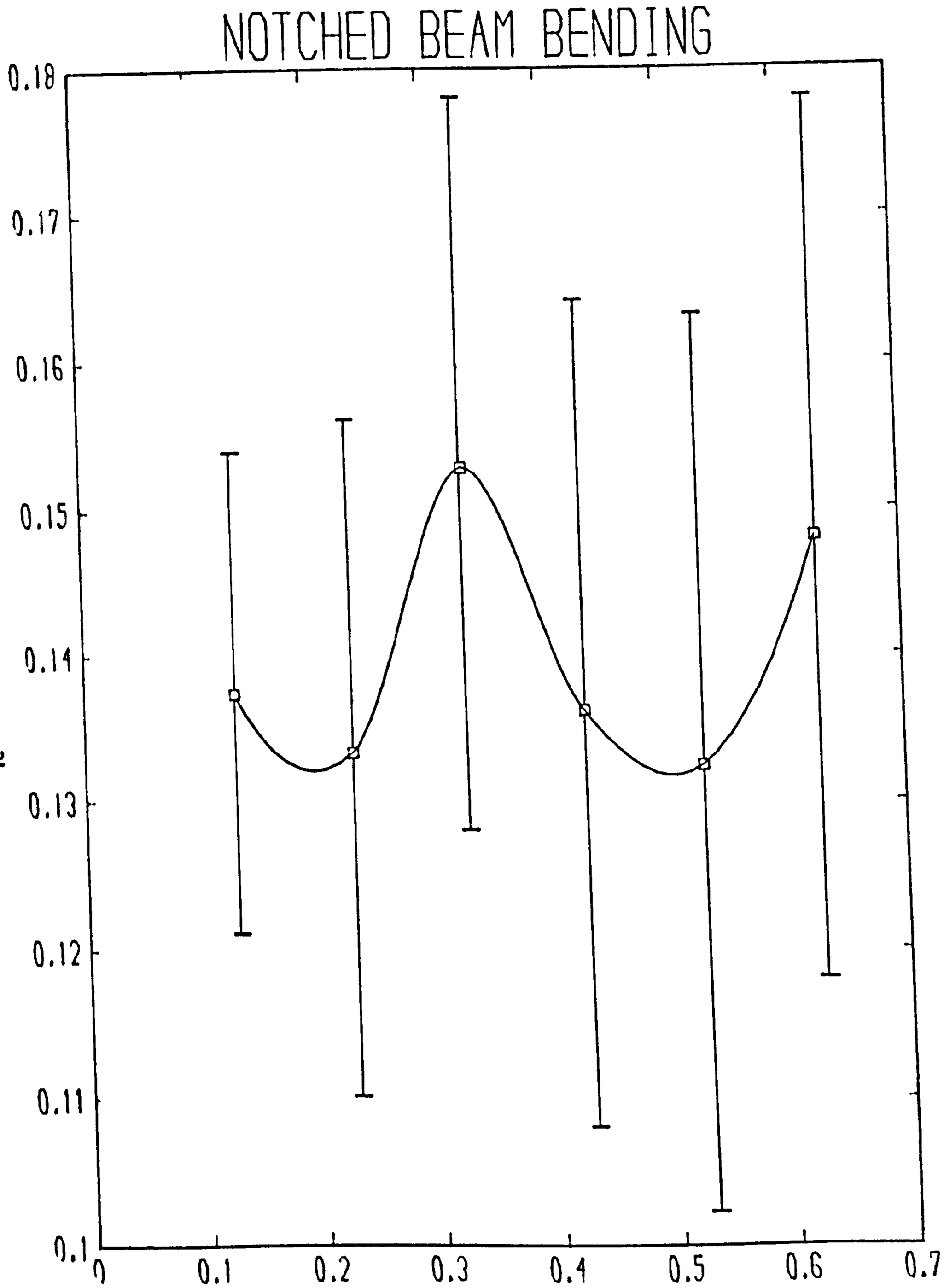

FIG. 4.79 K_{IC} VS NOTCH GEOMETRY FOR HERCULITE LX PLASTER

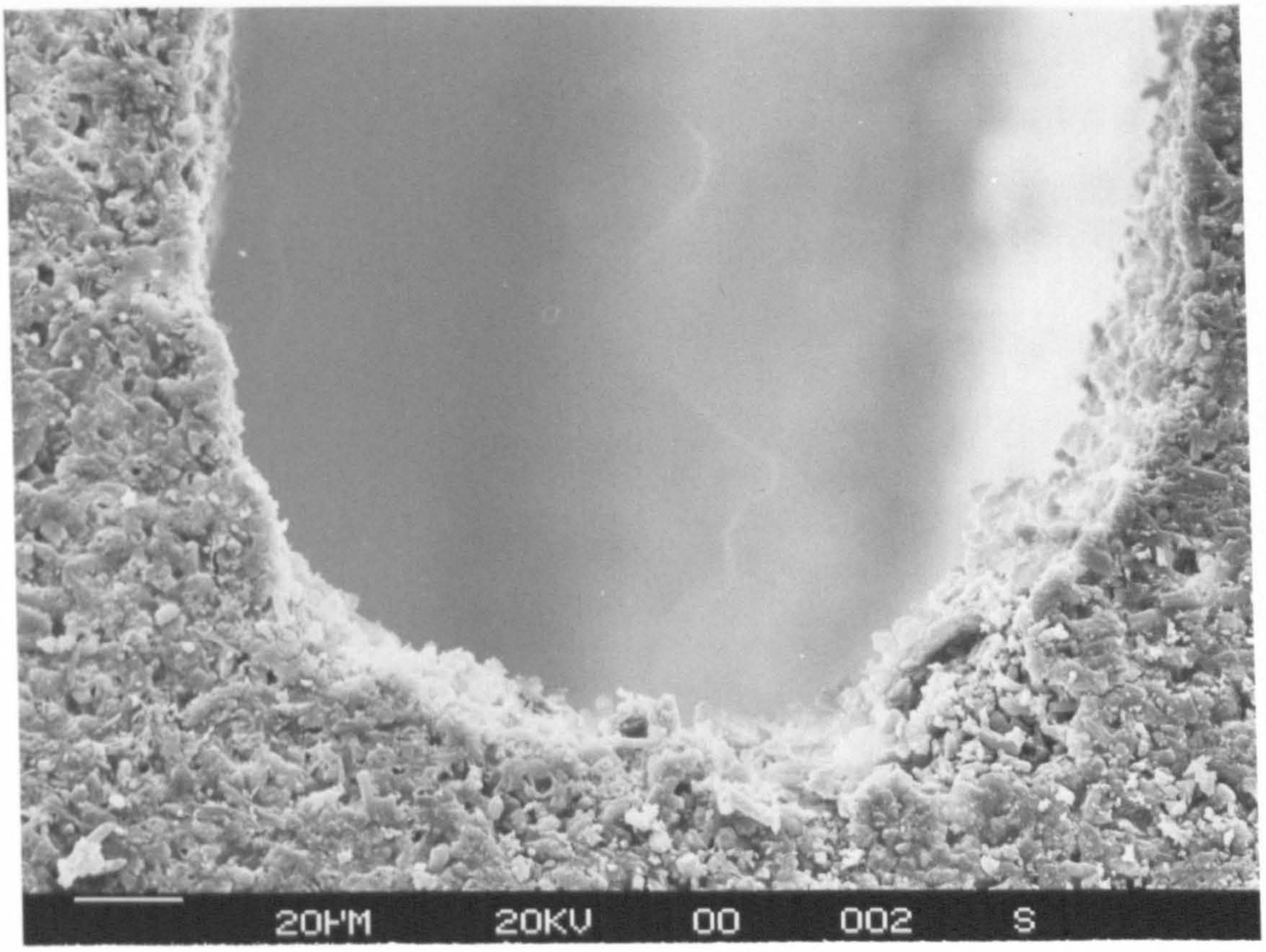

FIG. 4.80 TYPICAL SIDE VIEW OF A SAWN NOTCH ; x 500

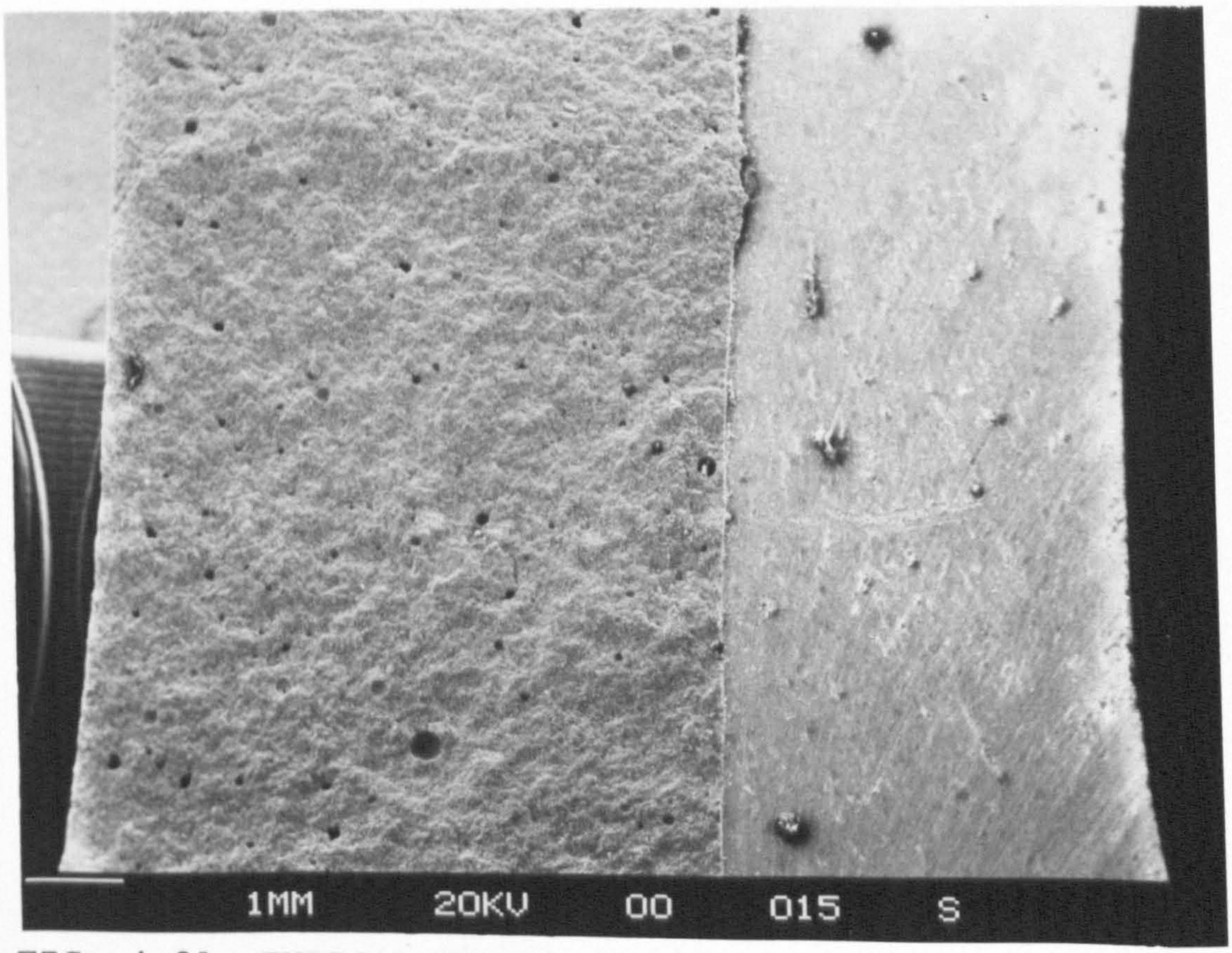

FIG. 4.81 TYPICAL FRACTURE SURFACE SHOWING A POROSITY STRUCTURE x 9

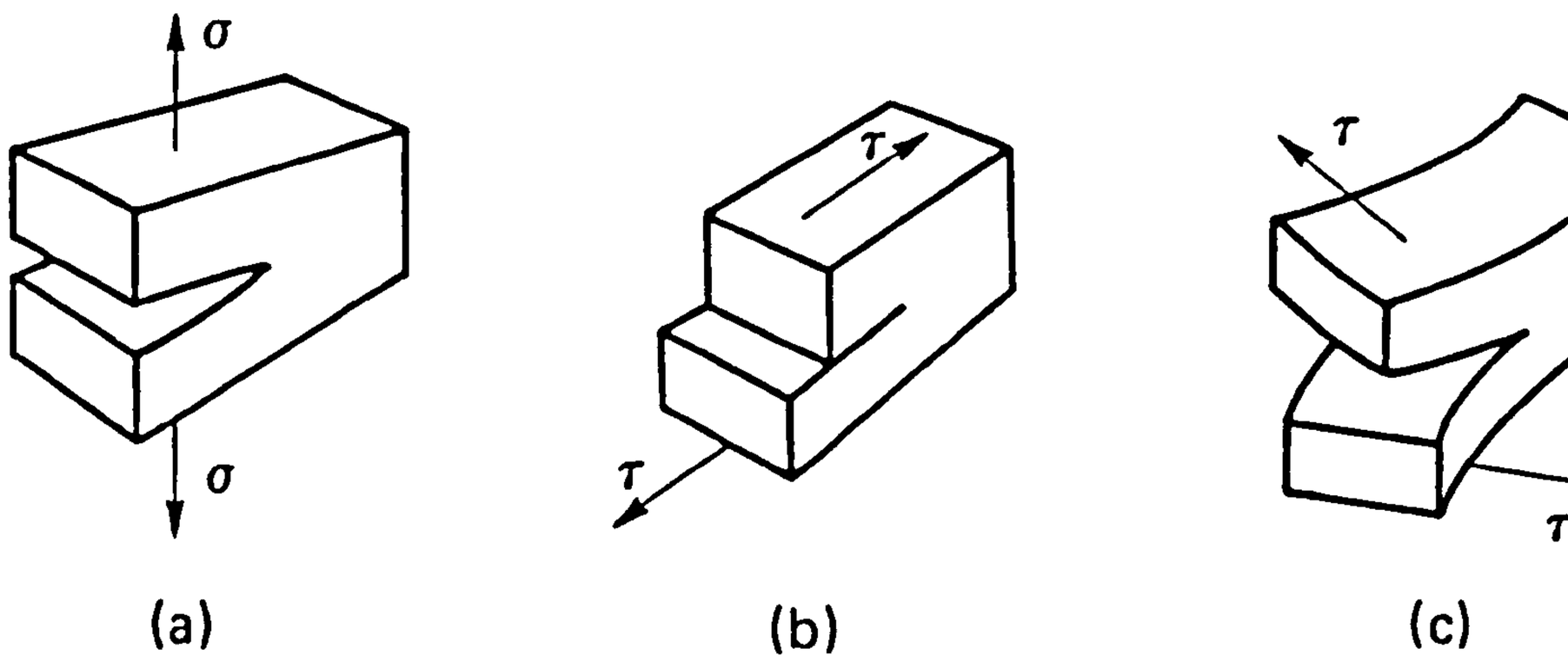

FIG. 4.82 BASIC MODES OF FRACTURE
(a) Opening Mode
(b) Shearing Mode
(c) Tearing Mode

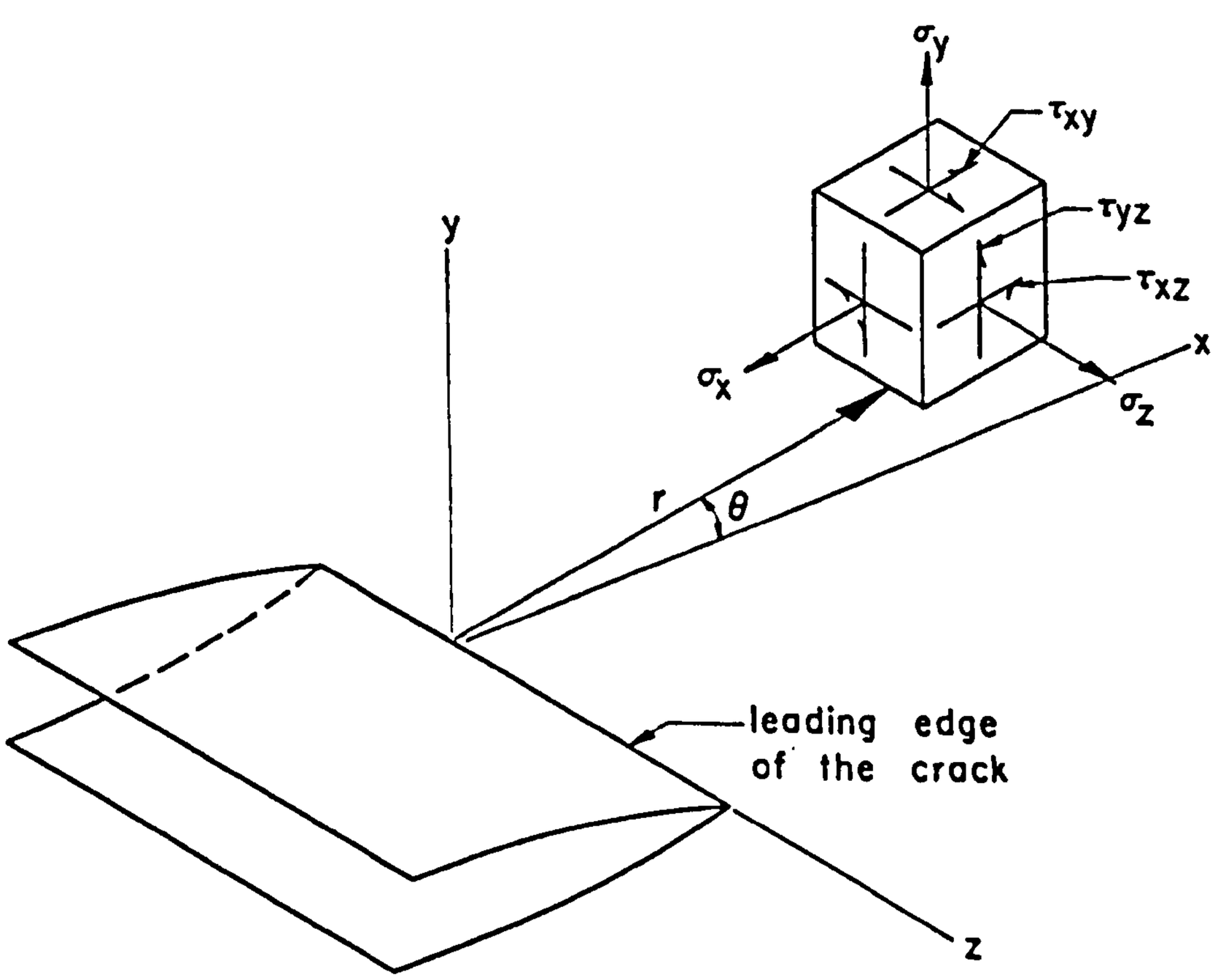

FIG. 4.83 THREE - DIMENSIONAL CRACK TIP COORDINATE AND STRESS SYSTEM

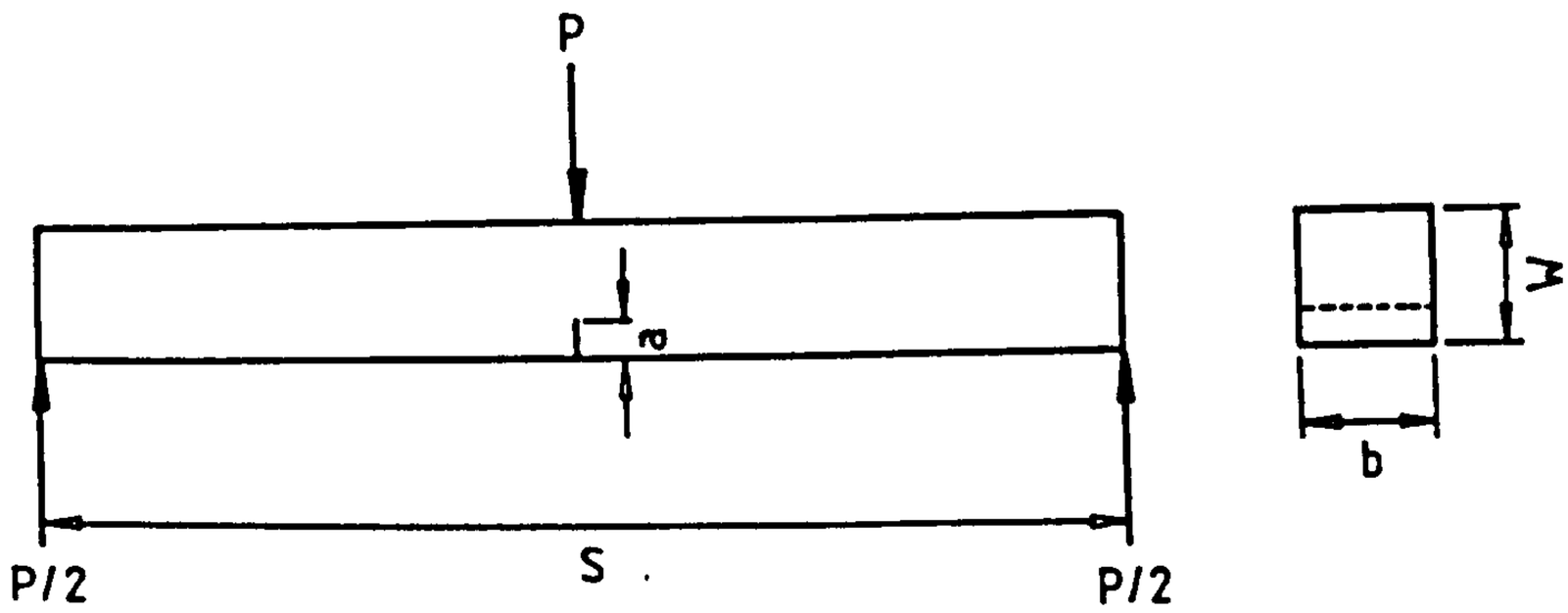

P = 1 Newton
S = 0·08 m
E = 6·89 × 10^{9} N/m**2
b = 0·01 m
W = 0·01 m
ν = 0·2

FIG.4.84 S.E.N BEAM BEND SPECIMEN AND MATERIAL PROPERTIES EMPLOYED IN ANALYSIS

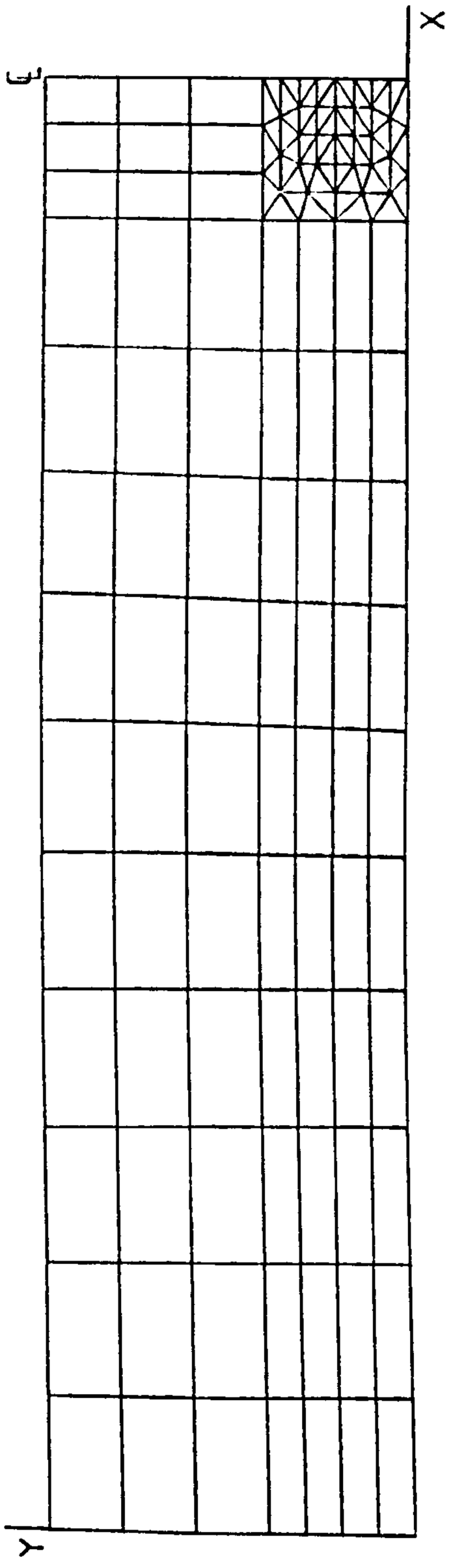

FIG. 4.85 FIRST IDEALIZATION OF A HALF SPECIMEN OF FIGURE 4.84 , a/W = 0·2

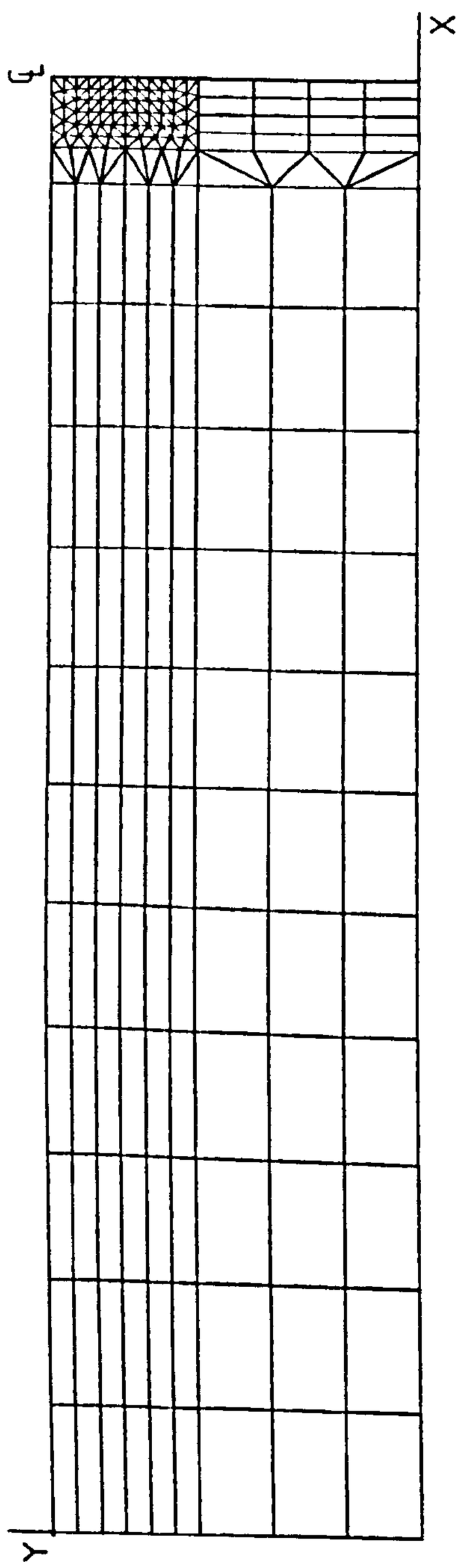

FIG. 4.86 SECOND IDEALIZATION OF A HALF SPECIMEN OF FIGURE 4.84 , a/W = 0·8

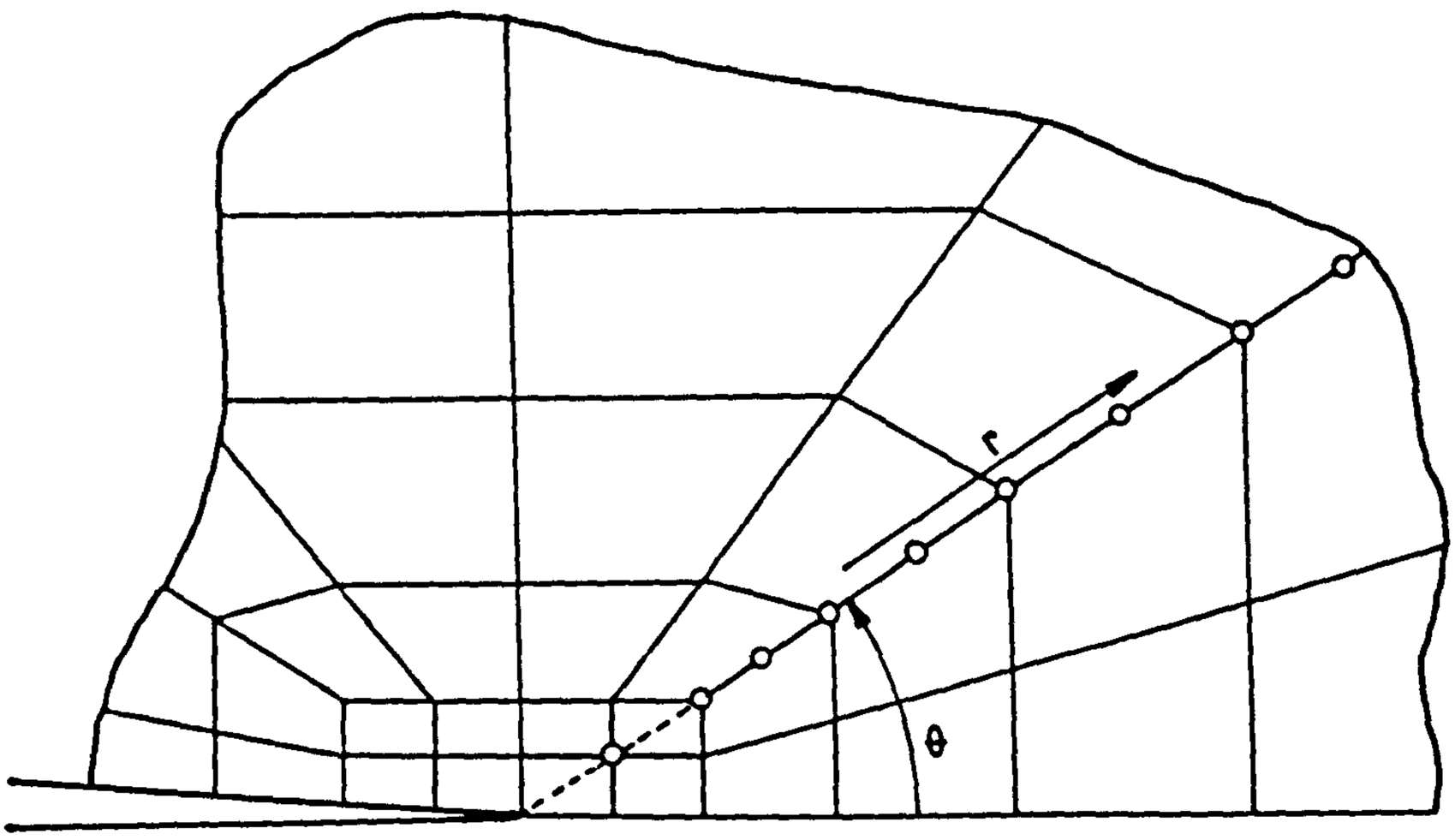

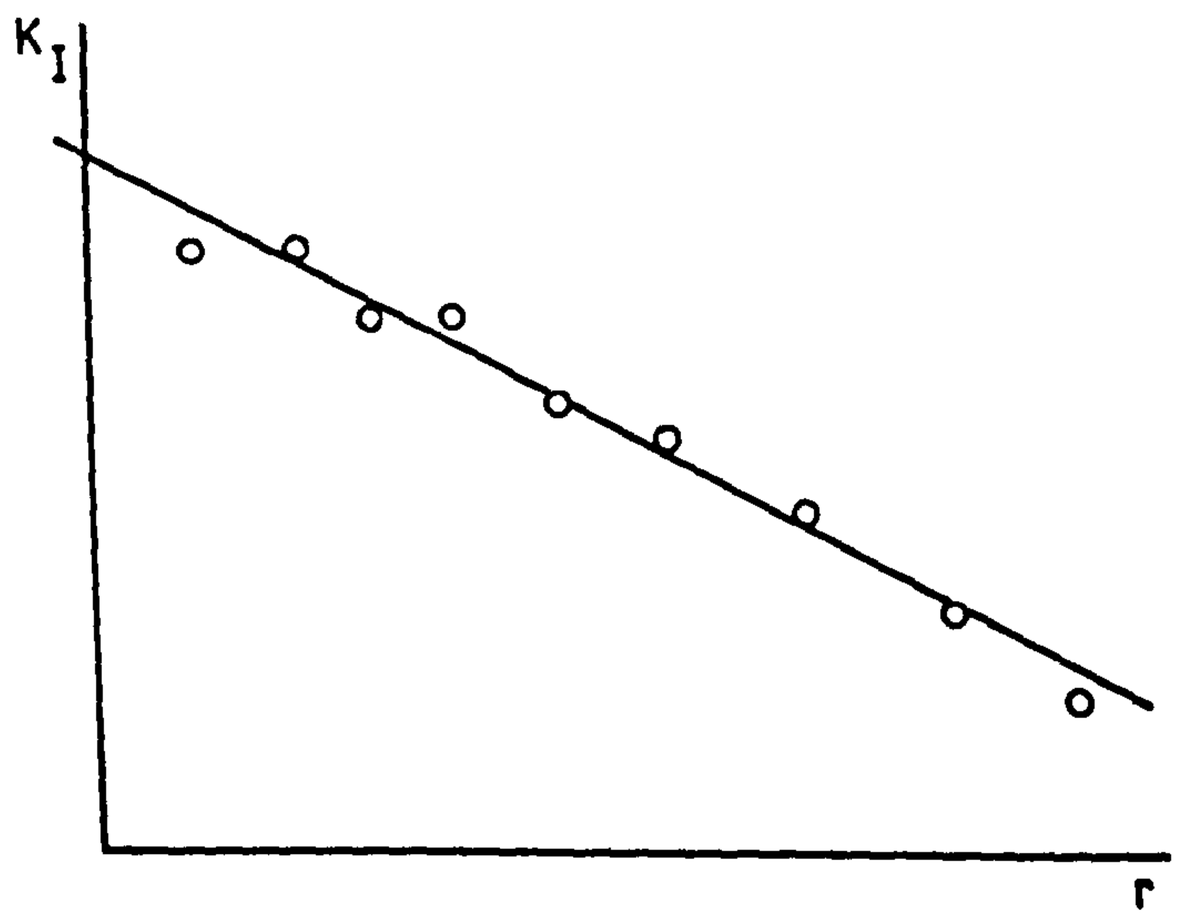

FIG. 4.87 STRESS INTENSITY FACTOR EVALUATION BY EXTRAPOLATION

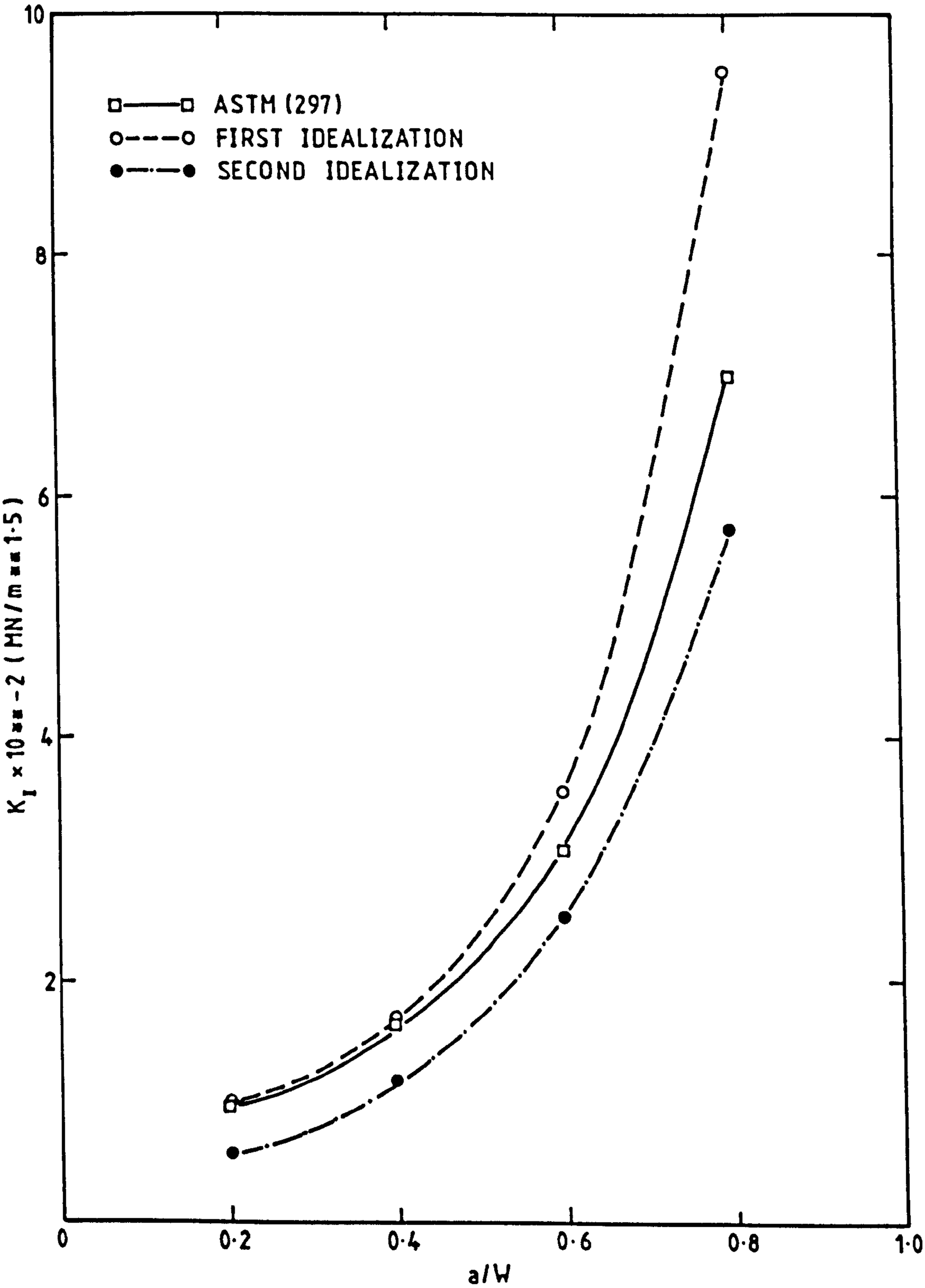

FIG. 4.88 STRESS INTENSITY FACTOR PLOT FOR STRESS EXTRAPOLATION

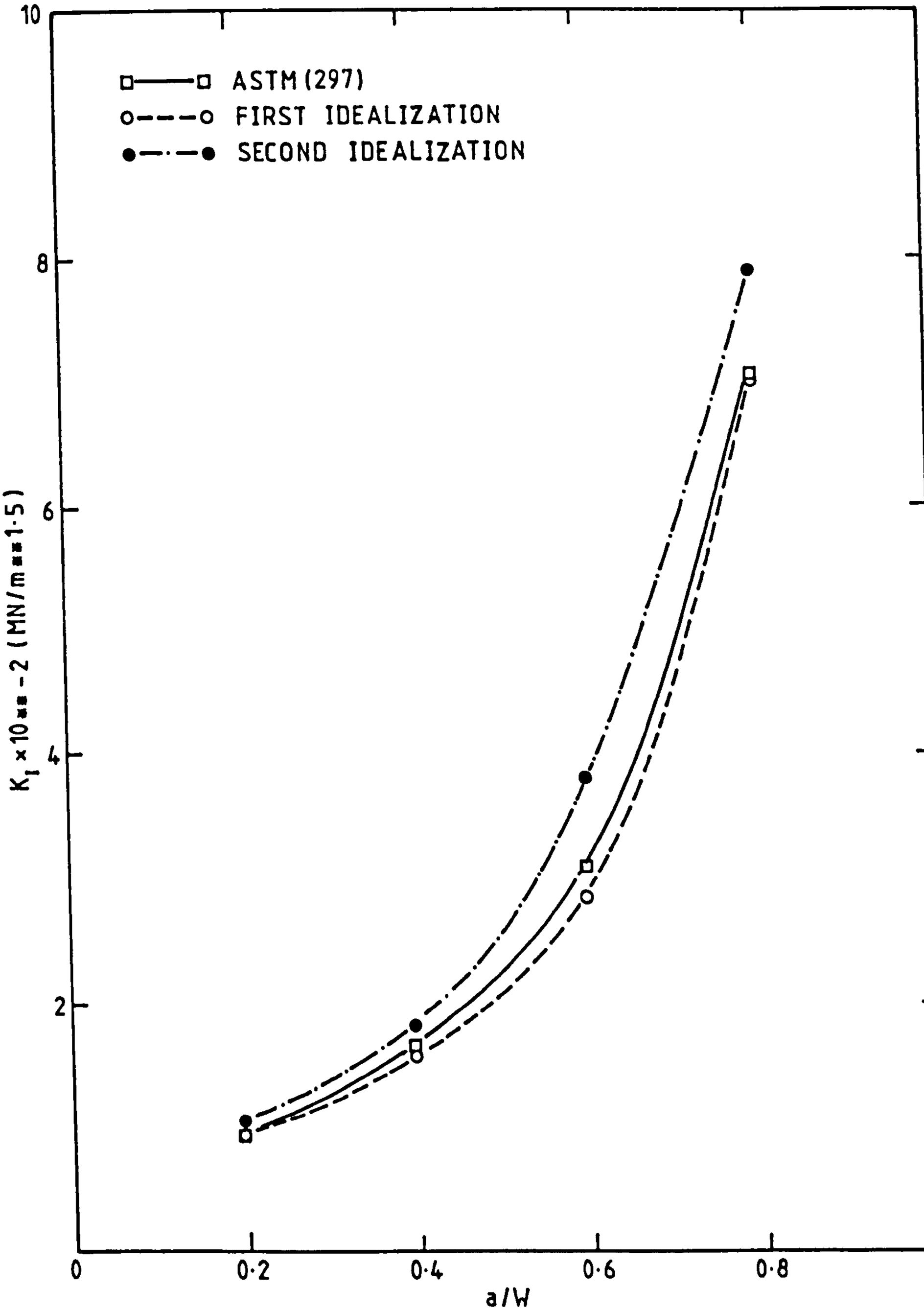

FIG. 4.89 STRESS INTENSITY FACTOR PLOT FOR DISPLACEMENT EXTRAPOLATION

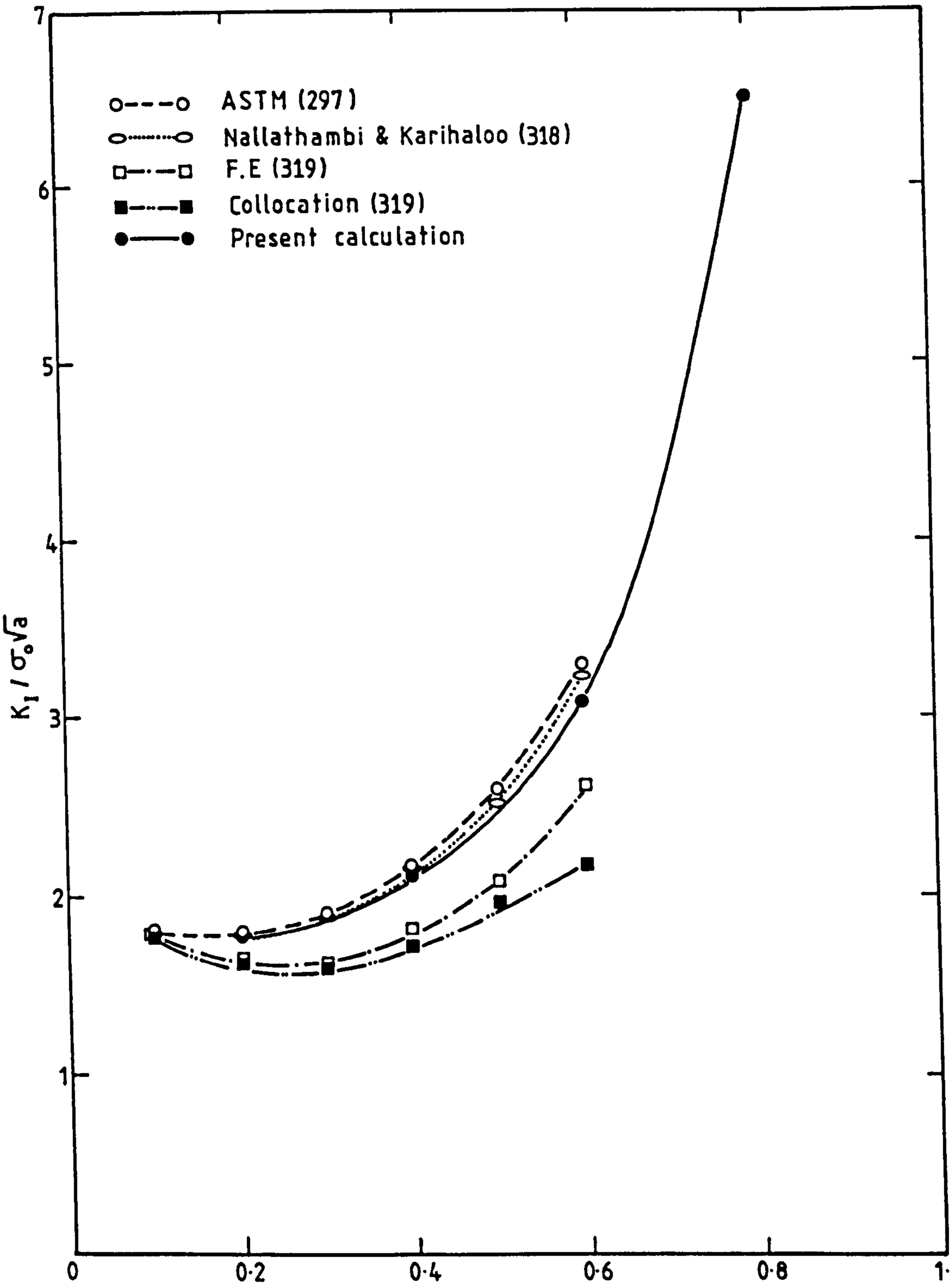

FIG. 4.90 COMPARISON OF RESULTS OF COLLOCATION AND FINITE ELEMENT SOLUTIONS

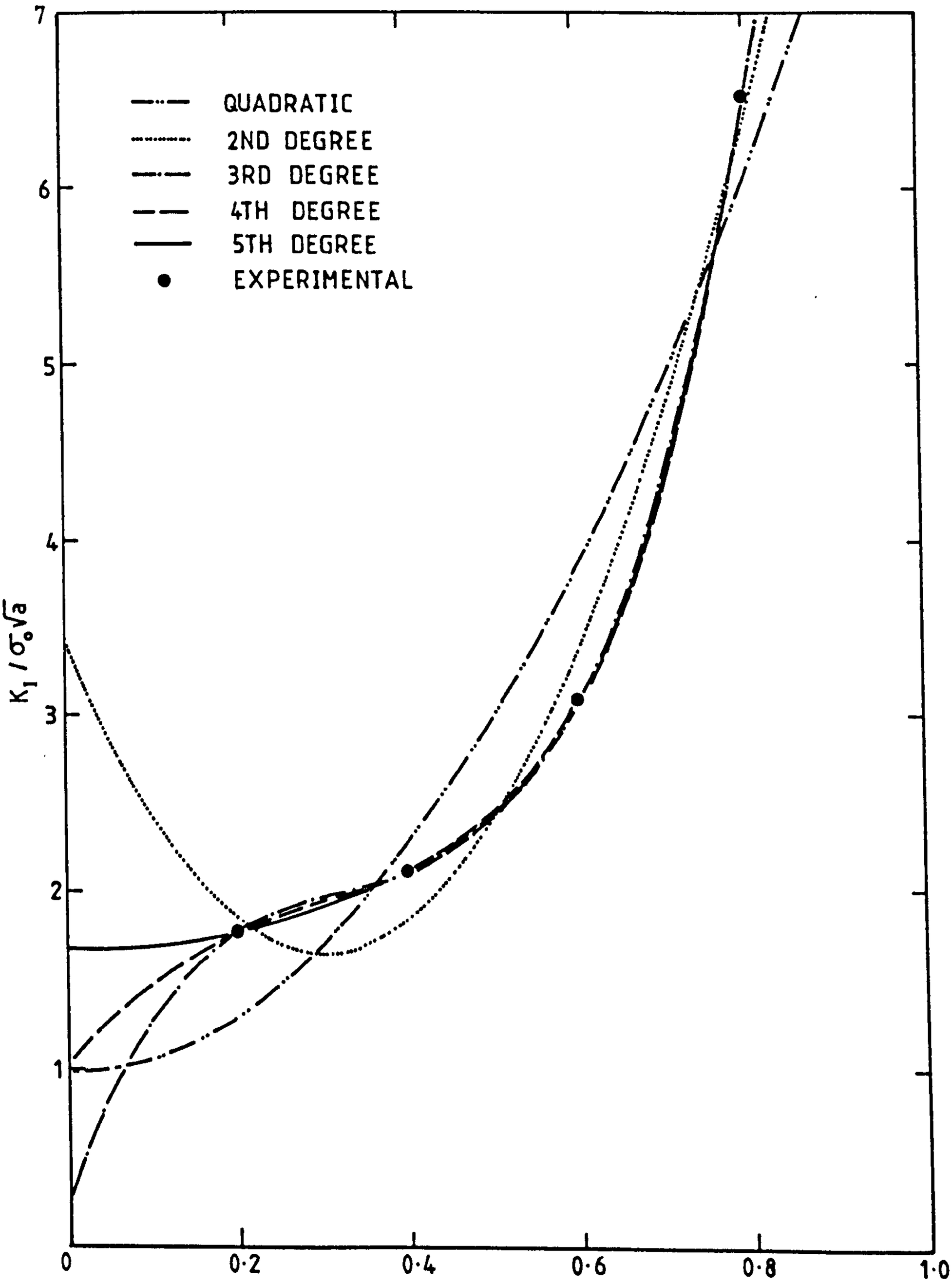

FIG. 4.91 LEAST-SQUARES CURVE FITTING FOR S.E.N BEAM BENDING